Titre: Title:	Application of perturbation theory to lattice calculations based on method of cyclic characteristics
Auteur: Author:	Monchai Assawaroongruengchot
Date:	2007
Type:	Mémoire ou thèse / Dissertation or Thesis
Référence: Citation:	Assawaroongruengchot, M. (2007). Application of perturbation theory to lattice calculations based on method of cyclic characteristics [Thèse de doctorat, École Polytechnique de Montréal]. PolyPublie. https://publications.polymtl.ca/8051/

UNIVERSITÉ DE MONTRÉAL

APPLICATION OF PERTURBATION THEORY TO LATTICE CALCULATIONS BASED ON METHOD OF CYCLIC CHARACTERISTICS

MONCHAI ASSAWAROONGRUENGCHOT
DÉPARTEMENT DE GÉNIE PHYSIQUE
ÉCOLE POLYTECHNIQUE DE MONTRÉAL

THÈSE PRÉSENTÉE EN VUE DE L'OBTENTION
DU DIPLÔME DE PHILOSOPHIÆ DOCTOR
(GÉNIE NUCLÉAIRE)
AUGUST 2007

Your file Votre référence
ISBN: 978-0-494-35505-3
Our file Notre référence
ISBN: 978-0-494-35505-3

UNIVERSITÉ DE MONTRÉAL

ÉCOLE POLYTECHNIQUE DE MONTRÉAL

Cette thèse intitulée:

APPLICATION OF PERTURBATION THEORY TO LATTICE CALCULATIONS BASED ON METHOD OF CYCLIC CHARACTERISTICS

présentée par: ASSAWAROONGRUENGCHOT MONCHAI
en vue de l'obtention du diplôme de: Philosophiæ Doctor
a été dûment acceptée par le jury d'examen constitué de:

M. TEYSSEDOU Alberto, Ph.D., président
M. MARLEAU Guy, Ph.D., membre et directeur de recherche
M. KOCLAS Jean, Ph.D., membre et codirecteur de recherche
M. ROY Robert, Ph.D., membre
M. NICHITA Eleodor, Ph.D., membre

To my parents and all of my teachers

ACKNOWLEDGMENTS

I would like to gratefully thank my research director, Professor Guy Marleau, and my research co-director, Professor Jean Koclas for their continuous guidance and support on this work. Their knowledge and motivation provided me with a good exemple on how a research work should proceed. I would also like to acknowledge the work of the committee members, Professor Alberto Teyssedou, Professor Robert Roy and Professor Eleodor Nichita for their interest and the valuable time they spent in reviewing this manuscript and providing insightful comments. Finally I would like to thank my friends for the supports and encouragement they have provided: Cornellia, Fan, Nihan, Romain, Alexi, Ovidiu, Hamid, Azadeh, Farshad, Karthikeyan, Djamila, Jing Sun and Yan Song. The financial support of this research by Natural Science and Engineering Research Council of Canada is also gratefully acknowledged.

ABSTRACT

Perturbation theory is a technique used for the estimation of changes in performance functionals, such as linear reaction rate ratio and eigenvalue affected by small variations in reactor core compositions. Here the algorithm of perturbation theory is developed for the multigroup integral neutron transport problems in 2D fuel assemblies with isotropic scattering. The integral transport equation is used in the perturbative formulation because it represents the interconnecting neutronic systems of the lattice assemblies via the tracking lines. When the integral neutron transport equation is used in the formulation, one needs to solve the resulting integral transport equations for the flux importance and generalized flux importance functions. The relationship between the generalized flux importance and generalized source importance functions is defined in order to transform the generalized flux importance transport equations into the integro-differential equations for the generalized adjoints.

Next we develop the adjoint and generalized adjoint transport solution algorithms based on the method of cyclic characteristics (MOCC) in DRAGON code. In the MOCC method, the adjoint characteristics equations associated with a cyclic tracking line are formulated in such a way that a closed form for the adjoint angular function can be obtained. The MOCC method then requires only one cycle of scanning over the cyclic tracking lines in each spatial iteration. We also show that the source importance function by CP method is mathematically equivalent to the adjoint function by MOCC method. In order to speed up the MOCC solution algorithm, a group-reduction and group-splitting techniques based on the structure of the adjoint scattering matrix are implemented. A combined forward flux/adjoint function iteration scheme, based on the group-splitting technique and the common use of a large number of variables storing tracking-line data and exponential values, is proposed to reduce the computing time when both direct and adjoint solutions

are required.

A problem that arises for the generalized adjoint problem is that the direct use of the negative external generalized adjoint sources in the adjoint solution algorithm results in negative generalized adjoint functions. During the multigroup iterations, using such negative values in the adjoint rebalance scheme shall cause errors in the rebalance factors, and numerical oscillations in the solutions. A coupled flux biasing/decontamination scheme is applied to make the generalized adjoint functions positive using the adjoint functions in such a way that it can be used for the multigroup rebalance technique. After multigroup convergence is reached, the decontamination procedure extracts from the generalized adjoints the component parallel to the adjoint function. Three types of biasing/decontamination schemes are investigated in this study. To demonstrate the efficiency of these algorithms, calculations are performed on the 17×17 PWR, 37 pin CANDU and the Watanabe-Maynard lattice problems. Numerical comparisons of adjoint functions, generalized adjoint functions and k_{eff} results obtained by the MOCC and CP methods are presented. Numerical results of perturbative estimates and sensitivity coefficients are also presented as well as the group-based sensitivity analyses of eigenvalue with respect to nuclide densities.

Next we consider the application of the perturbation theory to the reactor problems. Since the coolant void reactivity (CVR) is a important factor in reactor safety analysis, we have decided to select this parameter for optimization studies. We consider the optimization and adjoint sensitivity techniques for the adjustments of CVR at beginning of burnup cycle (BOC) and k_{eff} at end of burnup cycle (EOC) for a 2D Advanced CANDU Reactor (ACR) lattice. The sensitivity coefficients are evaluated using the perturbation theory based on the integral transport equations. Three sets of parameters for CVR-BOC and k_{eff}-EOC adjustments are studied: 1) Dysprosium density in the central pin with Uranium enrichment in the outer fuel rings, 2) Dysprosium density and Uranium enrichment both in the central pin,

and 3) the same parameters as in the first case but the objective is to obtain a negative checkerboard CVR at beginning of cycle (CBCVR-BOC). To approximate the sensitivity coefficient at EOC, we perform constant-power burnup/depletion calculations for 600 full power days (FPD) using a slightly perturbed nuclear library and the unperturbed neutron fluxes to estimate the variation of nuclide densities at EOC. Sensitivity analyses of CVR and eigenvalue are included in the study.
In addition the optimization and adjoint sensitivity techniques are applied to the CBCVR-BOC and k_{eff}-EOC adjustment of the ACR lattices with Gadolinium in the central pin. Finally we apply these techniques to the CVR-BOC, CVR-EOC and k_{eff}-EOC adjustment of a CANDU lattice of which the burnup period is extended from 300 to 450 FPDs. The cases with the central pin containing either Dysprosium or Gadolinium in the natural Uranium are considered in our study.

RÉSUMÉ

La théorie des perturbations est une technique utilisée en physique des réacteurs nucléaires pour évaluer les changements dans des fonctionelles de performance, telles que celles utilisées dans le calcul des valeurs propres et des rapports de taux de réactions, résultant de faibles variations dans la composition du réacteur. Cette technique est développée pour des problèmes de transport neutronique dans des réseaux 2-D de cellules contenant du combustible. Nous utilisons ici la formulation intégrale de l'équation de transport car elle représente un ensemble de systèmes neutroniques couplés entre eux par des trajectoires linéaires (les lignes caractéristiques du système) alors que la formulation intégro-différentielle correspond plutôt à un équilibre local des neutrons à l'intérieur d'un volume infinitésimal. Nous présenterons les relations entre les fonctions d'importance pour les flux et les fonctions d'importance pour les sources qui correspondent respectivement aux solutions de l'équations de transport intégro-différentielle et intégrale adjointes ainsi que l'extension de telles définitions aux problèmes adjoints généralisés.

Nous développons également des algorithmes de résolution de l'équation du transport adjointe basés sur la méthode de caractéristiques cycliques (MOCC) programmée dans le code DRAGON. Un des principaux avantages de cette méthode est qu'elle ne nécessite pas la connaissance des courants sur les frontières externes du domaine comme pour la méthode des caractéristiques standard utilisant des conditions aux frontières blanches. En utilisant la méthode MOCC, les équations de caractéristiques adjointes peuvent être formulées sous une forme fermée impliquant la fonction angulaire adjointe. Cette méthode exige alors seulement un cycle de balayage des lignes d'intégration pour chaque boucle de l'itération spatiale. L'équivalence mathématique entre la fonction adjointe obtenue par la méthode des probabilités de collision (CP) et la fonction adjointe par la méthode de MOCC est démontrée. Afin d'accélérer l'algorithme de résolution du problème itératif généré

par cette dernière méthode, une technique basée sur la forme de la matrice de diffusion, qui consiste à ordonner les groupes d'une façon différente ("group reduction method ") et à les réarranger en différents ensembles ("group splitting method"), est mise en oeuvre. De plus, on propose un processus itératif pour résoudre en parallèle les équations de transport pour les flux et les fonctions adjointes ce qui permet d'utiliser un grand nombre de variables communes contenant les données associées aux lignes caractéristiques et les facteurs d'atténuation exponentiels. Ceci a pour effet de réduire sensiblement les temps de calcul lorsque les solutions pour les flux et les fonctions adjointes sont toutes les deux requises.

Un des problèmes majeurs que l'on rencontre lors de l'évaluation des adjoints généralisés est la présence des sources négatives. Ces sources sont dues à la présence d'adjoints généralisés pouvant prendre des valeurs négatives et ce contrairement aux fonctions adjointes et au flux qui eux sont strictement positifs. C'est en fait la technique de rééquilibrage multigroupe utilisée pour accélérer l'itération couvrant les différents groupes d'énergie qui alors se détraque. En effet, certains facteurs de rééquilibrage deviennent négatifs menant à des changements dans le signe des adjoints généralisés qui induisent des oscillations numériques dans les solutions. Nous proposons de résoudre ce problème en utilisant une procédure couplée de contamination/décontamination. Le processus de contamination consiste à ajouter aux adjoints généralisés une contribution venant des fonctions adjointes rendant la source adjointe généralisée strictement positive et pouvant alors être utilisée pour la solution multigroupe et qui rendra le processus de rééquilibrage stable. Les adjoints ainsi produits sont ensuite décontaminés avant d'être utilisés au niveau des itérations de puissance. Nous suggérons trois types de combinaison contamination/décontamination que nous analysons et évaluons. Nous démontrons l'efficacité des algorithmes de résolution des équations MOCC en utilisant un calcul d'assemblage REP 17×17, une cellule CANDU à 37 crayons et une cellule Watanabe-Maynard. Des comparaisons numériques des fonctions adjointes,

des fonctions adjointes généralisées et du k_{eff} obtenus par les méthodes MOCC et CP sont présentées. Les algorithmes utilisés pour les calculs de perturbations généralisées sont vérifiés en utilisant les mêmes assemblages REP et cellules CANDU. Finalement nous présentons des résultats numériques pour différents coefficients de sensibilité obtenus en utilisant la méthode des perturbations généralisées pour différentes densités isotopiques de noyaux présents dans la cellule.

Dans la seconde partie de ce travail, nous considérons l'application de la théorie des perturbations à des problèmes d'optimisation de la composition isotopique de cellules de réacteurs nucléaires. Comme l'effet en réactivité résultant de la vidange du caloporteur (CVR) est un facteur crucial dans les analyses de sûreté des réacteurs, c'est à ce problème que nous nous sommes attaqués. Ici nous montrons comment les techniques de calcul des coefficients de sensibilité basées sur le calcul des fonctions adjointes peuvent être utilisées afin d'ajuster le CVR au début du cycle d'évolution du combustible (BOC) et le facteur de multiplication (k_{eff}) à la fin du cycle (EOC) pour une cellule du réacteur CANDU avancé (le ACR). Trois ensembles d'ajustement du CVR initial de la cellule (CVR-BOC) et de son k_{eff} final (k_{eff}-EOC) ont été étudiés : 1) la densité de dysprosium dans le crayon central combiné à l'enrichissement en uranium dans les anneaux externes de combustible; 2) la densité de dysprosium et l'enrichissement du combustible en uranium dans le crayon central; et 3) les mêmes paramètres que dans le premier cas, mais en ajustant aussi le CVR-BOC pour une vidange du caloporteur en damier (CBCVR-BOC). Dans ces analyses, nous approximons les coefficients de sensibilité en fin de cycle en utilisant le flux neutronique 600 jours pleine puissance dans le combustible de référence pour mettre à jour une bibliothèque perturbée.

Nous étudierons également l'ajustement de CBCVR-BOC et k_{eff}-EOC pour une cellule ACR contenant du gadolinium dans le crayon central. Finalement nous considérerons le prolongement de 300 à 450 jours de la période d'irradiation à pleine puissance d'une cellule CANDU-6 légèrement enrichie et dont le crayon central est

empoisonné avec du dysprosium ou du gadolinium. Dans ces cas, nous imposerons des contraintes sur le CVR de début et de fin de cycle et sur le k_{eff} final.

CONDENSÉ EN FRANÇAIS

La théorie des perturbations est une technique utilisée en physique des réacteurs nucléaires pour l'évaluation de changements dans des fonctionelles de performance, telles que celles utilisées dans le calcul des valeurs propres et des rapports de taux de réactions, résultant de faibles variations dans la composition du réacteur. Elle est basée sur un formalisme utilisant les solutions directes et adjointes aux équations du système à analyser. Ici, l'algorithme de la théorie des perturbations est développé pour des problèmes de transport neutronique dans des réseaux 2-D de cellules contenant du combustible. Nous utiliserons une formulation intégrale de l'équation de transport en supposant que les sources dues à la diffusion sont isotropes. L'équation adjointe correspondante produira des solutions connues sous le nom de "fonctions d'importance pour les flux". Celles-ci différent des solutions adjointes de l'équation intégro-différentielle équivalente et qui elles sont connues sous le nom de "fonctions d'importance pour les sources". Nous présenterons les relations entre ces deux types de fonctions d'importance ainsi que l'extension de telles définitions aux problèmes adjoints généralisés. Ici, nous utilisons principalement la formulation intégrale de l'équation de transport car elle représente un ensemble de systèmes neutroniques couplés entre eux par des trajectoires linéaires (les lignes caractéristiques du système) alors que la formulation intégro-différentielle correspond plutôt à un équilibre local des neutrons à l'intérieur d'un volume infinitésimal.

Les fonctions adjointes étant requises si l'on désire utiliser la théorie des perturbations généralisées, nous développons également des algorithmes de résolution de l'équation adjointe du transport basés sur la méthode des caractéristiques cycliques (MOCC) programmée dans le code DRAGON. Les avantages principaux de cette méthode sont les suivants: Elle exige moins d'espace en mémoire et les calculs sont plus performants (réduction du temps de calcul CPU) que la méthode des probabilités de collision (CP) lorsque les mêmes lignes d'intégration cycliques sont

utilisées (conditions aux frontières spéculaires). Elle ne nécessite pas la connaissance des courants sur les frontières externes du domaine comme pour la méthode des caractéristiques utilisant des conditions aux frontières blanches (MOC). Elle permet en plus d'analyser les problèmes de transport en utilisant une description exacte de la géométrie. En utilisant la méthode MOCC, les équations de caractéristiques adjointes peuvent être formulées sous une forme fermée impliquant la fonction angulaire adjointe. Cette méthode exige alors seulement un cycle de balayage des lignes d'intégration pour chaque boucle de l'itération spatiale. Le temps requis pour effectuer une itération spatiale est donc inférieur à celui exigé pas la méthode MOC lorsque les mêmes lignes caractéristiques sont considérées. L'équivalence mathématique entre la fonction adjointe obtenue par la méthode CP et la fonction adjointe par la méthode de MOCC est aussi démontrée.

Afin d'accélérer l'algorithme de résolution du problème itératif généré par la méthode MOCC, une technique basée sur la forme de la matrice de diffusion, qui consiste à ordonner les groupes d'une façon différente ("group reduction method ") et à les réarranger en différents ensembles ("group splitting method"), est mise en oeuvre. De plus, on propose un processus itératif qui permet de résoudre en parallèle les équations de transport pour les flux et les fonctions adjointes ce qui permet d'utiliser un grand nombre de variables communes contenant les données associées aux lignes caractéristiques et les facteurs d'atténuations exponentiels. Ceci a pour effet de réduire sensiblement les temps de calcul lorsque les solutions pour les flux et les fonctions adjointes sont toutes les deux requises.

Un des problèmes majeurs que l'on rencontre lors de l'évaluation des adjoints généralisés est la présence des sources adjointes généralisées négatives dans l'algorithme de solution adjointe. Ces sources négatives sont dues à la présence d'adjoints généralisés pouvant prendre des valeurs négatives et ce contrairement aux fonctions adjointes et au flux qui sont eux strictement positifs. C'est en fait la technique de rééquilibrage multigroupe utilisée pour accélérer l'itération couvrant les

différents groupes d'énergie qui se détraque à cause de la présence de sources et d'adjoints négatifs. En effet, certains facteurs de rééquilibrage deviennent alors négatifs menant à des changements dans le signe des adjoints généralisés qui induisent des oscillations numériques dans les solutions. Nous proposons de résoudre ce problème en utilisant une procédure couplée de contamination/décontamination. Le processus de contamination consiste à ajouter aux adjoints généralisés une contribution venant des fonctions adjointes rendant la source adjointe généralisée strictement positive et pouvant alors être utilisée pour la solution multigroupe et qui rendra le processus de rééquilibrage stable. Les adjoints ainsi produits sont ensuite décontaminés avant d'être utilisés au niveau des itérations de puissance. Nous proposons dans notre étude trois types de combinaison contamination/décontamination que nous analysons et évaluons.

Nous démontrons dans cette thèse l'efficacité des algorithmes de résolution des équations MOCC en utilisant un calcul d'assemblage REP 17 × 17, une cellule CANDU à 37 crayons et une cellule Watanabe-Maynard. Des comparaisons numériques des fonctions adjointes, des fonctions adjointes généralisées et du k_{eff} obtenus par les méthodes MOCC et CP sont présentées. De plus, les algorithmes utilisés pour les calculs de perturbations généralisées sont vérifiés en utilisant les mêmes assemblages REP et les mêmes cellules CANDU. Finalement nous présentons des résultats numériques pour différents coefficients de sensibilité obtenus en utilisant la méthode des perturbations généralisées pour différentes densités isotopiques de noyaux présents dans la cellule. Nous analysons aussi les coefficients de sensibilité associés à la valeur propre en fonction des densités isotopiques.

Dans la seconde partie de ce travail, nous considérons l'application de la théorie des perturbations à des problèmes d'optimisation de la composition isotopique de cellules de réacteur nucléaires. Comme l'effet en réactivité résultant de la vidange du caloporteur (CVR) est un facteur crucial dans les analyses de sûreté des réacteurs, c'est à ce problème que nous nous sommes attaqués. Ici nous présentons com-

ment les techniques de calcul des coefficients de sensibilité utilisant les fonctions adjointes peuvent être utilisées afin d'ajuster le CVR au début du cycle d'évolution de la combustion nucléaire (BOC) et le facteur de multiplication (k_{eff}) à la fin du cycle (EOC) pour une cellule du réacteur CANDU avancé (le ACR). Les coefficients de sensibilité sont évalués en utilisant la théorie des perturbations basée sur les équations intégrales de transport. Les flux et les adjoints seront obtenus à partir des solutions numériques générées sur la méthode MOCC.

Trois ensembles de paramètres pour l'ajustement du CVR initial de la cellule (CVR-BOC) et de son k_{eff} final (k_{eff}-EOC) ont été étudiés : 1) la densité de dysprosium dans le crayon central combiné à l'enrichissement en uranium dans les anneaux externes de combustible; 2) la densité de dysprosium et l'enrichissement du combustible en uranium dans le crayon central; et 3) les mêmes paramètres que dans le premier cas, mais en ajustant aussi le CVR-BOC pour une vidange du caloporteur en damier (CBCVR-BOC). Nos objectifs sont d'obtenir un CVR-BOC négatif de -2 mk, un k_{eff}-EOC de 0.900 pour les deux premières options d'optimisation, et en plus un CBCVR-BOC de -2 mk pour le troisième cas. Des analyses de sensibilité pour le CVR et la valeur propre sont également incluses dans l'étude.

Dans ces analyses, nous proposons d'utiliser une méthode approximative pour accélérer le calcul des coefficients de sensibilité en fin de cycle. Cette méthode consiste à traiter premièrement l'évolution du combustible pendant 600 jours à pleine puissance (600 FPD) en utilisant une bibliothèque de référence. Nous utiliserons ensuite ces flux de référence pour faire évoluer la bibliothèque perturbée et on utilisera les propriétés de la bibliothèque perturbée à 600 jours pour évaluer les coefficients de sensibilité à la fin du cycle d'évolution.

Finalement nous appliquerons aussi ces mêmes techniques de calcul des coefficients de sensibilité utilisant les fonctions adjointes aux cas suivants. Nous étudierons l'ajustement de CBCVR-BOC et k_{eff}-EOC pour une cellule ACR contenant du gadolinium dans le crayon central. Nous considérerons aussi le prolongement de

300 à 450 jours de la période d'irradiation à pleine puissance d'une cellule CANDU-6 légèrement enrichie et dont le crayon central est empoisonné avec du dysprosium ou du gadolinium. Dans ces cas, nous imposerons des contraintes sur le CVR de début et de fin de cycle et sur le k_{eff} final.

Les principales conclusions de cette thèse peuvent être classées en trois catégories : efficacité des algorithmes de résolution, précision de la méthode des perturbation généralisées et performance de la méthode lors de calculs d'optimisation.

L'algorithme de résolution de l'équation de transport pour les fonctions adjointes et adjointes généralisées que nous avons développé pour la méthode des caractéristiques cycliques fait en sorte que cette technique atteint presque la performance de la méthode des probabilités de collision. De plus, étant moins vorace en termes de ressources mémoire, elle peut être utilisée pour la résolution de problèmes impliquant un nombre d'inconnu beaucoup plus élevé. Nous avons aussi démontré l'équivalence entre les adjoints obtenus par MOCC et la méthode CP.

Un des problèmes majeurs dans l'utilisation de la forme intégrale de l'équation de transport dans des calculs perturbatifs réside dans la nécessité d'évaluer l'effet de la perturbation sur l'opérateur de transport. Deux méthodes approximatives ont été proposées et validées. La première méthode, correspondant à l'approximation isotrope (IA), fonctionne très bien pour tous les types de cellules considérés (REP et CANDU) lorsque les perturbations sont faibles tout en étant un peu moins fiable pour les cellules de type CANDU. Nous avons aussi démontré que la fiabilité des calculs perturbatifs pour ce dernier type de cellules est grandement améliorée en utilisant la méthode d'approximation linéaire (LA).

Finalement nous avons aussi appliqué la théorie des perturbations à des problèmes pratiques en physique des réacteurs nucléaires. Les coefficients de sensibilité dérivés en utilisant les fonctions adjointes de l'équation de transport ont été utilisés de façon à optimiser les propriété du combustible dans des cellules CANDU et ACR. Il a donc été possible de déterminer l'enrichissement et la concentration en poi-

sons consommables des crayons de combustible dans ces cellules qui minimisent le coefficient de réactivité du vide tout en optimisant l'utilisation du combustible.

TABLE OF CONTENTS

LIST OF FIGURES

LIST OF NOTATIONS AND SYMBOLS

Abbreviations

2D:	Two dimensions
3D:	Three dimensions
ACR:	Advanced CANDU reactor
BOC:	Beginning of fuel burnup cycle
CANDU:	Canadian Deuterium Uranium reactor
CANFLEX:	CANDU flexible fuelling
CBCVR:	Checkerboard-patterned coolant-voided reactivity
CBVOID:	Checkerboard-patterned coolant voiding
CP:	Collision probability
CVR:	Coolant-voided reactivity
EOC:	End of fuel burnup cycle
EVO:	Evolution (burnup/depletion) module in DRAGON
FPD:	Full power day
GPT:	Generalized perturbation theory
IA:	Isotropic approximation method
LA:	Linearization approximation method
MCNP:	Monte Carlo Neutral Transport Code
MOC:	Method of characteristics
MOCC:	Method of cyclic characteristics
PWR:	Pressurized light water reactor
TNOS:	Total number of one-group solution

LIST OF TABLES

LIST OF APPENDICES

INTRODUCTION

Reactor physics studies involve the computation of neutron distribution and fission power generation inside the lattices of a reactor core. The main activities include the calculations of criticality, coolant void reactivity, absorber reactivity worths, reaction rates, burnup-depletion, coupled kinetics-thermalhydraulics analysis, fuel cycle optimization, sensitivity and uncertainty analyses of system parameters, radiation shielding and protection, etc. The neutronic system is often modelled by the deterministic neutron diffusion and transport equations or by a stochastic model that uses Monte Carlo methods. Most computations in reactor physics are time-consuming especially when repetitive computations are required such as for lattice design (including the calculation of k_{eff}, reaction rates, coolant void reactivity, pin power, etc.) for multiple parameters (e.g. the operating temperature, U235 enrichment, fixed/soluble poison densities, coolant/moderator densities, lattice pitches, etc.). To reduce these repetitive calculations, a perturbation theory can be applied to approximate the reactor parameters for the cases involving small variation in the system parameters.

Lattice Physics Calculations in DRAGON

In our research, we focus on the lattice calculations based on the deterministic neutron transport model using the lattice physics code DRAGON Version 3.05 developed at Institut de génie nucléaire, École Polytechnique de Montréal (MARLEAU et al., 2006). Major functions of DRAGON are: macroscopic library generation using the available microscopic libraries (such as WIMSLIB, WNEA, IAEA); 2D/3D isotropic and 2D cyclic tracking generation modules (ROY et al., 1991; ROY et al., 1994); neutron transport solutions based on the interface current, CP,

MOC and MOCC methods as well as a 3D isotropic-tracking MOC option recently implemented (ROY, 1998; ROY, 2003; WU and ROY, 2003); space-dependent burnup/depletion calculations with fixed flux or constant power using the regional fluxes obtained from the transport solutions; self-shielding calculation based on the modified Stamm'ler method (STAMM'LER and M.J.ABBATE, 1983; HÉBERT and MARLEAU, 1991) and the other various advanced self-shielding methods (such as the extended Ribon, subgroup methods) available in DRAGON Version 4.0 (HÉBERT, 2005; HÉBERT, 2006a; HÉBERT, 2006b); homogenization, super-homogenization (SPH), condensation and reaction-rate calculations (HÉBERT, 1993); generalized adjoint transport and perturbation theory (COURAU, 2001; COURAU and MARLEAU, 2002), etc. In addition a 2D/3D isotropic-tracking MOC method is included in DRAGON Version 4.0 (LE TELLIER and HÉBERT, 006a). A parallel 3D MOCC module can also be found in another version of DRAGON (DAHMANI and ROY, 2005).

The DRAGON code is applied to various research works in lattice physics such as the 3D modelling of CANDU reactivity control devices using the CP and MOC methods (ROY et al., 1994; LE TELLIER et al., 006b), a few groups homogenization/condensation cross section generation for full core diffusion calculation (MARLEAU et al., 2006), the coupled DRAGON/DONJON codes for full core history-based burnup simulations (VARIN and MARLEAU, 2006), the simulation for Co60 isotope production in CANDU-6, the generalized perturbation theory based on the CP equation (COURAU, 2001), the perturbative estimate of 3D reactivity control device in CANDU-6 (MARLEAU, 2004a), the 3D space-dependent ACR-lattice burnup/depletion calculation using either CP and MOC methods, the validation of pin power, k_{eff} and coolant void reactivities in CANDU and ACR lattices, 3D heterogeneous full core calculation using the parallel MOC method (DAHMANI and ROY, 2005).

Perturbation Theory

The perturbation theory for nuclear reactor analysis is a technique used for the estimation of changes in reactor properties that are affected by small variations in reactor core compositions. The method is similar to classical perturbation theory for a linear system. In its early development, perturbation theory is applied to the estimation of eigenvalue changes due to the adjustment of core composition. Later the generalized perturbation theory (GPT) is established for problems in reactor core design such as computation of reaction rate ratio, fuel burnup, power density distribution, kinetic problems and penetration calculation of neutron-photon for shielding as well as applications in the field of parametric sensitivity and uncertainty analysis.

In performing reactor analysis and design calculation, a nuclear engineer may encounter many situations in which perturbation theory can reduce substantially the calculation time in obtaining a solution. The following problems illustrate cases for which the application of perturbation theory is often considered (WILLIAMS, 1986):

- The examination of parametric alterations to the reactor lattice and core designs
- The repetitive computations with varying sources or varying initial conditions in time dependent problems
- The estimation of small reactivity changes due to small changes in reactor core compositions
- Determination of space-dependent reactivity coefficients
- Design of experiments which exhibit the correct parameter sensitivity

- Calculation of the sensitivity parameters
- Adjustment of multigroup cross-sections to improve the calculation of integral parameters
- Calculation of burnup sensitivity and fuel cycle optimization, etc.

Perturbation theories can be classified into three types:

- Perturbation theory for neutron field problems (or static perturbation theory) is the theory associated with the static reactor systems affected by the core composition changes. For this case, the reactor systems are represented by time-independent diffusion or transport equations.
- Perturbation theory for nuclide field problems is the theory associated with the reactor systems for which the nuclide densities are time-varying due to fuel burnup/depletion. Thus the reactor systems are represented by the coupled time-dependent isotopic burnup/depletion and neutron transport equations.
- Boundary perturbation theory is the theory associated with the static reactor systems affected by the changes in boundary conditions such as reflector thickness, reflector properties, etc.

In the following sections, the literature review of developments in the perturbation theory is presented in the following order:

- Perturbation theory for neutron field problems
- Perturbation theory for nuclide field problems
- Boundary perturbation theory

Literature Review on Perturbation Theory for Neutron Field Problems

The static perturbation theory is applied to problems of estimating the changes in k_{eff}, reactivity worth, etc. that are affected by the variations in reactor core compositions. Wigner is the first to introduce the perturbation theory in reactor core analysis (WIGNER, 1945; WILLIAMS, 1986). Davison proposes the derivation of adjoint transport equation, adjoint integral solution and the perturbation theory for critical size calculation (DAVISON, 1957). He also introduces the variational method to estimate the bilinear reaction rate affected by direct flux and adjoint flux variations. Usachev (USACHEV, 1964) proposes the interpretation of neutron importance and presents an algorithm for neutron importance function computation. Usachev also presents the generalized perturbation formulation to compute the changes in breeding ratio. Lewins extends Usachev works by introducing the variational principle to compute a change in arbitrary reaction rate ratio. Lewins proposes the adjoint residue equations to obtain the accurate estimation of reaction rate ratio (LEWINS, 1966). Gandini generalizes the work by Usachev and Lewins to the generalized perturbation theory for bilinear functional. He also proposes the iterative algorithms for computation of the generalized adjoint fluxes (GANDINI, 1967).

Stacey proposes the variational approach for GPT to estimate the changes in reactivity worth and reaction rate ratio (STACEY, 1972). His variational method provides the first order correction taking into account the changes in the direct and adjoint fluxes. The relationship between the variational theory and the generalized perturbation theory proposed by Gandini is proven. Stacey expands the variational methods to various types of problems such as linear and bilinear functionals, linear and bilinear ratio functionals (STACEY, 1974). The generalized adjoint and generalized forward flux equations emerge from variational conditions

required to determine the solution. In addition, the applications of variational estimates to reactor physics such as reactivity worth, reactor kinetics radiation shielding are demonstrated. Pomraning proposes a perturbation theory approach for calculation of eigenvalue changes by deriving functional from one group neutron diffusion equation with the use of its self-adjoint properties (POMRANING, 1983). Belblidia proposes the Taylor-generalized perturbation theory applied to one dimension power density distribution (BELBLIDIA et al., 1983). The second order perturbation formulation using Taylor-series expansion is introduced with the numerical examples using the one group neutron diffusion equations. Williams summarizes the development of perturbation, generalized perturbation (WILLIAMS, 1986), higher-order perturbation, time dependent perturbation theories as well as the various applications of these techniques to reactor physics calculations. Lewins introduces the new higher-order perturbation theory based on Taylor-series expansion and proposes perturbation formulation for linear functional of thermal utilization using Lagrange method incorporated with the one group diffusion equation. This method relies on the use of the self-adjoint property of the diffusion equation (LEWINS et al., 1986).

Bruna applies GPT to estimate the changes in the axial power offset ratio functional (BRUNA et al., 1990). Laurin-Kovitz proposes the perturbation algorithm based on the variational nodal method in the DIF3D code (LAURIN-KOVITZ and LEWIS, 1996a). The perturbation formulation for k_{eff} is derived directly from the response matrix equation. The numerical examples of various test cases using P1 and P3 nodal methods are demonstrated. Courau and Marleau introduce the multigroup generalized adjoint transport solution by the method of collision probability (COURAU and MARLEAU, 2002). The newly defined pseudo-adjoint and generalized pseudo-adjoint fluxes are introduced in the technique in order to use a similar algorithm for direct flux calculation. They propose the new formulation of

generalized perturbation theory using CP equation to estimate the changes in k_{eff} and homogenized cross-sections (COURAU and MARLEAU, 2003). The test cases of CANDU and PWR cells are carried out with numerical results for changes in k_{eff} and homogenized cross-sections as well as the sensitivity coefficients of various actinides. Recently Takeda introduces the generalized perturbation theory based on the integro-differential transport equations for the sensitivity analysis of U238 capture to Pu239 fission reaction rate ratio in LWR and fast reactors (TAKEDA et al., 2006). The forward flux, adjoint- and generalized adjoint transport solutions are carried out by the discrete ordinate method in TWOTRAN-II code. The splitting source method is applied to separate the positive and negative sources. The generalized adjoint transport equation is split into 2 equations corresponding to these sources that need to be solved separately. The generalized adjoint solutions are obtained by the iterative method of Neumann series without the rebalancing scheme.

Monte Carlo method can also be used for perturbation calculations. Hoffman applies a perturbative Monte Carlo method to estimate the k_{eff} change using the particle tracking technique in KENO code (HOFFMAN et al., 1978). Hoogenboom proposes a collision kernel sampling to determine direct and adjoint fluxes for k_{eff} calculation (HOOGENBOOM, 1981). Rief proposes a Monte Carlo perturbation theory to estimate the first and second order derivative terms used in perturbation theory (RIEF, 1984). The methods of collision kernel estimator and tracking length estimator are applied in his technique. Rief provides the review of Monte Carlo techniques in perturbation theory such as correlated tracking, derivative operator sampling and the neutron importance techniques (RIEF, 1986). Morillion proposes the multiple estimate and Taylor expansion methods for determination of high order derivative operators that are used in perturbation calculations (MORILLON, 1998). Favorite proposes an alternative Monte-Carlo based F-A (Forward-Adjoint)

method to implement the differential operator for estimating k_{eff} changes due to the very small sample perturbation (FAVORITE, 2002). Rearden proposes the Monte Carlo method to determine the direct and adjoint angular fluxes. By applying the spherical harmonic expansion method (P_N) to the recorded angular fluxes generated in a Monte Carlo algorithm, the angular elements are then determined (REARDEN, 2004). The sensitivity coefficients are formulated by using the same cross section data generated in Monte Carlo algorithm.

Literature Review on Perturbation Theory for Nuclide Field Problems

During normal reactor operation, the fuel composition is varying according to burnup level in reactor. The direct calculation of time-varying densities of fuel isotopes is complicated and time-consuming in fuel cycle optimization processes. Perturbation theory is often applied to reduce the calculation time. Since the perturbation theory is first developed by Usachev (USACHEV, 1964), Gandini extends Usachev work to the time-dependent generalized perturbation theory problems of estimating the time dependent nuclide concentration and sensitivity coefficients of nuclides (GANDINI et al., 1977). The extension of his work to higher-order terms in a generalized perturbative formulation is developed to take into account large flux variations (GANDINI, 1978). The third order perturbative formulation for linear functionals is demonstrated. The importance conservation principle approach for higher-order GPT is developed with the linear functional case (GANDINI, 1981).

Takeda demonstrates the application of GPT to the burnup sensitivity analysis in a fast breeder reactor (TAKEDA and UMANO, 1985). The sensitivity coefficients to nuclide cross-sections are derived using a variational method. Williams summarizes the time dependent perturbation theories with the coupling between transport equations and burnup depletion equations (WILLIAMS, 1986). Yang ap-

plies the GPT method to constant core power depletion calculations (YANG and DOWNAR, 1988). The extension of this work to the constrained equilibrium fuel cycle problem with shuffling and refueling is developed (YANG and DOWNAR, 1989). Maldonado considers the higher-order GPT to minimize the PWR fuel enrichment in fuel cycle optimization (MALDONADO et al., 1995). The adjoint flux solution from the time-dependent adjoint nodal diffusion equation is used in this higher-order GPT formulation. Gandini proposes the heuristically based GPT for analysis of accelerator driven subcritical reactors having external sources (GANDINI, 2001). The sensitivity formulation of actinides is developed. The direct flux and generalized adjoint flux solutions are obtained from the point kinetic models.

Literature Review on Boundary Perturbation Theory

The boundary perturbation theory is a technique used for estimation of the changes in reactor properties affected by the variations in boundary conditions (e.g. thickness of reflectors). Larsen and Pomraning first propose the perturbation formalism for calculation of first order change in k_{eff} due to a small perturbation in the boundary shape of reactive systems which are governed by diffusion and transport equations (LARSEN and POMRANING, 1981). Rahnema proposes the boundary perturbation theory to estimate the changes of arbitrary linear functionals in fixed source problem (RAHNEMA and POMRANING, 1983). They also extend the boundary perturbation theory to the ratio of linear functionals (RAHNEMA, 1989). A numerical example of spatial homogenization is given. They also develop the boundary perturbation theory to estimate the flux change affected by the perturbation in boundary conditions in the fixed source problem (RAHNEMA, 1994).

Structure of Thesis

In the Chapter 1 we present the neutron/adjoint transport problems and the recent developments in the perturbation theory. The development of the research work is presented in Chapter 2. In Chapter 3 we present the additional results of the CVR-BOC, CVR-EOC and k_{eff}-EOC adjustments in a CANDU lattice problem. In Chapter 4 we present the additional results of CBCVR-BOC and k_{eff}-EOC adjustments in a ACR lattice with Gadolinium in the central pin. Conclusion and recommendation for the future works are presented in the last chapter. In addition "ARTICLE I: Perturbation theory based on the method of cyclic characteristics" can be found in Appendix I (ASSAWAROONGRUENGCHOT and MARLEAU, 2007c). Next "ARTICLE II: Multigroup adjoint transport solution using the method of cyclic characteristics" is presented in Appendix II (ASSAWAROONGRUENGCHOT and MARLEAU, 2007b). Finally "ARTICLE III: Coolant void reactivity adjustments in advanced CANDU lattices using the adjoint sensitivity technique" can be found in Appendix III (ASSAWAROONGRUENGCHOT and MARLEAU, 2007a).

CHAPTER 1

BACKGROUND AND RECENT DEVELOPMENTS

1.1 Deterministic Neutron and Adjoint Transport Problems

1.1.1 Neutron Transport Problem

Generally the reactor system is represented either by diffusion or transport neutronic models. The diffusion model is mathematically equivalent to the first-order spherical harmonic expansion of the transport model (HENRY, 1975; BELL and GLASSTONE, 1979); therefore the reactor systems governed by transport models exhibit more accurate neutronic characteristics than diffusion models. In our research, we consider the multigroup discrete ordinate neutron transport equations in direction $\vec{\Omega}_l$ for a multiplicative k_{eff} problem with isotropic scattering as follows (LEWIS, 1993),

$$(A^g - \lambda B^g)\Phi^g(\vec{r}, \vec{\Omega}_l) = 0 \tag{1.1}$$

where

$$\begin{aligned} A^g\Phi^g(\vec{r}, \vec{\Omega}_l) &= \vec{\Omega}_l \cdot \vec{\nabla}\Phi^g(\vec{r}, \vec{\Omega}_l) + \Sigma^g(\vec{r})\Phi^g(\vec{r}, \vec{\Omega}_l) - \sum_{g'=1}^{G} \Sigma_s^{g \leftarrow g'}(\vec{r})\phi^{g'}(\vec{r}) \\ B^g\Phi^g(\vec{r}, \vec{\Omega}_l) &= \sum_{g'=1}^{G} \chi^g(\vec{r})\nu\Sigma_f^{g'}(\vec{r})\phi^{g'}(\vec{r}) \\ \phi^g(\vec{r}) &= \sum_{l=1}^{N^\Omega} W_l^\Omega \Phi^g(\vec{r}, \vec{\Omega}_l) \end{aligned} \tag{1.2}$$

Here, $\lambda = k_{eff}^{-1}$, and $\vec{\Omega}_l$ is the l-th discretized unit angular directional vector. $\Phi^g(\vec{r}, \vec{\Omega}_l)$ and $\phi^g(\vec{r})$ are the forward angular and scalar fluxes. $\Sigma^g(\vec{r})$ and $\Sigma_s^{g \leftarrow g'}(\vec{r})$ are the transport-corrected total and isotropic scattering cross sections respectively where the transport correction takes partially into account the linearly anisotropic contributions to the scattering cross sections (MACFARLANE, 1984). $\Sigma_f^g(\vec{r})$ is the fission cross sections, $\chi^g(\vec{r})$ is the fission production spectrum, and ν is the average number of neutrons generated per fission. Finally, W_l^Ω and N^Ω are respectively the weight and order of the angular quadrature defining the discrete ordinate problem.

The general boundary conditions used in neutron transport problems are of the form,

$$\Phi^{g,-}(\vec{r_s'}, \vec{\Omega}_l') = \alpha \cdot \Phi^{g,+}(\vec{r}_s, \vec{\Omega}_l) \tag{1.3}$$

where $(+)$ and $(-)$ indicate the outgoing and incoming directions, α is the albedo or the transmission coefficient at the domain boundary, and $\vec{r}_s$ and $\vec{r_s'}$ are points on the boundary.

For reflective boundary conditions, the variables in (1.3) become,

$$\begin{aligned} \vec{r_s'} &= \vec{r}_s \\ \vec{\Omega}_l' &= \vec{\Omega}_l - 2(\vec{n} \cdot \vec{\Omega}_l)\vec{n} \\ \vec{\Omega}_l' \cdot \vec{n} &< 0 \text{ and } \vec{\Omega}_l \cdot \vec{n} > 0 \end{aligned}$$

where $\vec{\Omega}_l$ and $\vec{\Omega}_l'$ are the unit directional vectors of the angular functions impinging on and reflected from the boundary at point $\vec{r}_s$, and $\vec{n}$ is the unit outward vector normal to boundary surface at $\vec{r}_s$.

When periodic boundary conditions are considered, the variables in (1.3) become,

$$\vec{r}_s' = \vec{\mathcal{P}}(\vec{r}_s \rightarrow \vec{r}_s', \vec{\Omega}_l) \cdot \vec{r}_s$$
$$\vec{\Omega}_l' = \vec{\Omega}_l$$

where $\vec{\mathcal{P}}(\vec{r}_s \rightarrow \vec{r}_s', \vec{\Omega}_l)$ is the periodicity or translation operator.

The neutron transport equations (1.1) can also be cast in an equivalent integral form written as,

$$(\mathcal{L}^g - \lambda \mathcal{F}^g)\Phi^g(\vec{r}, \vec{\Omega}_l) = 0 \tag{1.4}$$

where

$$\mathcal{L}^g \Phi^g(\vec{r}, \vec{\Omega}_l) = \Phi^g(\vec{r}, \vec{\Omega}_l) - \mathcal{T}_l^{g,-1} \sum_{g'=1}^{G} \Sigma_s^{g \leftarrow g'}(\vec{r}) \phi^{g'}(\vec{r})$$
$$\mathcal{F}^g \Phi^g(\vec{r}, \vec{\Omega}_l) = \mathcal{T}_l^{g,-1} \sum_{g'=1}^{G} \chi^g(\vec{r}) \nu \Sigma_f^{g'}(\vec{r}) \phi^{g'}(\vec{r})$$
$$\mathcal{T}_l^{g,-1}(\vec{r}) = \mathcal{T}^{g,-1}(\vec{r}, \vec{\Omega}_l) = (\vec{\Omega}_l \cdot \vec{\nabla} + \Sigma^g(\vec{r}))^{-1} \tag{1.5}$$

and $\mathcal{T}_l^{g,-1}$ is the inverse transport operator.

The solution methods for the transport equations (1.1) and (1.4) can be classified as:

- Analytical methods such as the spherical harmonic method, analytical discrete ordinate method, analytic P_N method, analytic DP_N method etc. (DAVISON, 1957; BELL and GLASSTONE, 1979; SANCHEZ and MCCORMICK, 1982; LEWIS, 1993).
- Integro-differential transport solution methods which are the numerical meth-

ods associated with the integro-differential form of transport equation. These methods are such as the finite difference discrete ordinate methods, S_N method, finite element method (SANCHEZ and MCCORMICK, 1982; LEWIS, 1993).

- Integral transport solution methods which are the numerical methods associated with the integral forms of transport equation. These methods are the interface current method, collision probability method, method of characteristics, transverse nodal method (SANCHEZ and MCCORMICK, 1982; LEWIS, 1993).

- Surface integral transport solution methods which are the numerical methods associated with the surface-integral forms of transport equation. These methods are the C_N and F_N methods (SANCHEZ and MCCORMICK, 1982).

In general, the analytical methods are not suited for problems having heterogeneous structures, while the numerical methods of integro-differential and integral types are applicable to such problems. Generally the integro-differential transport methods are appropriate for optically thick medium while the integral methods are appropriate for optically thin medium. In addition some integro-differential methods such as S_N method, may have problems of negative fluxes and ray effects or spatial oscillations in flux solutions.

1.1.2 Adjoint Transport Problem

One can associate with the integro-differential neutron transport equation (1.1) an adjoint transport equation using the following conservation relations (BELL and

GLASSTONE, 1979; LEWIS, 1993),

$$\left\langle \Phi^{*g}(\vec{r},\vec{\Omega}_l), (A^g - \lambda B^g)\Phi^g(\vec{r},\vec{\Omega}_l) \right\rangle = \left\langle \Phi^g(\vec{r},\vec{\Omega}_l), (A^{*g} - \lambda B^{*g})\Phi^{*g}(\vec{r},\vec{\Omega}_l) \right\rangle = 0 \tag{1.6}$$

where the inner product is defined,

$$\langle \Phi^{*g}(\vec{r},\vec{\Omega}_l), F^g(\vec{r},\vec{\Omega}_l)\Phi^g(\vec{r},\vec{\Omega}_l) \rangle = \sum_{g=1}^{G}\sum_{l=1}^{N^\Omega} W_l^\Omega \int_D d^3r \Phi^{*g}(\vec{r},\vec{\Omega}_l)F^g(\vec{r},\vec{\Omega}_l)\Phi^g(\vec{r},\vec{\Omega}_l) \tag{1.7}$$

and D is the spatial domain for the problem.

The adjoint transport equations derived from (1.6) take the form (BELL and GLASSTONE, 1979; LEWIS, 1993),

$$(A^{*g} - \lambda B^{*g})\Phi^{*g}(\vec{r},\vec{\Omega}_l) = 0 \tag{1.8}$$

where

$$A^{*g}\Phi^{*g}(\vec{r},\vec{\Omega}_l) = -\vec{\Omega}_l \cdot \vec{\nabla}\Phi^{*g}(\vec{r},\vec{\Omega}_l) + \Sigma^g(\vec{r})\Phi^{*g}(\vec{r},\vec{\Omega}_l) - \sum_{g'=1}^{G} \Sigma_s^{g'\leftarrow g}(\vec{r})\phi^{*g'}(\vec{r})$$

$$B^{*g}\Phi^{*g}(\vec{r},\vec{\Omega}_l) = \sum_{g'=1}^{G} \chi^{g'}(\vec{r})\nu\Sigma_f^g(\vec{r})\phi^{*g'}(\vec{r})$$

$$\phi^{*g}(\vec{r}) = \sum_{l=1}^{N^\Omega} W_l^\Omega \Phi^{*g}(\vec{r},\vec{\Omega}_l)$$

$\Phi^{*g}(\vec{r},\vec{\Omega}_l)$ and $\phi^{*g}(\vec{r})$ are the adjoint angular and adjoint scalar functions (or angular and scalar source importances (WILLIAMS, 1986)) respectively. One can see that the adjoint streaming operator has the negative sign from the forward streaming operator and the adjoint scattering matrix is the group-transposition of

the forward scattering matrix.

Similar to the neutron transport solution, the adjoint transport equations can be solved using analytical or numerical methods (WACHSPRESS, 1966; CARLSON and LATHROP, 1968; HENRY, 1975; DUDERSTADT and HAMILTON, 1976; LEWIS, 1993). In our research, we focus on the application of the method of cyclic characteristics (MOCC) with the cyclic tracking lines to solve 2D adjoint and generalized adjoint transport problems. The literature review on the method of characteristics and the adjoint transport solution methods are presented in the next sections.

1.1.3 Literature Review on the Method of Characteristics

The development of the method of characteristics (MOC) (particularly the step characteristics method or the MOC method with flat sources) for the neutron transport equation began in 1959 and was first applied by Vladimirov to simple geometries. Askew develops a MOC method to solve the neutron transport equation in the general 2D geometries (ASKEW, 1972). Halsall first applies MOC method to reactor core analysis (HALSALL, 1980). WIMS-CACTUS module is developed for solving the transport equation in complicated 2D geometries. The WIMS8-CACTUS characteristic solver is developed further for 3D problem (HUTTON, 2000). The 2D cyclic characteristics method is proposed to solve multigroup neutron transport problems in general geometries with reflective boundary conditions (ROY, 1998). The Korean 2D MOC solver (CRX code) based on isotropic tracking is developed for rectangular and hexagonal lattices (HONG and CHO, 1998). The reflective white boundary condition is treated in the problems. Roy extends the work on the method of cyclic characteristics to take into account anisotropic scattering problems (ROY, 1999). Spherical harmonic expansion method is used

for treating the anisotropic terms in the characteristics formulation. The numerical results for one group transport equation with fixed source are given. The MOC method in CHAR code is extended to solve 2D multigroup transport problems with linearly anisotropic scattering (POSTMA and VUJIC, 1999). Synthetic acceleration techniques developed for the 2D MOC method are based on diffusion-like cell balancing where flux correction factors are determined in order to satisfy cell neutron balance equation (SANCHEZ and CHETAINE, 2000). Angular flux equations within cell are derived using MOC method for estimating the current vectors at cell walls. The multigroup 3D MOC solver for general geometries is implemented in DRAGON (WU and ROY, 1999; WU and ROY, 2000). The self-collision rebalancing acceleration technique is introduced by using the self-collision probability to reduce the numbers of inner iterations. In addition the track merging technique is proposed to minimize the track density. The equivalence between collision probability and MOC methods is proven for finite 3D domain.

Another type of the MOC method, the short characteristics method with flat sources (i.e. the characteristics lines start and end within a spatial subdomain or cell containing multiple regions), is developed for 2D transport problems (MASIELLO and ZMIJAREVIC, 2006). The advantage is that the common tracking lines can be used for the cells having the same geometries. One also needs to homogenize the outgoing angular fluxes on the surfaces between the connected cells so that these angular surface fluxes can be applied in the cell interface conditions. In addition the linear characteristics method is a MOC method based on linearly interpolated sources within a region. The source inside a region is obtained from the interpolation between the artificial surface sources at both ends of a line segment. Recently the simplified linear characteristics method, is extended from the linear MOCC method in order to maintain the continuity of the source within a material that contains serveral connected regions (LE TELLIER and HÉBERT, 006a).

1.1.4 Literature Review on Deterministic Adjoint Transport Solution Methods

As a result of perturbation formulation, the adjoint and generalized adjoint equations have emerged from perturbation conditions. When the reactor system is governed by either neutron diffusion or transport equations, the perturbation formulation is associated with adjoint diffusion or adjoint transport equations respectively. Since the neutron transport models shall be used in this research, solving the associated adjoint transport equations is required to determine the desired solutions.

Deterministic adjoint transport solution methods are often developed closedly with the perturbation methods summarized in the previous chapter. An adjoint transport solution method is first proposed by Davison (DAVISON, 1957). He presents the derivation of integral solution of adjoint scalar fluxes from one group integro-differential transport equations. Carlson and Lathrop propose the S_N method for adjoint transport solution of k_{eff} problem with 6 group spherical geometry (CARLSON and LATHROP, 1968). Bell presents the P_1 solution method for adjoint transport equation and the equivalence to adjoint diffusion equation (BELL and GLASSTONE, 1979). Laurin-Kovitz develops the adjoint transport solution algorithm based on the variational nodal method in DIF3D code (LAURIN-KOVITZ and LEWIS, 1996b). Sjoden applies S_N discrete ordinate method using the PENTRAN code to solve adjoint transport equation for the detector responses (SJODEN, 2002). The study case is a 3D He-3 neutron detector model with 47 energy groups. Courau and Marleau introduce the method of collision probability (CP) to solve the multigroup adjoint and generalized adjoint transport equations in the PWR and CANDU lattice problems (COURAU and MARLEAU, 2002; COURAU and MARLEAU, 2003).

1.2 Recent Developments on Perturbation Theory based on Neutron Transport Equations

With the use of integro-differential transport equation (1.1), the classical first order approximation of perturbed eigenvalue $\Delta\lambda$ is in the form (BELL and GLASSTONE, 1979; ROZON, 1998),

$$\Delta\lambda = \frac{\langle \Phi^{*g}, (\Delta A^g - \lambda \Delta B^g)\Phi^g \rangle}{\langle \Phi^{*g}, B^g \Phi^g \rangle} \tag{1.9}$$

where the variations in first order forward fluxes are eliminated using the adjoint functions. Here ΔA^g and ΔB^g are the perturbations on the transport and fission operators defined in Eq. (1.1) (see also Eq. (I.61)).

To consider the generalized perturbation theory of linear reaction rate ratio, we first define the performance functional,

$$R_1 = \frac{\langle \Sigma^g_\kappa, \Phi^g \rangle}{\langle \Sigma^g_\zeta, \Phi^g \rangle} \tag{1.10}$$

where Σ^g_κ and Σ^g_ζ are nuclear cross sections.

The first order approximation for ΔR_1 using the GPT method can then be obtained (COURAU, 2001; COURAU and MARLEAU, 2003),

$$\Delta R_1 = \frac{(\langle \Delta\Sigma^g_\kappa, \Phi^g \rangle - R_1 \langle \Delta\Sigma^g_\zeta, \Phi^g \rangle)}{\langle \Sigma^g_\zeta, \Phi^g \rangle} + \langle \Gamma^{*g}_\beta, -(\Delta A^g - \lambda \Delta B^g)\Phi^g \rangle \tag{1.11}$$

where $\Delta\Sigma^g_\kappa$ and $\Delta\Sigma^g_\zeta$ are the perturbations in Σ^g_κ and Σ^g_ζ respectively and,

$$\begin{aligned} \langle \Gamma^{*g}, (A^g - \lambda B^g)\Delta\Phi^g \rangle &= \langle \Gamma^{*g}, -(\Delta A^g - \lambda \Delta B^g - \Delta\lambda B^g)\Phi^g \rangle \\ &= \langle \Gamma^{*g}_\beta, -(\Delta A^g - \lambda \Delta B^g)\Phi^g \rangle \end{aligned} \tag{1.12}$$

Here we have used the transport equation for the generalized adjoint angular function $\Gamma^{*g}(\vec{r},\vec{\Omega}_l)$,

$$(A^{*g} - \lambda B^{*g})\Gamma^{*g}(\vec{r},\vec{\Omega}_l) = S^{*g} \tag{1.13}$$

to eliminate the effect of first order flux variations (COURAU, 2001; COURAU and MARLEAU, 2003). S^{*g} is the external generalized adjoint source defined as,

$$S^{*g} = \frac{(\Sigma^g_\kappa - R_1\Sigma^g_\zeta)}{\langle \Sigma^g_\zeta, \Phi^g \rangle} \tag{1.14}$$

We also imposed the condition,

$$\langle \Gamma^{*g}_\beta, B^g\Phi^g \rangle = 0 \tag{1.15}$$

to eliminate the term $\Delta\lambda B^g\Phi^g$ in Eq. (1.12).

The general solutions $\Gamma^{*g}_\beta(\vec{r},\vec{\Omega}_l)$ of the inhomogeneous transport equation (1.13) are of the form

$$\Gamma^{*g}_\beta = \Gamma^{*g} + \beta\Phi^{*g} \tag{1.16}$$

Here we select β as

$$\beta = -\frac{\langle \Gamma^{*g}, B^g\Phi^g \rangle}{\langle \Phi^{*g}, B^g\Phi^g \rangle} \tag{1.17}$$

in order to satisfy Eq. (1.15).

Recent work on the variational method based on the integro-differential transport equations is applied to functional of reactivity worth and it requires to solve the resulting generalized forward transport equation (TAKEDA et al., 2006). In fact the

variation in reactivity worth can be obtained indirectly from $-\Delta\lambda$ using the perturbation theory and thus the generalized forward transport solution can be avoided (MARLEAU, 2004a). In addition, to avoid the negative generalized adjoint sources, the splitting source method is introduced by solving the two generalized forward transport equations associated with the positive and negative source components. The generalized adjoint transport solution is based on the method of Neumann series (TAKEDA et al., 2006).

1.3 Sensitivity Coefficient

The sensitivity coefficient of the functional R with respect to a reactor parameter α_q is defined as the relative change in R due to a relative change in α_q as follows,

$$S_R^q = \frac{\alpha_q}{R}\frac{\partial R}{\partial \alpha_q} \tag{1.18}$$

where α_q is the q-th parameter of a reactor core.

For the case where R_1 is given by equation (1.10), the sensitivity coefficient of R_1 with respect to α_q based on the integral transport equations is,

$$\begin{aligned} S_{R_1}^q &= \frac{\alpha_q}{R_1}\left[\frac{(\langle\frac{\partial\Sigma_\kappa^g}{\partial\alpha_q},\Phi^g\rangle - R_1\langle\frac{\partial\Sigma_\zeta^g}{\partial\alpha_q},\Phi^g\rangle)}{\langle\Sigma_\zeta^g,\Phi^g\rangle} + \langle\Gamma_\beta^{*g},-(\frac{\partial A^g}{\partial\alpha_q}-\lambda\frac{\partial B^g}{\partial\alpha_q})\Phi^g\rangle\right] \\ &= \frac{\alpha_q}{R_1\Delta\alpha_q}\left[\frac{(\langle\Delta\Sigma_\kappa^g,\Phi^g\rangle - R_1\langle\Delta\Sigma_\zeta^g,\Phi^g\rangle)}{\langle\Sigma_\zeta^g,\Phi^g\rangle} + \langle\Gamma_\beta^{*g},-(\Delta A^g-\lambda\Delta B^g)\Phi^g\rangle\right] \end{aligned} \tag{1.19}$$

The sensitivity coefficient of eigenvalue with respect to α_q using (1.9) is,

$$S_\lambda^q = \sum_{g=1}^{G} S_\lambda^{q,g} = \frac{\alpha_q}{\lambda\Delta\alpha_q}\frac{\langle\phi^{*g},(\Delta A^g-\lambda\Delta B^g)\Phi^g\rangle}{\langle\phi^{*g},B^g\Phi^g\rangle} \tag{1.20}$$

where $S_{\lambda}^{q,g}$ are the group-based sensitivity coefficients of eigenvalue to α_q.

CHAPTER 2

DEVELOPMENT IN RESEARCH

2.1 Research Objectives

We first develop the MOCC algorithm for the adjoint and generalized adjoint transport solutions that are used in the perturbative estimates and sensitivity calculations (see the appendix: ARTICLE I and II). The MOCC method is applied to compute the non-leakage probabilities that are used in the rebalance technique for speeding up the direct and adjoint solutions (i.e., when albedo factors of the boundary are less than unity). In addition, for speeding up the solutions, we introduce the group-splitting technique and the combined forward flux/adjoint function iteration scheme that relies on the common use of a large number of exponential variables and tracking line data. We also extract the MOCC response matrix using the MOCC method and the common use of exponential variables similar to the combined forward/adjoint scheme. The computing time of forward fluxes and adjoint functions using the MOCC response matrix method is found to be lower than the time required by the MOCC method. We show that the MOCC response matrix is mathematically equivalent to the collision probability matrix, and the adjoint and generalized adjoint functions by the MOCC method are equivalent to those by the CP method. Three types of biasing and decontamination schemes are introduced for the generalized adjoint transport solutions.

Secondly we develop the perturbation theory based on the integral transport equations to compute the perturbative estimates and sensitivity coefficients of eigenvalues and linear reaction rate ratios (see the appendix: ARTICLE I). The isotropic

(IA) and linearization (LA) approximations based on the MOCC method are introduced to evaluate the perturbed integral transport functionals. The results obtained using the LA method are more accurate than those computed using the perturbation theory based on the integro-differential transport equations for the problems with the anisotropic fluxes.

Finally we apply the optimization and adjoint sensitivity techniques to CVR-BOC, CBCVR-BOC and k_{eff}-EOC adjustments in the ACR lattices (see the appendix: ARTICLE III). We use the perturbation theory to compute the sensitivity coefficients at BOC. To approximate the sensitivity coefficients at EOC, we perform constant-power burnup/depletion calculations using a slightly perturbed nuclear library and the unperturbed neutron fluxes to estimate the variation of nuclide densities at EOC. The resulting perturbed nuclide densities are used in computing the perturbative estimates and coefficients at EOC. In our study we consider the adjustments of CVR-BOC, CBCVR-BOC and k_{eff}-EOC by searching the Dy density in the central pin and U235 enrichment in the central pin or outer rings. Our goal is to obtain a desired target CVR-BOC, CBCVR-BOC of -2 mk and k_{eff}-EOC of 0.900. We also consider a case with Gd in the central pin in order to study the effective use of Dy and Gd in the CBCVR adjustments (see Chapter 4).

In addition we apply the similar techniques to the CANDU lattice with the burnup period extended from 300 to 450 FPDs (see Chapter 3). The goal is to obtain the target CVR-BOC, CVR-EOC and k_{eff}-EOC, of 10 mk, 8 mk and 0.900 respectively, by searching for the optimal Dy, Gd densities and U235 enrichment. The sensitivity analyses of CVR, CBCVR and eigenvalues at BOC and EOC are included in our study.

2.2 Summary of Perturbation Theory based on Integral Neutron Transport Equation

From the past development the perturbation theory is applied to the neutronic system represented by the diffusion equation (DAVISON, 1957; LEWINS, 1966; STACEY, 1972; WILLIAMS, 1986). A few applications to integro-differential neutron transport system can be found such as the perturbation theory based on the variational nodal transport method and the discrete ordinate method (CARLSON and LATHROP, 1968; LAURIN-KOVITZ and LEWIS, 1996a; SJODEN, 2002; TAKEDA et al., 2006). A perturbation theory is also applied to the system represented by the collision probability equations (COURAU and MARLEAU, 2002; COURAU and MARLEAU, 2003).

In ARTICLE I we propose the perturbation theory based on the integral neutron transport equations to estimate the changes in eigenvalue and functional of linear reaction rate ratio affected by small parameter variations. As mentioned earlier, the proposed method provides more accurate perturbative estimates and sensitivity coefficients than the method based on the integro-differential transport equation for problems with anisotropic fluxes such as those found in the CANDU and ACR lattices (e.g., the high fast angular fluxes in the fuel regions have a direction toward the moderator while the thermal angular fluxes are high in the moderator regions and have the directions toward the central regions). The integral transport equation is used in the perturbative formulation because it represents the interconnecting neutronic systems of the lattice assemblies via tracking lines. On the other hand, the integro-differential transport equation represents the neutron balance inside an infinitesimal volume. The resulting classical first order perturbative estimate (BELL and GLASSTONE, 1979; ROZON, 1998) of eigenvalue with the use of

integral neutron transport equation is obtained,

$$\Delta\lambda = \frac{\langle \phi^{\dagger g}, (\Delta\mathcal{L}^g - \lambda\Delta\mathcal{F}^g)\Phi^g \rangle}{\langle \phi^{\dagger g}, \mathcal{F}^g\Phi^g \rangle} \tag{2.1}$$

By using the following conservation relations,

$$\langle \Phi^{\dagger g}(\vec{r},\vec{\Omega}_l), (\mathcal{L}^g - \lambda\mathcal{F}^g)\Phi^g(\vec{r},\vec{\Omega}_l) \rangle = \langle \Phi^g(\vec{r},\vec{\Omega}_l), (\mathcal{L}^{\dagger g} - \lambda\mathcal{F}^{\dagger g})\Phi^{\dagger g}(\vec{r},\vec{\Omega}_l) \rangle$$

with the integral transport equations (1.4), one obtains the flux importance transport equations in the form,

$$(\mathcal{L}^{\dagger g} - \lambda\mathcal{F}^{\dagger g})\Phi^{\dagger g}(\vec{r},\vec{\Omega}_l) = 0 \tag{2.2}$$

where

$$\mathcal{L}^{\dagger g}\Phi^{\dagger g}(\vec{r},\vec{\Omega}_l) = \Phi^{\dagger g}(\vec{r},\vec{\Omega}_l) - \sum_{g'=1}^{G} \Sigma_s^{g'\leftarrow g}(\vec{r}) \sum_{l'=1}^{N^\Omega} W_{l'}^\Omega \mathcal{T}_{l'}^{*g',-1} \Phi^{\dagger g'}(\vec{r},\vec{\Omega}_{l'}) \tag{2.3}$$

$$\mathcal{F}^{\dagger g}\Phi^{\dagger g}(\vec{r},\vec{\Omega}_l) = \sum_{g'=1}^{G} \chi^{g'}(\vec{r})\nu\Sigma_f^g(\vec{r}) \sum_{l'=1}^{N^\Omega} W_{l'}^\Omega \mathcal{T}_{l'}^{*g',-1} \Phi^{\dagger g'}(\vec{r},\vec{\Omega}_{l'}) \tag{2.4}$$

$$\begin{aligned} \mathcal{T}_l^{*g,-1} &= \mathcal{T}^{*g,-1}(\vec{r},\vec{\Omega}_l) = ((\vec{\Omega}_l\cdot\vec{\nabla} + \Sigma^g(\vec{r}))^*)^{-1} \\ &= (-\vec{\Omega}_l\cdot\vec{\nabla} + \Sigma^g(\vec{r}))^{-1} \end{aligned} \tag{2.5}$$

$$\phi^{\dagger g}(\vec{r}) = \sum_{l=1}^{N^\Omega} W_l^\Omega \Phi^{\dagger g}(\vec{r},\vec{\Omega}_l) \tag{2.6}$$

with $\Phi^{\dagger g}(\vec{r},\vec{\Omega}_l)$ and $\phi^{\dagger g}(\vec{r})$ the angular and scalar flux importance functions respectively. Note that the flux importance function is the adjoint function of the integral neutron transport equation while the source importance function (or typical adjoint function or adjoint flux) is the adjoint function of the integro-differential transport equation (WILLIAMS, 1986).

The flux importance equation (2.2) can be written in the explicit integral form,

$$\Phi^{\dagger g}(\vec{r},\vec{\Omega}_l) = \sum_{g'=1}^{G}\left[\Sigma_s^{g'\leftarrow g}(\vec{r}) + \lambda\chi^{g'}(\vec{r})\nu\Sigma_f^g(\vec{r})\right] \sum_{l'=1}^{N^\Omega} W_{l'}^\Omega \int_0^\infty dS e^{-\tau^{g'}(\vec{r}+S\vec{\Omega}_{l'},\vec{r})}\Phi^{\dagger g'}(\vec{r}+S\vec{\Omega}_{l'},\vec{\Omega}_{l'}) \tag{2.7}$$

Note that, on the first term on the RHS of equation (2.3), $\Phi^{\dagger g}(\vec{r},\vec{\Omega}_l)$ is isotropic because the sources of the forward transport equation are isotropic.

The adjoint angular function is related to the angular flux importance (WILLIAMS, 1986) by,

$$\Phi^{*g}(\vec{r},\vec{\Omega}_l) = \mathcal{T}_l^{*g,-1}\Phi^{\dagger g}(\vec{r},\vec{\Omega}_l) \tag{2.8}$$

Operating on both sides of (2.2) with $\mathcal{T}_l^{*g,-1}$ and using (2.8), one can transform the flux importance transport equation (2.2) into the integro-differential adjoint transport equation (1.8).

To determine the scalar flux importances using the adjoint scalar functions, we apply (2.8) to (2.2) and integrate the resulting equations over the angular domain using the angular quadrature technique as follows,

$$\phi^{\dagger g}(\vec{r}) = \sum_{g'=1}^{G}[\Sigma_s^{g'\leftarrow g}(\vec{r}) + \lambda\chi^{g'}(\vec{r})\nu\Sigma_f^g(\vec{r})]\phi^{*g'}(\vec{r}) \tag{2.9}$$

The scalar flux importance function (2.9) is equivalent to the total adjoint source (adjoint fission plus scattering sources) of the integro-differential adjoint transport problem with isotropic scattering. The main differences between eigenvalue estimates using the integro-differential and integral transport equations are:

- for the integral transport perturbation problem represented by equation (2.1), the first order forward flux variations are eliminated by the scalar flux importance functions instead of the angular adjoint functions that are used in the integro-differential transport problem;

- the perturbed integral transport operators $(\Delta\mathcal{L}^g - \lambda\Delta\mathcal{F}^g)\Phi^g$ depend on the first order variations in the cross-sections and inverse transport operator (i.e., $\Delta(\mathcal{T}^{g,-1})$) where the latter takes into account the changes in neutron transfer characteristics between the discretized regions via the tracking lines. On the other hand, the perturbed integro-differential transport operators $(\Delta A^g - \lambda\Delta B^g)\Phi^g$ depend only on the first order variations in cross-sections.

The integration of $\mathcal{T}^{g,-1}$ over the angular domain and regional volume is equivalent to the MOCC response matrix. Accordingly we can write $\Delta\mathcal{T}^{g,-1}$ as,

$$\Delta\mathcal{T}^{g,-1} \rightarrow [\Delta P_{VV}] = [P_{VV}(\Sigma + \Delta\Sigma)] - [P_{VV}(\Sigma)] \tag{2.10}$$

where the neutron fluxes and cross-sections are assumed constant within each region and $[P_{VV}]$ is the MOCC response matrix.

From the concept of neutron importance or adjoint function (HENRY, 1975), we extend this concept to the integral form of neutron importance written as follows,

$$\Phi^{*g}(\vec{r},\vec{\Omega}_l) = \int_0^\infty dS e^{-\tau^g(\vec{r}+S\vec{\Omega}_l,\vec{r})} \sum_{g'=1}^{G} \left[\Sigma_s^{g'\leftarrow g}(\vec{r}+S\vec{\Omega}_l) + \lambda\chi^{g'}\nu\Sigma_f^g(\vec{r}+S\vec{\Omega}_l)\right] \sum_{l'=1}^{N^\Omega} W_{l'}^\Omega \Phi^{*g'}(\vec{r}+S\vec{\Omega}_l,\vec{\Omega}_{l'}) \tag{2.11}$$

Neutron importance of a unit flux introduced at point $\vec{r}$ and direction $\vec{\Omega}_l$ is conserved and equal to the line integration of all the secondary neutron importance

of neutrons generated by scattering and fission reactions at point $\vec{r} + S\vec{\Omega}_l$ (corresponding to the total collision by a neutron that originates at $\vec{r}$ and $\vec{\Omega}_l$, escapes and reaches at $\vec{r} + S\vec{\Omega}_l$). This line integration of total neutron importance is performed over S for $S \in [0, \infty]$ on the tracking line in direction $\vec{\Omega}_l$.

From the relationship between neutron importance and flux importance function in (2.8), we can write this relationship in the integral form as follows,

$$\Phi^{*g}(\vec{r}, \vec{\Omega}_l) = \int_0^\infty dS e^{-\tau^g(\vec{r}+S\vec{\Omega}_l, \vec{r})} \Phi^{\dagger g}(\vec{r} + S\vec{\Omega}_l, \vec{\Omega}_l) \tag{2.12}$$

The neutron importance of a unit flux at point $\vec{r}$ and direction $\vec{\Omega}_l$ is equal to the line integration of angular flux importance function of a neutron that originates at $\vec{r}$ and $\vec{\Omega}_l$, escapes and undergoes total collision at $\vec{r} + S\vec{\Omega}_l$ where all its secondary neutrons are generated.

The flux importance of a unit flux at $\vec{r}$ and $\vec{\Omega}_l$ written as,

$$\Phi^{\dagger g}(\vec{r}, \vec{\Omega}_l) = \sum_{g'=1}^{G} \left[\Sigma_s^{g' \leftarrow g}(\vec{r}) + \lambda \chi^{g'} \nu \Sigma_f^g(\vec{r}) \right] \sum_{l'=1}^{N^\Omega} W_{l'}^\Omega \Phi^{*g'}(\vec{r}, \vec{\Omega}_{l'}) \tag{2.13}$$

is equal to the sum of all secondary neutron importance of the secondary neutrons generated by scattering and fission reactions into all direction $\vec{\Omega}_{l'}$ and group g'. These secondary neutrons emerge from the scatter and fission reactions after a total collision reaction by a unit neutron flux introduced at $\vec{r}$ and $\vec{\Omega}_l$.

Next we extend the perturbation theory to the generalized perturbation theory (GPT) based on the integral transport equation where a functional of linear reaction rate ratio is defined,

$$R_1 = \frac{\langle \Sigma_\kappa^g, \Phi^g \rangle}{\langle \Sigma_\zeta^g, \Phi^g \rangle} \tag{2.14}$$

where Σ_κ^g and Σ_ζ^g are nuclear cross sections.

The resulting first order GPT estimate of the linear reaction rate ratio that uses the integral transport equation is,

$$\Delta R_1 = \frac{(\langle \Delta\Sigma_\kappa^g, \Phi^g\rangle - R_1\langle \Delta\Sigma_\zeta^g, \Phi^g\rangle)}{\langle \Sigma_\zeta^g, \Phi^g\rangle} + \langle \Gamma_\beta^{\dagger g}, -(\Delta\mathcal{L}^g - \lambda\Delta\mathcal{F}^g)\Phi^g\rangle \tag{2.15}$$

where we use the generalized flux importance transport equations to eliminate the first order flux variations (see Eq. I.43),

$$(\mathcal{L}^{\dagger g} - \lambda\mathcal{F}^{\dagger g})\Gamma^{\dagger g}(\vec{r}, \vec{\Omega}_l) = S^{\dagger g}(\vec{r}) \tag{2.16}$$

with $S^{\dagger g}$ is the external generalized adjoint source:

$$S^{\dagger g} = \frac{(\Sigma_\kappa^g - R_1\Sigma_\zeta^g)}{\langle \Sigma_\zeta^g, \Phi^g\rangle}$$

and the generalized angular flux importance function $\Gamma^{\dagger g}(\vec{r}, \vec{\Omega}_l)$ is isotropic for the problem with isotropic scattering. The differences between the GPT estimates using the integro-differential and integral transport equations are similar to that for the eigenvalue estimates as discussed previously.

The general solutions $\Gamma_\beta^{\dagger g}(\vec{r}, \vec{\Omega}_l)$ of the inhomogeneous transport equation (2.16) are of the form

$$\Gamma_\beta^{\dagger g} = \Gamma^{\dagger g} + \beta\Phi^{\dagger g} \tag{2.17}$$

Here we select β as

$$\beta = -\frac{\langle \Gamma^{\dagger g}, \mathcal{F}^g\Phi^g\rangle}{\langle \Phi^{\dagger g}, \mathcal{F}^g\Phi^g\rangle} \tag{2.18}$$

in order to satisfy $\langle \Gamma_\beta^{\dagger g}, \mathcal{F}^g \Phi^g \rangle = 0$.

Similar to the mathematical relationship between flux importance and source importance functions (2.8), the relationship between the generalized adjoint function and the generalized flux importance is defined,

$$\Gamma^{*g}(\vec{r}, \vec{\Omega}_l) = \mathcal{T}_l^{*g,-1} \Gamma^{\dagger g}(\vec{r}, \vec{\Omega}_l) \tag{2.19}$$

Operating on both sides of (2.16) with $\mathcal{T}_l^{*g,-1}$ and using (2.19), we can arrange the resulting equations into the integro-differential generalized adjoint transport equation,

$$(A^{*g} - \lambda B^{*g}) \Gamma^{*g}(\vec{r}, \vec{\Omega}_l) = S^{*g} \tag{2.20}$$

where $S^{*g} = S^{\dagger g}$, $\Gamma^{*g}(\vec{r}, \vec{\Omega}_l)$ and $\Gamma^{*g}(\vec{r})$ are the generalized angular and scalar source importance functions respectively.

We can indirectly compute the generalized flux importances $\Gamma_\beta^{\dagger g}(\vec{r})$ from the generalized adjoints $\Gamma_\beta^{*g}(\vec{r})$ by applying (2.17), (2.18) and (2.19) to (2.16), and integrating the resulting equations over the angular domain,

$$\Gamma_\beta^{\dagger g}(\vec{r}) = \sum_{g'=1}^{G} [\Sigma_s^{g' \leftarrow g}(\vec{r}) + \lambda \chi^{g'}(\vec{r}) \nu \Sigma_f^g(\vec{r})] \Gamma_\beta^{*g'}(\vec{r}) + S^{\dagger g} \tag{2.21}$$

One can find that the generalized scalar flux importance is equivalent to the total generalized adjoint source (generalized adjoint fission, scattering and external generalized adjoint sources) of the integro-differential generalized adjoint transport problem with isotropic scattering.

When the integral form is used, one needs to compute the perturbed integral transport functionals $\left\langle Y^{\dagger g}, (\Delta \mathcal{L}^g - \lambda \Delta \mathcal{F}^g) \Phi^g \right\rangle$ where $Y^{\dagger g}$ is either $\Phi^{\dagger g}$ or $\Gamma_\beta^{\dagger g}$. Two meth-

ods are applied to approximate these functionals: the isotropic approximation (IA) and linearization approximation (LA) methods. The IA method is performed by assuming that the angular term $\Delta\Sigma^g\Phi^g$ on RHS of the following modified transport equation is isotropic,

$$\vec{\Omega}_l \cdot \vec{\nabla}\Phi^g(\vec{r},\vec{\Omega}_l) + \Sigma^g\Phi^g(\vec{r},\vec{\Omega}_l) + \Delta\Sigma^g\Phi^g(\vec{r},\vec{\Omega}_l) = \sum_{g'=1}^{G}[\Sigma_s^{g\leftarrow g'} + \lambda\chi^g\nu\Sigma_f^{g'}]\phi^{g'}(\vec{r}) + \Delta\Sigma^g\Phi^g(\vec{r},\vec{\Omega}_l) \quad (2.22)$$

The resulting perturbative estimate is equivalent to the estimate based on the integro-differential transport equations. For the LA method, the angular term in the modified transport equation is assumed anisotropic. We indirectly approximate the perturbed integral transport functional by linearizing the term $[P_{VV}(\Sigma + \Delta\Sigma)][Q]$ with respect to the total cross section in each mixture and energy group. The linearization factors of the m-th mixture are defined as follows,

$$\hat{\Xi}_{m,j}^g = -\frac{1}{d\Sigma_m^g}\sum_{i=1}^{N_J}(p_{j\rightarrow i}^g(\Sigma^g + d\Sigma_m^g) - p_{j\rightarrow i}^g(\Sigma^g))q_i^g \quad (2.23)$$

where we use $d\Sigma_m^g = 10^{-4}\Sigma_m^g$. The resulting perturbative estimate using LA method is equivalent to the perturbative estimate based on the CP equations (COURAU and MARLEAU, 2002). The advantage of the MOCC method is that it requires lower computing time than the CP method (one cycle of spatial iteration over tracking lines and total regional neutron sources with the use of perturbed total cross section $(\Sigma+\Delta\Sigma)$ for each mixture and group) to evaluate the linearization factors. On the other hand, the linearization using the CP method (COURAU and MARLEAU, 2002) is time-consuming because one needs to evaluate the perturbed CP matrices $[P_{VV}(\Sigma + \Delta\Sigma)]$ for each mixture and group. For a CANDU lattice with 69 group nuclear library and the use of cyclic tracking lines, the CP computing

time for linearization is approximately $N_{mix} \times 85$ min. (where N_{mix} is total number of mixtures) while the MOCC computing time is approximately $N_{mix} \times 1.1$ min. The testing computer is a PENTIUM 4-3.2GHz CPU with 1 GB RAM on an Intel D865GLC motherboard.

2.2.1 Sensitivity Coefficients

For the case where R_1 is given by equation (2.14), using (1.18) and (2.15) the sensitivity coefficient of R_1 with respect to α_q based on the integral transport equations is,

$$S^q_{R_1} = \frac{\alpha_q}{R_1}\left[\frac{(\langle\frac{\partial\Sigma^g_\kappa}{\partial\alpha_q},\Phi^g\rangle - R_1\langle\frac{\partial\Sigma^g_\zeta}{\partial\alpha_q},\Phi^g\rangle)}{\langle\Sigma^g_\zeta,\Phi^g\rangle} + \langle\Gamma^{\dagger g}_\beta, -(\frac{\partial\mathcal{L}^g}{\partial\alpha_q} - \lambda\frac{\partial\mathcal{F}^g}{\partial\alpha_q})\Phi^g\rangle\right]$$
$$= \frac{\alpha_q}{R_1\Delta\alpha_q}\left[\frac{(\langle\Delta\Sigma^g_\kappa,\Phi^g\rangle - R_1\langle\Delta\Sigma^g_\zeta,\Phi^g\rangle)}{\langle\Sigma^g_\zeta,\Phi^g\rangle} + \langle\Gamma^{\dagger g}_\beta, -(\Delta\mathcal{L}^g - \lambda\Delta\mathcal{F}^g)\Phi^g\rangle\right] \quad (2.24)$$

and the sensitivity coefficient of eigenvalue to α_q using (2.1) becomes,

$$S^q_\lambda = \sum_{g=1}^{G} S^{q,g}_\lambda = \frac{\alpha_q}{\lambda\Delta\alpha_q}\frac{\langle\phi^{\dagger g},(\Delta\mathcal{L}^g - \lambda\Delta\mathcal{F}^g)\Phi^g\rangle}{\langle\phi^{\dagger g},\mathcal{F}^g\Phi^g\rangle} \quad (2.25)$$

where $S^{q,g}_\lambda$ are the group-based sensitivity coefficients of eigenvalue to α_q. For the parameters of which the macroscopic cross sections are not the linear function, such as fuel temperature (T_f), we will use the first order finite difference method to approximate the derivative terms (e.g., $\partial\Sigma/\partial T_f \approx \Delta\Sigma/\Delta T_f$) in sensitivity evaluation.

2.2.2 Conclusions on Perturbation Theory

The advantage of using the integral transport equation is that the GPT estimates take into account the variations in the cross sections and the neutron transfer characteristics between each region. For problems with isotropic sources, these estimates depend on the generalized scalar flux importances while GPT estimates based on the integro-differential transport equation still depend on the generalized angular source importance functions.

The relationship between generalized adjoint function and generalized flux importance is defined in order to transform the generalized flux importance integral transport equations into the integro-differential form. The generalized adjoint scalar functions are related to the generalized flux importances by the linear transformation using CP matrix, i.e., $[\Gamma^*] = [P_{VV}][\Gamma^\dagger]$. Our numerical results show that the MOCC generalized adjoint functions are similar to the CP generalized source importances.

In order to evaluate the perturbed integral transport functionals in the GPT estimates, the isotropic approximation (IA) and linear approximation (LA) methods are applied to approximate the term $\Delta(\mathcal{T}_l^{g,-1})$. Using the IA method, the first order GPT estimate based on the integral transport equation is found equivalent to the GPT estimate based on the integro-differential transport equation where the adjoint angular functions are assumed isotropic as reported in the GPT based on the CP equation (COURAU and MARLEAU, 2003). The GPT estimates of the homogenized cross-sections due to the perturbations in the fuel, clad and coolant temperature result in the absolute relative error as low as 2.3×10^{-4} for the perturbations in temperature of 10% or less. The GPT estimate using IA method is comparable to the estimate using the LA method because in the PWR lattice the angular neutron fluxes are relatively isotropic due to the fuel rods that are uniformly

distributed over the assembly. The high-order angular terms in $(\Delta\Sigma^g\Phi^g)$ then produce low effect in the GPT estimation using the LA method. For the CANDU case, the angular neutron fluxes are generally more anisotropic and the LA method then results in more accurate GPT estimates for perturbations in temperature from 0 to 10%. For the sensitivity evaluation, the same behaviors are observed, provided that the linearization factors are evaluated using small perturbed cross-sections $(d\Sigma_m^g = 1.0^{-4}\Sigma^g)$.

2.3 Summary of Adjoint and Generalized Adjoint Transport Solutions using MOCC Method

In ARTICLE I and II, we have developed the adjoint and generalized adjoint transport solution algorithms based on the MOCC method. The main advantages of the MOCC method are: it requires lower computational time and memory space than the collision probability method (CP); it does not require the boundary surface currents as for the method of characteristics (MOC) with the isotropic tracking. The exact geometries can be treated directly in the algorithm. The MOCC method performs only one cycle of scanning over the cyclic tracking lines in each spatial iteration loop. Thus the spatial iteration time is lower in the MOCC method than in the MOC method when the same tracking lines are used. In the MOCC method the adjoint characteristics equations associated with a cyclic tracking line are formulated in such a way that we can derive a closed form for the adjoint angular function on an infinite line based on the solution for a finite number of line segments.

The boundary conditions associated with the adjoint transport problems that arise

from the derivation of adjoint transport equations are,

$$\Phi^{*g,+}(\vec{r}_s, \vec{\Omega}_l) = \alpha \cdot \Phi^{*g,-}(\vec{r_s'}, \vec{\Omega}_l') \tag{2.26}$$

Since $\mathcal{T}^{*g,-1}(\vec{r}, \vec{\Omega}_l) = \mathcal{T}^{g,-1}(\vec{r}, -\vec{\Omega}_l)$ in Eq. (2.5), the integrations of $\mathcal{T}_l^{*g,-1}$ over the angular domain and regional volume then result in the same MOCC response matrix,

$$p_{j\to i}^{*g} = \frac{1}{V_j}\int_{V_j} d^3r \sum_{l=1}^{N^\Omega} W_l^\Omega \mathcal{T}^{*g,-1}(\vec{r}, \vec{\Omega}_l)\delta_i(\vec{r}) = p_{j\to i}^{g} \tag{2.27}$$

where we assume that the angular quadrature is selected in such a way that $W_l^{-\Omega} = W_l^\Omega$. From the equivalence between $\mathcal{T}^{*g,-1}(\vec{r}, \vec{\Omega}_l)$ and $\mathcal{T}^{g,-1}(\vec{r}, -\vec{\Omega}_l)$, one notes that the $\vec{\Omega}_l$-directed adjoint transport equation must be solved in the opposite angular direction from the $\vec{\Omega}_l$-directed forward transport equation (i.e., the inverse adjoint transport operator is the same as the inverse transport operator for the $-\vec{\Omega}_l$ directed transport equation).

In order to start the MOCC procedure for the adjoint transport solution, we first derive the adjoint characteristics equation of the segment L_k in the direction $\vec{\Omega}_l$ using the integro-differential adjoint transport equation (1.8) as follows,

$$\Phi^{*g}(\vec{p}_k, \vec{\Omega}_l) = \Phi^{*g}(\vec{p}_{k+1}, \vec{\Omega}_l)e^{-\frac{\Sigma_k^g \gamma_k}{\sin(\theta)}} + \frac{q_k^{*g}}{\Sigma_k^g}[1 - e^{-\frac{\Sigma_k^g \gamma_k}{\sin(\theta)}}] \tag{2.28}$$

The average adjoint angular function on the segment L_k in the direction $\vec{\Omega}_l$ is,

$$L_k \overline{\Phi}_k^{*g}(\vec{\Omega}_l) = \frac{\Phi^{*g}(\vec{p}_{k+1}, \vec{\Omega}_l)}{\Sigma_k^g}[1 - e^{\frac{-\Sigma_k^g \gamma_k}{\sin(\theta)}}] + \frac{q_k^{*g}}{\Sigma_k^g \Sigma_k^g}\left[\frac{\Sigma_k^g \gamma_k}{\sin\theta} - [1 - e^{\frac{-\Sigma_k^g \gamma_k}{\sin(\theta)}}]\right] \tag{2.29}$$

For the case where the segment L_k is located in a void region, the adjoint characteristics equation for the segment L_k in the void region becomes,

$$\Phi^{*g}(\vec{p}_k, \vec{\Omega}_l) = \Phi^{*g}(\vec{p}_{k+1}, \vec{\Omega}_l) + \frac{\gamma_k}{\sin\theta} q_k^{*g} \tag{2.30}$$

while the average adjoint angular function equation in the void region is given by,

$$L_k \overline{\Phi}_k^{*g}(\vec{\Omega}_l) = \Phi^{*g}(\vec{p}_{k+1}, \vec{\Omega}_l) \frac{\gamma_k}{\sin\theta} + \left[\frac{\gamma_k}{\sin\theta}\right]^2 \frac{q_k^{*g}}{2} \tag{2.31}$$

For a cyclic tracking line having K segments in direction $\vec{\Omega}_l$, we can write the adjoint characteristics equation (derived in direction $(-\vec{\Omega}_l)$) as follows,

$$\Phi^{*g}(\vec{p}_1, \vec{\Omega}_l) = \Phi^{*g}(\vec{p}_{K+1}, \vec{\Omega}_l) \prod_{k'=1}^{K} [H(k')\beta_{alb}(k')] + M(K) \tag{2.32}$$

where $H(k)$ and $\beta_{alb}(k)$ are defined in equation (II.22).

The closed form for the adjoint angular function $\Phi^{*g}(\vec{p}_1, \vec{\Omega}_l)$ is determined by,

$$\Phi^{*g}(\vec{p}_1, \vec{\Omega}_l) = \frac{M(K)}{[1 - \prod_{k'=1}^{K} [H(k')\beta_{alb}(k')]]} \tag{2.33}$$

In the characteristics formalism, the discretized form of average adjoint scalar equation of region j of the spatial domain (D) is written as,

$$V_j \phi_j^{*g} = \sum_{l=1}^{N^\Omega} \sum_{i=1}^{N^\perp(l)} W_i^\perp W_l^\Omega \sum_{k=1}^{K} [F_j(\vec{T}(\vec{P}_i, \vec{\Omega}_l), \vec{p}_{k+1/2}) L_k \overline{\Phi}_k^{*g}(\vec{\Omega}_l)] \tag{2.34}$$

where ϕ_j^{*g} is the average adjoint scalar function in group g and region j, where $j = 1$ to N_J, and N_J is the total number of regions in the spatial domain (D). Here V_j is the volume of region j. $\overline{\Phi}_k^{*g}(\vec{\Omega}_l)$ is the average adjoint angular function

for the segment L_k on $\vec{T}(\vec{P}_i, \vec{\Omega}_l)$, $W_i^{\perp}$ is the quadrature weight for a starting point $\vec{P}_i$ of $\vec{T}(\vec{P}_i, \vec{\Omega}_l)$, $N^{\perp}(l)$ is the total number of tracking lines in direction $\vec{\Omega}_l$, and $\vec{p}_{k+1/2}$ is the center point of segment L_k. Note that, when the generalized adjoint transport problem is considered, a similar adjoint MOCC procedure is applied. The difference is mainly that constant external generalized adjoint sources are added in the total generalized adjoint sources.

In addition one can find that performing the adjoint angular function integrations over the tracking lines and characteristics domains using the MOCC procedure is equivalent to integrating the collision probability over the adjoint sources. (COURAU, 2001; COURAU and MARLEAU, 2002) The average adjoint scalar equation (2.34) can be written in the form,

$$\begin{aligned}\phi_j^{*g} &= \frac{1}{V_j}\sum_{i=1}^{N_J}\left[\int_{V_j} d^3r \int_{V_i} d^3r' \cdot \frac{e^{-\tau^g(\vec{r'},\vec{r})}}{\|\vec{r'}-\vec{r}\|^2}\cdot q^{*g}(\vec{r'})\right] \\ &= \sum_{i=1}^{N_J} p_{j\to i}^{g}\cdot q_i^{*g}\end{aligned} \tag{2.35}$$

where we assume that the total adjoint source ($q^{*g}(\vec{r'}) = q_i^{*g}$) is constant over the region i with,

$$q_i^{*g} = \sum_{g'=1}^{G}[\Sigma_{s,i}^{g'\leftarrow g} + \frac{1}{k_{eff}}\chi_i^{g'}\nu\Sigma_{f,i}^{g}]\phi_i^{*g'} \tag{2.36}$$

$$p_{j\to i}^{g} = \frac{1}{V_j}\int_{V_j} d^3r \int_{V_i} d^3r' \frac{e^{-\tau^g(\vec{r'},\vec{r})}}{\|\vec{r'}-\vec{r}\|^2} \tag{2.37}$$

We can write the MOCC average adjoint scalar function equation (2.35) in matrix form,

$$[\phi_{MOCC}^{*}] = [P_{VV}][Q^{*}] \tag{2.38}$$

where $[P_{VV}]$ is the MOCC response matrix equivalent to collision probability matrix

in the CP method.

2.3.1 Group-splitting Technique and Combined Forward Flux/Adjoint Function Iteration Scheme

In this section we consider the group-splitting technique where the energy groups are divided according to the structure of the adjoint scattering matrix. We may first write the forward scattering matrix for a mixture that contains up-scattering cross sections at the highest energy group. The adjoint scattering matrix is obtained by transposing the forward scattering matrix. From the adjoint scattering matrix, we can divide the energy groups into two sets. The first set contains all the groups without up-scattering (G_1: $g \leq g_u$ groups, where g_u is the lowest group containing no up-scattering). The second set contains the remaining groups (G_2: $g > g_u$ groups) where the adjoint scattering sources depend only on the adjoint functions in G_2. We can improve the multigroup iterations by first solving the G_2 adjoint transport equations to obtain the converged adjoint function solutions which are then used to compute the adjoint scattering sources required for solving the G_1 adjoint transport equations. Note that in the non-splitting scheme, these G_1 adjoint scattering sources are computed with the un-converged G_2 solutions. Therefore, inefficient computations in G_1 can be avoided in such a group-splitting procedure. In addition, we perform the backward iteration (G_1^-) from g_u to 1 groups because the adjoint scattering matrix is upper triangular in this group set (adjoint scattering sources in higher groups depend on the adjoint functions in lower groups). Here G_x^+ and G_x^- represent the forward and backward group iterations on the group set G_x respectively (e.g., G_1^+ represents the forward group iteration from 1 to g_u groups).

We also introduce the combined forward and adjoint iteration schemes to reduce the computing time when both forward and adjoint solutions are required. The

combined iteration scheme implemented in the multigroup iteration is based on the group-splitting technique and the common use of the large number of routine variables such as those used for storing exponential values and tracking line data. From the forward and adjoint scattering matrices we can divide the energy groups into 2 sets (G_1: $g \leq g_u$ and G_2: $g > g_u$) as discussed previously. The G_1 forward scattering sources ($q_{sc,G1}$) depend only on the fluxes (ϕ_{G1}). Similarly the G_2 adjoint scattering sources ($q^*_{sc,G2}$) depend only on the G_2 adjoint functions (ϕ^*_{G2}). Therefore, we may divide the multigroup iteration into three steps as follows.

- The first step is the flux iteration for G_1. Because $q_{sc,G1}$ depend only on ϕ_{G1}, we first solve the G_1 forward transport equations to obtain the converged flux ϕ_{G1} which are then used to compute $q_{sc,G2}$ for solving the G_2 function transport equations in the next step. The forward group iterations G_1^+ is performed because the forward scattering matrix is lower triangular (forward scattering sources in lower groups depend on forward fluxes in higher groups).

- The second step is the combined forward and adjoint iterations for G_2. The large number of exponential function evaluations and tracking-line variables calculations that are used both by the flux and adjoint function computation algorithms are the key procedure to reducing the computing time. We then solve simultaneously group-by-group the G_2 forward and adjoint transport equations to obtain the converged solutions ϕ_{G2} and ϕ^*_{G2}.

- The third step consists in solving the adjoint functions for G_1 where the adjoint scattering sources $q^*_{sc,G1}$ are computed using the converged adjoint functions ϕ^*_{G2}. The backward group iterations G_1^- is performed because the adjoint scattering matrix is upper triangular in this case.

During the combined forward/adjoint iterations, the flux and adjoint function converge at different rates. We have isolated the convergence checking routines for

flux and adjoint function in such a way that they can be turned off independently when either the flux or the adjoint has converged.

The group-reduction scheme consists in monitoring the convergence of the adjoint functions in the most thermal groups and activating the multigroup iterations only on the un-converged groups.

2.3.2 Multigroup Rebalance Technique

In the multigroup adjoint iterations, the convergence rate depends on the ratio of the within-group and up-scattering cross section to the total cross section. In fact the thermal adjoint functions G_2 converge before the fast adjoint functions G_1 (e.g., the adjoint sources in the fast groups generally depend on the down-scattering cross sections and the related adjoint functions in the lower groups; while the thermal adjoint sources depend on the up-scattering cross sections and the associated adjoint functions in the upper groups.). In addition, the higher up-scattering cross-sections from the thermal to intermediate groups result in higher thermal adjoint scattering sources ($q_{sc}^{*g}(\vec{r}) = \sum_{g'=1}^{G} \Sigma_s^{g' \leftarrow g} \phi^{*g'}(\vec{r})$) that cause longer multigroup iterations. When the within-group scattering to total cross-section ratio approaches unity, the multigroup iteration converges slowly (similar to the forward multigroup iterations). In fact the adjoint function must satisfy both adjoint transport and balance equations. By correcting the adjoint scalar functions using the adjoint balance equations after each spatial iteration loop, one can accelerate the calculation process. For the problems with albedo boundary conditions, the adjoint balance equations are obtained by integrating (1.8) over all angles and domain volumes as follows,

$$\Theta^{*g}[\phi^*] = Q^{*g} \tag{2.39}$$

where

$$\Theta^{*g}[\phi^*] = \mathcal{L}^{*g} + \sum_{j=1}^{N_J} \Sigma_j^g \phi_j^{*g} V_j - \sum_{j=1}^{N_J} \sum_{g'=1}^{G} \Sigma_{s,j}^{g' \leftarrow g} \phi_j^{*g'} V_j \tag{2.40}$$

$$Q^{*g} = \frac{1}{k_{eff}} \sum_{j=1}^{N_J} \sum_{g'=1}^{G} \chi_j^{g'} \nu \Sigma_{f,j}^g \phi_j^{*g'} V_j \tag{2.41}$$

$\mathcal{L}^{*g}$ is the total adjoint leakage in group g, and the subscript j indicates the variable associated with region j.

The total adjoint leakage $\mathcal{L}^{*g}$ can be determined indirectly by (MARLEAU, 2004b),

$$\mathcal{L}^{*g} = \sum_{j=1}^{N_J} \left[\left(1 - P_{NL,j}^g\right) \sum_{g'=1}^{G} \left(\Sigma_{s,j}^{g' \leftarrow g} + \frac{1}{k_{eff}} \chi_j^{g'} \nu \Sigma_{f,j}^g \right) \phi_j^{*g'} V_j \right] \tag{2.42}$$

where

$$P_{NL,j}^g = \sum_{i=1}^{N_J} p_{j \to i}^g \Sigma_i^g \tag{2.43}$$

$P_{NL,j}^g$ is the non-leakage probability of a neutron in region j in energy group g. We can determine $P_{NL,j}^g$ using the MOCC method by solving the adjoint transport equations with the imposed adjoint sources defined as follows,

$$q_i^{*g} = \Sigma_i^g \tag{2.44}$$

Using the MOCC adjoint scalar equation (2.35) in the MOCC response matrix equation, we can find that the adjoint results with adjoint sources (2.44) are equal to the non-leakage probabilities.

We can then rewrite (2.39) using (2.42) and (2.43) as follows,

$$\sum_{j=1}^{N_J} \Sigma_j^g \phi_j^{*g} V_j - \sum_{j=1}^{N_J} P_{NL,j}^g \sum_{g'=1}^{G} \Sigma_{s,j}^{g' \leftarrow g} \phi_j^{*g'} V_j = \frac{1}{k_{eff}} \sum_{j=1}^{N_J} P_{NL,j}^g \sum_{g'=1}^{G} \chi_j^{g'} \nu \Sigma_{f,j}^g \phi_j^{*g'} V_j \tag{2.45}$$

The corrected adjoint scalar function is defined as follows,

$$\widetilde{\phi}_j^{*g} = f_c^g \phi_j^{*g} \tag{2.46}$$

where f_c^g is the correction factor associated with energy group g. Applying (2.46) to the LHS of (2.45), we then solve the G resulting equations to obtain the correction factors f_c^g. All final correction factors shall converge to 1.0 at the end of multigroup iterations. For the problems with no leakage ($\alpha = 1$), $P_{NL,j}^g$ are set to unity.

2.3.3 Biasing and Decontamination Schemes for the Generalized Adjoint Transport Solution

Because of the negative external generalized adjoint sources, direct use of these sources in the adjoint solution algorithm shall result in negative generalized adjoints (unlike the forward fluxes and adjoint functions which are strictly positive). During the multigroup iterations, using such negative values in the adjoint rebalance scheme can cause errors in the rebalance factors and provoke numerical oscillations in the solutions (e.g., the negative rebalance factors change the signs of the generalized adjoints which then induce numerical oscillations). The rebalance scheme then becomes less effective to speed up the solutions. This problem arises because, in the adjoint balance equations, adjoint functions and spatial-integrated adjoint balance sources (adjoint fission plus external sources) must be positive, and the cancellations between positive and negatives sources may lead to inadequate rebalance factors. The generalized adjoints are made positive using a biasing scheme

defined as follows,

$$[\Gamma^*_{\text{bias}}] = [\Gamma^*] + C_{\text{bias}}[\phi^*] \tag{2.47}$$

$$C_{\text{bias}} = \max_{i,g}\left(\frac{f_b q_i^{*g} - S_i^{*g}}{q_i^{*g}}\right) \tag{2.48}$$

$$q_i^{*g} = \sum_{g'=1}^{G}(\Sigma_{s,i}^{g'\leftarrow g} + \frac{1}{k_{eff}}\chi_i^{g'}\nu\Sigma_{f,i}^{g})\phi_i^{*g'} \tag{2.49}$$

where C_{bias} is the biasing factor defined in terms of f_b a predetermined positive source biasing factor. Index i indicates the i-th region. q_i^{*g} are the standard adjoint fission plus scattering sources. The adjoint functions are used in the biasing because they are the homogeneous solutions of the generalized adjoint transport equations and they are strictly positive. The biased generalized adjoints are determined so that they result in positive total generalized adjoint sources. For a specific f_b, the biasing factor may not always result in positive generalized adjoints. The selection of f_b is discussed in ARTICLE I. After the multigroup iteration is completed, the orthogonal generalized adjoints $\Gamma_\perp^{*g}$ are extracted using a decontamination scheme given by,

$$[\Gamma^*_\perp] = [\Gamma^*_{\text{bias}}] - C_{\text{decon}}[\phi^*] \tag{2.50}$$

$$C_{\text{decon}} = \frac{[\Gamma^*_{\text{bias}}]^T[\phi^*]}{[\phi^*]^T[\phi^*]} \tag{2.51}$$

in order to satisfy $[\Gamma^*_\perp]^T[\phi^*] = 0$, where C_{decon} is the required decontamination factor. One can find that the decontamination scheme removes the homogeneous solutions from the total inhomogeneous solutions (biased adjoints). Note that this decontamination scheme is performed only in the power iteration loop. When the convergence is reached, we then evaluate the selected solution $[\Gamma^*_\beta]$ using Eq. (2.17).

In addition, the decontamination scheme developed in the generalized adjoint trans-

port solution by the CP method (while the biasing factor is kept constant at 10^5) is performed in order to satisfy the condition $[\Gamma^*_\perp]^T[B\Phi] = 0$, i.e., $\Gamma^{*g}_\perp = \Gamma^{*g}_\beta$; (COURAU, 2001). One may see that the elements of vector $[B\Phi]$ at low energy group as well as the elements in the regions without fissile isotopes become null. By using this scheme, Γ^{*g}_β that satisfy the above condition are not unique. This may undesirably result in the longer power iterations.

In our study, we examine three types of biasing and decontamination schemes as follows,

- *Scheme 1* consists of a two step biasing/decontamination scheme. In the first step the generalized adjoints are biased once in the first power iteration loop using Eq. (2.47). We then use these biased generalized adjoints in the power and multigroup iterations. The rebalance procedure in the multigroup iteration is turned on but the decontamination procedure is turned off in this step. When the biased generalized adjoints converge, the orthogonal generalized adjoints are extracted using Eq. (2.50). The first step is stopped and then the second step begins. In this second step the generalized adjoints are kept unbiased. The orthogonal generalized adjoints are directly used in the power and multigroup iterations. The rebalance procedure is turned off as well as decontamination in the power iterations. When the power iterations converge, once again the last decontamination is performed to extract the required orthogonal generalized adjoints Γ^{*g}_β.

- *Scheme 2* consists of a single-step biasing/decontamination scheme that is performed in each power iteration loop. The generalized adjoints are biased at the beginning of each power iteration loop and then used in the power and multigroup iterations. When multigroup iterations converge, the orthogonal generalized adjoints are extracted and used in the next power iteration

loop. The convergence of multigroup iterations relies on the biased generalized adjoints while convergence of power iterations relies on the orthogonal generalized adjoints.

- *Scheme 3* is a 2 step biasing/decontamination scheme similar to Scheme 1 except that, in the first step, the biasing and decontamination are performed in each power iteration (as described in Scheme 2).

2.3.4 The Computation of MOCC Response Matrix

In addition we extract the MOCC response matrices using the MOCC method to scan over the cyclic tracking lines using identity matrix sources of dimension $N_J \times N_J$ for each group. It is found that the MOCC computing time is lower than the time required by the CP method where the CP matrices are evaluated using the same cyclic tracking lines. This is because the calculation loops for region-to-region CP integrations on cyclic tracking lines is time-consuming ($N_J \times N_J \times G$ loops) while, in the MOCC method, the calculation relies on the propagation of the unit source in the i-th region to the flux in j-th region with the common use of a large number of tracking line data and exponential variables for each group. The computing time by the CP, MOCC and MOCC response matrix methods are presented in Table 2.1.

Finally the validation of adjoint and generalized adjoint MOCC algorithm is performed on the 37 pin CANDU, 17×17 PWR and Watanabe-Maynard lattice problems together with the numerical comparison of the direct and adjoint solutions between the MOCC and CP methods. Full details of numerical results are presented in ARTICLE I and II.

Table 2.1 The Computing Time of the Direct Flux and Adjoint Function by the CP, MOCC and MOCC Response Matrix Methods

Problems	Computation time (min.)		
	CP method	MOCC method	MOCC response matrix method
CANDU	85	58	19
PWR	227	121	93
ACR	243	150	78

2.3.5 Conclusions on Adjoint and Generalized Adjoint Transport Solutions by MOCC Method

The MOCC method is a good alternative solution method for the adjoint and generalized adjoint transport problems in two-dimensional heterogeneous geometries. The numerical results of adjoint function and k_{eff} by MOCC method are similar to the source importance function and k_{eff} results by CP method as expected. Since the source importance CP equation can be derived from the MOCC adjoint scalar function equation, the source importance function by CP method is equivalent to the adjoint function by MOCC method.

In order to satisfy the boundary conditions in the adjoint transport problems, we need to solve the $\vec{\Omega}$-directed adjoint transport equation along the tracking line in the backward direction $(-\vec{\Omega})$. The adjoint characteristics equation is in the same form as the characteristics equation in neutron transport problem except the adjoint characteristics equation is formulated in the direction $(-\vec{\Omega})$. With the use of closed form, the solution of adjoint angular function associated with the cyclic tracking line is directly determined.

By taking into account the structure of the adjoint scattering matrix, the group-

oriented and group-splitting iterations result in speed-up of computations. Because the adjoint functions converge faster in the thermal groups than in the fast groups, the group-reduction procedure is implemented by monitoring the convergence in the most thermal groups and activating the multigroup iterations only for the adjoint functions in the un-converged groups.

The combined forward-adjoint iterations scheme based on the group-splitting technique and the common use of the large number of routine variables storing tracking line data and exponential values give lower computing time than the total time required for the individual forward and adjoint calculations. The 3 step scheme (e.g., 1 to 26 (forward), 27 to 69 (forward & adjoint) and 26 to 1 (adjoint)) can be applied for both PWR and CANDU cases. This is because the forward fluxes converge slower than the adjoint functions in these cases. The iterations in the second step rely on the convergence of the flux iterations where the iteration for 27 to 69 groups give lower computing time than the iterations for 69 to 27 groups.

In the generalized adjoint transport solutions, the biasing and decontamination schemes in each power iteration loop (scheme 2) results in the lowest computing time among the 3 schemes proposed. This is because, in each power iteration, the decontamination scheme extracts the orthogonal generalized adjoints and in the meantime remove the undesired contaminated components which are the linear function of the standard adjoint functions. Therefore, the orthogonal generalized adjoint functions converge faster than the generalized adjoint functions, which are iterated with the contaminated components as in scheme 1 and 3.

2.4 Summary of the Application of Adjoint Sensitivity Technique to the CVR, CBCVR and k_{eff}-EOC Adjustments in the CANDU and ACR lattices

As presented in ARTICLE III, we apply the optimization and adjoint sensitivity techniques to the adjustments of CVR at the beginning of burnup cycle (BOC), and k_{eff} at the end of burnup cycle (EOC) by searching Dysprosium (Dy) density and U235 enrichment percentage for a CANFLEX-fueled ACR lattice. The sensitivity coefficients are evaluated using the perturbation theory based on the integral transport equations with isotropic scattering. To approximate the EOC sensitivity coefficient, we estimate the variations in nuclide densities at EOC by introducing a very small perturbation in the lattice parameters at BOC and perform constant-power burnup/depletion calculations for 600 FPDs using the unperturbed neutron fluxes.

Our objective is to obtain the negative CVR-BOC of -2 mk and k_{eff}-EOC of 0.900 (to meet the exit-burnup requirement). We have studied 3 situations: 1) the simultaneous adjustment of Dy density in the central pin and U235 enrichment in the outer fuel rings, 2) the adjustment of Dy density and U235 enrichment both in the central pin, and 3) the adjustment of Dy and U235 enrichment similar to the first case but to obtain the CBCVR-BOC of -2 mk. Dy is selected for the adjustment because it has wide and large resonance capture cross sections. Increasing Dy density shall result in higher absorption rate partly caused by the hardened neutron spectrum and subsequently lower the CVR. Because the increasing Dy density also lowers the k_{eff} of the cooled lattice, one needs to increase fission rates by altering U235 to compensate the higher Dy absorption rate.

2.4.1 The Optimization Problem

In order to obtain the target CVR-BOC and k_{eff}-EOC, we define an optimization problem to search for the Dy density and U235 enrichment that minimizes a cost functional J given by,

$$\begin{aligned} J &= W_c(CVR_{tar,BOC} - CVR_{BOC})^2 + W_\lambda(\lambda_{tar,EOC} - \lambda_{EOC})^2 \\ &\quad + W_F F_{50mk}^2(\lambda_{o,BOC} - \lambda_{BOC}) \end{aligned} \tag{2.52}$$

where $CVR = (\lambda - \lambda_{void})$. W_c, W_λ and W_F are the weights of CVR_{BOC}, λ_{EOC} and function $F_{50mk}(\lambda_{BOC} - \lambda_{o,BOC})$ respectively. The function F_{50mk} serves as a penalty function for λ_{BOC} where $F_B(x) = x$ when $|x| > B$, otherwise 0. By defining the penalty function for λ_{BOC}, the optimal solution shall not result in a λ_{BOC} change larger than 50 mk. $CVR_{tar,BOC}$ and $\lambda_{tar,EOC}$ are the target CVR_{BOC} and λ_{EOC} respectively. $\lambda_{o,BOC}$ is the nominal eigenvalue of the lattices at BOC. For the CBCVR adjustment in the third case, CVR is replaced by CBCVR in Equation (2.52).

2.4.2 Sensitivity Calculation

We apply the perturbation theory method based on the integral neutron transport equations in Eq. (1.4) to determine the eigenvalue sensitivity coefficient to

parameter P_i defined as follows,

$$\begin{aligned}\frac{\partial \lambda_{V,X}}{\partial P_i} &= \frac{1}{\Delta P_i}\frac{\langle \Phi^{\dagger g}, (\Delta \mathcal{L}^g - \lambda \Delta \mathcal{F}^g)\Phi^g \rangle_{V,X}}{\langle \Phi^{\dagger g}, \mathcal{F}^g \Phi^g \rangle_{V,X}} \\ &\approx -\left[\frac{\left\langle [\phi^\dagger], [\Delta P_{VV}][Q] \right\rangle + \left\langle [P_{VV}][\phi^\dagger], ([\Delta \Sigma_s][\phi] + \lambda [\chi][\Delta(\nu\Sigma_f)][\phi]) \right\rangle}{\Delta P_i \langle \Phi^{\dagger g}, \mathcal{F}^g \Phi^g \rangle}\right]_{V,X} \\ &\equiv S^{P_i}_{\lambda_{V,X}} = \sum_{g=1}^{G} S^{g,P_i}_{\lambda_{V,X}} \end{aligned} \tag{2.53}$$

where $S^{g,P_i}_{\lambda_{V,X}}$ is a group-based eigenvalue sensitivity coefficient to P_i, P_i is either %wt Dy-BOC density or U235-BOC enrichment percentage, X is either BOC or EOC, and V is either void or cooled conditions. In addition we define the CVR sensitivity coefficient using Eq. (2.53) as,

$$\begin{aligned}\frac{\partial CVR_X}{\partial P_i} &= S^{P_i}_{CVR_X} = \sum_{g=1}^{G} S^{g,P_i}_{CVR_X} \\ &= \frac{\partial(\lambda - \lambda_{void})_X}{\partial P_i} \end{aligned} \tag{2.54}$$

where $S^{g,P_i}_{CVR_X}$ is a group-based CVR sensitivity coefficient to P_i.

2.4.3 The Approximation of Sensitivity Coefficients at BOC and EOC

The burnup sensitivity method can be used to compute the eigenvalue sensitivity at EOC for a few groups problem (YANG and DOWNAR, 1988; GANDINI, 2001). The method requires to solve the coupled time-dependent adjoint nuclide burnup equations and generalized adjoint transport equations backward in time (when the void coefficients at EOC are required, one also needs to solve another coupled problem associated with the coolant-voided conditions). One can expect that the solution of these coupled problems would be time-consuming. The method is then useful when various types of sensitivity coefficients are required. In our problem

we only need two types of eigenvalue coefficients $S_{\lambda_{EOC}}^{Dy_{BOC}}$ and $S_{\lambda_{EOC}}^{U235_{BOC}}$ at EOC. We propose to use a simpler method to approximate the EOC perturbed nuclide densities with the use of perturbation theory described in the previous section that requires only the flux importance functions at BOC and EOC.

First we compute the sensitivity coefficients at BOC. One needs to determine the BOC perturbed transport operators ($\Delta\mathcal{L}_{BOC}$ and $\Delta\mathcal{F}_{BOC}$ in Eq.(2.53)) associated with the parameter perturbation ΔP_i. We introduce a very small perturbation ΔP_i (e.g., 0.0001% U235-BOC and 0.01%wt Dy-BOC that results in $\Delta\lambda \approx 5 \times 10^{-5}$) in the lattice parameters and construct the BOC perturbed macroscopic cross-section library. Next we perform resonance self-shielding correction to the macroscopic cross sections in this perturbed library and construct the BOC perturbed transport operators for the sensitivity calculations using Eq.(2.53). For the void sensitivity coefficients at BOC, we impose the vacuum condition to the coolant mixtures in the BOC perturbed library, then perform self-shielding correction and evaluate the coolant-voided perturbed transport operators.

To evaluate the sensitivity coefficients at EOC, we need to approximate the EOC perturbed nuclide densities $\tilde{N}_{EOC}$ associated with the perturbed parameter $\tilde{P}_i$ by solving the burnup/depletion equations,

$$\left[\frac{d\tilde{N}_\kappa}{dt}\right] = C([\tilde{N}_\kappa], [\phi_\kappa], \tilde{P}_i) \tag{2.55}$$

with the use of DRAGON-EVO module (MARLEAU et al., 2006). Here C is the nuclide burnup and decay functions, $\tilde{P}_i = P_i + \Delta P_i$, and κ is the burnup step. We perform the constant-power burnup/depletion calculation on the BOC perturbed library from 0 to 600 FPDs using the unperturbed fluxes (which have been calculated using the unperturbed library at each burnup periods). The differences between the perturbed and unperturbed fluxes due to this very small perturba-

tion are assumed small. Once the EOC nuclide densities have been obtained, we perform self-shielding correction on the resulting EOC perturbed library, then approximate the perturbed transport operators $\Delta\mathcal{L}_{EOC}([\tilde{N}_{EOC}], [\phi_{EOC}], \tilde{P}_i)$ and $\Delta\mathcal{F}_{EOC}([\tilde{N}_{EOC}], [\phi_{EOC}], \tilde{P}_i)$, and evaluate the EOC sensitivity coefficients using Eq. (2.53). For the evaluation of EOC void sensitivity coefficients, similar procedures are performed as for the BOC void coefficient.

A more accurate procedure consists in performing burnup/depletion calculations that use the perturbed fluxes associated with their perturbed library. However this method is time-consuming due to the evaluation of perturbed fluxes required at each burnup steps. This method was only used to evaluate the reference group-based coefficients for sensitivity analyses.

2.4.4 The Optimization Procedure

For the lattice burnup/depletion calculations, we perform the calculation for 600 FPDs using the constant 35 kW/kgU burnup power to evaluate the neutron fluxes, CVR, cooled and void k_{eff} at each burnup step. The flux importance functions of the cooled and void lattices are computed at BOC and EOC.

One can see that the optimization problem defined in (2.52) is a two variable problem. We can easily find the optimal Dy density and U235 enrichment percentage by scanning through the ranges of Dy density and U235 enrichment with the step change (e.g., 0.001). The cooled and void eigenvalues associated with the new parameters are approximated and applied in the cost functional for the optimal search,

$$\lambda_{V,X,new} = \lambda_{o,V,X} + \sum_{i}^{N_p} \frac{\partial \lambda_{V,X}}{\partial P_i}(\tilde{P}_i - P_{i,o}) \tag{2.56}$$

where $\tilde{P}_i$ is either the step-searching Dy or U235, $P_{i,o}$ is the nominal values of Dy-BOC or U235-BOC of the lattices for which the coefficients are evaluated, and λ_o is the eigenvalue of the lattices associated with the parameters $P_{i,o}$.

In the first step of the optimizing process, we compute the fluxes, flux importance functions and sensitivity coefficients of the lattices with the nominal Dy and U235. Then we use these coefficients to search the optimal Dy and U235 that minimizes the cost functional. Next we apply the computed optimal Dy and U235 to the lattices, build the new lattice library, and compute the new CVR-BOC and k_{eff}-EOC. If these new CVR-BOC and k_{eff}-EOC do not meet their target values, we begin the second step and reevaluate the fluxes, flux importance functions and sensitivity coefficients of the new lattices with the optimal Dy and U235 obtained from the previous step. The same procedure is repeated until the CVR-BOC and k_{eff}-EOC meet their target values. The stopping criteria are to obtain the absolute relative errors (%) of the CVR-BOC and k_{eff}-EOC less than ϵ and 0.1ϵ respectively, where ϵ is a small real value.

The numerical results and the effects of Dy density and U235 enrichment on the CVR-BOC on CBCVR-BOC are presented in ARTICLE III as well as the group-based sensitivity analyses of CVR and eigenvalue at BOC and EOC with respect to Dy density and U235 enrichment. In addition we extend the optimization and adjoint sensitivity techniques to the CVR-BOC, CVR-EOC and k_{eff}-EOC adjustments of a CANDU lattice with the burnup period extended from 300 to 450 FPDs. The objective is to obtain the target CVR-BOC, CVR-EOC and k_{eff}-EOC of +10 mk, +8 mk and 0.956510 (equal to k_{eff} of the initial-designed lattice at 300 FPDs) respectively. For the CANDU lattice, we consider 4 cases in our study: 1) The simultaneous adjustment of Dy in the central pin and U235 in the outer fuel rings to obtain the target CVR-BOC and k_{eff}-EOC; 2) The adjustment similar to case 1 but to obtain the target CVR-BOC, CVR-EOC and k_{eff}-EOC; 3) Similar to case 1

but replace Dy with Gd in the central pin, and 4) Similar to case 2 but replace Dy with Gd in the central pin. The numerical results and the effects of Dy, Gd and U235 on CVR-BOC, CVR-EOC and CBCVR-BOC are presented in Chapter 3 as well as the sensitivity analyses of CVR and eigenvalue at BOC and EOC to Dy, Gd and U235. Finally we apply the optimization and adjoint sensitivity techniques to the CBCVR-BOC and k_{eff}-EOC adjustments of the ACR lattice with Gadolinium in the central pin. The numerical results, the Gd effects and the sensitivity analyses of CVR and eigenvalue are presented in Chapter 4.

2.4.5 Conclusions on Application of Adjoint Sensitivity Technique

The simple optimization and adjoint sensitivity techniques are applied to adjust the CVR-BOC, CBCVR-BOC and k_{eff}-EOC of the ACR lattices. In the first adjustment case, the optimal Dy density in the central pin and U235 enrichment in the outer rings are 8.26 %wt and 2.107%, and gives approximately a CVR-BOC and k_{eff}-EOC of -2.0 mk and 0.900. By slightly altering Dy and U235 to their optimal values, one can adjust the positive CVR (for the first 120 FPDs) to be negative over the burnup period. In the second case, we obtain the optimal Dy and U235 of 19.614%wt and 20.995% both in the central pin. The resulting CVRs are all negative as expected. In the third case, the optimal CBCVR-BOC is of -1.18 mk while its target is -2.0 mk. This is because the Dy approaches its maximum limit in the central pin. According to the optimal Dy and U235 of 99.838%wt and 2.406% the resulting CBCVRs are entirely negative, while the initial CBCVRs are all positive. In addition the sensitivity analysis method is used in analyzing the groupwise characteristics of eigenvalues, CVR and CBCVR (at BOC and EOC) with respect to Dy density and U235 enrichment.

CHAPTER 3

CVR ADJUSTMENTS IN 37 PIN CANDU-6 LATTICES USING ADJOINT SENSITIVITY TECHNIQUE

3.1 Problem Descriptions

In this chapter we study the CVR-BOC, CVR-EOC and k_{eff}-EOC adjustments for a CANDU-6 lattice of which the fuel burnup period is extended from 300 to 450 full power days (FPDs) (MARLEAU et al., 2006). The major characteristics of the CANDU-6 lattice are: overmoderated lattice with 37 pin natural Uranium fuel bundle, and heavy water moderator and coolant. The moderator is separated from the coolant channel by means of pressure and calendria tubes with a Helium gap. Our objectives here are to obtain the CVR-BOC and CVR-EOC equal or less than the target values of +10 and +8 mk respectively, and to obtain k_{eff}-EOC equal to the target k_{eff}-EOC of 0.956510 (equal to the k_{eff} of the initial-designed CANDU-6 lattice at 300th FPD). Here we study 4 adjustment cases: 1) the adjustments of Dysprosium (Dy) in the central pin and U235 enrichment in the outer rings (2nd to 4th rings) to obtain the target CVR-BOC and k_{eff}-EOC (CVR-EOC is unconstrained), 2) similar to the first case but to obtain the target CVR-BOC, CVR-EOC and k_{eff}-EOC, 3) similar to the first case but the adjustment of Galdolinium (Gd) instead of Dysprosium and 4) similar to the second case but the adjustment of Gd instead of Dy.

In fact Gd has larger thermal and resonance absorption cross sections than Dy between 0 and 200 eV, but Dy has larger resonance absorption in the intermediate spectrum between 200 eV and 10 keV. The CANDU flux spectrum is relatively

softened due to the overmoderated lattice. When the same amount of either Gd or Dy is added in the CANDU lattice, Gd shall be consumed at a faster rate than Dy. Gd is then suitable for eliminating the excess reactivity and reducing CVR-BOC, while ensuring higher k_{eff} at EOC than the lattice with Dy. For the case of CVR-BOC adjustment, one can see that the lattice with Gd in the central pin requires lower U235 enrichment than the lattice with Dy. In the case of CVR-BOC and CVR-EOC adjustment, the lattice with Dy in the central pin shall have some Dy left at EOC that can reduce CVR-EOC, while the lattice with Gd requires excessive amount of Gd to minimize CVR-EOC due to its fast burning rate. In this case, the lattice with Dy requires lower U235 than the lattice with Gd. We also need to adjust for higher U235 enrichment so that the lattice can produce the thermal power for the extended burnup period, and k_{eff}-EOC meets the requirements of discharged fuels.

3.2 The Optimization Problem

The problem here is to optimize the CVR-BOC, CVR-EOC and k_{eff}-EOC to meet their target requirements. The cost functional J is defined,

$$\begin{aligned} J &= W_{c,BOC}F_{0mk}^2(CVR_{BOC} - CVR_{tar,BOC}) \\ &\quad + W_{c,EOC}(CVR_{EOC} - CVR_{tar,EOC})^2 \\ &\quad + W_{\lambda,EOC}(\lambda_{tar,EOC} - \lambda_{EOC})^2 + W_{\lambda,BOC}F_{100mk}^2(\lambda_{o,BOC} - \lambda_{BOC}) \end{aligned} \quad (3.1)$$

where $CVR = (\lambda - \lambda_{void})$ and $\lambda = 1/k_{eff}$. $W_{c,BOC}$, $W_{c,EOC}$, $W_{\lambda,BOC}$ and $W_{\lambda,EOC}$ are the weights of CVR_{BOC}, CVR_{EOC}, λ_{BOC} and λ_{EOC} respectively. The function F_{0mk} and F_{100mk} serves as the penalty functions for CVR_{BOC} and λ_{BOC} respectively where $F_B(x) = x$ when $x > B$, otherwise 0. λ_{tar} and CVR_{tar} are the target values

of λ and CVR. $\lambda_{o,BOC}$ is the nominal eignevalue of the initial-unadjusted lattices at BOC.

The calculation of BOC sensitivity coefficients, the approximation of EOC sensitivity coefficients, and the optimization procedures are similar to those presented in ARTICLE III.

3.3 Effects of Gadolinium, Dysprosium and U235 on CVR-BOC and CBCVR-BOC

As illustrated in Figure 3.1, we study the effects of U235 enrichment in the outer rings on CVR-BOC, CVR-EOC and CBCVR-BOC for a lattice with 0.0% Dysprosium, 0.0% Gadolinium and 0.7114% U235 in the central pin. Both CVR-BOC and CBCVR-BOC decrease with the increasing U235 enrichment because U235, having large resonance capture cross sections, tends to increase the resonance capture that is caused by the hardened flux spectrum, and then results in lower fissions during coolant voiding. For U235 between 0.7 to 1.5%, CVR-EOC increases with U235 enrichment due to the higher Pu239 production that results in a higher fission rate upon coolant voiding. We find that the Pu239-EOC concentration increases with the U235-BOC enrichment and reaches a maximum value at 2.0% U235 ($\sim$1.8% increase in density compared with Pu239 in the natural U235 lattice). When U235 $>$ 2.0%, CVR-EOC is lower due to the decrease of Pu239 production and the increase of U235 resonance capture. As mentioned in ARTICLE III, CBCVR-BOC is lower than CVR-BOC because the CANDU-6 lattice is overmoderated. This leads to weak spatial-coupling among the adjacent cells and the fact that the coolant-voided spectrum shift is very localized in space. The checkerboard-voided (CBVOID) lattices then have higher resonance capture and lower fission reactions than that of the fully voided lattices.

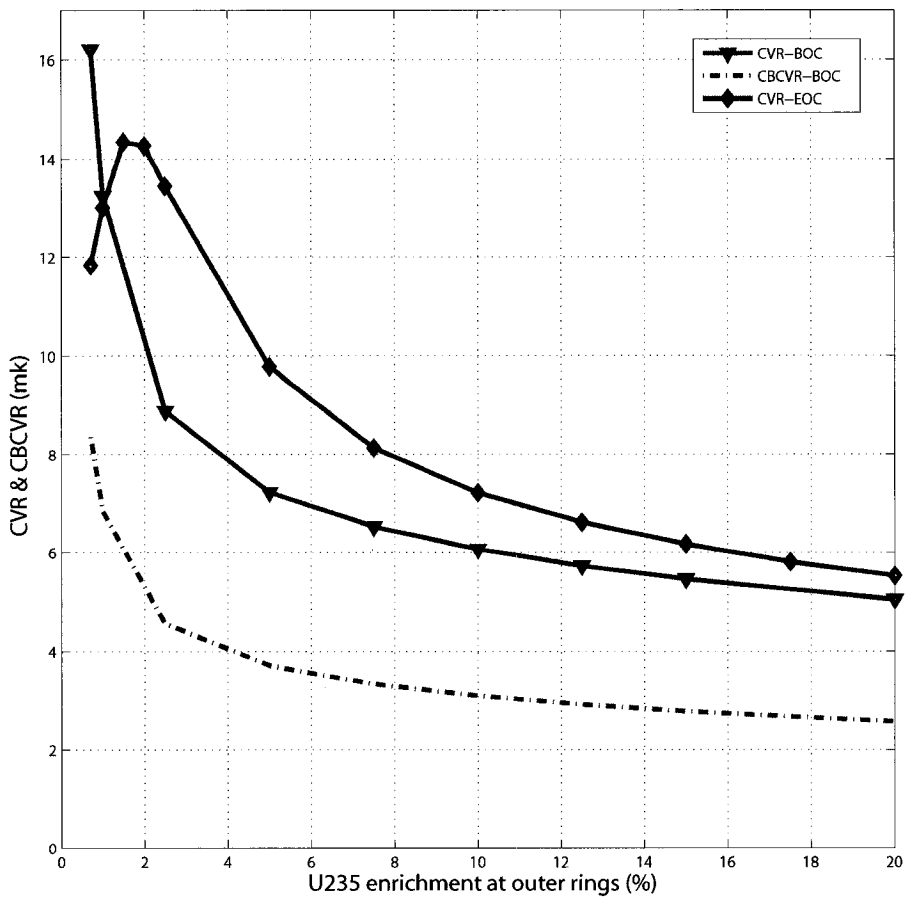

Figure 3.1 Effects of U235 enrichment (%) in the outer rings on CVR-BOC, CVR-EOC and CBCVR-BOC

The effects of Dy density in the central pin on CVR-BOC, CVR-EOC and CBCVR-BOC are presented in Figure 3.2. The increasing Dysprosium density directly decreases the CVRs because its large absorption partially eliminates the fission effect in the fuel pins during the coolant voiding. When the Dysprosium density is greater than 20%, the CVRs decrease more slowly due to self-shielding effects of Dy that already suppresses thermal and resonance neutron fluxes in the central pin and surrounding regions.

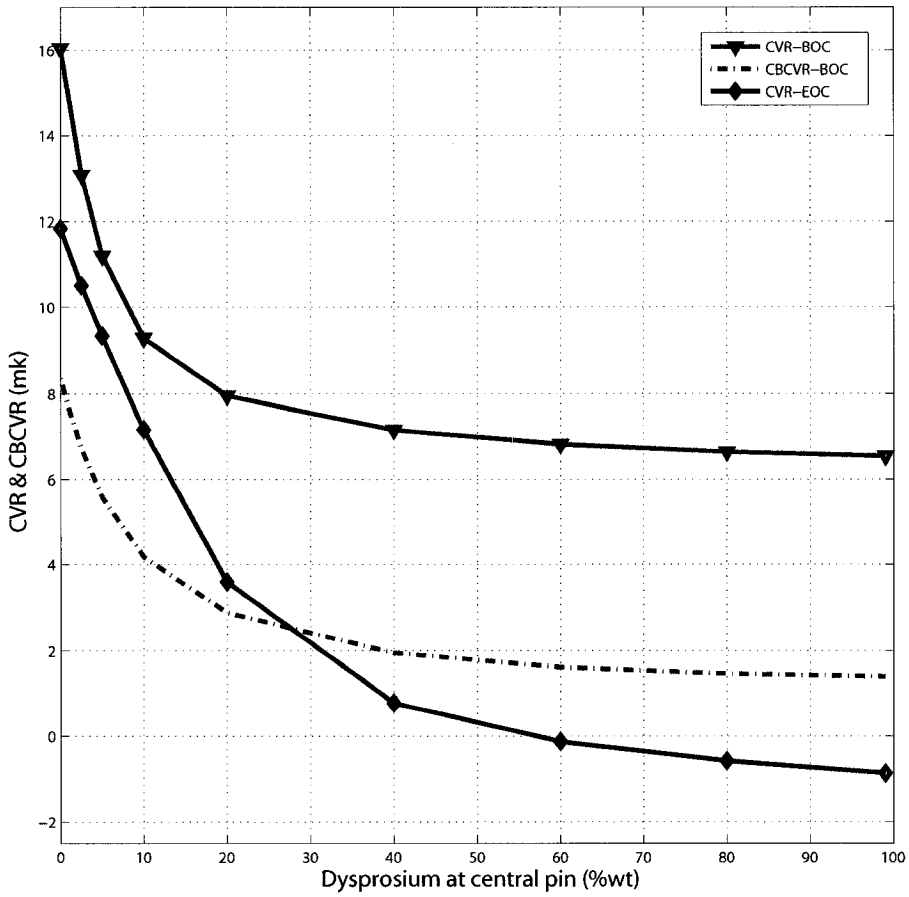

Figure 3.2 Effects of Dy density (%wt) on CVR-BOC, CVR-EOC and CBCVR-BOC

The effects of Gd density in the central pin on CVR-BOC, CVR-EOC and CBCVR-BOC are presented in Figure 3.3. For $0 < Gd < 1\%$, Gd abruptly decreases CVR-BOC and CBCVR-BOC because its large absorption cross section partially eliminates the fission increased upon coolant voiding. When the Gd is greater than 1%, these CVRs change slowly due to the dominating self-shielding effects of Gd. For Gd between 0 and 20%, CVR-EOC remains almost constant due to Gd being mostly consumed at EOC. When $Gd \geq 20\%$, excessive Gd is left from the fuel burnup process at EOC and effectively reduces the CVR-EOC.

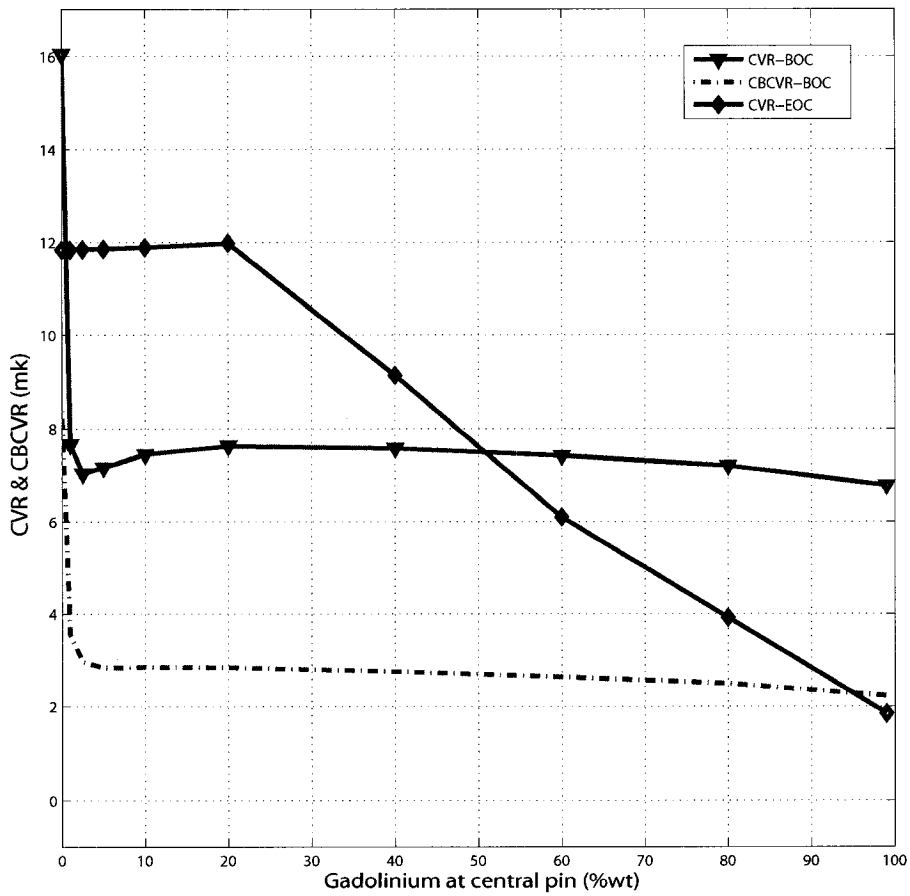

Figure 3.3 Effects of Gd density (%wt) on CVR-BOC, CVR-EOC and CBCVR-BOC

3.4 CANDU Eigenvalue and CVR Sensitivity Analyses

3.4.1 CANDU Eigenvalue and CVR Sensitivity Analysis to Dysprosium Density

We first consider the sensitivity coefficients of CVR and eigenvalues to Dysprosium density for a lattice with 0.0% Dysprosium in the central pin and 0.7114% U235 in each fuel pin. The group sensitivity of cooled (100% coolant-filled) and void eigenvalues (at BOC) to Dy presented in Figure 3.4 are positive due to the increasing absorption rate corresponding to the increase of Dy. The sensitivity of void eigenvalue is slightly higher than that of the cooled eigenvalue. Generally during coolant voiding the neutrons are less thermalized. The neutron fluxes become hardened. However the up-scattering reactions of thermal neutrons are lower due to voiding of hot coolant. The thermal fluxes then become more themalized. As one can see in Figure 3.5, the thermal flux spectrum (between 0 and 0.1 eV) in the central pin is shifted toward the lower energy group. The flux spectrums in the central pin, 4th fuel ring, coolant and moderator regions are illustrated in Figure 3.5 to 3.8 and all fluxes are normalized with respect to a unit neutron production rate in the lattice. Since Dy has large thermal absorption cross sections, the higher thermal fluxes due to voiding of hot coolant results in higher absorption rates. These increasing absorptions in Dy shall compensate the decreasing coolant absorptions, resonance capture and the increasing fissions (due to the shifted thermal spectrum in fuel pins), and subsequently mitigate the positive CVR effect during coolant voiding.

The group sensitivity of cooled and void eigenvalues at EOC to Dy are presented in Figure 3.9. The group coefficients are positive between 10^{-5} to 10^{3} eV due to the fact that some Dy still remains in the pin and because there is a higher U235 and converted Pu239 contents at EOC (e.g., when Dy-BOC is increased by 0.1%,

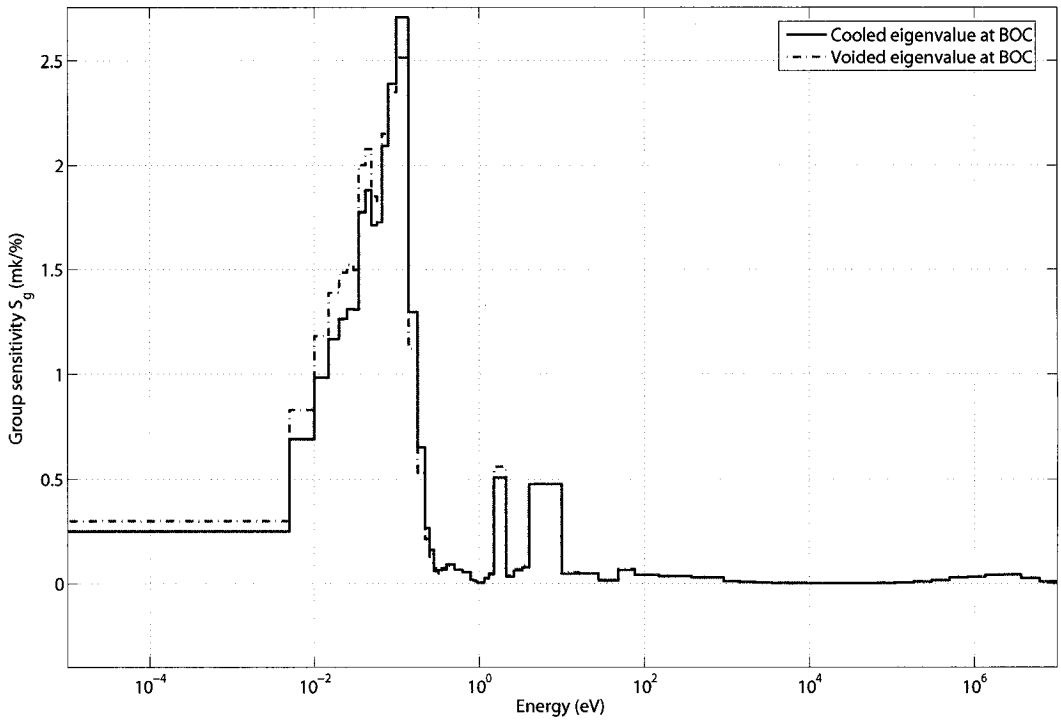

Figure 3.4 CANDU: Group sensitivity of cooled and voided eigenvalues (at BOC) to Dy density

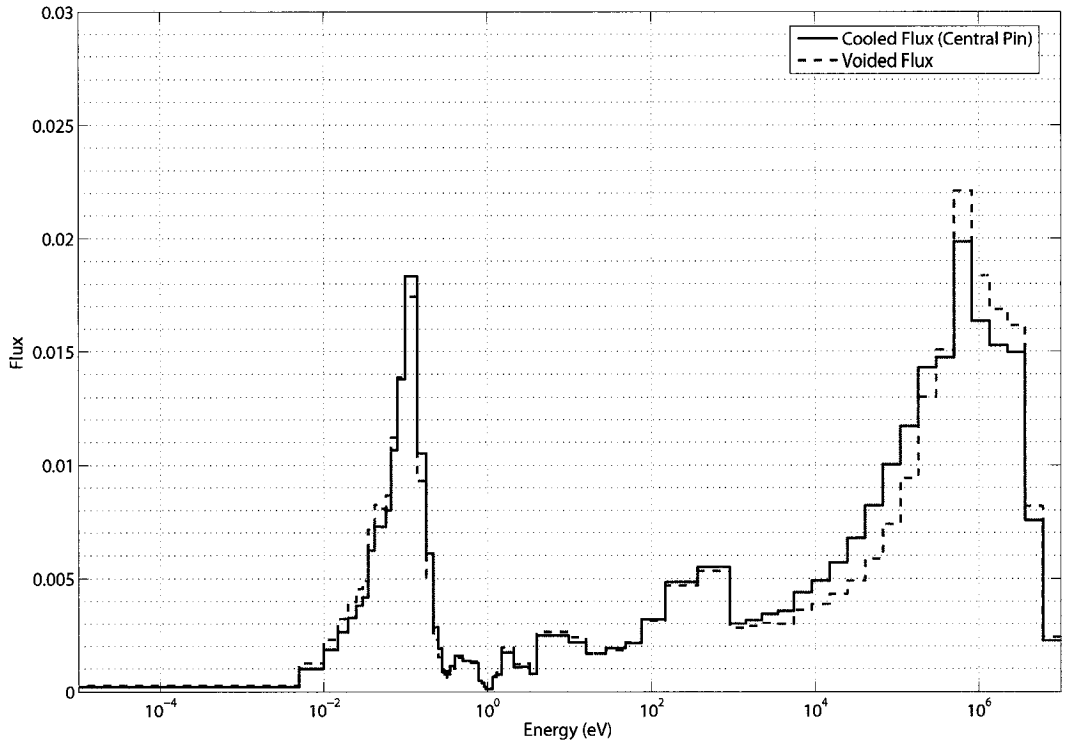

Figure 3.5 CANDU: Cooled and voided flux spectrums in the central pin

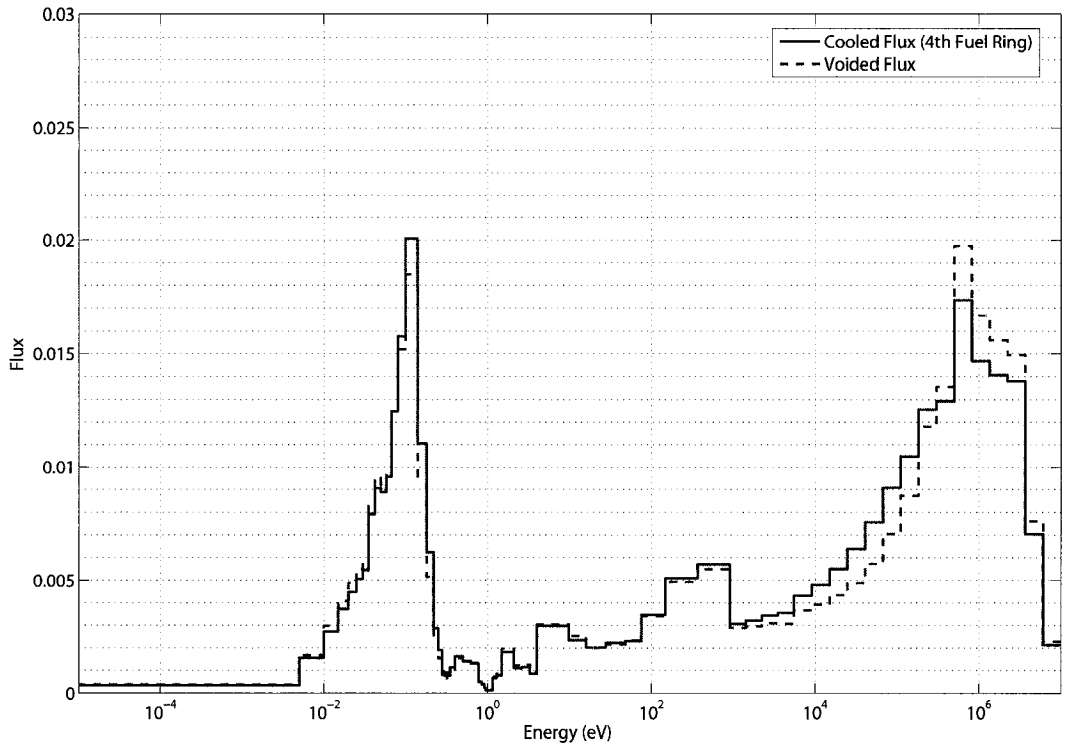

Figure 3.6 CANDU: Cooled and voided flux spectrums in the 4th fuel ring

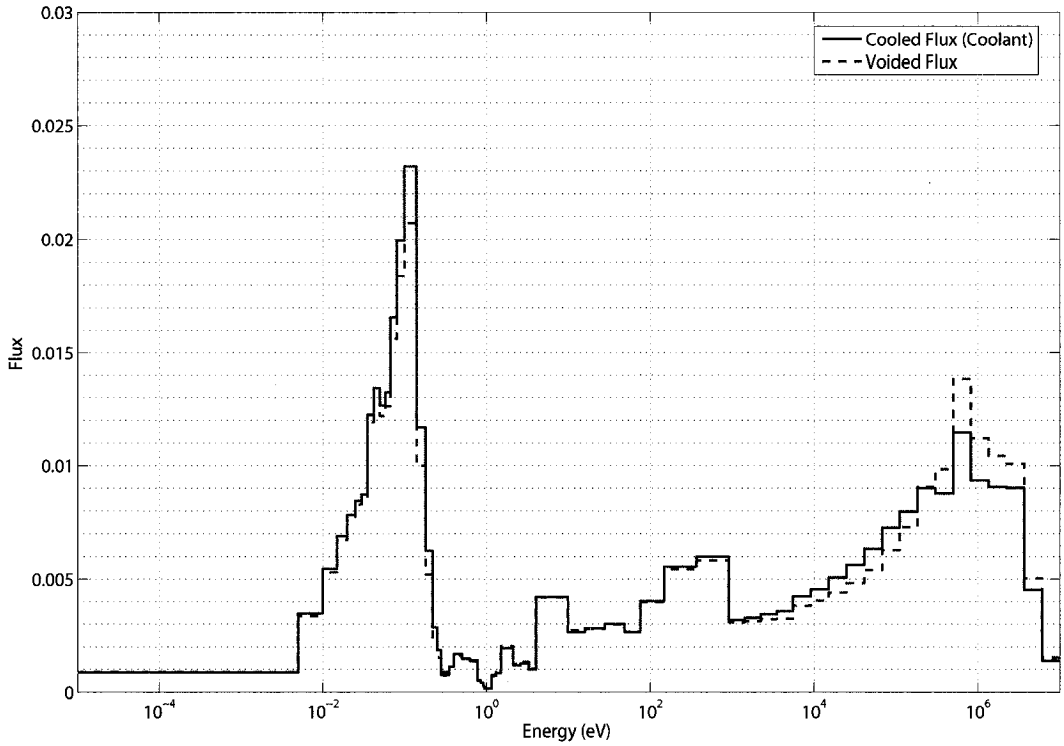

Figure 3.7 CANDU: Cooled and voided flux spectrums in the coolant

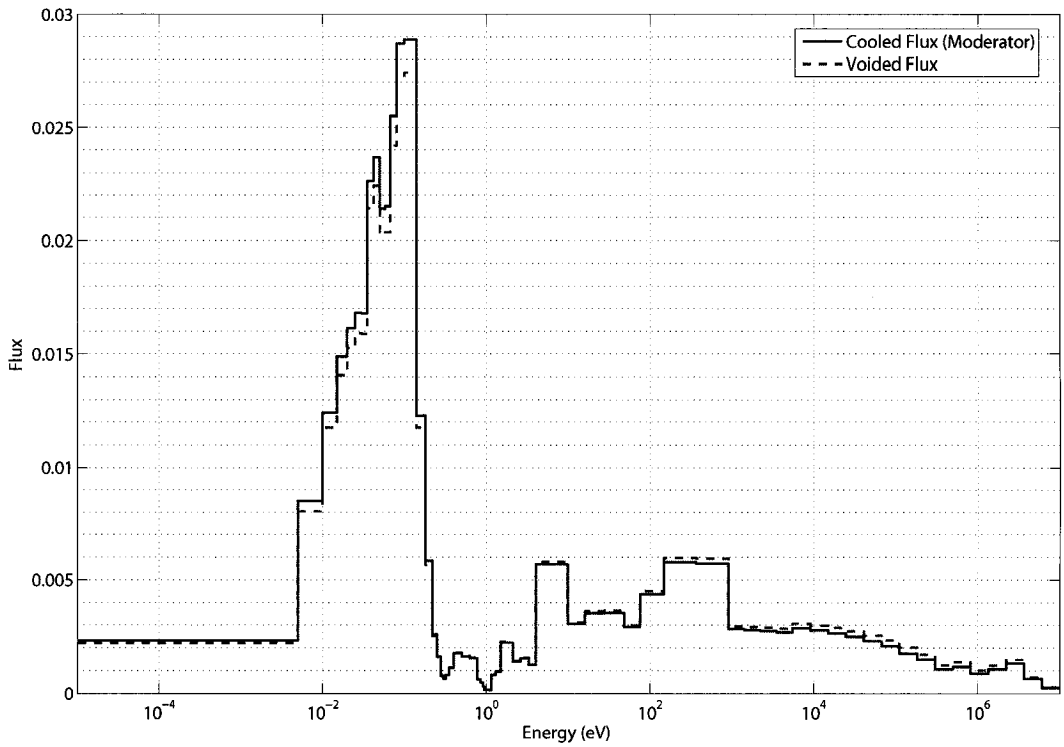

Figure 3.8 CANDU: Cooled and voided flux spectrums in the moderator

U235-EOC and Pu239-EOC are increased approximtely by 8.9E-3 and 3.1E-3% in the 4th ring). The higher thermal fluxes due to loss of hot coolant also results in a more positive sensitivity of void eigenvalue at low energy. The negative sensitivity at high energy is due to increasing fission neutron productions. This is because the burnable Dy poison is mainly consumed and the presence of higher remaining U235 and Pu239 with their fission reactions become the dominant effect.

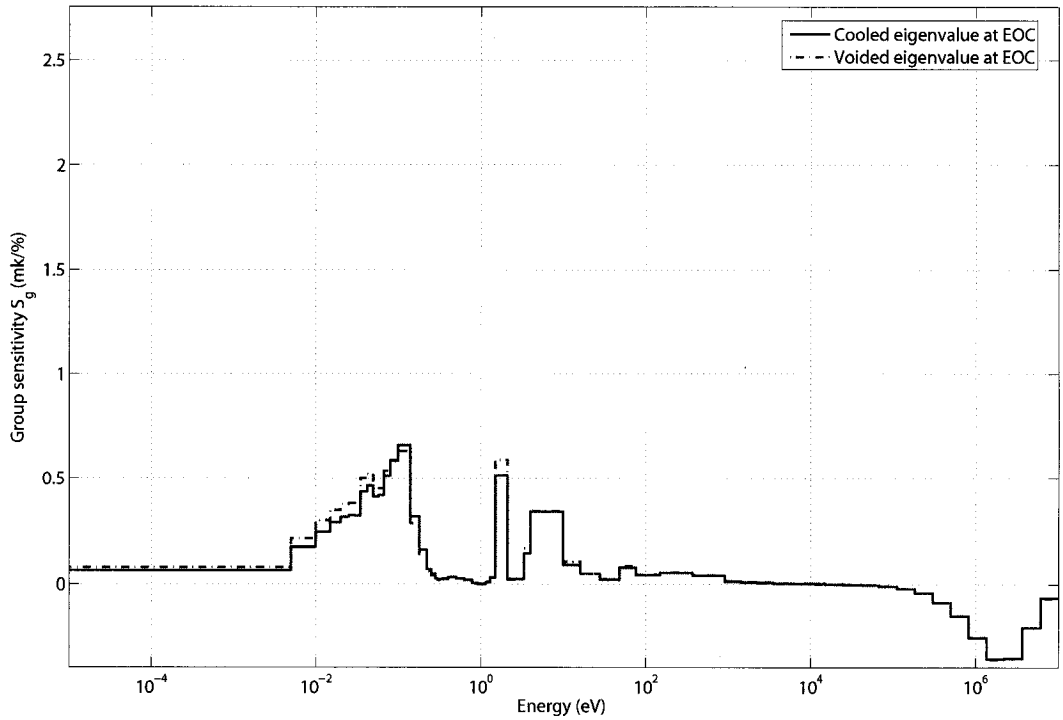

Figure 3.9 CANDU: Group sensitivity of cooled and voided eigenvalues (at EOC) to Dy density

The group sensitivity coefficients of CVR-BOC and CVR-EOC to Dy in Figure 3.10 are mainly negative due to the increasing absorptions by the higher thermal fluxes (thermal spectrum shifted) as mentioned previously. The positive sensitivity between 10^{-1} to 1.0 eV is due to the decreasing coolant scattering reactions and

shifted flux spectrum. CVR-EOC sensitivity is similar to the CVR-BOC sensitivity except for its smaller magnitude because Dy is mainly consumed at EOC.

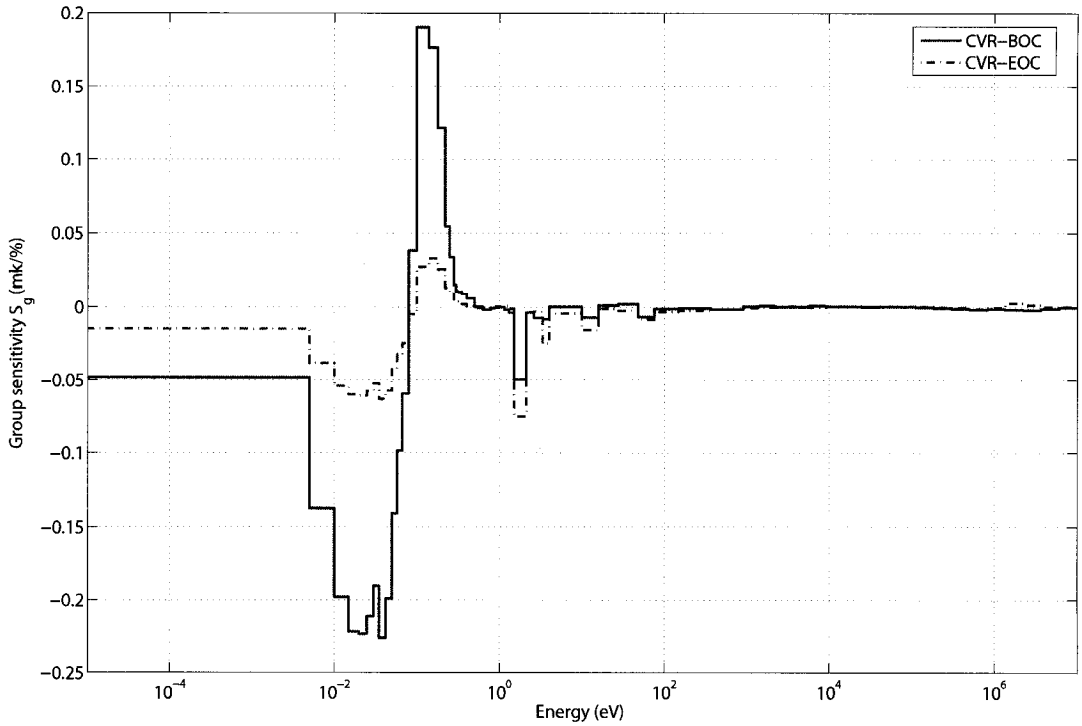

Figure 3.10 CANDU: Group sensitivity of CVR-BOC and CVR-EOC to Dy density

3.4.2 CANDU Eigenvalue and CVR Sensitivity Analysis to Gadolinium Density

We next consider the sensitivity coefficients of CVR and eigenvalues to Gadolinium density. The group sensitivity of cooled and void eigenvalues (at BOC) to Gd presented in Figure 3.11 are positive due to the increasing absorption rate corresponding to the increase of Gd. The sensitivity of void eigenvalue is higher than that of the cooled eigenvalue because of the higher thermalized fluxes (due to lower

up-scattering by hot coolant). One can see that the magnitude of eigenvalue sensitivity to Gd is approximately 10 times larger than eigenvalue coefficient to Dy because of the large thermal absorption cross sections of Gd compared with the Dy cross sections. The group sensitivity of cooled and void eigenvalues at EOC to Gd are presented in Figure 3.12. Both EOC eigenvalue coefficients are mostly diminished because the Gd having fast burning rate is depleted at EOC.

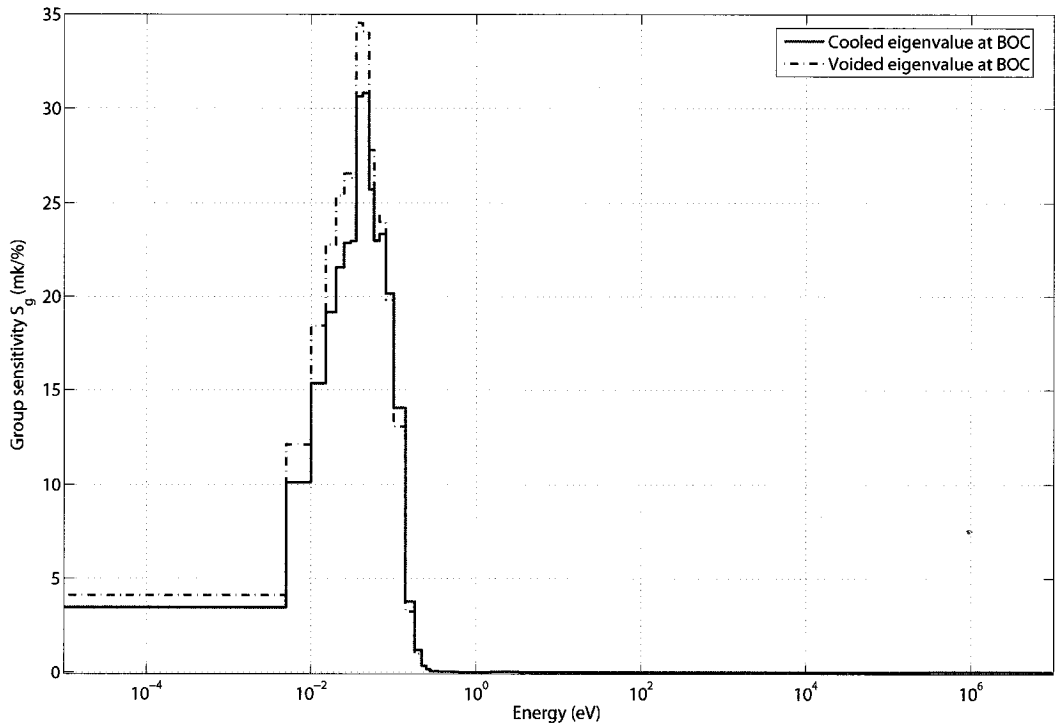

Figure 3.11 CANDU: Group sensitivity of cooled and voided eigenvalues (at BOC) to Gd density

The group sensitivity coefficients of CVR at BOC to Gd as presented in Figure 3.13 are mainly negative due to the increasing absorptions by the higher thermal fluxes as mentioned above. But the CVR-EOC sensitivity coefficient vanishes due to Gd burnout at EOC. One can see that the magnitude of CVR-BOC sensitivity to Gd is much higher than that of Dy. Gd is then more suitable for eliminating

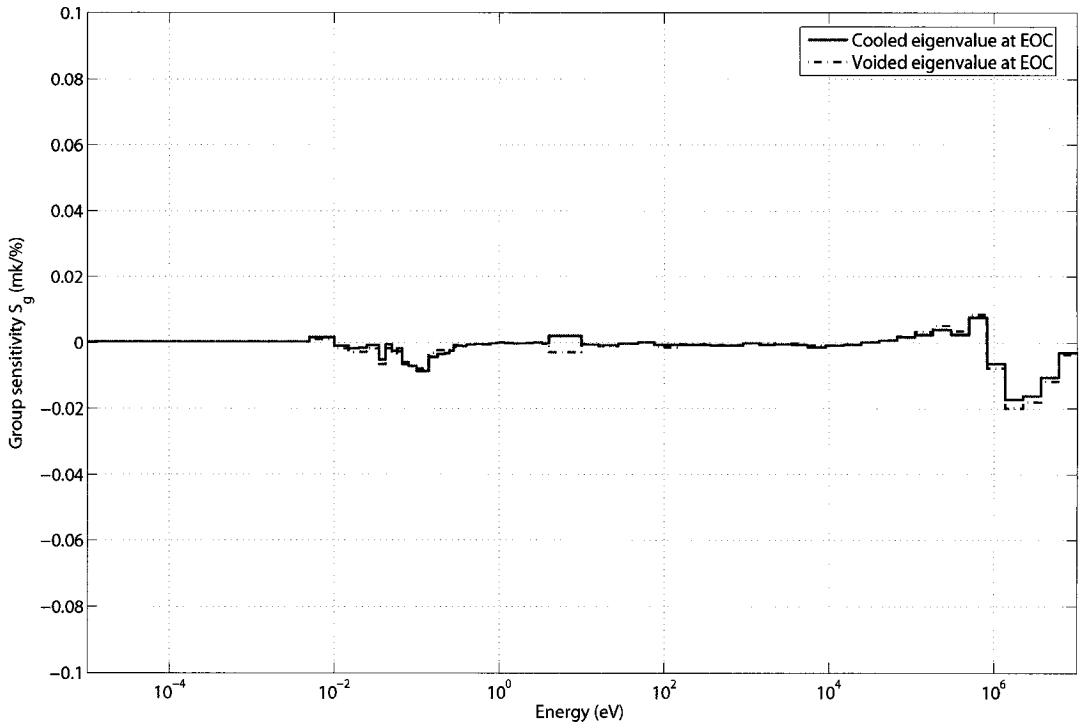

Figure 3.12 CANDU: Group sensitivity of cooled and voided eigenvalues (at EOC) to Gd density

CVR-BOC than Dy but Dy is more suitable for eliminating CVR-EOC. This is because Dy is consumed slower and remains at EOC, while Gd is mostly consumed at EOC (provided that Gd-BOC is lower than 20% otherwise the excessive Gd left from burnup process starts having a large impact at EOC).

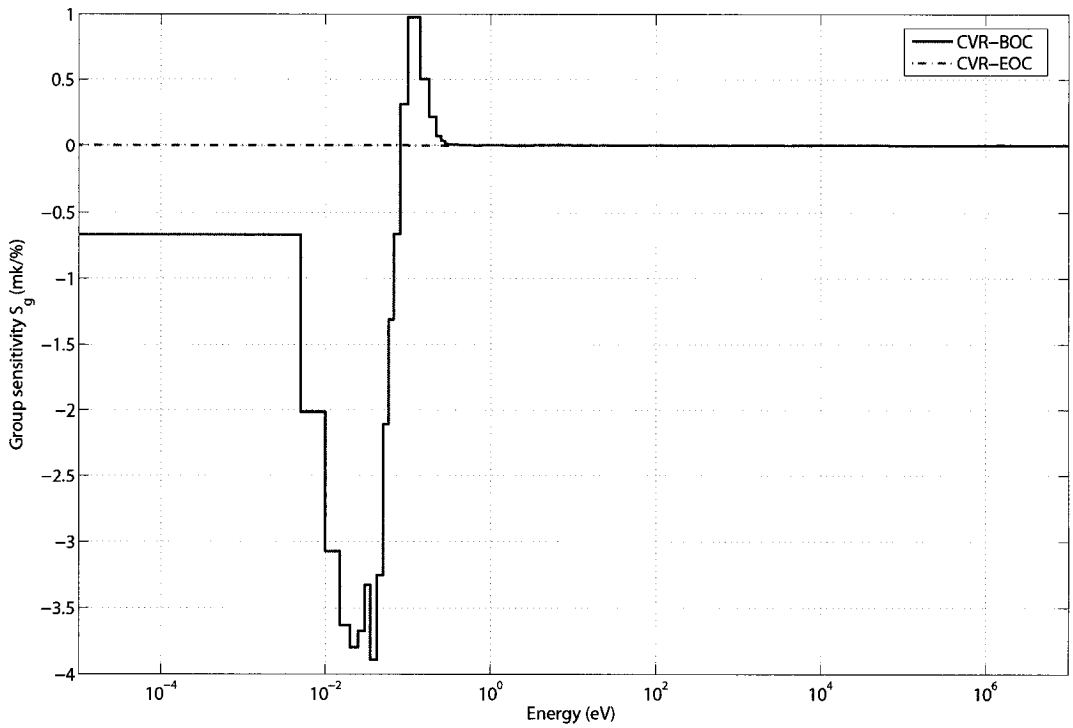

Figure 3.13 CANDU: Group sensitivity of CVR-BOC and CVR-EOC to Gd density

3.4.3 CANDU Eigenvalue and CVR Sensitivity Analysis to U235 Enrichment

The group sensitivity of cooled and void eigenvalues (at BOC) to Uranium enrichment in the outer rings are presented in Figure 3.14. The sensitivity coefficients are positive at low energy due to the increasing absorption rate corresponding to

the increase of U235. But absorption-to-fission neutron productions cause negative sensitivities at high energy. The sensitivity of void eigenvalue at low energy is slightly higher than the cooled because of the more thermalized fluxes as mentioned previously. From the U235 effects on CVR-BOC, the higher U235 results in the higher resonance capture that reduces the fissions upon coolant voiding. The sensitivity of void eigenvalue is then slightly more positive than the cooled sensitivity at high energy.

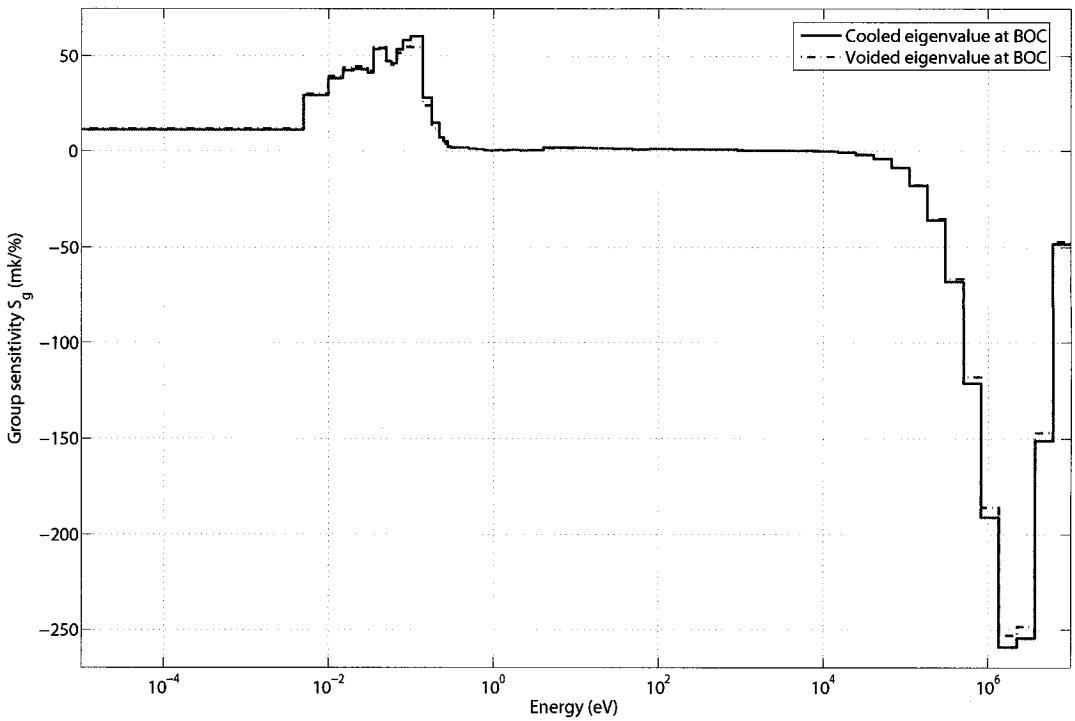

Figure 3.14 CANDU: Group sensitivity of cooled and voided eigenvalues (at BOC) to U235 enrichment

The group sensitivity of cooled and void eigenvalues (at EOC) to Uranium enrichment in the outer rings in Figure 3.15 are similar to those at BOC except the magnitude is much smaller because U235 are mainly consumed at EOC. The main difference is that the void sensitivity at high energy is more negative than the

cooled sensitivity. This is because the burnable poisons are mostly depleted and there is higher Pu239 produced at EOC when U235 is increased (see section 3.3). The coolant-voided fission then dominates at EOC and results in higher fission neutron productions.

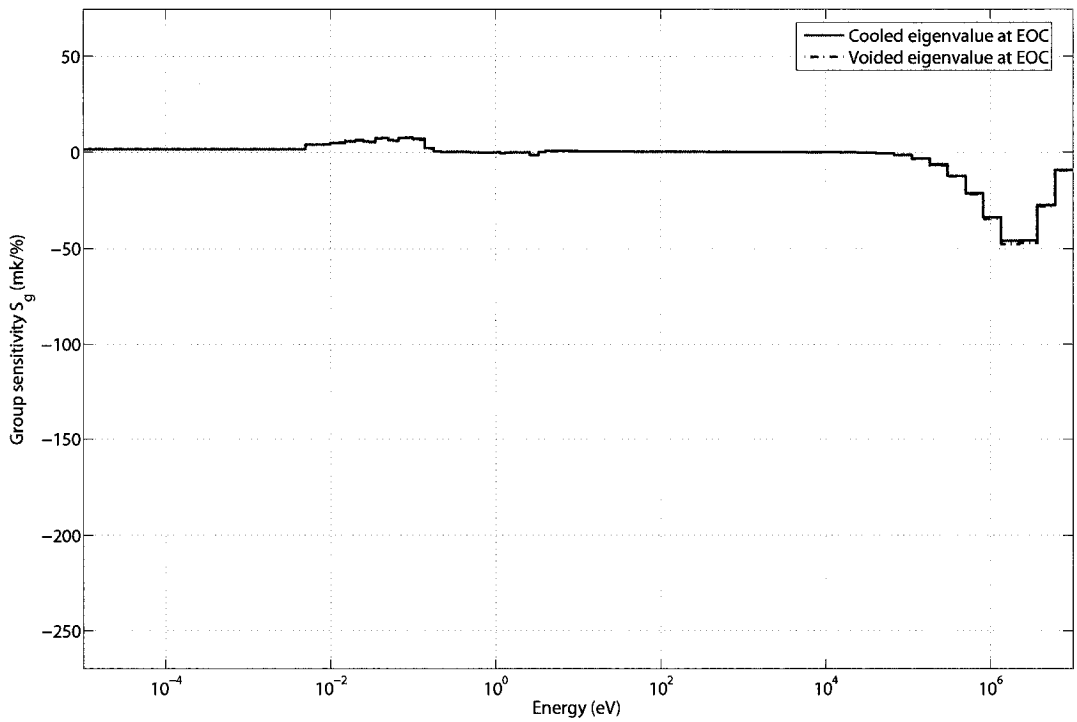

Figure 3.15 CANDU: Group sensitivity of cooled and voided eigenvalues (at EOC) to U235 enrichment

As presented in Figure 3.16, the CVR-BOC sensitivity is negative at high energy because of the increasing resonance capture in U235; on the other hand, the CVR-EOC sensitivity becomes positive due to the higher Pu239 at EOC.

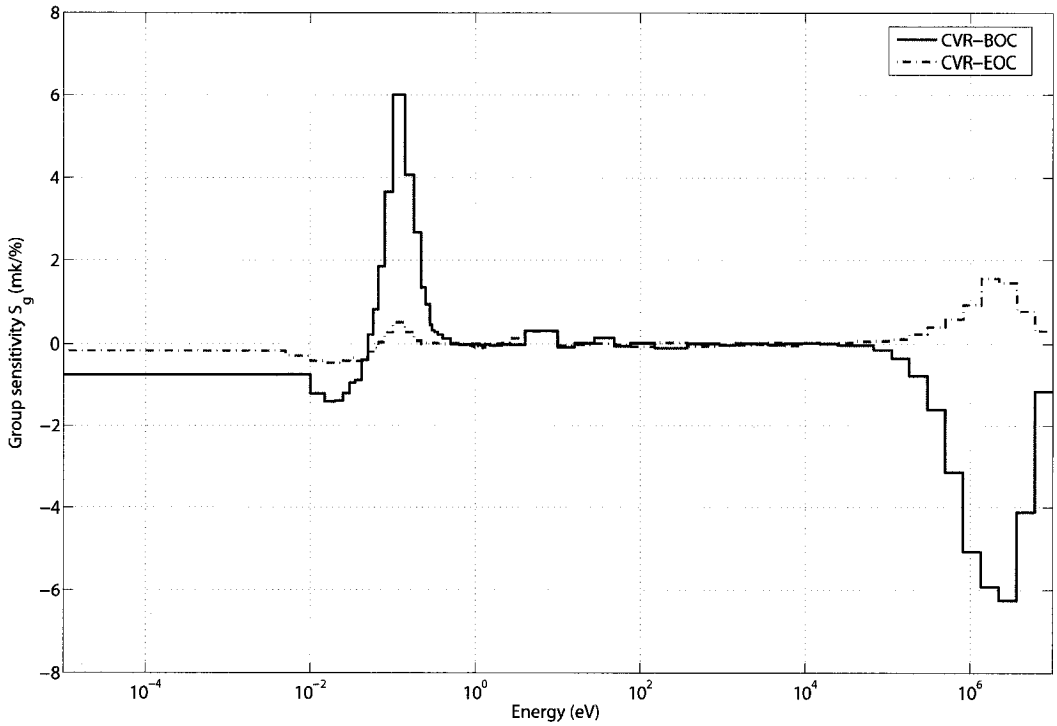

Figure 3.16 CANDU: Group sensitivity of CVR-BOC and CVR-EOC to U235 enrichment

3.5 Optimization Results

In our calculation procedures, we first discretize a 2-D 37 pin CANDU lattice into 42 regions according to the exact geometries. The 69 energy group nuclear cross sections are obtained from the WIMS-AECL library with 63 burnup/depleted nuclides. Exception made here is that the nuclear library of Gd152, Gd154, Gd156, Gd158 and Gd160 nuclides is not available in the WIMS-AECL library. Only the nuclear library of Gd155 and Gd157 is used in our calculations. The azimuthal angular integration for the MOCC method is performed using a 19 point Gaussian quadrature (ROY et al., 1991) while the polar integration consists in a 10 point Gauss-Legendre quadrature. The tracking density is 21 lines/cm. Periodic boundary conditions are used for this problem. For the lattice burnup/depletion calculations, we perform the calculation for 450 FPDs using the constant 31.9713kW/kgU burnup power to evaluate the neutron fluxes, CVR, cooled and void k_{eff} at each burnup step. The adjoint and flux importance functions of the cooled and void lattices are computed at BOC and EOC. The 19 burnup steps are at 0, 1, 5, 10, 20, 30, .., 50, 70, 90, ..,150, 200, 250, ..., 450 FPDs. The cooled and voided macroscopic cross sections in the library are corrected separately to take into account the self-shielding effects due to heavy nuclides at each step. Here we study 4 adjustment cases as follow,

1. The CVR-BOC and k_{eff}-EOC adjustments by searching the optimal Dy density in the central pin and U235 enrichment in the outer rings.
2. The CVR-BOC, CVR-EOC and k_{eff}-EOC adjustments by searching the Dy density and U235 enrichment.
3. The adjustments similar to Case 1 except that Dy is replaced with Gd.
4. The adjustments similar to Case 2 except that Dy is replaced with Gd.

Our objective is to obtain the desired CVR-BOC and CVR-EOC equal or less than the target values of +10 and +8 mk respectively, and to obtain k_{eff}-EOC equal to the target k_{eff}-EOC of 0.956510 (the same as the k_{eff} of the initial-unadjusted lattice at 300th FPD). The stopping criteria for optimization process is to obtain the relative errors of CVRs less than 1.0% and absolute relative error of k_{eff}-EOC less than 0.1%.

In the optimization process we first calculate the cooled and voided k_{eff} and sensitivity coefficients at BOC and EOC as explained in ARTICLE III for the cost function in (3.1). The weights $W_{c,BOC}$, $W_{c,EOC}$ and $W_{\lambda,BOC}$ are set to unity but $W_{\lambda,EOC}$ is set to 1000. This is because the adjustment of k_{eff}-EOC for extended burnup period is more important than the CVR adjustment. There is also a large difference between initial and target k_{eff}-EOC (-60mk) while the differences between initial and target CVR-BOC and CVR-EOC are approximately 6 mk. By setting all weights to unity we may instead obtain an optimal solutions that satisfy only the target CVRs. According to these weight selection, we allow the optimal results for CVRs and k_{eff}-BOC to slightly violate our predefined optimization constraints. For the case 1 and 3 where CVR-EOC is unconstrained, $W_{c,EOC}$ is set to zero.

3.5.1 Case 1: CVR-BOC and k_{eff}-EOC Adjustments with Dy

The first case is the CVR-BOC and k_{eff}-EOC adjustment of the CANDU lattice with the extended burnup period except that the CVR-EOC is unconstrained. The results for each adjustment step are presented in Table 3.1. From the final result, we obtain CVR-BOC of 10 mk (initial 16.2 mk) and k_{eff}-EOC of 0.956816 that meet our target requirements. The CVR and k_{eff} plots versus burnup time are presented in Figure 3.17 and 3.18. CVR rises quickly from 0th FPD to the first peak at 5th

FPD due to the Xe (marginal Sm) buildup, and it decreases gradually afterward. However, CVR rises up again at 50th FPD and reaches the 2nd peak at 400th FPD because of the Dy depletion. CVR-EOC of 12.58 mk is found higher than the initial CVR-EOC because of the higher U235-BOC that increases Pu239 production at EOC (see section 3.3). One also find that CBCVR of the final adjustment is lower than CVR over the burnup period as expected and the maximum CBCVR of 6.54 mk is found at 350th FPD. A problem then arises because the final BOC excess reactivity is approximately +100 mk higher than the excess reactivity of the initial-unadjusted lattice. This is because the lattice needs to produce the constant power for the extended period and must satisfy the k_{eff}-EOC requirement at 450th FPD. One may require the additional procedures to eliminate the excess reactivity such as the soluble poisoning or refueling schemes for full-core system. If one tries to lower k_{eff}-BOC by increasing Dy, the increasing Dy shall also lower k_{eff}-EOC (due to the higher Dy left at EOC) and thus the additional U235 is required to compensate the lower k_{eff}-EOC.

3.5.2 Case 2: CVR-BOC, CVR-EOC and k_{eff}-EOC Adjustments with Dy

For the second case, we extend the first case to the CVR-BOC, CVR-EOC and k_{eff}-EOC adjustment. The results of Dy, U235 and sensitivity coefficients from the 4th step of the first case is used as the initial step. The adjustment results are presented in Table 3.2. From the final result, we obtain the desired CVR-BOC, CVR-EOC and k_{eff}-EOC that meet our target requirements. We obtain the optimal Dy and U235 of 14.44 and 1.3848% that are higher than the optimal result in the first case. This is because higher Dy is required to reduce the CVR-EOC but in the mean time Dy also lower k_{eff}-EOC. We then need the additional U235 to compensate the higher Dy absorption and increase k_{eff}-EOC. The CVR and k_{eff} plots are shown

Table 3.1 Case 1 : Adjustment Results

Steps	Dy (%)	$U235$ in Outer rings (%)	$S^{Dy_{BOC}}_{CVR_{BOC}}$ $S^{Dy_{BOC}}_{\lambda_{EOC}}$ [mk/%]	$S^{U235_{BOC}}_{CVR_{BOC}}$ $S^{U235_{BOC}}_{\lambda_{EOC}}$ [mk/%]	CVR_{BOC} CVR_{MAX} CVR_{EOC} [mk]	$k_{eff,BOC}$ $k_{eff,EOC}$
1	0.000	0.7114	-1.39591E+0 6.38469E+0	-1.46040E+1 -9.74368E+1	16.20 16.87 12.10	1.116370 0.905379
2	1.296	1.000	-1.00749E+0 5.56666E+0	-6.66887E+0 -1.37302E+2	11.79 12.89 12.56	1.220517 0.936448
3	1.842	1.185	-8.32429E-1 5.17047E+0	-3.93659E+0 -1.52715E+2	10.29 13.02 12.94	1.275732 0.964822
4	2.380	1.145	-7.66093E-1 5.00957E+0	-4.52711E+0 -1.50222E+2	10.04 12.65 12.55	1.254704 0.955292
5	2.380	1.153	-	-	10.00 12.67 12.58	1.257608 0.956816

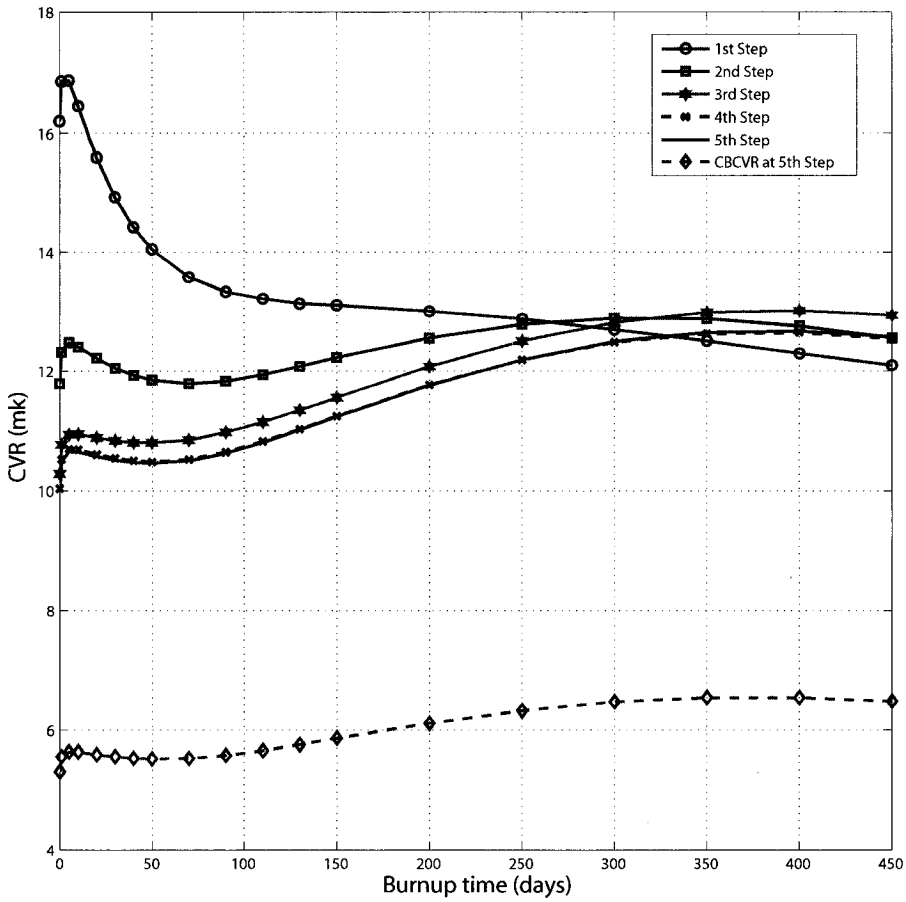

Figure 3.17 CANDU Case 1 : CVR plot versus burnup time

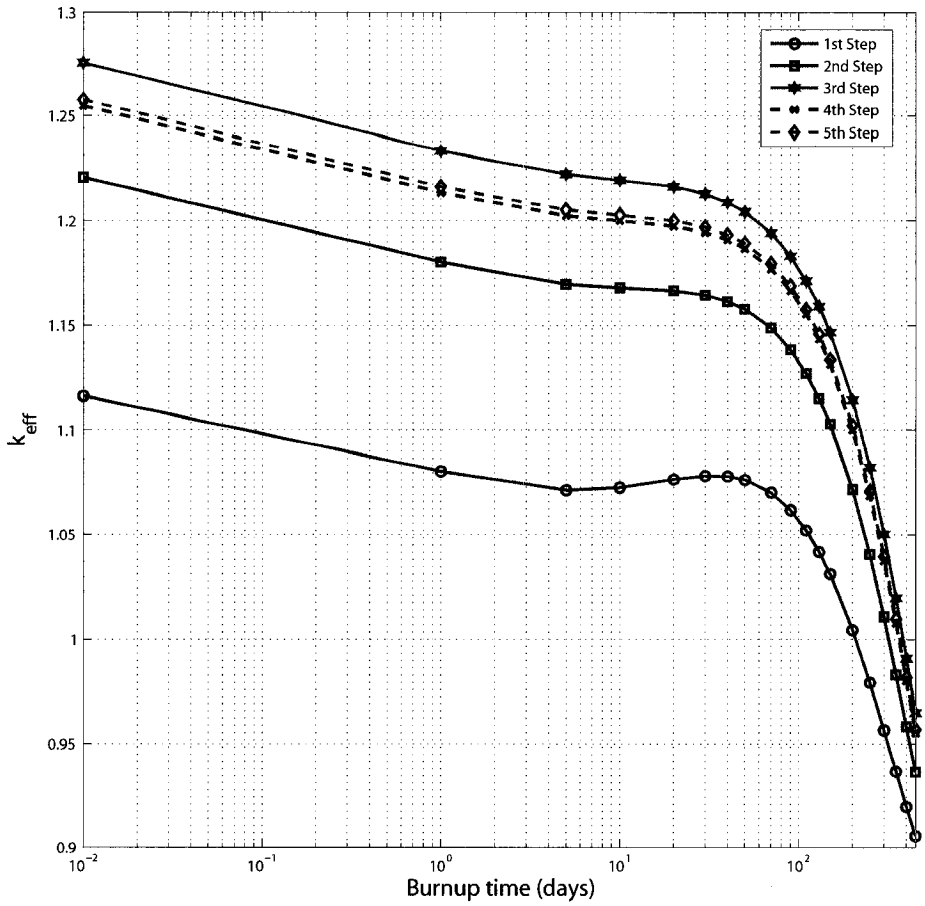

Figure 3.18 CANDU Case 1 : k_{eff} plot versus burnup time

in Figure 3.19 and 3.20. The CVR is found lower than 8.07 mk over the complete burnup period. Initially we assume that the 2nd CVR peak would be higher than the target CVR-EOC of 8mk. But the CVR does not reach its 2nd peak within 450 FPDs due to the high Dy-BOC of 14.44%. CBCVR is lower than CVR over the burnup period as expected. A maximum CBCVR of +4.68 mk is found at EOC.

Table 3.2 Case 2 : Adjustment Results

Steps	Dy (%)	$U235$ in Outer rings (%)	$S^{Dy_{BOC}}_{CVR_{BOC}}$ $S^{Dy_{BOC}}_{CVR_{EOC}}$ $S^{Dy_{BOC}}_{\lambda_{EOC}}$ [mk/%]	$S^{U235_{BOC}}_{CVR_{BOC}}$ $S^{U235_{BOC}}_{CVR_{EOC}}$ $S^{U235_{BOC}}_{\lambda_{EOC}}$ [mk/%]	CVR_{BOC} CVR_{MAX} CVR_{EOC} [mk]	$k_{eff,BOC}$ $k_{eff,EOC}$
1	2.380	1.145	-7.66093E-1 -5.11821E-1 5.00957E+0	-4.52711E+0 2.79499E+0 -1.50222E+2	10.04 12.65 12.55	1.254704 0.9552921
2	15.932	1.605	-8.55872E-2 -1.79952E-1 1.71087E+0	-1.44173E+0 1.73542E+0 -1.66564E+2	5.25 8.13 8.13	1.314581 0.994706
3	14.156	1.346	-1.00747E-1 -2.45397E-1 2.25648E+0	-2.25450E+0 2.67412E+0 -1.66179E+2	5.80 8.06 8.06	1.252365 0.949774
4	14.710	1.397	-1.00262E-1 -2.26840E-1 2.11180E+0	-1.67601E+0 2.23442E+0 -1.67644E+2	5.65 8.02 8.02	1.265510 0.957757
5	14.440	1.385	-	-	5.70 8.07 8.07	1.262722 0.956195

3.5.3 Case 3: CVR-BOC and k_{eff}-EOC Adjustments with Gd

The third case is the CVR-BOC and k_{eff}-EOC adjustments for the CANDU lattice with the extended burnup period but CVR-EOC is unconstrained. The results for each step are presented in Table 3.3. From the final result we obtain CVR-BOC

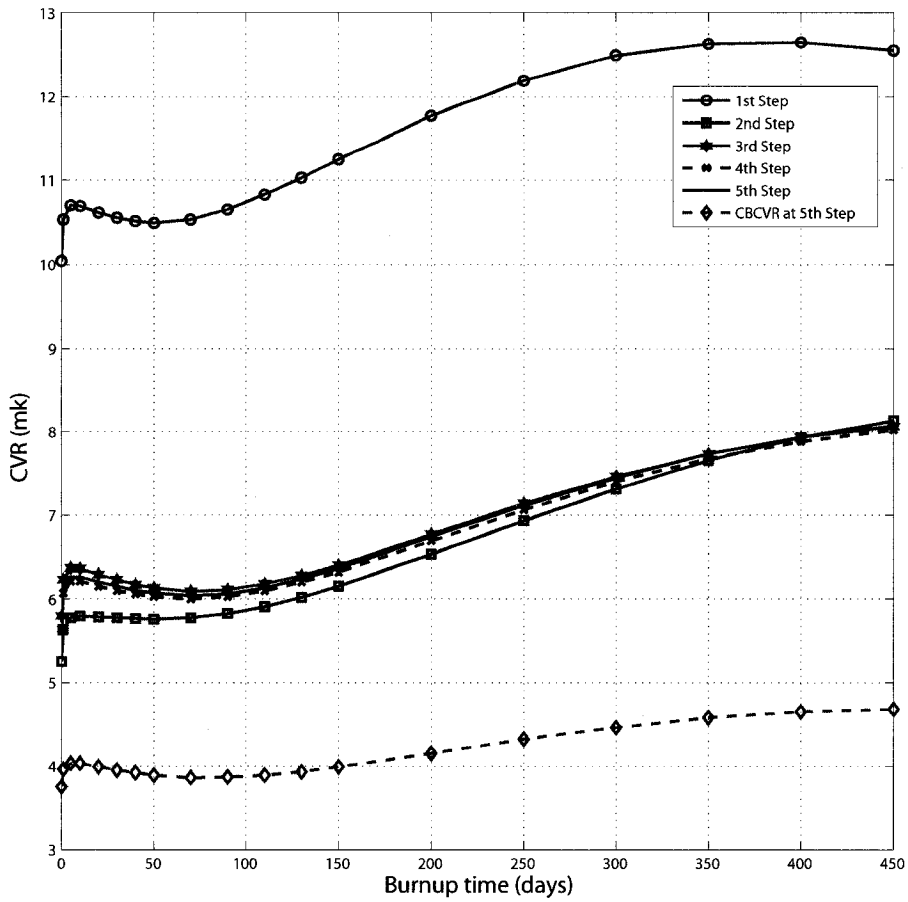

Figure 3.19 CANDU Case 2 : CVR plot versus burnup time

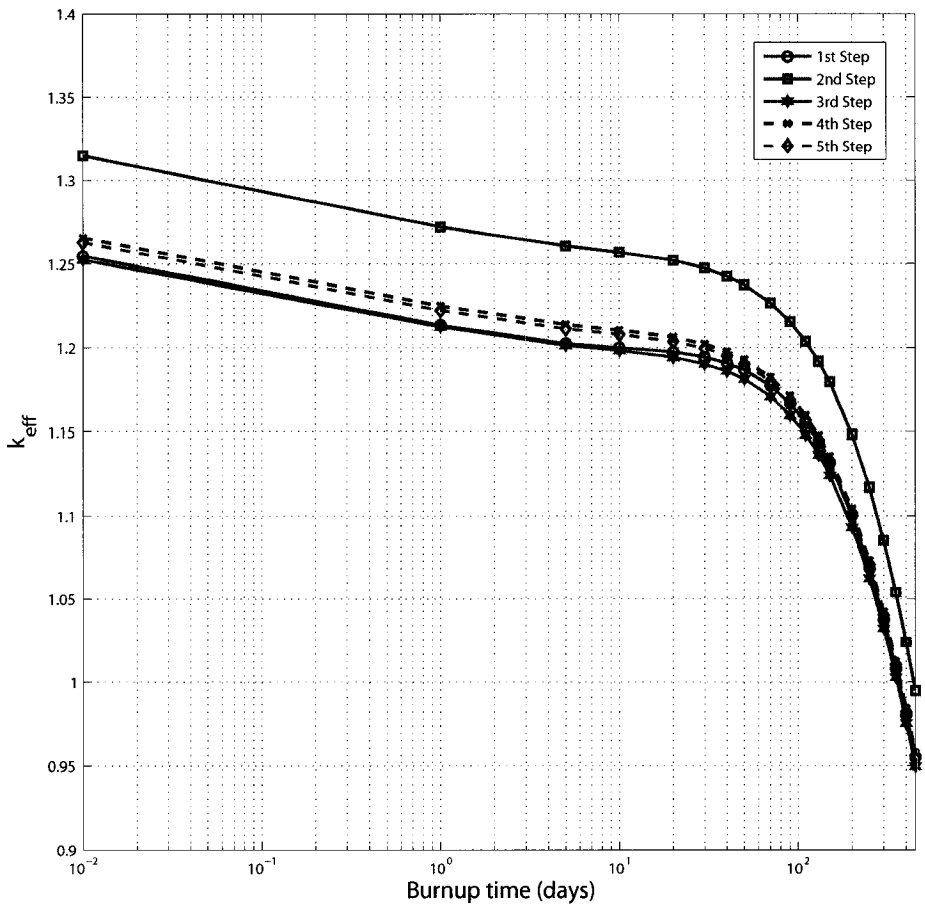

Figure 3.20 CANDU Case 2 : k_{eff} plot versus burnup time

of +6.00 mk and k_{eff}-EOC of 0.956789 that meet our targets. The CVR and k_{eff} plots are presented in Figure 3.21 and 3.22. From the CVR plot in the final step, the CVR first rises quickly from 0th FPD, reaches the first peak at 5th FPD and decreases gradually afterward. However, at 50th FPD the CVR rises again and continues rising until 450th FPD due to the Gd depletion. CVR is found equal or below +10 mk for the first 300 FPDs and above +10 mk afterward. CVR-EOC become higher than the initial-unadjusted CVR-EOC of 12.1 mk because of the increasing U235-BOC and higher Pu239 produced at EOC (see the effect of U235 on CVR-EOC in Section 3.3). In addition CBCVR is found lower than CVR over the burnup period as expected. From the final result Gd is mainly consumed at EOC. The CVR and eigenvalue coefficients at EOC then become insensitive to Gd. The BOC excess reactivity is +24.22 mk higher than that of the initial lattice. One may need a procedure to eliminate this excess reactivity.

3.5.4 Case 4: CVR-BOC, CVR-EOC and k_{eff}-EOC Adjustments with Gd

The fourth case is the extension of the third case for the CVR-BOC, CVR-EOC and k_{eff}-EOC adjustments. We select the initial Gd of 50% corresponding to CVR-EOC of +8 mk from the Gd effect on CVR-EOC in Figure 3.3. An initial U235-BOC of 1.25% is selected. The adjustment results for each step are presented in Table 3.4 We obtain the desired CVR-BOC, CVR-EOC and k_{eff}-EOC within our criteria. The CVR and k_{eff} plots versus burnup period are shown in Figure 3.23 and 3.24. The CVR is equal or lower than +8.28 mk over the burnup period. CBCVR is always lower than CVR over the complete burnp period as expected. In this case the BOC excess reactivity is ~94mk higher than the initial lattice. The soluble poisons may be required to eliminate this excess reactivity.

Table 3.3 Case 3 : Adjustment Results

Steps	Gd (%)	$U235$ in Outer rings (%)	$S^{Gd_{BOC}}_{CVR_{BOC}}$ $S^{Gd_{BOC}}_{\lambda_{EOC}}$ [mk/%]	$S^{U235_{BOC}}_{CVR_{BOC}}$ $S^{U235_{BOC}}_{\lambda_{EOC}}$ [mk/%]	CVR_{BOC} CVR_{MAX} CVR_{EOC} [mk]	$k_{eff,BOC}$ $k_{eff,EOC}$
1	0.000	0.7114	-2.96420E+1 -1.95191E-1	-1.47250E+1 -9.70769E+1	16.20 16.87 12.10	1.116370 0.905379
2	0.9305	1.314	-1.25212E+0 0.00000E+0	-1.34164E+0 -1.57058E+2	6.10 14.25 14.25	1.277315 0.998094
3	4.9420	1.037	2.41733E-2 -1.98835E-2	-2.79566E+0 -1.40362E+2	5.90 13.76 13.42	1.153371 0.948812
4	28.300	1.097	-6.47398E-3 -2.90267E-2	-2.99308E+0 -1.45626E+2	5.88 14.07 13.83	1.162653 0.961774
5	28.518	1.058	- -	- -	6.00 13.68 13.68	1.147395 0.956789

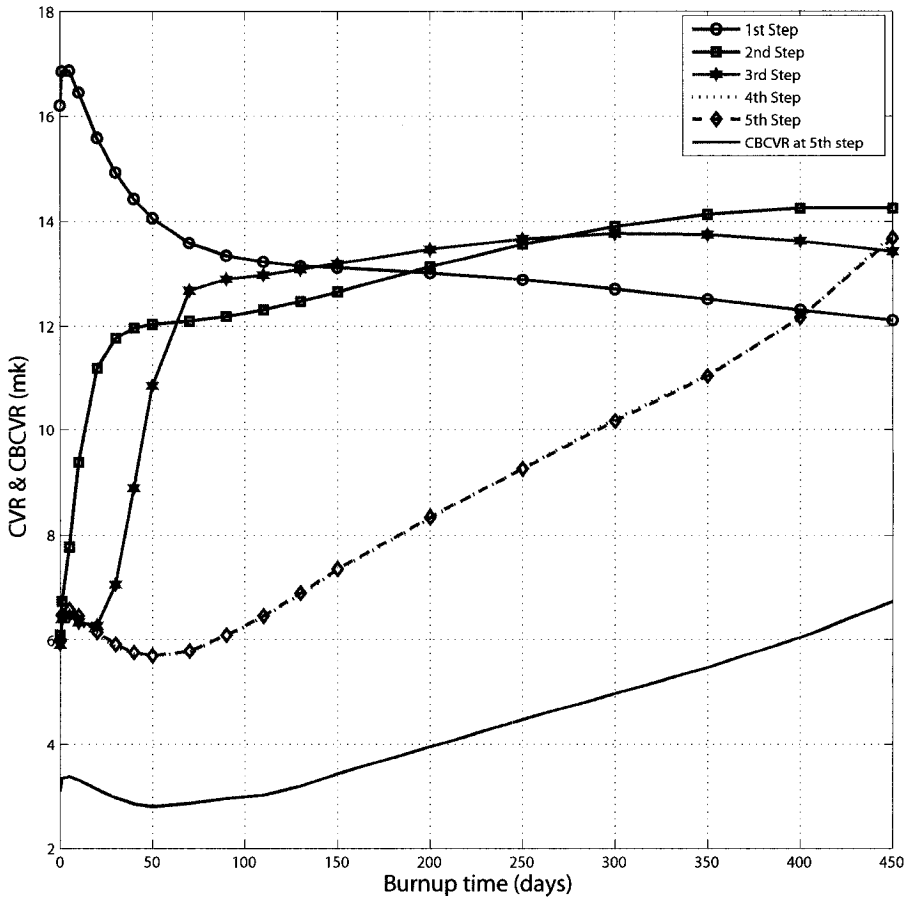

Figure 3.21 CANDU Case 3 : CVR plot versus burnup time

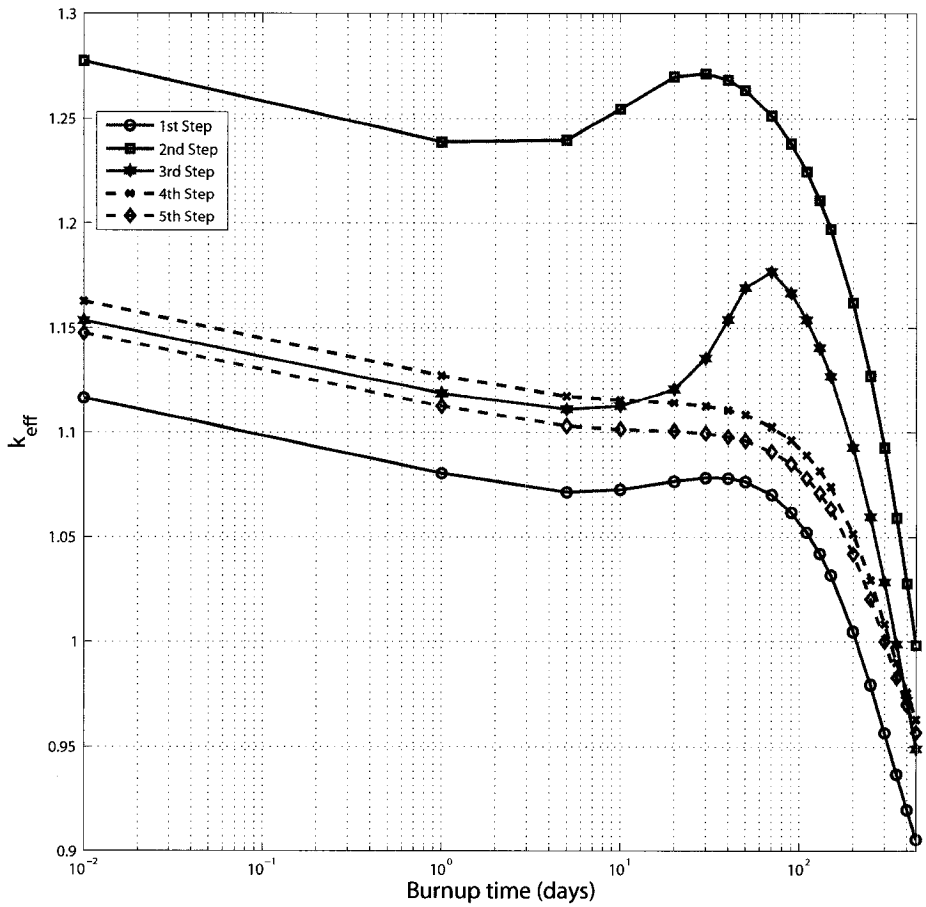

Figure 3.22 CANDU Case 3 : k_{eff} plot versus burnup time

3.6 Conclusion

Here the optimization and adjoint sensitivity techniques are applied to the CVR-BOC, CVR-EOC and k_{eff}-EOC adjustments for a CANDU lattice with the extended burnup period of 450 FPDs. In the first and third adjustment cases, we can reduce the control reactivity worths for positive CVR protection by 4.20 and 3.19 mk respectively, and obtain the CVR-BOC and k_{eff}-EOC according to the target requirements. In the second and fourth adjustment cases, we can reduce the control reactivity worths by 8.80 and 8.59 mk respectively. For the CVR-BOC and k_{eff}-EOC adjustments, Gd is more suitable than Dy to lower the CVR-BOC because the CANDU lattice with Gd requires lower U235 enrichment. For the CVR-BOC, CVR-EOC and k_{eff}-EOC adjustments, the CANDU lattice with Gd is also more suitable due to its lower U235 requirement. This will not be the case if one tries to lower CVR-EOC in the fourth case to exact 8.07 mk. The lattice with Gd then requires slightly higher U235 enrichment. In our study here, we allow the optimal CVRs to slightly violate the predefined constraints because we consider the k_{eff}-EOC adjustment to be more important than the CVR adjustments in the extended burnup problem. In addition, when combining the fast and slow burning effects of Gd and Dy, Gd effectively reduces the CVR and excess reactivity at the beginning of cycle (as in the third case). After Gd is mainly consumed, Dy then takes effect to reduce CVR until the end of cycle similar to the second case (CVR-EOC is more sensitive to Dy than Gd). By combining Gd and Dy effects in the central pin, the lattice would require lower Dy than in the second case, and then lower Gd and U235 than that in the fourth case.

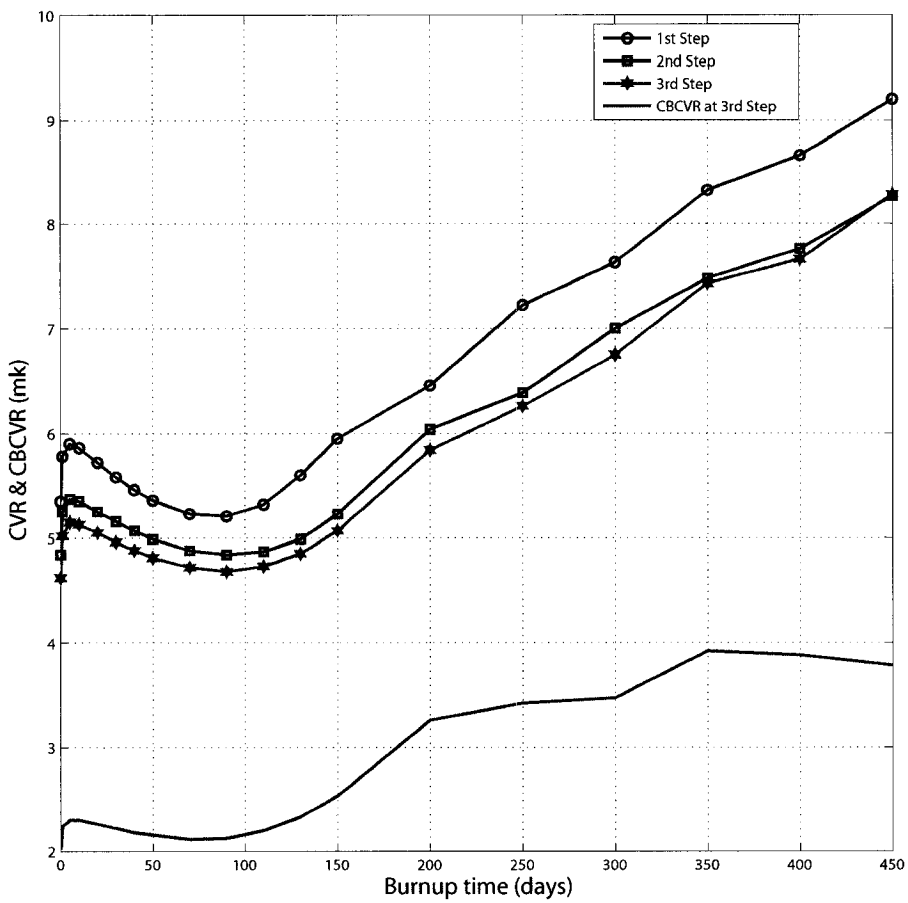

Figure 3.23 CANDU Case 4 : CVR plot versus burnup time

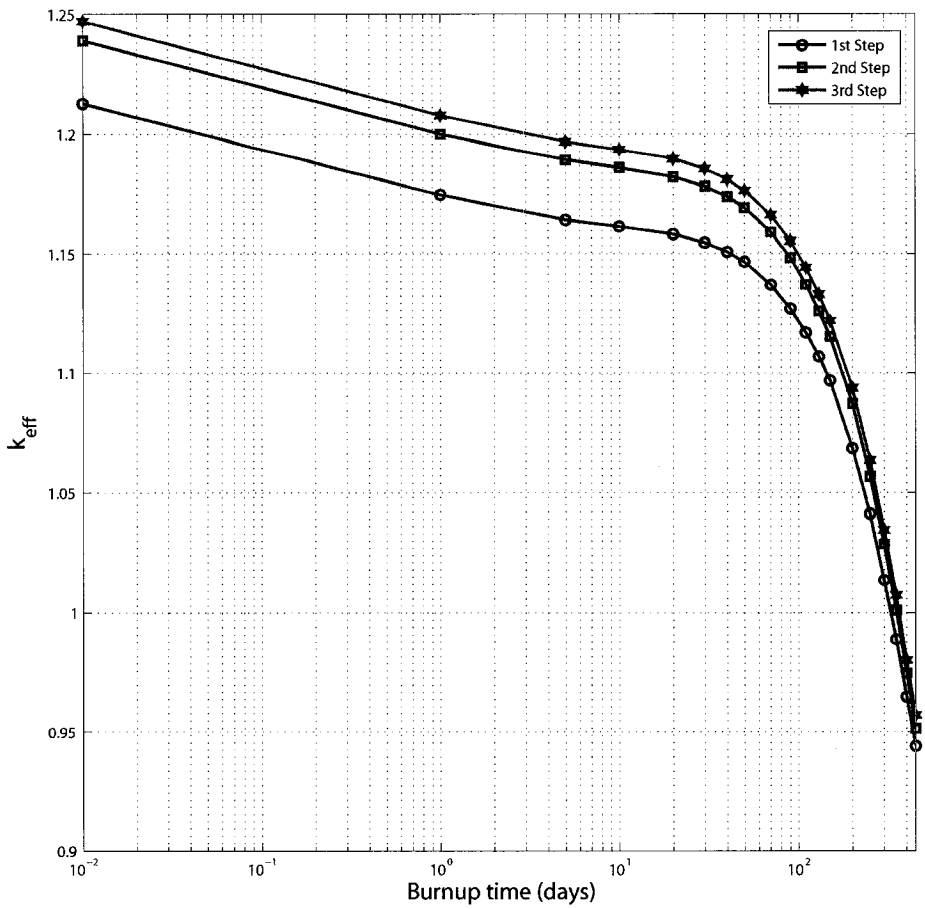

Figure 3.24 CANDU Case 4 : k_{eff} plot versus burnup time

Table 3.4 Case 4 : Adjustment Results

Steps	Gd (%)	$U235$ in Outer rings (%)	$S^{Gd_{BOC}}_{CVR_{BOC}}$ $S^{Gd_{BOC}}_{CVR_{EOC}}$ $S^{Gd_{BOC}}_{\lambda_{EOC}}$ [mk/%]	$S^{U235_{BOC}}_{CVR_{BOC}}$ $S^{U235_{BOC}}_{CVR_{EOC}}$ $S^{U235_{BOC}}_{\lambda_{EOC}}$ [mk/%]	CVR_{BOC} CVR_{MAX} CVR_{EOC} [mk]	$k_{eff,BOC}$ $k_{eff,EOC}$
1	50.000	1.250	-8.01583E-3 -1.03930E-2 1.21387E-1	-2.01753E+0 1.72835E+0 -1.65866E+2	5.35 9.20 9.20	1.212576 0.944034
2	59.980	1.341	-7.75474E-3 -1.10496E-2 9.90696E-2	-1.63741E+0 3.39929E+0 -1.72462E+2	4.84 8.26 8.26	1.239124 0.951564
3	62.478	1.374	-	-	4.62 8.28 8.28	1.246963 0.956821

CHAPTER 4

CBCVR ADJUSTMENT IN CANFLEX-FUELED ACR LATTICES WITH GADOLINIUM IN CENTRAL PIN

4.1 Problem Descriptions

In this chapter we study the CBCVR-BOC and k_{eff}-EOC adjustments for a CANFLEX ACR lattice similar to the third case study in ARTICLE III except that Dysprosium is replaced with Gadolinium in the central pin. The objective of this study is to obtain the target CBCVR-BOC of -2 mk and k_{eff}-EOC of 0.900 by searching for the optimal Gd density (%wt) in the central pin and U235 enrichment (%) in the 42 outer fuel pins. As mentioned in the previous chapter, Gd having larger absorption cross sections than Dy shall be consumed at a faster rate. When the same amount of Dy and Gd is applied, the ACR lattice with Gd has a higher k_{eff}-EOC than the ACR lattice with Dy and thus requires lower U235 enrichment to obtain the same k_{eff}-EOC. Here CBCVR-EOC is unconstrained in the optimization process because the Gd effect on CBCVR-BOC and CBCVR-EOC (explained in the next section) indicates that the Gd density of 99% is required to lower CBCVR-BOC down to the minimum value of $\sim$+3 mk and the corresponding CBCVR-EOC of -2.82 mk is obtained at this Gd density. We can then avoid the calculation of sensitivity coefficients of CBCVR-EOC and checkerboard-voided (CBVOID) eigenvalue with respect to Gd and U235 at EOC. In addition the U235 effect on CBCVR-BOC and CBCVR-EOC shows that the minimum CBCVR-BOC is positive. One can foresee that the optimized CBCVR-BOC would not meet the target CBCVR-BOC of -2 mk. The cost functional for optimization procedure is similar to that defined in Eq. (3.1) except that CVR is replaced with CBCVR.

$W_{c,BOC}$, $W_{\lambda,EOC}$ and $W_{\lambda,BOC}$ are set equal to unity so that the equal importance for CBCVR-BOC, k_{eff}-EOC and the penalty functional of k_{eff}-BOC is imposed on the optimization process. $W_{c,EOC}$ is set to zero due to the unconstrained CBCVR-EOC. The burnup/depletion calculation, the calculation of sensitivity coefficients and optimization procedures are similar to that presented in ARTICLE III.

4.2 Effects of U235 and Gadolinium on ACR-CVR and ACR-CBCVR

As illustrated in Figure 4.1, we first study the effects of U235 enrichment in the outer rings on CBCVR-BOC, CBCVR-EOC and CVR-BOC for a lattice with 4.6% Gd and 0.7114% U235 in the central pin. Similar to that presented in ARTICLE III, both CVR-BOC and CBCVR-BOC rapidly decrease with the increasing U235 enrichment between 0 to 4% because the higher U235 having large resonance capture cross sections increases the resonance capture due to the hardened flux spectrum and subsequently lowers the fast fissions upon coolant voiding. For U235 between 0.5 to 2.0%, CBCVR-EOC is increased with U235 due to the higher Pu239 production that results in higher CBVOID fission. We find that Pu239-EOC increases with the U235-BOC and reaches the maximum value at 5.0% U235 (~20% increase in density compared with Pu239 in the initial 2% U235 ACR lattice). When U235 > 2.0%, CBCVR-EOC starts decreasing because the resonance capture in the increasing U235-EOC dominates over the coolant-voided fast fission in Pu239-EOC. As mentioned in ARTICLE III, CVR-BOC is lower than CBCVR-BOC because ACR lattices have the strong spatial coupling among the adjacent lattice that causes the coupled coolant-moderation between the cooled and voided lattices, the less hardened CBVOID spectrum and the lower resonance captures.

The effects of Gd density in the central pin on CBCVR-BOC, CBCVR-EOC and CVR-BOC is presented in Figure 4.2. For $0 < Gd < 5\%$, Gd abruptly decreases

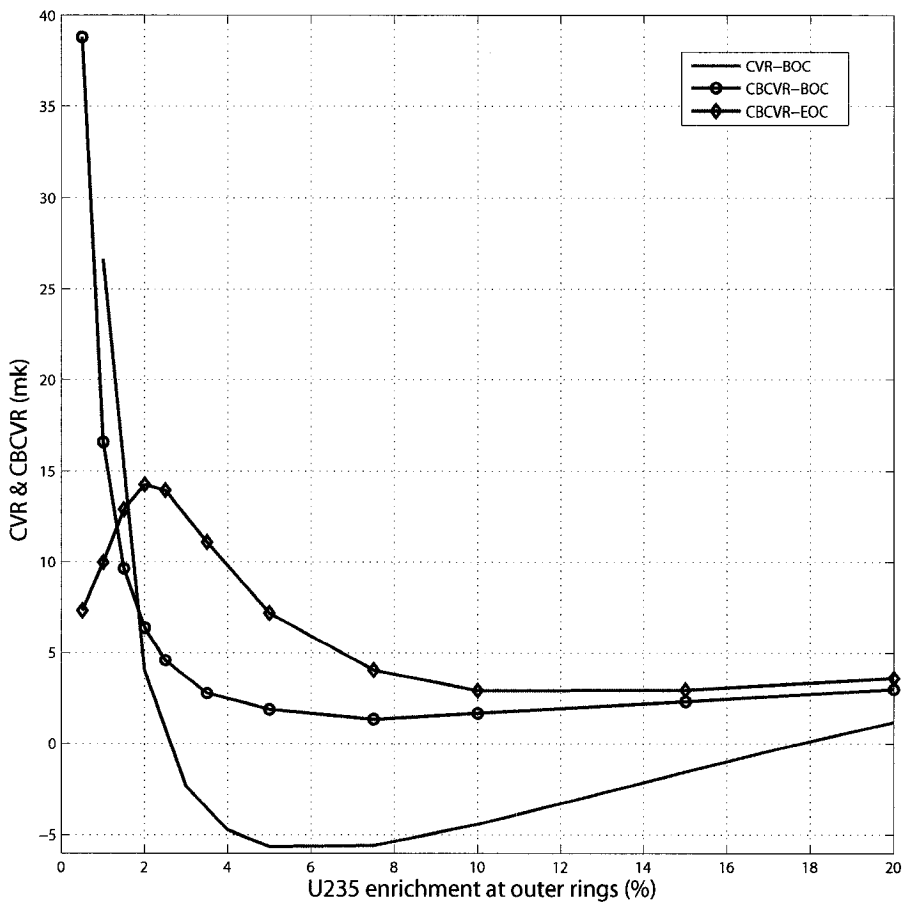

Figure 4.1 ACR: U235 effect on CBCVR-BOC, CBCVR-EOC and CVR-BOC

CVR-BOC and CBCVR-BOC because its large thermal and resonance absorption cross sections partially eliminates the fast fission due to the hardened flux spectrum. When the Gd is greater than 5%, CVR-BOC and CBCVR-BOC change slowly due to the dominating self-shielding effects of Gd. For Gd between 0 and 20%, CBCVR-EOC remains in the same level because Gd is mainly consumed at EOC. For Gd $\geq$ 20%, the excessive Gd is left from the fuel burnup at EOC and effectively lowers CBCVR-EOC. In our case, the target CBCVR-BOC is set to -2 mk. One can estimate that the optimal Gd would be as high as 100% and the optimal CBCVR-BOC would not meet its target value.

4.3 ACR Eigenvalue and CVR Sensitivity Analysis to Gadolinium Density

Next we study the sensitivity coefficients of CVR and eigenvalues to Gadolinium density. The group sensitivity of cooled and void eigenvalues (at BOC) to Gd presented in Figure 4.3 are positive due to the increasing absorption rate corresponding to the increasing Gd. The sensitivity of void eigenvalue is higher than the cooled because of the hardened flux spectrum during the coolant voiding.

The group sensitivity of cooled and void eigenvalues at EOC to Gd are presented in Figure 4.4. Both EOC eigenvalue coefficients at low energy are diminished because the Gd is mainly depleted at EOC. However, when Gd is increased at BOC, there are higher Pu239 and U235 left at EOC that result in the higher neutron production and the negative coefficients at high energy. The void coefficient is more negative than the cooled at high energy because the burnable poisons including Gd are depleted and the coolant-voided fission becomes dominant at EOC.

The group sensitivity coefficients of CVR at BOC to Gd as presented in Figure 4.5

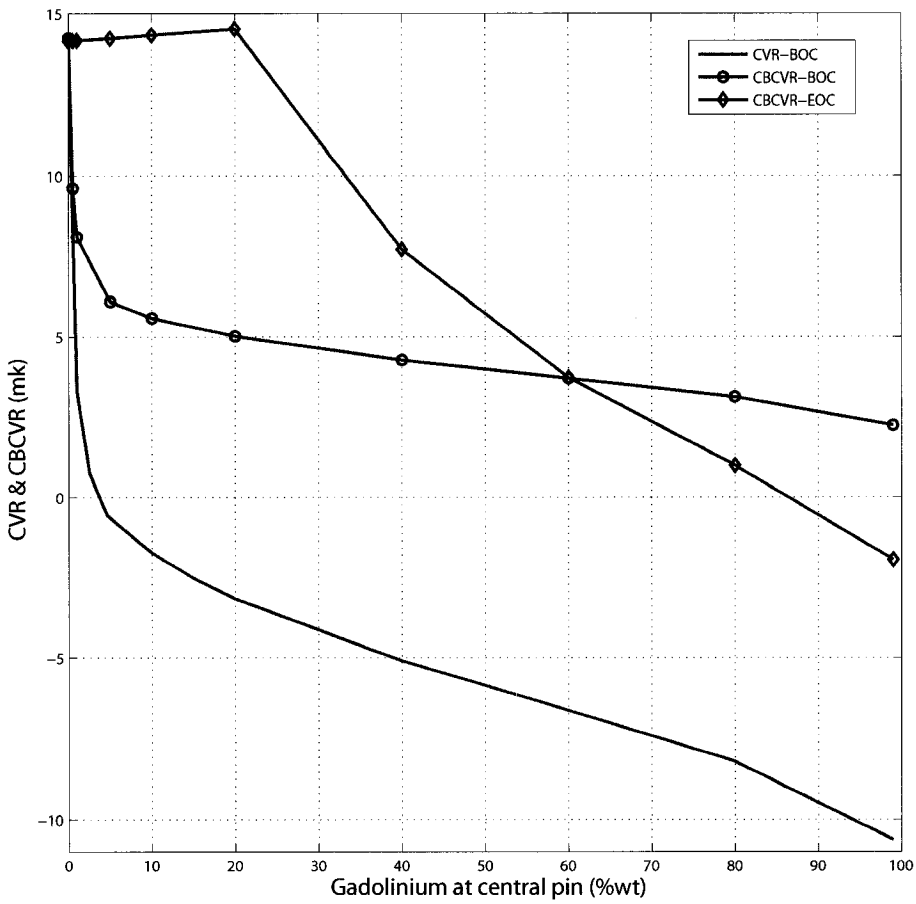

Figure 4.2 ACR: Gadolinium effect on CBCVR-BOC, CBCVR-EOC and CVR-BOC

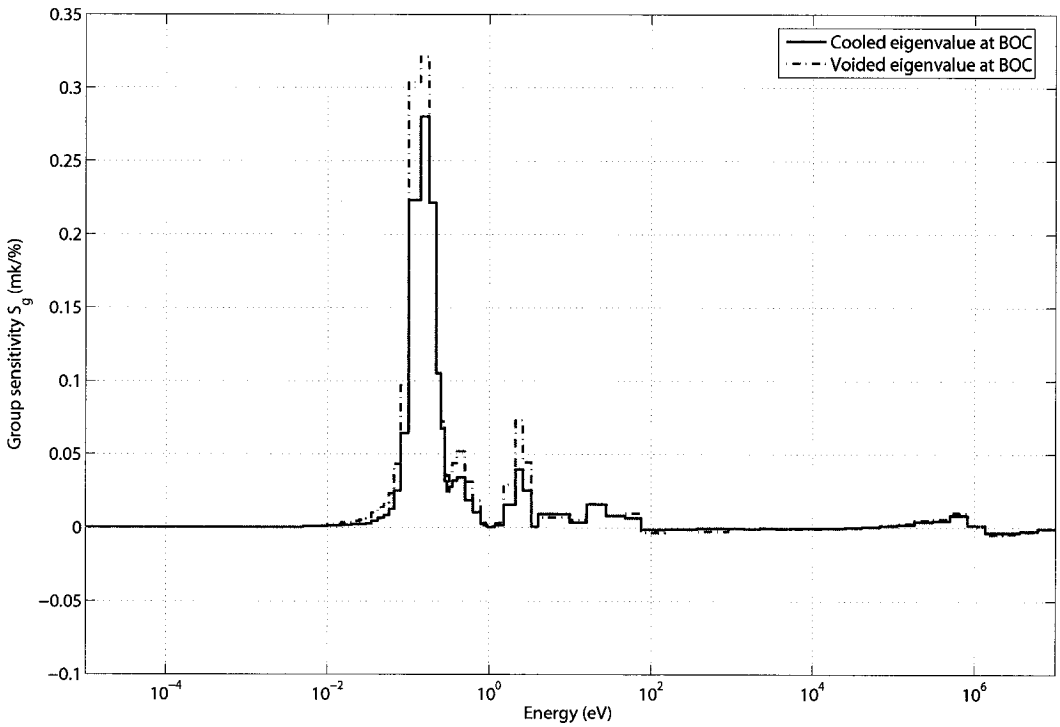

Figure 4.3 ACR : Group sensitivity of cooled and void eigenvalues (at BOC) to Gadolinium density

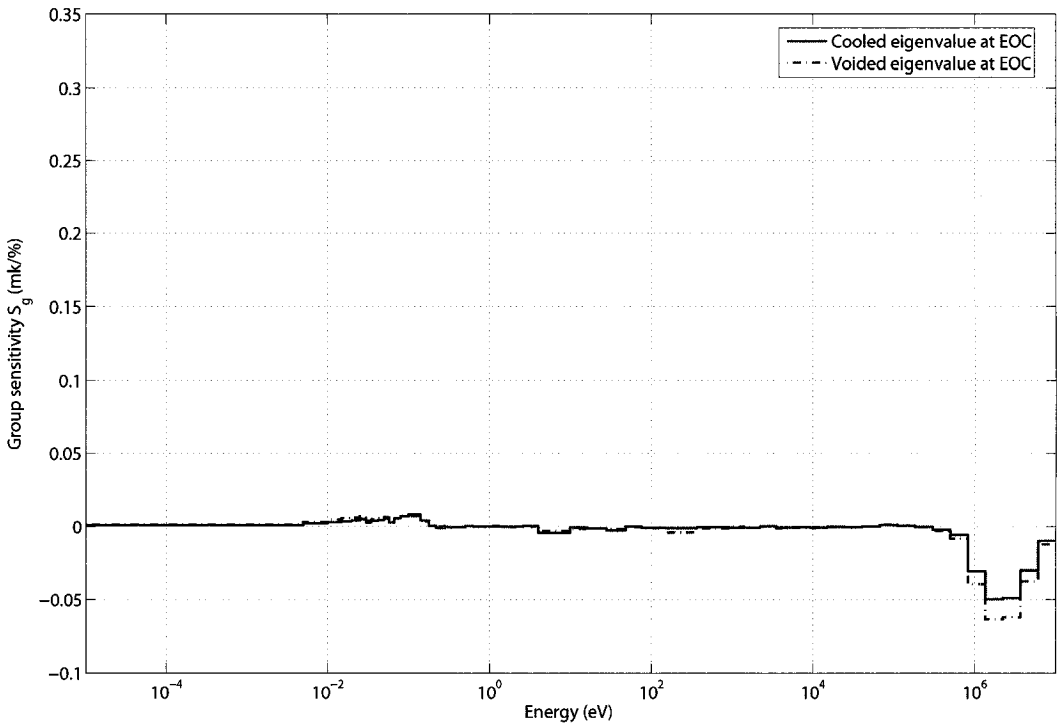

Figure 4.4 ACR : Group sensitivity of cooled and void eigenvalues (at EOC) to Gadolinium density

are mainly negative due to the increasing absorptions by the hardened spectrum as mentioned previously. The CVR-EOC sensitivity coefficients at low energy mostly diminish due to Gd burnout but it becomes positive at high energy due to the higher neutron productions by the increasing Pu239 and U235 at EOC.

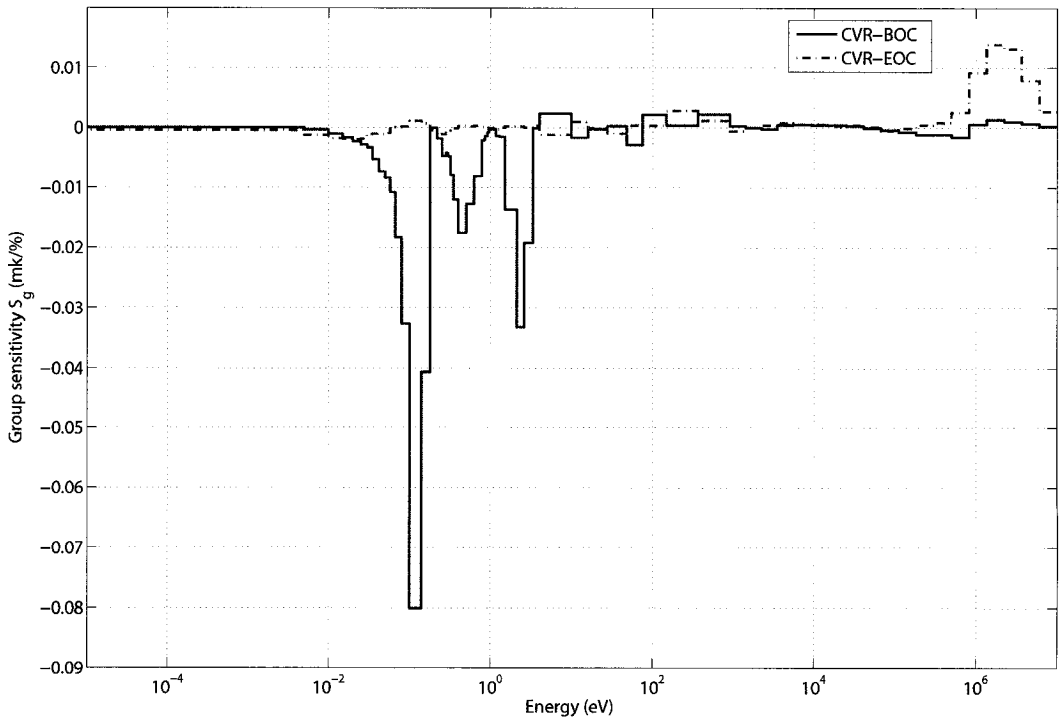

Figure 4.5 ACR : Group sensitivity of CVR-BOC and CVR-EOC to Gadolinium density

The group sensitivity of checkerboard void (CBVOID) eigenvalues (at BOC and EOC) to Gd density illustrated in Figure 4.6 to 4.7 are similar to the group sensitivity of fully void eigenvalues at BOC and EOC except that their magnitudes are smaller. This is because CBVOID flux spectrum is softer than the fully void spectrum. Similarly the CBCVR sensitivity presented in Figure 4.8 has the same structure as the CVR sensitivity except for their smaller magnitudes.

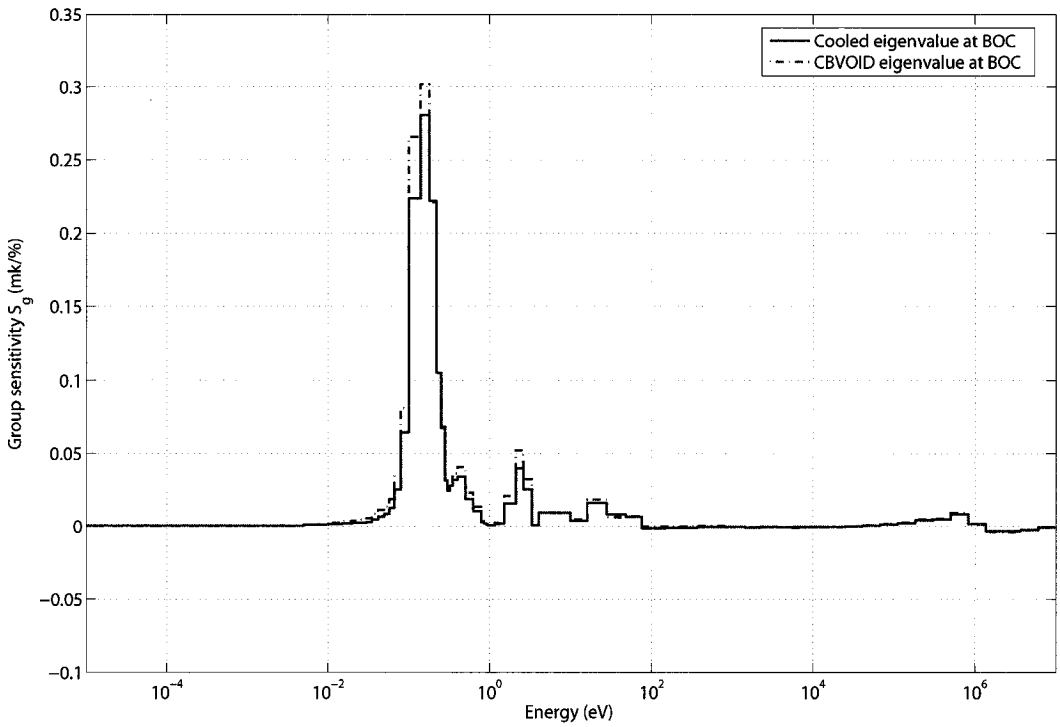

Figure 4.6 ACR : Group sensitivity of cooled and checkerboard void eigenvalues at BOC to Gadolinium density

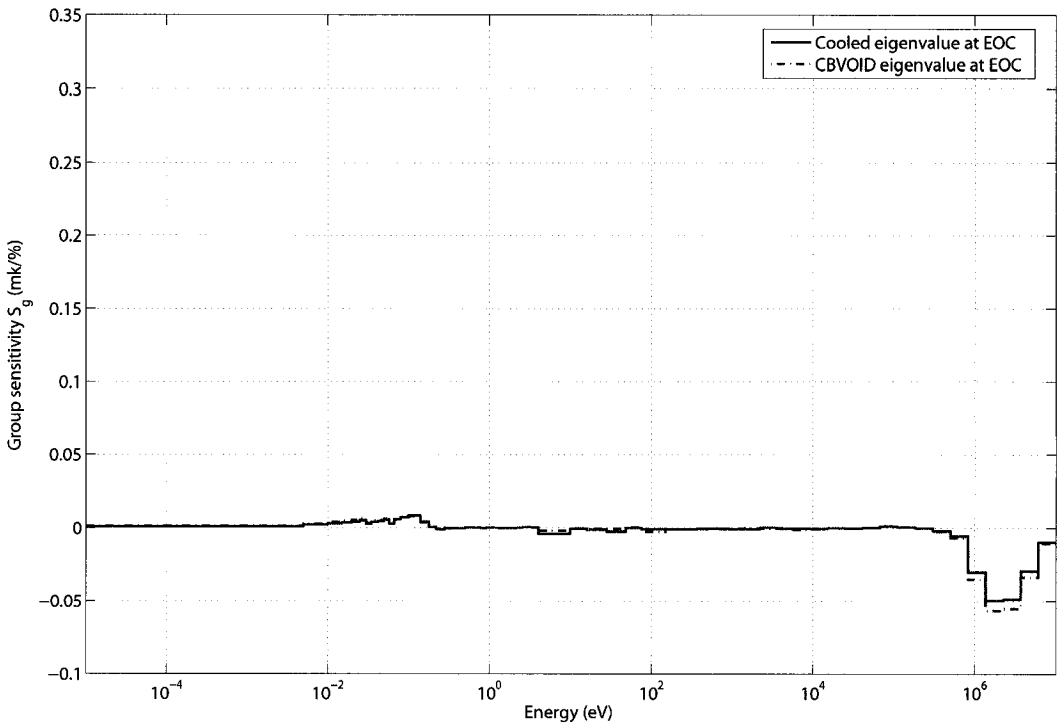

Figure 4.7 ACR : Group sensitivity of cooled and checkerboard void eigenvalues at EOC to Gadolinium density

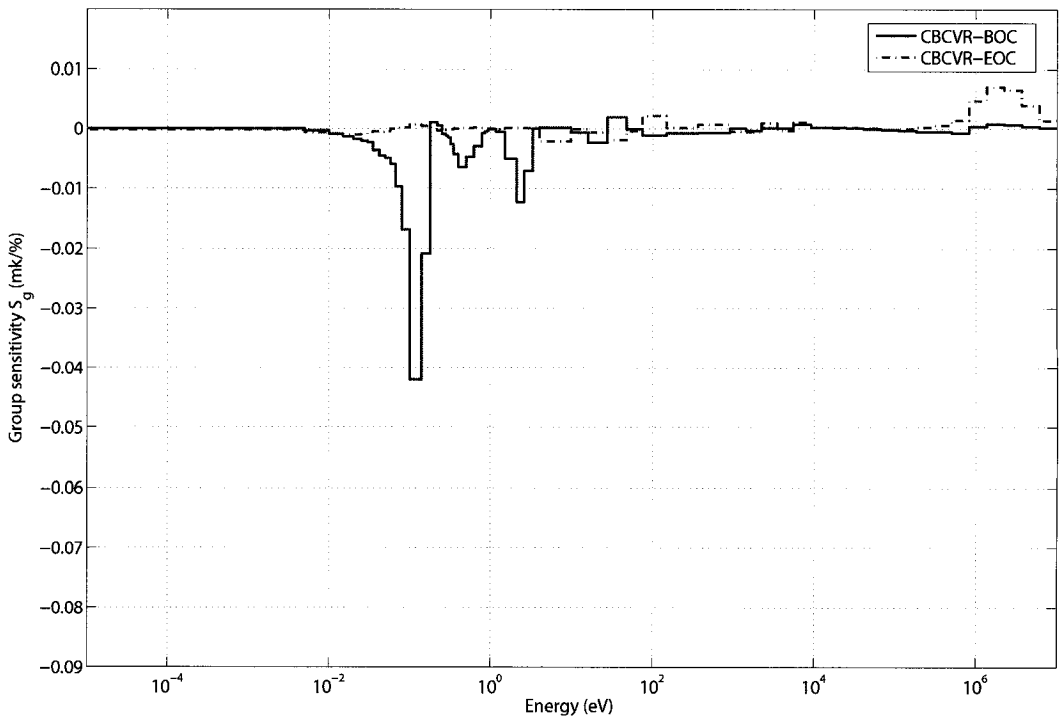

Figure 4.8 ACR : Group sensitivity of CBCVR-BOC and CBCVR-EOC to Gadolinium density

4.4 Optimization Results

The adjustment results of Gd in the central pin and U235 in the outer fuel rings are presented in Table 4.1. As mentioned previously in the Gd effect on CBCVR-BOC, Gd as high as 99.8% is required to obtain the lowest CBCVR-BOC. The final result shows that the CBCVR-BOC and maximum CBCVR are of +1.54 and +2.26 mk respectively. In this case the CBCVR-BOC can not meet the target value of -2 mk because the final Gd density is approaching its maximum limit. In fact CBCVR-BOC can be decreased further by increasing the U235 enrichment but it shall result in higher k_{eff}-EOC. One would then needs to select an extended burnup period where the new optimal Gd and U235 exist within the limits. In the first step, the eigenvalue sensitivity to 4.6% Gd-BOC at EOC is negative because Gd is mainly consumed at EOC and the higher Gd also causes higher Pu239 and U235 left at EOC. From the 2nd to final steps, the eigenvalue sensitivity to Gd-BOC at EOC become positive because of the excessive Gd left from burnup process that effectively decreases the k_{eff}-EOC and results in the negative CBCVR-EOC. As a result of the final adjustment, the CVR, CBCVR and k_{eff} plots versus burnup time are presented in Figure 4.9 to 4.11. In the first step CBCVR rises quickly from 6.39 mk to the first peak at 5th FPD due to the Xe buildup. Because Gd of 4.6% is burnt out quickly, CBCVR continue rising to the 2nd peak at 450th FPD. From the 2nd to final optimization steps, the 2nd CBCVR peak diminishes because the high Gd density effectively lowers CBCVR along the burnup period. From the final result, CBCVR is found positive for the first 350 FPDs and becomes negative afterward. In addition CVR is entirely negative over the burnup period. The CVR-BOC and maximum CVR-BOC are -11.56 and -10.30 mk respectively.

4.5 Conclusion

From the adjustment result, we obtain the optimal CBCVR-BOC of 1.54 mk while the target is -2.00 mk. This is because Gd approaches its maximum limit in the central pin. In fact, one can lower CBCVR-BOC by increasing the U235 enrichment and extending the burnup period. The maximum CBCVR over the burnup period is 2.26 mk for the ACR lattice with optimal Gd and U235. To compare with the ACR lattice with Dy (see the 3rd case of ARTICLE III), the lattice with optimal 99.838% Dy in the central pin and 2.406% U235 in the outer rings results in CBCVR-BOC and maximum CBCVR of -1.18 and -0.54 mk respectively. One can see that the ratio of $|S^{Gd_{BOC}}_{\mathrm{CBCVR_{BOC}}}/S^{Gd_{BOC}}_{\lambda_{EOC}}|$ with respect to Gd (at the 4th adjustment step) is higher than that with respect to Dy (at fifth step in ARTICLE III). This may indicate that Gd is more effective to reduce the CBBCVR-BOC than Dy at high percentage, while Gd also produces less absorption effects to the lattice at EOC.

We also approximate Dy to obtain the maximum CBCVR of ~2.26 mk when U235 is fixed at 2.268% as same as the Gd case. The k_{eff}-EOC is found below the target k_{eff} of 0.900. Thus the ACR lattice with Dy requires higher U235 than the lattice with Gd to obtain the same maximum CBCVR and target k_{eff}-EOC. By considering the fuel cost, the ACR lattice with Gd is more suitable than the lattice with Dy due the lower U235 requirement, provided one installs the control mechanisms that can compensate the maximum CBCVR of 2.26 mk (initially 10.16 mk in the typical ACR lattice with 4.6% Dy and 2.0% U235).

One may consider instead a combination of Dy and Gd in the central pin in order to lower the maximum CBCVR (e.g. removing some Dy and adding Gd with the same amount as in the 3rd case of ARTICLE III). This could then slightly decrease the maximum CBCVR-BOC below -0.54 mk because the magnitude of CBCVR-BOC sensitivity coefficient to Gd is higher than that of Dy.

Table 4.1 ACR-Gd: Adjustment Results

Step	Gd	U235 in Outer Rings	$S^{Gd_{BOC}}_{\mathrm{CBCVR_{BOC}}}$ $S^{Gd_{BOC}}_{\lambda_{EOC}}$ [mk/%]	$S^{U235_{BOC}}_{\mathrm{CBCVR_{BOC}}}$ $S^{U235_{BOC}}_{\lambda_{EOC}}$ [mk/%]	CBCVR_{BOC} CBCVR_{MAX} CBCVR_{EOC} [mk]	$k_{eff,BOC}$ $k_{eff,EOC}$
1	4.6 %	2.0%	-1.73789E-1 -5.67193E-2	-3.97500E+0 -1.09145E+2	6.39 14.69 14.30	1.225102 0.916789
2	57.102%	1.811%	-2.65770E-2 2.47717E-1	-4.83956E+0 -1.11427E+2	5.05 5.78 -1.65	1.169795 0.861900
3	99.802%	2.344%	-8.24546E-2 1.92702E-1	-2.70467E+0 -1.16194E+2	1.60 2.32 -1.07	1.241538 0.908654
4	99.800%	2.252%	-8.30815E-2 3.09357E-1	-1.96316E+0 -1.21823E+2	1.58 2.30 -1.58	1.229283 0.898504
5	99.800%	2.268%	-	-	1.54 2.26 -1.50	1.231421 0.900486

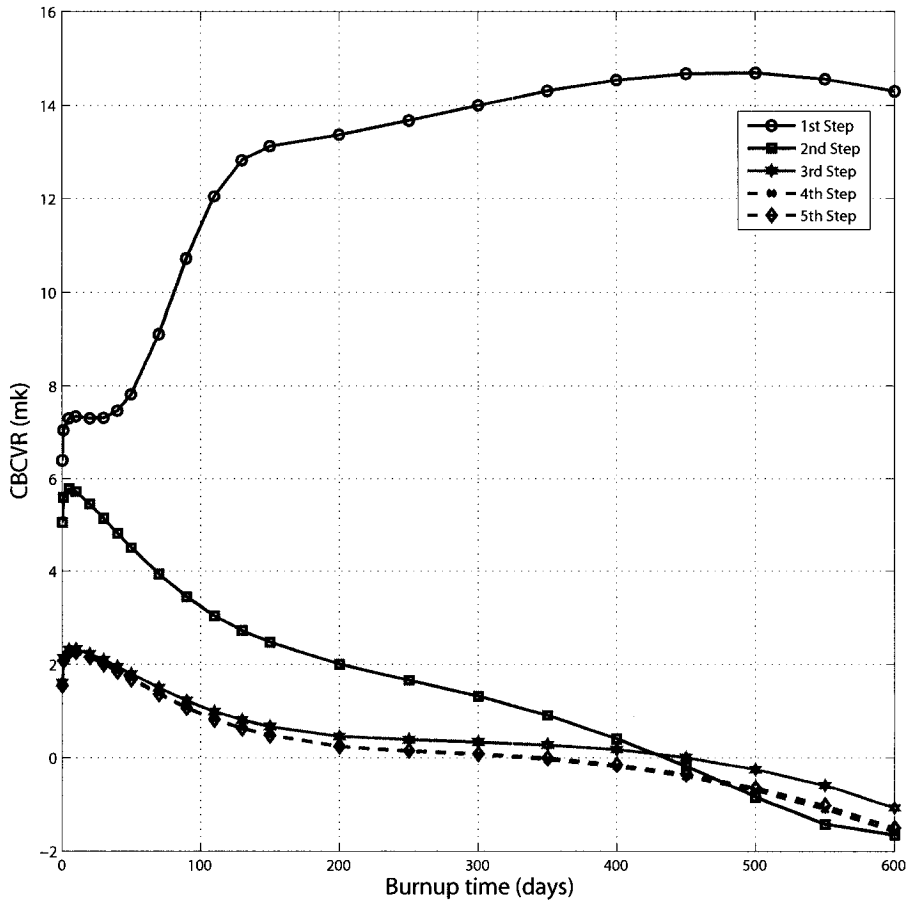

Figure 4.9 ACR-Gd : CBCVR versus burnup time

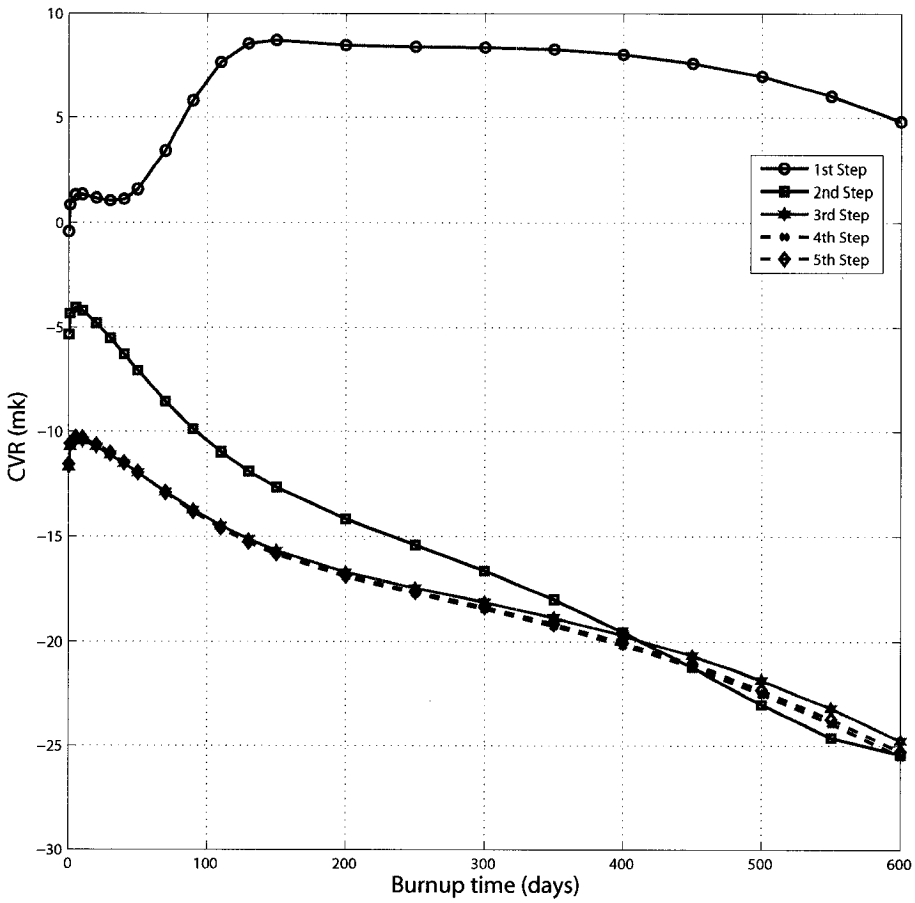

Figure 4.10 ACR-Gd : CVR versus burnup time

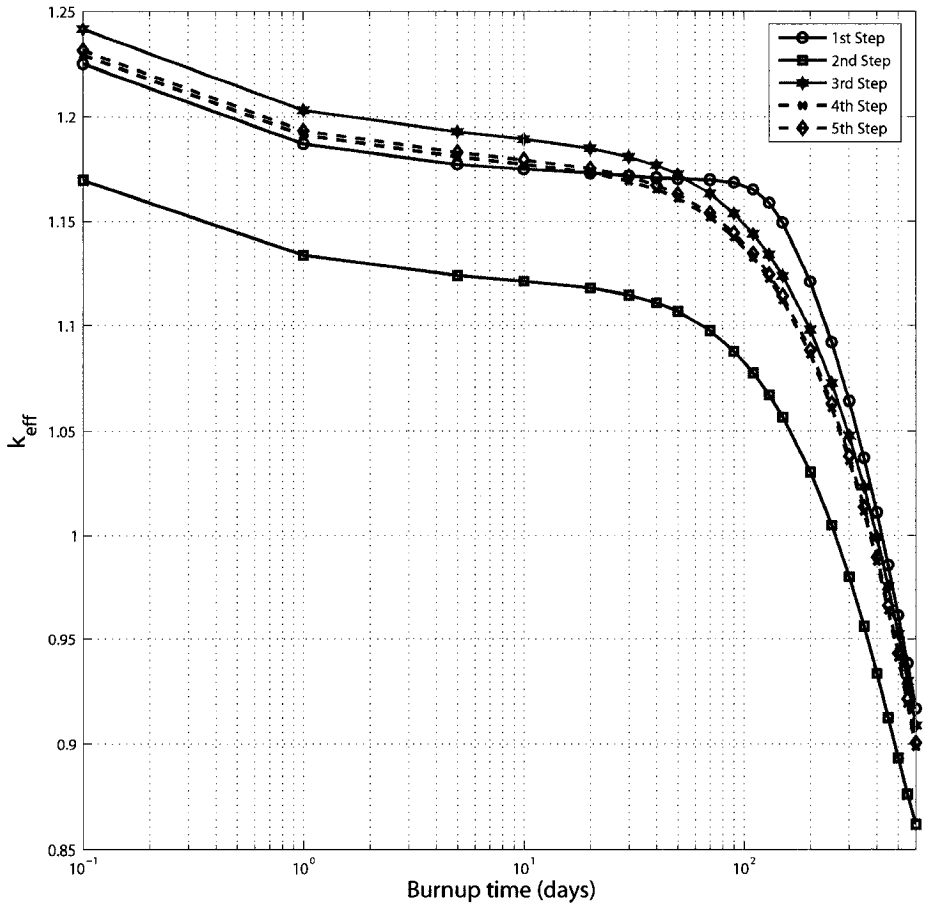

Figure 4.11 ACR-Gd : $k_{eff}^{'}$ plot versus burnup time

CONCLUSIONS AND RECOMMENDATIONS

We have developed the perturbation theory based on the integral neutron transport equation for the perturbative estimation and sensitivity calculations of eigenvalue and linear reaction rate ratios. The advantage of using the integral transport equation is that the perturbative estimates take into account the variations in cross sections and neutron transfer characteristics between regions. For problems with isotropic sources, the perturbative estimates depend on the scalar (or generalized scalar-) flux importances while the perturbative estimates based on the integro-differential transport equation depend on the angular (or generalized angular-) source importance functions. The relationship between generalized adjoint function and generalized flux importance is defined in order to transform the generalized flux importance integral transport equations into the integro-differential form. The generalized adjoint scalar functions are related to the generalized scalar flux importances by the linear transformation using MOCC response matrix, i.e. $[\Gamma^*] = [P_{VV}][\Gamma^\dagger]$. The resulting adjoint and generalized adjoint transport equations are then solved using the MOCC method.

We have also developed the MOCC solution algorithm for the adjoint and generalized adjoint transport problems in 2D heterogeneous geometries. In order to satisfy the boundary conditions in the adjoint transport problems, we need to solve the $\vec{\Omega}$-directed adjoint transport equation along the tracking line in the backward direction $(-\vec{\Omega})$. The adjoint characteristics equation is in the same form as the characteristics equation in neutron transport problem except the adjoint characteristics equation is formulated in the direction $(-\vec{\Omega})$. With the use of closed form, the solution of adjoint angular function associated with the cyclic tracking line is directly determined.

By taking into account the structure of adjoint scattering matrix, the group-oriented and group-splitting iterations result in speed-up of computations. Because the adjoint functions converge faster in the thermal groups than in the fast groups, the group-reduction procedure is implemented by monitoring the convergence in the most thermal groups and activating the multigroup iterations only for the adjoint functions in the un-converged groups.

The combined forward-adjoint iterations scheme based on the group-splitting technique and the common use of the large number of routine variables storing tracking line data and exponential values require lower computing time than the total time required for the individual forward and adjoint calculations. The 3 step scheme (e.g. 1 to 26 (forward), 27 to 69 (forward & adjoint) and 26 to 1 (adjoint)) can be applied for both PWR and CANDU cases. This is because the forward fluxes converge slower than the adjoint functions in these cases. The iterations in the second step rely on the convergence of the flux iterations where the iteration for 27 to 69 groups give lower computing time than the iterations for 69 to 27 groups. The numerical results of adjoint function and k_{eff} by MOCC method are similar to the source importance function and k_{eff} results by CP method. Since the source importance CP equation can be derived from the MOCC adjoint scalar function equation, the source importance function by CP method is equivalent to the adjoint function by MOCC method.

For the generalized adjoint transport solutions by MOCC method, the biasing and decontamination schemes in each power iteration loop (scheme 2) results in the lowest computing time among the 3 schemes proposed. This is because, in each power iteration, the decontamination scheme extracts the orthogonal generalized adjoints and in the meantime removes the undesired contaminated components which are the linear function of the standard adjoint functions. Therefore the orthogonal generalized adjoint functions converge faster than the generalized adjoint

functions, which are iterated with the contaminated components allowed, in scheme 1 and 3.

To evaluate the perturbed integral transport functionals in the perturbative estimates, the isotropic approximation (IA) and linear approximation (LA) methods are applied to approximate the term related to $[\Delta P_{VV}]$. Using the IA method, the perturbative estimate based on the integral transport equations is found equivalent to the perturbative estimate based on the integro-differential transport equation where the adjoint angular functions in the perturbative formulation are assumed isotropic.

In the PWR lattice, the perturbative estimates of the homogenized cross-section due to the perturbations in the fuel, clad and coolant temperature result in a maximum absolute relative error of 2.3×10^{-4} for perturbations in temperature of 10% or less. The perturbative estimate using IA method is comparable to the estimate using the LA method because in the PWR lattice the angular neutron fluxes are relatively isotropic due to the fuel rods are uniformly distributed over the assembly. Therefore the high-order angular terms in $(\Delta\Sigma^g\Phi^g)$ produce low effect in the perturbative estimation using the LA method. For the CANDU case, the angular neutron fluxes are generally more anisotropic and the LA method then results in more accurate estimations for the perturbations in temperature from 0 to 10%. For the sensitivity evaluation, the same behaviors are observed, provided that the linearization factors are evaluated using small perturbed cross-sections $(d\Sigma_m^g = 1.0^{-4}\Sigma^g)$.

Finally we consider an application of the perturbation theory to practical problems. We apply the simple optimization and adjoint sensitivity techniques to adjust the CVR (or CBCVR) and k_{eff}-EOC of the CANDU-6 and ACR-700 lattices by searching the Dysprosium (or Gadolinium) density and the U235 enrichment that mini-

mize an objective cost functional. For the first adjustment case of ACR lattice, we can obtain the optimal Dy density in the central pin and U235 enrichment in the outer rings are of 8.26 %wt and 2.107% that results in the desired target k_{eff}-EOC and negative CVR over burnup period of 600 FPDs. For the 2nd adjustment case, we obtain the optimal Dy and U235 of 19.614%wt and 20.995% both in the central pin that results in the desired negative CVR and k_{eff}-EOC as expected. In the 3rd case where the objective is to adjust CBCVR-BOC and k_{eff}-EOC, the optimal Dy and U235 of 99.838%wt and 2.406% results in the negative CBCVR over 600 FPDs while the initial CBCVR are all positive. For the last case where the Dy is replaced with Gd in the central pin, we can obtain the optimal Gd and U235 of 99.8%wt and 2.268% that results in the target k_{eff}-EOC. The CBCVR-BOC can not be reduced lower than 1.54 mk (even if the target CBCVR-BOC is -2.0 mk) because the Gd density reach the maximum limit in the central pin. The optimized CBCVR is below 2.26 mk for the first 400 FPDs and becomes negative afterward. By considering only the cost of fuel, the ACR lattice with Gd is more suitable than the lattice with Dy due to the lower U235 requirement when the same maximum CBCVR and k_{eff}-EOC are obtained.

For the first adjustment case of a CANDU-6 lattice with extended burnup from 300 to 450 FPDs, we obtain the optimal Dy and U235 of 2.380% and 1.153% that results in the desired CVR-BOC and k_{eff}-EOC. For the 2nd case, we obtain the optimal Dy and U235 of 14.440% and 1.385% that results in the desired CVR-BOC, CVR-EOC and k_{eff}-EOC. The CVR is equal or below 8.07 mk over the burnup period of 450 FPDs (while the maximum CVR of the initial-unadjusted lattice is 16.87 mk). For the 3rd case with Gd and U235 adjustments, we can obtain the optimal Gd and U235 of 28.518%wt and 1.058% that results in the target CVR-BOC and k_{eff}-EOC. For the last case, the optimal Gd and U235 of 62.478%wt and 1.374% results in the required CVR-BOC, CVR-EOC and k_{eff}-EOC. The CVR is equal or below

8.28 mk over the burnup period. For the CVR-BOC, CVR-EOC and k_{eff}-EOC adjustments, the CANDU lattice with Gd in the central pin is more suitable than the lattice with Dy due to its lower U235 requirement. In addition the sensitivity analysis method is used in analyzing the groupwise characteristics of eigenvalues, CVR and CBCVR (at BOC and EOC) with respect to Dy, Gd and U235. By using these simple techniques, one can design lattices that meet both safety and burnup performance requirements.

General Discussions

As mentioned previously, the perturbation theory based on integral transport equations provides more accurate perturbative estimates than the theory based on integrodifferential transport equations where the angular adjoint functions in the perturbed transport functional are assumed isotropic. This may not be true when the angular adjoint functions and angular fluxes are directly used in computing the perturbed transport functional. One may have to provide large memory space to store these angular direct fluxes and adjoint functions for each group and region (e.g. $2 \times N^{\Omega} \times G \times N_{reg}$ elements).

An application of the perturbation theory to the anisotropic scattering problems may be considered by arranging for the anisotropic scattering term as follows,

$$(\mathcal{L}^{\dagger g} - \lambda \mathcal{F}^{\dagger g})\Phi^{\dagger g}(\vec{r}, \vec{\Omega}_l) = 0 \tag{4.1}$$

where

$$\mathcal{L}^{\dagger g}\Phi^{\dagger g}(\vec{r},\vec{\Omega}_l) = \Phi^{\dagger g}(\vec{r},\vec{\Omega}_l) - \sum_{l'=1}^{N^\Omega} W_{l'}^\Omega \sum_{g'=1}^{G} \Sigma_s^{g'\leftarrow g}(\vec{r},\vec{\Omega}_{l'} \leftarrow \vec{\Omega}_l)\mathcal{T}_{l'}^{*g',-1}\Phi^{\dagger g'}(\vec{r},\vec{\Omega}_{l'})$$

$$\mathcal{F}^{\dagger g}\Phi^{\dagger g}(\vec{r},\vec{\Omega}_l) = \sum_{g'=1}^{G} \chi^{g'}(\vec{r})\nu\Sigma_f^g(\vec{r}) \sum_{l'=1}^{N^\Omega} W_{l'}^\Omega \mathcal{T}_{l'}^{*g',-1}\Phi^{\dagger g'}(\vec{r},\vec{\Omega}_{l'})$$

The same relationship between flux importance and source importance functions (as well as for the generalized flux importance functions) can be defined to transform the above transport equations into the integro-differential form.

Instead of linearization for the term $[\Delta P_{VV}][Q]$, one may directly linearize the MOCC response matrix $[P_{VV}]$ with respect to the total macroscopic cross sections in each region and group. The approximated perturbed response matrix $[P_{VV}(\Sigma + \Delta\Sigma)]$ may be used for approximation of the perturbed fluxes for the higher order perturbative approximation.

In addition the conjugate gradient algorithm for the solution of large sparse matrix equation can be applied to compute both forward fluxes and adjoint functions in the same time. The adaptive biasing schemes may be considered in calculating the biasing factor in each power iteration loop in order to ensure the positive spatial-integrated total generalized adjoint sources for the rebalancing scheme. The procedure to preevaluate the biasing factor can then be avoided.

The perturbation theory based on the integral transport equation can be performed with the use of other integral transport solution methods such as 2D and 3D MOC, 3D MOCC, and interface current methods where the additional calculation of adjoint currents is required at boundary surfaces. The similar linearization approximation methods for the perturbed integral transport functional can be directly used.

An extension to the geometrical perturbation may be considered such as for the small perturbations in fuel rod size, moderator volume, clad thickness (a preliminary test indicates that this works well for a 2 group unit cell). The sensitivity coefficients with respect to the geometrical parameters could be obtained.

Due to more accurate sensitivity coefficients obtained for the problem with anisotropic fluxes, the integral transport perturbation theory is suitable for the uncertainty analysis of the performance functionals to variations in the microscopic nuclear library. More accurate covariance of the performance functionals to variations in nuclear cross sections can be obtained.

Recommendation for Future Works

One may consider the applications of perturbation theory based on the integral transport equations as follows: sensitivity analyses of eigenvalue and performance functionals to cross-sectional data in CANDU and ACR lattices, and applications to uncertainty analyses of reactor parameters under variations in nuclear cross-section (LEWINS and BECKER, 1982); a perturbation theory with the adjoint and generalized adjoint transport solutions using 3D MOC and MOCC methods (WU and ROY, 2003; DAHMANI and ROY, 2005); the sensitivity analyses of CVR and CBCVR in a 3D CANDU supercell under the checkerboard voiding condition; an application of perturbation theory based on integral transport equations to subcritical reactor problems; an extension of the perturbation theory and sensitivity analysis to radiation transport and shielding problems; and the application of adjoint sensitivity and optimization techniques to a extended-burnup/fuel cycle optimization problem based on transport equations.

REFERENCES

AECL R&D Advisory Panel (1992). *Report of The AECL Research and Development Advisory Panel for 1992.* AECL.

ASKEW, J. (1972). A characteristics formulation of the neutron transport equation in complicated geometries. *Winfrith: United Kingdom Atomic Energy Establishment*, **Report AEEW-M 1108**.

ASSAWAROONGRUENGCHOT, M. and MARLEAU, G. (2005). Multigroup adjoint transport solution using the method of cyclic characteristics. In *Proc. Int. Topl. Mtg. on Mathematics and Computation, Supercomputing, Reactor Physics and Nuclear and Biological Applications, Sep. 12-15, Avignon, France.*

ASSAWAROONGRUENGCHOT, M. and MARLEAU, G. (2006). Generalized perturbation theory based on the method of cyclic characteristics. In *ANS Proc. Int. Topl. Mtg. on Reactor Physics, Sep. 10-14, Vancouver, BC, Canada.*

ASSAWAROONGRUENGCHOT, M. and MARLEAU, G. (2007a). Coolant void reactivity adjustments in advanced CANDU lattices using adjoint sensitivity technique. *Ann. Nucl. Energy (accepted for publication July 2007).*

ASSAWAROONGRUENGCHOT, M. and MARLEAU, G. (2007b). Multigroup adjoint transport solution using the method of cyclic characteristics. *Nuc. Sci. Eng.*, **155**, 37–52.

ASSAWAROONGRUENGCHOT, M. and MARLEAU, G. (2007c). Perturbation theory based on method of cyclic characteristics. *Nuc. Sci. Eng.*, **157**, 30–50.

BELBLIDIA, L. A., KALLFELZ, J. M., and CACUCI, D. G. (1983). Generalized perturbation theory with derivative operators for power density investigations in nuclear reactors. *Nuc. Sci. Eng.*, **84**, 206–225.

BELL, G. and GLASSTONE, S. (1979). *Nuclear reactor theory.* R. E. Krieger Pub. Co., Huntington, N.Y.

BRUNA, G., AIGLE, R., and LOUSSOUARN, O. (1990). Generalized perturbation theory for the reconstruction of the axial offset in a pressurized water reactor. *Nuc. Sci. Eng.*, **105**, 290–296.

CARLSON, B. G. and LATHROP, K. D. (1968). *Discrete Ordinate Method.* in Computing Methods in Reactor Physics, Greenspan, H., Okrent, D., Kelber, C. N. editors., Gordon and Breach, New York, USA.

CONSTANTIN, M. and BEALACEANU, V. (2002). Void reactivity and pin power calculation for a typical CANDU cell using CPS and a two-stratified coolant model. *Ann. Nucl. Energy*, **29**, 791.

CONSTANTIN, M., GUGIU, D., and BEALACEANU, V. (2003). Void reactivity and pin power calculation for a CANDU cell using the SEU-43 fuel bundles. *Ann. Nucl. Energy*, **30**, 301.

COTTON, C., LEE, D., and DOWNAR, T. (2004). Coolant void reactivity analysis of CANDU and ACR-700 lattices. *Trans. Am. Nucl. Soc.*, **90**, 587.

COTTON, C., LEE, D., KOZLOWSKI, T., DOWNAR, T., and CARLSON, D. (2005). Physics analysis of coolant voiding in the ACR-700 lattices. *Trans. Am. Nucl. Soc.*, **92**, 685.

COURAU, T. (2001). *Application de la théorie des perturbations généralisées aux calculs de cellules utilisant la méthode des probabilités de collision.* Thèse de doctorat, École Polytechnique de Montréal, Département de génie mécanique, Montréal, Canada.

COURAU, T. and MARLEAU, G. (2002). Adjoint and generalized adjoint flux calculations using the collision probability technique. *Nuc. Sci. Eng.*, **141**, 46–54.

COURAU, T. and MARLEAU, G. (2003). Perturbation theory for lattice cell calculations. *Nuc. Sci. Eng.*, **143**, 19–32.

DAHMANI, M. and ROY, R. (2005). Parallel solver based on the three-dimensional characteristics method: design and performance analysis. *Nuc. Sci. Eng.*, **150**, 155–69.

DAVISON, B. (1957). *Neutron Transport Theory*. Original ed., Oxford Clarendon Press, Oxford.

DUDERSTADT, J. J. and HAMILTON, L. J. (1976). *Nuclear Reactor Analysis*. Original ed. Wiley. 650p., New York.

FAVORITE, J. (2002). An alternative implementation of the differential operator (Taylor series) perturbation method for Monte Carlo criticality problems. *Nuc. Sci. Eng.*, **142**, 327–341.

GANDINI, A. (1967). A generalized perturbation method for bi-linear functionals of the real and adjoint neutron fluxes. *J. Nucl. Energy Part A/B*, **21**, 755–765.

GANDINI, A. (1978). Higher order time-dependent generalized perturbation theory. *Nuc. Sci. Eng.*, **67**, 91–106.

GANDINI, A. (1981). Generalized perturbation theory for nonlinear systems from the importance conservation principle. *Nuc. Sci. Eng.*, **77**, 316–343.

GANDINI, A. (2001). HGPT based sensitivity time-dependent methods for the analysis of subcritical systems. *Ann. Nucl. Energy.*, **28**, 1193–1217.

GANDINI, A., SALVATORES, M., and TONDINELLI, L. (1977). New developments in generalized perturbation methods in the nuclide field. *Nuc. Sci. Eng.*, **62**, 339–345.

HALSALL, M. J. (1980). CACTUS: A characteristics solution to the neutron transport equation in complicated geometries. *Winfrith: United Kingdom Atomic Energy Establishment.*, **Report AEEW-R 1291**.

HÉBERT, A. (1993). A consistent technique for the pin-by-pin homogenization of a pressurized water reactor assembly. *Nuc. Sci. Eng.*, **113**, 227–38.

HÉBERT, A. (2005). The Ribon extended self-shielding model. *Nuc. Sci. Eng.*, **151**, 1–24.

HÉBERT, A. (2006a). Applied reactor physics. *École Polytechnique de Montréal, Institut de génie nucléaire.*

HÉBERT, A. (2006b). Towards DRAGON version 4.0. In *ANS Proc. Int. Topl. Mtg. on Reactor Physics, Sep. 10-14, Vancouver, BC, Canada*, volume http://www.polymtl.ca/merlin/.

HÉBERT, A. and MARLEAU, G. (1991). Generalization of the Stamm'ler method for the self-shielding of resonant isotopes in arbitrary geometries. *Nuc. Sci. Eng.*, **108**, 230–239.

HENRY, A. F. (1975). *Nuclear Reactor Analysis.* MIT Press, Cambridge, Mass., USA.

HOFFMAN, T., PETRIE, L., and LANDERS, N. (1978). A Monte Carlo perturbation source method for reactivity calculations. *Nuc. Sci. Eng.*, **66**, 60–66.

HONG, S. G. and CHO, N. Z. (1998). CRX: a code for rectangular and hexagonal lattices based on the method of characteristics. *Ann. Nucl. Energy*, **25**, 547–565.

HOOGENBOOM, J. E. (1981). A practical adjoint Monte Carlo technique for fixed source and eigenvalue problems. *Nuc. Sci. Eng.*, **79**, 357–373.

HUTTON, J. (2000). New capabilities of the WIMS8 code. *Int. Conf. Physics of Nuclear Science and Technology. PHYSOR2000 Pittsburg. USA.*

Intel (June 2005). IA-32 Intel architecture optimization reference manual. *www.intel.com*, pages 2–66.

LARSEN, E. W. and POMRANING, G. C. (1981). Boundary perturbation theory. *Nuc. Sci. Eng.*, **77**, 415–425.

LAURIN-KOVITZ, K. F. and LEWIS, E. (1996a). Variational nodal transport perturbation theory. *Nuc. Sci. Eng.*, **123**, 369–380.

LAURIN-KOVITZ, K. F. and LEWIS, E. E. (1996b). Variational nodal transport perturbation theory. *Nuc. Sci. Eng.*, **123**, 369–380.

LE TELLIER, R. and HÉBERT, A. (2006a). On the integration scheme along a trajectory for the characteristics method. *Ann. Nucl. Energy*, **33**, 1260–69.

LE TELLIER, R., HÉBERT, A., and MARLEAU, G. (2006b). The implementation of a 3D characteristics solver for the generation of incremental cross sections for reactivity devices in a CANDU reactor. In *ANS Proc. Int. Topl. Mtg. on Reactor Physics, Sep. 10-14, Vancouver, BC, Canada.*

LEWINS, J. and BECKER, M. (1982). *Advances in nuclear science and technology Volume 14: Sensitivity and uncertainty analysis of reactor performance parameters.* Plenum Press, New York & USA.

LEWINS, J. D. (1966). A variational principle for ratios in critical systems. *J. Nucl. Energy Part A/B*, **20**, 141–143.

LEWINS, J. D., PARKS, G., and BABB, A. L. (1986). Higher order perturbation theory - an example for discussion. *Nuc. Sci. Eng.*, **94**, 380–392.

LEWIS, E. E. (1993). *Computational Methods of Neutron Transport.* American Nuclear Society, La Grange Park, Ill., USA.

MACFARLANE, R. E. (1984). TRANSX-CTR: A code for interfacing MATXS cross-section libraries to nuclear transport codes for fusion system analysis. *Los Alamos Scientific Laboratory, New Mexico, USA*, **Report LA-9863-MS**.

MALDONADO, G. I., TURINSKY, P. J., KROPACZEK, D. J., and PARKS, G. (1995). Employing nodal generalized perturbation theory for the minimization of feed enrichment during pressurized water reactor in-core nuclear fuel management optimization. *Nuc. Sci. Eng.*, **121**, 312–325.

MARLEAU, G. (2001). DRAGON theory manual: Part I- collision probability calculation. *École Polytechnique de Montréal, Institut de génie nucléaire*, **Rapport technique IGE-236 (www.polymtl.ca/nucleaire/en/index.php)**.

MARLEAU, G. (2004a). CANDU adjuster rods incremental cross section evaluation: A perturbative approach. In *ANS Proc. Int. Topl. Mtg. on Reactor Physics, April 25-29, Chicago, IL USA.*

MARLEAU, G. (2004b). DRAGON theory for 3D CANDU problems. *École Polytechnique de Montréal, Institut de génie nucléaire.*

MARLEAU, G., HÉBERT, A., and ROY, R. (2000). A user guide for DRAGON. *École Polytechnique de Montréal, Institut de génie nucléaire*, **Rapport technique IGE-174 Rev. 5 (www.polymtl.ca/nucleaire/en/index.php)**.

MARLEAU, G., HÉBERT, A., and ROY, R. (2006). A user guide for DRAGON version 3.05. *École Polytechnique de Montréal, Institut de génie nucléaire*, **Rapport technique IGE-174 Rev. 6 (www.polymtl.ca/nucleaire/en/index.php)**.

MASIELLO, E. and ZMIJAREVIC, I. (2006). Short characteristics method for 2D heterogeneous Cartesian cells. In *ANS Proc. Int. Topl. Mtg. on Reactor Physics, Sep. 10-14, Vancouver, BC, Canada.*

MORILLON, B. (1998). On the use of Monte Carlo perturbation in neutron transport problems. *Ann. Nucl. Energy.*, **25**, 1095–1117.

OVANES, M., CHAN, P., and MAO, J. (2002). Reactor physics innovation in ACR-700 design for the next CANDU generation. *23rd CNS Annual Conference, June 3-5.*

POMRANING, G. C. (1983). Perturbation theory in the diffusion approximation. *Nuc. Sci. Eng.*, **83**, 72–74.

POSTMA, T. and VUJIC, J. (1999). The method of characteristics in general geometry with anisotropic scattering. In *Intl. Conf. on Mathematics and Computation, Reactor Physics and Environmental Analysis in Nuclear Applications, Madrid, Spain, September 27-30.*

RAHNEMA, F. (1989). Boundary condition perturbation theory for use in spatial homogenization methods. *Nuc. Sci. Eng.*, **102**, 183–190.

RAHNEMA, F. (1994). Boundary condition perturbation of fixed-source problems. *Transactions of the American Nuclear Society*, **70**, 174–5.

RAHNEMA, F. and POMRANING, G. C. (1983). Boundary perturbation theory for inhomogeneous transport equations. *Nuc. Sci. Eng.*, **84**, 313–319.

REARDEN, B. (2004). Perturbation theory eigenvalue sensitivity analysis with Monte Carlo techniques. *Nuc. Sci. Eng.*, **146**, 367–382.

RICE, C. (November 2000). Introducing the Intel Pentium 4 processor. *www.intel.com*, page 4.

RIEF, H. (1984). Generalized Monte Carlo perturbation algorithms for correlated sampling and second order Taylor series approach. *Ann. Nucl. Energy.*, **11**, 455–476.

RIEF, H. (1986). Review of Monte Carlo techniques for analyzing reactor perturbation. *Nuc. Sci. Eng.*, **92**, 289–297.

RONEN, Y. (1986). *CRC Handbook of Nuclear Reactor Calculations Vol III.* CRC Press, Boca Raton, Fl., USA.

ROY, R. (1998). The cyclic characteristics method. In *Proc. Int. Topl. Mtg. on the Physics of Nuclear Science and Technology, Long Island, New York, October 5-8*, volume 1, pages 407–414.

ROY, R. (1999). The cyclic characteristics method with anisotropic scattering. In *Intl. Conf. on Mathematics and Computation, Reactor Physics and Environmental Analysis in Nuclear Applications, Madrid, Spain, September 27-30.*

ROY, R. (2003). *Théorie des probabilités de collision et méthode des caractéristiques.* École Polytechnique de Montréal, Institut de génie nucléaire, Rapport technique IGE-235 58p., Montréal, Canada.

ROY, R., MARLEAU, G., HÉBERT, A., and ROZON, D. (1991). A cyclic tracking procedure for collision probability calculation in 2D lattices. In *Proc. Int. Topl. Mtg. Advances in Mathematics, Computations and Reactor Physics, Pittsburgh, Pennsylvania, April 28 - May 2*, volume 1, pages 4–1 to 4–14.

ROY, R., MARLEAU, G., TAJMOUATI, J., and ROZON, D. (1994). Modelling of CANDU reactivity control devices with the lattice code DRAGON. *Ann. Nucl. Energy*, **21 No.2**, 115–132.

ROZON, D. (1998). *Introduction to Nuclear Reactor Kinetics.* Polytechnic International Press, Montréal, Canada.

SANCHEZ, R. and CHETAINE, A. (2000). Synthetic acceleration for a two-dimensional characteristic method in unstructured meshes. *Nuc. Sci. Eng.*, **136**, 122–139.

SANCHEZ, R. and MCCORMICK, N. (1982). A review of neutron transport approximations. *Nuc. Sci. Eng.*, **80**, 481–535.

SJODEN, G. E. (2002). Deterministic adjoint transport applications for He-3 neutron detector design. *Ann. Nucl. Energy*, **29**, 1055–1071.

STACEY, W. J. (1972). Variational estimates of reactivity worths and reaction rate ratios in critical nuclear reactors. *Nuc. Sci. Eng.*, **48**, 444–458.

STACEY, W. J. (1974). *Variational Methods in Nuclear Reactor Physics.* First ed. Academic Press, New York.

STAMM'LER, R. and M.J.ABBATE (1983). *Methods of steady-state reactor physics in nuclear design.* Academic Press, New York, USA.

TAKEDA, T., ASANO, K., and KITADA, T. (2006). Sensitivity analysis based on transport theory. *Journal of Nuclear Science and Technology*, **43 No.7**, 743–749.

TAKEDA, T. and UMANO, T. (1985). Burnup sensitive analysis in a fast breeder reactor - part I: Sensitivity calculation method with generalized perturbation theory. *Nuc. Sci. Eng.*, **91**, 1–10.

TALEBI, F., MARLEAU, G. ., and KOCLAS, J. . (2006). A model for coolant void reactivity evaluation in assemblies of CANDU cells. *Ann. Nucl. Energy*, **33**, 975.

USACHEV, L. (1964). Perturbation theory for the breeding ratio and for other number ratios pertaining to various reactor processes. *J. Nucl. Energy Part A/B*, **18**, 571–583.

VARIN, E. and MARLEAU, G. (2006). CANDU reactor core simulations using fully coupled DRAGON and DONJON calculations. *Ann. Nucl. Energy*, **33 No.8**, 682–691.

WACHSPRESS, E. L. (1966). *Iterative Solution of Elliptic Systems, and Applications to the Neutron Diffusion Equations of Reactor Physics.* Original ed. Prentice-Hall. 299p., Englewood Cliffs, N.J.

WIGNER, E. (1945). Effects of small perturbations on pile period. *Manhattan Project Report*, **CP-3048**.

WILLIAMS, M. (1986). *CRC Handbook of Nuclear Reactors Calculations.* First ed., RONEN, Y. Editor, CRC Press, Boca Raton, Fl.

WU, G. J. and ROY, R. (1999). Self-collision rebalancing technique for the MCI characteristics solver. *20th Annual Conf. Canadian Nuclear Society. Montreal. Canada. May 30 - June 2.*

WU, G. J. and ROY, R. (2000). New development of the three-dimensional characteristics solver MCI in DRAGON. *21st Annual Conf. Canadian Nuclear Society. Toronto. Canada. June 12-14.*

WU, G. J. and ROY, R. (2003). A new characteristics algorithm for 3D transport calculations. *Ann. Nucl. Energy*, **30**, 1–16.

YANG, W. and DOWNAR, T. J. (1988). Generalized perturbation theory for constant power core depletion. *Nuc. Sci. Eng.*, **99**, 353–366.

YANG, W. and DOWNAR, T. J. (1989). Depletion perturbation theory for the constrained equilibrium cycle. *Nuc. Sci. Eng.*, **102**, 365–380.

ZIKA, M. and ADAMS, M. (2000). Transport synthetic acceleration for long-characteristics assembly-level transport problems. *Nuc. Sci. Eng.*, **134**, 135–158.

APPENDIX I

ARTICLE I: PERTURBATION THEORY BASED ON THE METHOD OF CYCLIC CHARACTERISTICS

Monchai Assawaroongruengchot and Guy Marleau

Nuclear Science and Engineering,
Volume 157, Number 1, September 2007, Pages 30-50

Abstract

Generalized perturbation theory (GPT) is a technique used for the estimation of small changes in performance functionals, such as linear reaction rate ratios, eigenvalues, power density etc., affected by small variations in reactor core compositions. Here a GPT algorithm is developed for the multigroup integral neutron transport problems in two-dimensional fuel assemblies with isotropic scattering. We then use the relationship between the generalized flux importance and generalized source importance functions to transform the generalized flux importance transport equations into the integro-differential equations for the generalized adjoints. The resulting adjoint and generalized adjoint transport equations are then solved using the method of cyclic characteristics (MOCC). Because of the presence of negative adjoint sources, a coupled flux biasing/decontamination scheme is applied to make the generalized adjoint functions positive in such a way that it can be used for the multigroup rebalance technique. After convergence is reached, the decontamination procedure extracts from the generalized adjoints the component parallel to the adjoint function. Three types of biasing/decontamination schemes are investigated in the study. To demonstrate the efficiency of our solution algorithms, calculations are performed on the 17×17 PWR and 37 pin CANDU lattices. Numerical comparisons of the generalized adjoint functions and GPT estimates using the MOCC and CP methods are presented as well as sensitivity coefficients of nuclide densities.

I.1 Introduction

Generalized perturbation theory (GPT) is a technique used to estimate the change in performance functionals, such as linear reaction rate ratios, eigenvalues etc., affected by small changes in reactor core compositions. It can be applied to prob-

lems such as computations of power density distribution, fuel cycle optimization, burnup calculation, sensitivity and uncertainty analyses etc (WILLIAMS, 1986). The GPT method has been mostly applied to problems using the neutron diffusion equation (STACEY, 1972; POMRANING, 1983; WILLIAMS, 1986; LEWINS et al., 1986). For the neutron transport problems, a few applications can be found such as a variational nodal transport perturbation theory (LAURIN-KOVITZ and LEWIS, 1996a) based on the response matrix equations and GPT applications based on the collision probability technique (COURAU and MARLEAU, 2003). Here we present the algorithm for GPT estimation of small changes in eigenvalues and functionals of reaction rate ratio based on the multigroup neutron transport equations with isotropic scattering. We study the GPT estimates based on the integral neutron transport equations and discuss the mathematical relationship (WILLIAMS, 1986) between adjoint function (or source importance function) and flux importance function. In fact, the integral transport equations are used in our formulation because they represent the interconnecting neutronic systems of the fuel assemblies. On the other hand, the integro-differential transport equation represents the neutron balance inside an infinitesimal volume. Using this relationship, the flux importance integral transport equation that arise from a GPT formulation is transformed into an integro-differential adjoint (or source importance) transport equation. We also study isotropic and linear approximation methods to evaluate the perturbed integral transport functionals taking part in the GPT estimates.

The resulting adjoint and generalized adjoint transport equations, as well as the forward neutron transport equations, are then solved using the method of cyclic characteristics (MOCC) (ROY, 1998; ASSAWAROONGRUENGCHOT and MARLEAU, 2007b). The MOCC method does not require to evaluate the surface currents at boundaries as the method of characteristics (MOC), and requires only one cycle of scanning over tracking lines resulting in a more rapid spatial conver-

gence rate. The MOCC method requires lower computing time than MOC and CP methods to evaluate the perturbed integral transport functionals when high-order angular corrections to the fluxes are accounted for approximation. This is because the CP method needs to compute the full matrices associated with the perturbed total cross-sections of each mixture (COURAU and MARLEAU, 2003), while the MOCC method performs only spatial iterations over the total neutron sources for each group and mixture. On the other hand, the CP method is more efficient when one needs to compute many types of generalized adjoints because the CP matrices are evaluated only once.

The MOCC generalized adjoint solution algorithm, similar to the algorithm for the adjoint problem (ASSAWAROONGRUENGCHOT and MARLEAU, 2007b), is composed of power/multigroup/spatial iterations and multigroup rebalance scheme. Because of negative adjoint sources in the generalized adjoint problem, the direct use of these sources in the adjoint solution algorithm may result in negative generalized adjoints and cause errors in the rebalance factors and numerical oscillations in the adjoint solutions. This is because the adjoint functions and spatial-integrated adjoint balance sources (adjoint fission and external adjoint sources) must be positive in the multigroup adjoint balance equations. The cancellations between the positive and negative sources in the balance equation may also cause inappropriate corrections for the adjoint solutions. In order to remedy this problem, a flux biasing scheme is applied to make the generalized adjoints positive using the adjoint functions (that are also the homogeneous solutions of the generalized adjoint transport equations). After the convergence of the multigroup iterations is reached, the decontamination process extracts the component parallel to the adjoint functions from the biased generalized adjoints (where the homogeneous solutions are totally removed from the inhomogeneous solutions). In our study we shall investigate three types of biasing/decontamination schemes.

The verification of GPT algorithms is performed for a 17×17 PWR lattice problem. Comparisons of the generalized adjoint functions obtained by the MOCC method and the generalized source importance functions by CP method are presented. Numerical results of GPT estimates and sensitivity coefficients for nuclide densities in PWR and CANDU lattices are also presented.

In Section I.2 we present the forward and adjoint transport equations and the GPT formulations for eigenvalues and reaction rate ratios, and sensitivity coefficients. Section I.3 presents the MOCC formulation of the generalized adjoint transport problems, the relationship between the MOCC generalized adjoint functions and the CP generalized source importances, and the evaluation of the perturbed transport functionals. The MOCC generalized adjoint solution algorithm and the biasing/decontamination scheme are presented in Section I.4. The numerical results of the generalized adjoint solutions, GPT estimates, sensitivity coefficients are presented in Section I.5. The conclusion is presented in the last Section.

I.2 Formulation of Generalized Perturbation Theory

I.2.1 Forward and Adjoint Neutron Transport Equations

Let us first define the multigroup discrete ordinate forward neutron transport equations (LEWIS, 1993) in direction $\vec{\Omega}_l$ for a multiplicative k_{eff} problem with isotropic scattering as follows,

$$(A^g - \lambda B^g)\Phi^g(\vec{r}, \vec{\Omega}_l) = 0 \tag{I.1}$$

where

$$A^g\Phi^g(\vec{r},\vec{\Omega}_l) = \vec{\Omega}_l \cdot \vec{\nabla}\Phi^g(\vec{r},\vec{\Omega}_l) + \Sigma^g(\vec{r})\Phi^g(\vec{r},\vec{\Omega}_l) - \sum_{g'=1}^{G} \Sigma_s^{g\leftarrow g'}(\vec{r})\phi^{g'}(\vec{r})$$

$$B^g\Phi^g(\vec{r},\vec{\Omega}_l) = \sum_{g'=1}^{G} \chi^g(\vec{r})\nu\Sigma_f^{g'}(\vec{r})\phi^{g'}(\vec{r})$$

$$\phi^g(\vec{r}) = \sum_{l=1}^{N^\Omega} W_l^\Omega \Phi^g(\vec{r},\vec{\Omega}_l) \tag{I.2}$$

Here, $\lambda = k_{eff}^{-1}$, and $\vec{\Omega}_l$ is the l-th discretized unit angular directional vector. $\Phi^g(\vec{r},\vec{\Omega}_l)$ and $\phi^g(\vec{r})$ are the forward angular and scalar fluxes. $\Sigma^g(\vec{r})$ and $\Sigma_s^{g\leftarrow g'}(\vec{r})$ are the transport-corrected total and isotropic scattering cross sections respectively where the transport correction takes partially into account the linearly anisotropic contributions to the scattering cross sections (MACFARLANE, 1984). $\Sigma_f^g(\vec{r})$ is the fission cross sections, $\chi^g(\vec{r})$ is the fission production spectrum, and ν is the average number of neutrons generated per fission. Finally, W_l^Ω and N^Ω are respectively the weight and order of the angular quadrature defining the discrete ordinate problem. Here the explicit quadrature we will select is such that a set of cyclic tracking lines can be generated for a 2D Cartesian problem (MARLEAU, 2001).

The boundary conditions used in the neutron transport problem are of the form,

$$\Phi^{g,-}(\vec{r}_s,\vec{\Omega}'_l) = \alpha \cdot \Phi^{g,+}(\vec{r}_s,\vec{\Omega}_l) \tag{I.3}$$

where $\vec{\Omega}'_l = \vec{\Omega}_l - 2(\vec{n}\cdot\vec{\Omega}_l)\vec{n}$, the $+/-$ indicate the outgoing/incoming directions and $\vec{n}$ is the unit outward normal at the boundary surface. α is the albedo or transmission coefficient at the domain boundary. $\vec{\Omega}_l$ and $\vec{\Omega}'_l$ are the unit directional vectors of the angular fluxes impinging on and reflecting from the boundary at point $\vec{r}_s$.

The neutron transport equations (I.1) can also be cast in an equivalent integral form,

$$(\mathcal{L}^g - \lambda \mathcal{F}^g)\Phi^g(\vec{r}, \vec{\Omega}_l) = 0 \tag{I.4}$$

where

$$\begin{aligned}
\mathcal{L}^g\Phi^g(\vec{r}, \vec{\Omega}_l) &= \Phi^g(\vec{r}, \vec{\Omega}_l) - \mathcal{T}_l^{g,-1} \sum_{g'=1}^{G} \Sigma_s^{g \leftarrow g'}(\vec{r})\phi^{g'}(\vec{r}) \\
\mathcal{F}^g\Phi^g(\vec{r}, \vec{\Omega}_l) &= \mathcal{T}_l^{g,-1} \sum_{g'=1}^{G} \chi^g(\vec{r})\nu\Sigma_f^{g'}(\vec{r})\phi^{g'}(\vec{r}) \\
\mathcal{T}_l^{g,-1}(\vec{r}) &= \mathcal{T}^{g,-1}(\vec{r}, \vec{\Omega}_l) = (\vec{\Omega}_l \cdot \vec{\nabla} + \Sigma^g(\vec{r}))^{-1}
\end{aligned} \tag{I.5}$$

The transport equations (I.1) and (I.4) are solved using the collision probability method (COURAU and MARLEAU, 2002), MOCC method (ROY, 1998) or method of characteristics (MOC) (HALSALL, 1980; HONG and CHO, 1998; WU and ROY, 2003).

One can write (I.4) in the explicit integral form for the finite lattice domain unfolded to infinity,

$$\begin{aligned}
\Phi^g(\vec{r}, \vec{\Omega}_l) &= \mathcal{T}^{g,-1}(\vec{r}, \vec{\Omega}_l)q^g(\vec{r}) \\
&= \Phi^g(\vec{r} - S'\vec{\Omega}_l, \vec{\Omega}_l)e^{-\tau^g(\vec{r}-S'\vec{\Omega}_l,\vec{r})}\big|_{S'=\infty} + \int_0^{\infty} dS e^{-\tau^g(\vec{r}-S\vec{\Omega}_l,\vec{r})} q^g(\vec{r} - S\vec{\Omega}_l)
\end{aligned} \tag{I.6}$$

where

$$q^g(\vec{r}) = \sum_{g'=1}^{G} \left[\Sigma_s^{g \leftarrow g'}(\vec{r}) + \lambda \chi^g(\vec{r}) \nu \Sigma_f^{g'}(\vec{r}) \right] \phi^{g'}(\vec{r})$$

$$\tau^g(\vec{r} - S\vec{\Omega}_l, \vec{r}) = \int_0^S dS' \Sigma^g(\vec{r} - S'\vec{\Omega}_l)$$

The first term on RHS of (I.6) vanish due to $e^{-\tau^g(\vec{r}-S'\vec{\Omega}_l,\vec{r})}\big|_{S'=\infty} = 0$

The integration of the inverse transport operator $\mathcal{T}_l^{g,-1}$ over the angular domain and regional volume result in the collision probability when the operands are assumed isotropic and constant within each discretized region (MARLEAU, 2001) :

$$p_{j \to i}^g \equiv \frac{1}{V_j} \int_{V_j} d^3r \sum_{l=1}^{N^\Omega} W_l^\Omega \mathcal{T}^{g,-1}(\vec{r}, \vec{\Omega}_l) \delta_i(\vec{r}) \tag{I.7}$$

where the operand $\delta_i(\vec{r}) = 1$ when $\vec{r}$ is in region i otherwise it is equal to zero.

One can associate with the integro-differential neutron transport equation (I.1) an adjoint transport equation using the following conservation relations (BELL and GLASSTONE, 1979; LEWIS, 1993),

$$\left\langle \Phi^{*g}(\vec{r}, \vec{\Omega}_l), (A^g - \lambda B^g)\Phi^g(\vec{r}, \vec{\Omega}_l) \right\rangle = \left\langle \Phi^g(\vec{r}, \vec{\Omega}_l), (A^{*g} - \lambda B^{*g})\Phi^{*g}(\vec{r}, \vec{\Omega}_l) \right\rangle = 0 \tag{I.8}$$

where the inner product is defined,

$$\langle \Phi^{*g}(\vec{r}, \vec{\Omega}_l), F^g(\vec{r}, \vec{\Omega}_l)\Phi^g(\vec{r}, \vec{\Omega}_l) \rangle = \sum_{g=1}^{G} \sum_{l=1}^{N^\Omega} W_l^\Omega \int_D d^3r \Phi^{*g}(\vec{r}, \vec{\Omega}_l) F^g(\vec{r}, \vec{\Omega}_l) \Phi^g(\vec{r}, \vec{\Omega}_l) \tag{I.9}$$

and D is the spatial domain for the problem.

The adjoint transport equations derived from (I.8) take the form (BELL and GLASSTONE, 1979; LEWIS, 1993),

$$(A^{*g} - \lambda B^{*g})\Phi^{*g}(\vec{r}, \vec{\Omega}_l) = 0 \tag{I.10}$$

where

$$A^{*g}\Phi^{*g}(\vec{r}, \vec{\Omega}_l) = -\vec{\Omega}_l \cdot \vec{\nabla}\Phi^{*g}(\vec{r}, \vec{\Omega}_l) + \Sigma^g(\vec{r})\Phi^{*g}(\vec{r}, \vec{\Omega}_l) - \sum_{g'=1}^{G} \Sigma_s^{g' \leftarrow g}(\vec{r})\phi^{*g'}(\vec{r})$$

$$B^{*g}\Phi^{*g}(\vec{r}, \vec{\Omega}_l) = \sum_{g'=1}^{G} \chi^{g'}(\vec{r})\nu\Sigma_f^g(\vec{r})\phi^{*g'}(\vec{r})$$

$$\phi^{*g}(\vec{r}) = \sum_{l=1}^{N^\Omega} W_l^\Omega \Phi^{*g}(\vec{r}, \vec{\Omega}_l)$$

$\Phi^{*g}(\vec{r}, \vec{\Omega}_l)$ and $\phi^{*g}(\vec{r})$ are the adjoint angular and adjoint scalar functions (or angular and scalar source importances (WILLIAMS, 1986)) respectively. One can see that the adjoint streaming operator has the negative sign from the forward streaming operator and the adjoint scattering matrix is the group-transposition of the forward scattering matrix. Finally, the boundary conditions, associated with adjoint transport problems and boundary conditions (I.3) are,

$$\Phi^{*g,+}(\vec{r}_s, \vec{\Omega}_l) = \alpha \cdot \Phi^{*g,-}(\vec{r}_s, \vec{\Omega}'_l) \tag{I.11}$$

By using the conservation relations (I.8) with the integral transport equations (I.4), we can also obtain the flux importance transport equations in the form,

$$(\mathcal{L}^{\dagger g} - \lambda \mathcal{F}^{\dagger g})\Phi^{\dagger g}(\vec{r}, \vec{\Omega}_l) = 0 \tag{I.12}$$

where

$$\mathcal{L}^{\dagger g}\Phi^{\dagger g}(\vec{r},\vec{\Omega}_l) = \Phi^{\dagger g}(\vec{r},\vec{\Omega}_l) - \sum_{g'=1}^{G}\Sigma_s^{g'\leftarrow g}(\vec{r})\sum_{l'=1}^{N^\Omega} W_{l'}^{\Omega}\mathcal{T}_{l'}^{*g',-1}\Phi^{\dagger g'}(\vec{r},\vec{\Omega}_{l'}) \tag{I.13}$$

$$\mathcal{F}^{\dagger g}\Phi^{\dagger g}(\vec{r},\vec{\Omega}_l) = \sum_{g'=1}^{G}\chi^{g'}(\vec{r})\nu\Sigma_f^{g}(\vec{r})\sum_{l'=1}^{N^\Omega} W_{l'}^{\Omega}\mathcal{T}_{l'}^{*g',-1}\Phi^{\dagger g'}(\vec{r},\vec{\Omega}_{l'}) \tag{I.14}$$

$$\mathcal{T}_l^{*g,-1} = \mathcal{T}^{*g,-1}(\vec{r},\vec{\Omega}_l) = ((\vec{\Omega}_l\cdot\vec{\nabla}+\Sigma^g(\vec{r}))^*)^{-1} = (-\vec{\Omega}_l\cdot\vec{\nabla}+\Sigma^g(\vec{r}))^{-1} \tag{I.15}$$

$$\phi^{\dagger g}(\vec{r}) = \sum_{l=1}^{N^\Omega} W_l^{\Omega}\Phi^{\dagger g}(\vec{r},\vec{\Omega}_l) \tag{I.16}$$

with $\Phi^{\dagger g}(\vec{r},\vec{\Omega}_l)$ and $\phi^{\dagger g}(\vec{r})$ the angular and scalar flux importance functions respectively.

We can write the flux importance equation (I.12) in the explicit integral form,

$$\begin{aligned}\Phi^{\dagger g}(\vec{r},\vec{\Omega}_l) = &\sum_{g'=1}^{G}\left[\Sigma_s^{g'\leftarrow g}(\vec{r}) + \lambda\chi^{g'}(\vec{r})\nu\Sigma_f^{g}(\vec{r})\right] \\ &\sum_{l'=1}^{N^\Omega} W_{l'}^{\Omega}\int_0^\infty dS e^{-\tau^{g'}(\vec{r}+S\vec{\Omega}_{l'},\vec{r})}\Phi^{\dagger g'}(\vec{r}+S\vec{\Omega}_{l'},\vec{\Omega}_{l'})\end{aligned} \tag{I.17}$$

Note that, on the first term on the RHS of equation (I.13), $\Phi^{\dagger g}(\vec{r},\vec{\Omega}_l)$ is isotropic because the sources of the forward transport equation are isotropic.

Since $\mathcal{T}^{*g,-1}(\vec{r},\vec{\Omega}_l) = \mathcal{T}^{g,-1}(\vec{r},-\vec{\Omega}_l)$, the integrations of $\mathcal{T}_l^{*g,-1}$ over the angular domain and regional volume using (I.7) then result in the same collision probability (MARLEAU, 2001; COURAU and MARLEAU, 2002),

$$p_{j\rightarrow i}^{*g} = \frac{1}{V_j}\int_{V_j} d^3r\sum_{l=1}^{N^\Omega} W_l^{\Omega}\mathcal{T}^{*g,-1}(\vec{r},\vec{\Omega}_l)\delta_i(\vec{r}) = p_{j\rightarrow i}^{g} \tag{I.18}$$

where we assume that the angular quadrature is selected in such a way that $W_l^{-\Omega} = W_l^{\Omega}$. From the equivalence between $\mathcal{T}^{*g,-1}(\vec{r},\vec{\Omega}_l)$ and $\mathcal{T}^{g,-1}(\vec{r},-\vec{\Omega}_l)$, one notes that the $\vec{\Omega}_l$-directed adjoint transport equation must be solved in the opposite angular direction from the $\vec{\Omega}_l$-directed forward transport equation (i.e. the inverse adjoint transport operator is the same as the inverse transport operator for the $-\vec{\Omega}_l$ directed transport equation).

The adjoint angular function is related to the angular flux importance (WILLIAMS, 1986) by,

$$\Phi^{*g}(\vec{r},\vec{\Omega}_l) = \mathcal{T}_l^{*g,-1}\Phi^{\dagger g}(\vec{r},\vec{\Omega}_l) \tag{I.19}$$

Operating on both sides of (I.12) with $\mathcal{T}_l^{*g,-1}$ and using (I.19), we can transform the flux importance transport equations (I.12) into the integro-differential adjoint transport equations (I.10).

In order to determine the scalar flux importances using the adjoint scalar functions, we apply (I.19) to (I.12) and integrate the resulting equations over angular domain using the angular quadrature technique as follows,

$$\phi^{\dagger g}(\vec{r}) = \sum_{g'=1}^{G}[\Sigma_s^{g'\leftarrow g}(\vec{r}) + \lambda\chi^{g'}(\vec{r})\nu\Sigma_f^{g}(\vec{r})]\phi^{*g'}(\vec{r}) \tag{I.20}$$

The scalar flux importance function (I.20) is equivalent to the total adjoint source (adjoint fission plus scattering sources) of the integro-differential adjoint transport problem with isotropic scattering.

I.2.2 GPT Method

Here we present the GPT estimations of the eigenvalue and reaction rate ratio based on the integro-differential transport equations which we use as the reference cases. We then study the GPT estimations based on the integral transport equations and introduce the flux importance and generalized flux importance functions to eliminate the first order forward flux variations.

For the GPT estimation of eigenvalue, we assume that the system is perturbed according to,

$$(A_p^g - \lambda_p B_p^g)\Phi_p^g = 0 \tag{I.21}$$

where

$$A_p^g = A^g + \epsilon \Delta A^g \tag{I.22}$$

$$B_p^g = B^g + \epsilon \Delta B^g \tag{I.23}$$

$$\lambda_p = \lambda + \epsilon \Delta \lambda \tag{I.24}$$

$$\Phi_p^g = \Phi^g + \epsilon \Delta \Phi^g \tag{I.25}$$

and ϵ is an infinitesimal real constant. Here $\vec{r}$ and $\vec{\Omega}_l$ are omitted for simplicity.

With the use of (I.21), the classical first order approximation of perturbed eigenvalue $\Delta\lambda$ is in the form (BELL and GLASSTONE, 1979; ROZON, 1998),

$$\Delta\lambda = \frac{\langle \Phi^{*g}, (\Delta A^g - \lambda \Delta B^g)\Phi^g \rangle}{\langle \Phi^{*g}, B^g \Phi^g \rangle} \tag{I.26}$$

where the variations in first order forward fluxes are eliminated using the adjoint functions.

For the GPT estimation of eigenvalue based on the integral transport equation

$$(\mathcal{L}_p^g - \lambda_p \mathcal{F}_p^g)\Phi_p^g = 0 \tag{I.27}$$

we assume that

$$\mathcal{L}_p^g = \mathcal{L}^g + \epsilon\Delta\mathcal{L}^g$$
$$\mathcal{F}_p^g = \mathcal{F}^g + \epsilon\Delta\mathcal{F}^g$$

The first order approximation for $\Delta\lambda$ can be written,

$$\Delta\lambda = \frac{\langle \phi^{\dagger g}, (\Delta\mathcal{L}^g - \lambda\Delta\mathcal{F}^g)\Phi^g \rangle}{\langle \phi^{\dagger g}, \mathcal{F}^g\Phi^g \rangle} \tag{I.28}$$

The main differences between eigenvalue estimates in (I.26) and (I.28) are:

- for the integral transport problem represented by equation (I.28) the scalar flux importance functions are applied to eliminate the first order forward flux variations instead of the angular adjoint functions used for the integro-differential transport problem in (I.26);
- the perturbed system operators $(\Delta\mathcal{L}^g - \lambda\Delta\mathcal{F}^g)\Phi^g$ depend on the first order variations in the cross-sections and inverse transport operator (i.e. $\Delta(\mathcal{T}^{g,-1})$) where the latter takes into account the changes in neutron transfer characteristics between the discretized regions via the tracking lines.

It was shown in Eq. (I.7) that the integration of $\mathcal{T}^{g,-1}$ over the angular domain and the regional volume is equivalent to the CP matrix. Accordingly we can write $\Delta\mathcal{T}^{g,-1}$ as,

$$\Delta\mathcal{T}^{g,-1} \rightarrow [\Delta P_{VV}] = [P_{VV}(\Sigma + \Delta\Sigma)] - [P_{VV}(\Sigma)] \tag{I.29}$$

where the neutron fluxes and cross-sections are assumed constant within each region and $[P_{VV}]$ is the collision probability matrix (ASSAWAROONGRUENGCHOT and MARLEAU, 2007b; COURAU, 2001). On the other hand the perturbed system operators $(\Delta A^g - \lambda \Delta B^g)\Phi^g$ in (I.26) depend only on the first order variations in cross-sections (see Section I.3.3).

For the GPT estimation of linear reaction rate ratio, we first define the performance functional as follows,

$$R_1 = \frac{\langle \Sigma_\kappa^g, \Phi^g \rangle}{\langle \Sigma_\zeta^g, \Phi^g \rangle} \tag{I.30}$$

where Σ_κ^g and Σ_ζ^g are nuclear cross sections. Assuming that the cross sections are perturbed according to,

$$\Sigma_{\kappa,p}^g = \Sigma_\kappa^g + \epsilon \Delta \Sigma_\kappa^g \tag{I.31}$$

$$\Sigma_{\zeta,p}^g = \Sigma_\zeta^g + \epsilon \Delta \Sigma_\zeta^g \tag{I.32}$$

The perturbed functional $R_{1,p}$ becomes,

$$R_{1,p} = R_1 + \epsilon \Delta R_1 = \frac{\langle \Sigma_{\kappa,p}^g, \Phi_p^g \rangle}{\langle \Sigma_{\zeta,p}^g, \Phi_p^g \rangle} \tag{I.33}$$

Assuming the system is perturbed according to (I.21) and using (I.30) to (I.32) in (I.33), the first order approximation for ΔR_1 can then be obtained (COURAU,

2001; COURAU and MARLEAU, 2003),

$$\begin{aligned}\Delta R_1 &= \lim_{\epsilon\to 0}\left(\frac{R_{1,p}-R_1}{\epsilon}\right) = \frac{\left(\langle \Delta\Sigma_\kappa^g, \Phi^g\rangle - R_1\langle \Delta\Sigma_\zeta^g, \Phi^g\rangle\right)}{\langle \Sigma_\zeta^g, \Phi^g\rangle} + \langle S^{*g}, \Delta\Phi^g\rangle \\ &= \frac{\left(\langle \Delta\Sigma_\kappa^g, \Phi^g\rangle - R_1\langle \Delta\Sigma_\zeta^g, \Phi^g\rangle\right)}{\langle \Sigma_\zeta^g, \Phi^g\rangle} + \langle (A^{*g}-\lambda B^{*g})\Gamma^{*g}, \Delta\Phi^g\rangle \\ &= \frac{\left(\langle \Delta\Sigma_\kappa^g, \Phi^g\rangle - R_1\langle \Delta\Sigma_\zeta^g, \Phi^g\rangle\right)}{\langle \Sigma_\zeta^g, \Phi^g\rangle} + \langle \Gamma_\beta^{*g}, -(\Delta A^g - \lambda\Delta B^g)\Phi^g\rangle \end{aligned} \tag{I.34}$$

where

$$\begin{aligned}\langle \Gamma^{*g}, (A^g-\lambda B^g)\Delta\Phi^g\rangle &= \langle \Gamma^{*g}, -(\Delta A^g - \lambda\Delta B^g - \Delta\lambda B^g)\Phi^g\rangle \\ &= \langle \Gamma_\beta^{*g}, -(\Delta A^g - \lambda\Delta B^g)\Phi^g\rangle \end{aligned} \tag{I.35}$$

Here we have used the transport equation for the generalized adjoint angular function $\Gamma^{*g}(\vec{r}, \vec{\Omega}_l)$,

$$(A^{*g}-\lambda B^{*g})\Gamma^{*g}(\vec{r}, \vec{\Omega}_l) = S^{*g} \tag{I.36}$$

to eliminate the effect of first order flux variations (COURAU, 2001; COURAU and MARLEAU, 2003). We also imposed the condition,

$$\langle \Gamma_\beta^{*g}, B^g\Phi^g\rangle = 0 \tag{I.37}$$

to eliminate the term $\Delta\lambda B^g\Phi^g$ in Eq. (I.35).

In Eq. (I.36), S^{*g} is the external generalized adjoint source defined as follows,

$$S^{*g} = \frac{(\Sigma_\kappa^g - R_1\Sigma_\zeta^g)}{\langle \Sigma_\zeta^g, \Phi^g\rangle} \tag{I.38}$$

Note that the particular solution to (I.36) exists when the condition ($\langle S^{*g}, \Phi^g\rangle = 0$)

is satisfied (WILLIAMS, 1986). The generalized adjoint scalar function $\Gamma^{*g}(\vec{r})$ is computed using angular quadrature technique as follows,

$$\Gamma^{*g}(\vec{r}) = \sum_{l=1}^{N^{\Omega}} W_l^{\Omega} \Gamma^{*g}(\vec{r}, \vec{\Omega}_l) \tag{I.39}$$

The general solutions $\Gamma_{\beta}^{*g}(\vec{r}, \vec{\Omega}_l)$ of the inhomogeneous transport equation (I.36) are of the form

$$\Gamma_{\beta}^{*g} = \Gamma^{*g} + \beta \Phi^{*g} \tag{I.40}$$

Here we select β as

$$\beta = -\frac{\langle \Gamma^{*g}, B^g \Phi^g \rangle}{\langle \Phi^{*g}, B^g \Phi^g \rangle} \tag{I.41}$$

in order to satisfy Eq. (I.37).

For the GPT estimation of linear reaction rate ratio based on the integral transport equation we assume that the system is perturbed according to (I.27). Using (I.30) to (I.32) in (I.33), the first order approximation for ΔR_1 based on the integral neutron transport equations is obtained,

$$\Delta R_1 = \frac{(\langle \Delta \Sigma_{\kappa}^g, \Phi^g \rangle - R_1 \langle \Delta \Sigma_{\zeta}^g, \Phi^g \rangle)}{\langle \Sigma_{\zeta}^g, \Phi^g \rangle} + \langle \Gamma_{\beta}^{\dagger g}, -(\Delta \mathcal{L}^g - \lambda \Delta \mathcal{F}^g) \Phi^g \rangle \tag{I.42}$$

where we use the generalized flux importance transport equations to eliminate the first order flux variations,

$$(\mathcal{L}^{\dagger g} - \lambda \mathcal{F}^{\dagger g}) \Gamma^{\dagger g}(\vec{r}, \vec{\Omega}_l) = (\mathcal{L}^{\dagger g} - \lambda \mathcal{F}^{\dagger g}) \Gamma^{\dagger g}(\vec{r}) = S^{\dagger g}(\vec{r}) \tag{I.43}$$

with $S^{\dagger g}$ is the external generalized adjoint source:

$$S^{\dagger g} = \frac{(\Sigma_\kappa^g - R_1 \Sigma_\zeta^g)}{\langle \Sigma_\zeta^g, \Phi^g \rangle}$$

and $\Gamma^{\dagger g}(\vec{r}, \vec{\Omega}_l)$ the generalized angular flux importance function is isotropic. The differences between the GPT estimates (I.34) and (I.42) are similar to those for the eigenvalue estimates as discussed previously.

Similar to the mathematical relationship between flux importance and source importance functions (I.19), the relationship between the generalized adjoint function and the generalized flux importance is,

$$\Gamma^{*g}(\vec{r}, \vec{\Omega}_l) = \mathcal{T}_l^{*g,-1} \Gamma^{\dagger g}(\vec{r}, \vec{\Omega}_l) \tag{I.44}$$

Operating on both sides of (I.43) with $\mathcal{T}_l^{*g,-1}$ and using (I.44), we can arrange the resulting equations into the integro-differential generalized adjoint transport equations (I.36).

We can indirectly compute the generalized flux importances $\Gamma_\beta^{\dagger g}(\vec{r})$ from the generalized adjoints $\Gamma_\beta^{*g}(\vec{r})$ by applying (I.40), (I.41) and (I.44) to (I.43), and integrating the resulting equations over angular domain,

$$\Gamma_\beta^{\dagger g}(\vec{r}) = \sum_{g'=1}^{G} [\Sigma_s^{g' \leftarrow g}(\vec{r}) + \lambda \chi^{g'}(\vec{r}) \nu \Sigma_f^g(\vec{r})] \Gamma_\beta^{*g'}(\vec{r}) + S^{\dagger g} \tag{I.45}$$

One can find that the generalized scalar flux importance is equivalent to the total generalized adjoint source (generalized adjoint fission, scattering and external generalized adjoint sources) of the integro-differential generalized adjoint transport problem with isotropic scattering. The evaluation of the perturbed transport functionals including the perturbed transport operators is discussed in Section I.3.3.

I.2.3 Sensitivity Coefficients

The sensitivity coefficient of the performance functional R with respect to a reactor parameter α_q is defined as the relative change in R due to a relative change in α_q as follows,

$$S_R^q = \frac{\alpha_q}{R}\frac{\partial R}{\partial \alpha_q} \tag{I.46}$$

where α_q is the q-th parameter of a reactor core.

For the case where R_1 is given by equation (I.30), using (I.42) the sensitivity coefficient of R_1 with respect to α_q based on the integral transport equations is,

$$\begin{aligned} S_{R_1}^q &= \frac{\alpha_q}{R_1}\left[\frac{(\langle\frac{\partial\Sigma_\kappa^g}{\partial\alpha_q},\Phi^g\rangle - R_1\langle\frac{\partial\Sigma_\zeta^g}{\partial\alpha_q},\Phi^g\rangle)}{\langle\Sigma_\zeta^g,\Phi^g\rangle} + \langle\Gamma_\beta^{\dagger g},-(\frac{\partial\mathcal{L}^g}{\partial\alpha_q}-\lambda\frac{\partial\mathcal{F}^g}{\partial\alpha_q})\Phi^g\rangle\right] \\ &= \frac{\alpha_q}{R_1\Delta\alpha_q}\left[\frac{(\langle\Delta\Sigma_\kappa^g,\Phi^g\rangle - R_1\langle\Delta\Sigma_\zeta^g,\Phi^g\rangle)}{\langle\Sigma_\zeta^g,\Phi^g\rangle} + \langle\Gamma_\beta^{\dagger g},-(\Delta\mathcal{L}^g-\lambda\Delta\mathcal{F}^g)\Phi^g\rangle\right] \end{aligned} \tag{I.47}$$

Using (I.28) the sensitivity coefficient of the eigenvalue with respect to α_q is,

$$S_\lambda^q = \sum_{g=1}^{G} S_\lambda^{q,g} = \frac{\alpha_q}{\lambda\Delta\alpha_q}\frac{\langle\phi^{\dagger g},(\Delta\mathcal{L}^g-\lambda\Delta\mathcal{F}^g)\Phi^g\rangle}{\langle\phi^{\dagger g},\mathcal{F}^g\Phi^g\rangle} \tag{I.48}$$

where $S_\lambda^{q,g}$ are the group-based sensitivity coefficients of eigenvalue to α_q. For the parameters of which the macroscopic cross sections are not the linear function, such as fuel temperature (T_f), we will use the first order finite difference method to approximate the derivative terms (e.g. $\partial\Sigma/\partial T_f \approx \Delta\Sigma/\Delta T_f$) in sensitivity evaluation.

I.3 The MOCC Method and Evaluation of the Perturbed Transport Operators

I.3.1 MOCC Method

In this section we briefly present the characteristics formulation of the generalized adjoint problem which is similar to the formulation for the adjoint transport problem (ASSAWAROONGRUENGCHOT and MARLEAU, 2007b). The boundary conditions associated with the generalized adjoint problem are similar to the boundary conditions of the adjoint problem defined in (I.11). When a void boundary ($\alpha = 0$) is considered, these boundary conditions give the zero outgoing generalized angular adjoints at boundary. Therefore we need to solve the generalized adjoint transport equation in the backward direction ($-\vec{\Omega}_l$).

Let us now consider the spatial domain D having infinite length along Z axis as shown in figure I.1. A tracking line generated across D in direction $\vec{\Omega}_l$ is composed of line segments indexed by L_k. The total generalized adjoint sources q_k^{*g} and total cross sections Σ_k^g on L_k are assumed constant. For two dimensional problems in the X-Y plane, $\Gamma^{*g}(\vec{r}, \vec{\Omega})$ is independent of Z. We then write the generalized adjoint characteristics equation for L_k as follows,

$$\Gamma^{*g}(\vec{p}_k, \vec{\Omega}_l) = \Gamma^{*g}(\vec{p}_{k+1}, \vec{\Omega}_l) e^{-\frac{\Sigma_k^g \gamma_k}{\sin(\theta)}} + \frac{q_k^{*g}}{\Sigma_k^g}[1 - e^{-\frac{\Sigma_k^g \gamma_k}{\sin(\theta)}}] \tag{I.49}$$

where $L_k = \gamma_k / \sin(\theta)$, and $\vec{p}_k$ and $\vec{p}_{k+1}$ are the projections $\vec{r_k}$ and $\vec{r}_{k+1}$ on X-Y plane respectively. Next we determine the average generalized adjoint angular function on L_k,

$$L_k \overline{\Gamma}_k^{*g}(\vec{\Omega}_l) = \frac{\Gamma^{*g}(\vec{p}_{k+1}, \vec{\Omega}_l)}{\Sigma_k^g}[1 - e^{\frac{-\Sigma_k^g \gamma_k}{\sin(\theta)}}] + \frac{q_k^{*g}}{\Sigma_k^g \Sigma_k^g}\left[\frac{\Sigma_k^g \gamma_k}{\sin\theta} - [1 - e^{\frac{-\Sigma_k^g \gamma_k}{\sin(\theta)}}]\right] \tag{I.50}$$

In a rectangular spatial domain unfolded to infinity using reflective boundary con-

ditions, a cyclic tracking line is defined in such a way that each line starts and ends at the same point after periodically translating along the infinite tracking lines (MARLEAU, 2001). Since the starting and ending points of a cyclic tracking line are the same point in the finite domain, we find that $\Gamma^{*g}(\vec{p}_1, \vec{\Omega}_l) = \Gamma^{*g}(\vec{p}_{K+1}, \vec{\Omega}_l)$. The generalized adjoint angular function $\Gamma^{*g}(\vec{p}_1, \vec{\Omega}_l)$ is then determined by,

$$\Gamma^{*g}(\vec{p}_1, \vec{\Omega}_l) = \frac{M(K)}{[1 - \prod_{k'=1}^{K}[H(k')\beta_{alb}(k')]]} \tag{I.51}$$

when $M(K)$ is finite and $\prod_{k'=1}^{K} H(k')\beta_{alb}(k') < 1$. Here we define,

$$M(K) = \sum_{k=1}^{K} \left[\left(\prod_{k'=1}^{k-1} [H(k')\beta_{alb}(k')] \right)^{\varrho(k)} \left(\frac{1 - e^{\frac{-\Sigma_k^g \gamma_k}{\sin\theta}}}{\Sigma_k^g} \right)^{\vartheta(k)} \left(\frac{\gamma_k}{\sin\theta} \right)^{1-\vartheta(k)} \right] q_k^{*g}$$

with $H(k) = \exp[-(\Sigma_k^g \gamma_k)/\sin\theta]$, $\varrho(k) = 1$ for $k > 1$ otherwise it is equal to 0, $\vartheta(k) = 0$ when L_k is in void region otherwise it is equal 1, and $\beta_{alb}(k) = \alpha(k)$ when L_k is in contact with the boundary at point $\vec{p}_k$, otherwise it is equal 1.

Next we determine the average generalized adjoint scalar function in region j using the characteristics formalism (WU and ROY, 2003; ASSAWAROONGRUENGCHOT and MARLEAU, 2007b) as follows,

$$V_j \Gamma_j^{*g} = \sum_{l=1}^{N^\Omega} \sum_{i=1}^{N^\perp(l)} W_i^\perp W_l^\Omega \sum_{k=1}^{K} [F_j(\vec{\Upsilon}(\vec{P}_i, \vec{\Omega}_l), \vec{p}_{k+1/2}) L_k \overline{\Gamma}_k^{*g}(\vec{\Omega}_l)] \tag{I.52}$$

where $\vec{\Upsilon}(\vec{P}, \vec{\Omega})$ is a tracking line defined by its reference starting point $\vec{P}$ and a direction vector $\vec{\Omega}$. $F_j(\vec{\Upsilon}, \vec{P} + S\vec{\Omega})$ is equal to 1 when the point $(\vec{P} + S\vec{\Omega})$ on $\vec{\Upsilon}(\vec{P}, \vec{\Omega})$ is in the region j, otherwise it takes a value of 0. $W_i^\perp$ is the quadrature weight for a starting point $\vec{P}_i$ of $\vec{\Upsilon}(\vec{P}_i, \vec{\Omega}_l)$, $N^\perp(l)$ is the total number of tracking lines in direction $\vec{\Omega}_l$, and $\vec{p}_{k+1/2}$ is the center point of L_k. The procedures for solving the generalized adjoint transport equations, such as power, multigroup and

spatial iterations, biasing/decontaminations schemes, and evaluation of Γ_{β}^{*g}, will be explained in section I.4.

I.3.2 Relationship Between Generalized Adjoint Functions by MOCC and CP Methods

The MOCC adjoint scalar function can be written in the form of collision probability equation as follows, (ASSAWAROONGRUENGCHOT and MARLEAU, 2007b)

$$[\phi^*] = [P_{VV}][Q^*] \tag{I.53}$$

$$[Q^*] = \left[[\Sigma_s]^T + \lambda\,[[\chi]\cdot[\nu\Sigma_f]]^T\right][\phi^*] \tag{I.54}$$

Here $[\phi^*]$ is the vector of MOCC adjoint scalar functions, $[P_{VV}]$ is the MOCC response matrix which is equivalent to collision probability matrix, $[\Sigma_s]$ and $[\nu\Sigma_f]$ are respectively matrices of scattering and fission neutron production cross sections, and $[\chi]$ is the matrix of probability of fission neutron production.

The relationship between the adjoint scalar function (source importance function) and the scalar flux importance is defined (WILLIAMS, 1986; COURAU and MARLEAU, 2002; ASSAWAROONGRUENGCHOT and MARLEAU, 2007b),

$$[\phi^*] = [P_{VV}][\phi^\dagger] \tag{I.55}$$

Using (I.55) in (I.53), we obtain the MOCC flux importance equation,

$$[\phi^\dagger] = [Q^*] = \left[[\Sigma_s]^T + \lambda\,[[\chi]\cdot[\nu\Sigma_f]]^T\right][P_{VV}][\phi^\dagger] \tag{I.56}$$

One can again find that the flux importances are the total adjoint sources of the integro-differential adjoint transport problem.

For the generalized adjoint transport problem, the characteristics formulation is similar to the formulation for the adjoint problem except that external sources S^{*g} are now included. The MOCC generalized adjoint functions can then be cast in the matrix form using (I.53),

$$[\Gamma^*] = [P_{VV}][Q^*_\Gamma] \tag{I.57}$$

$$[Q^*_\Gamma] = \left[[\Sigma_s]^T + \lambda\,[[\chi]\cdot[\nu\Sigma_f]]^T\right][\Gamma^*] + [S^*] \tag{I.58}$$

where $[\Gamma^*]$ and $[S^*]$ are the vector of the generalized adjoints and external sources.

The generalized adjoint MOCC equation (I.57) is the same as the generalized source importance CP equation (COURAU and MARLEAU, 2003). Thus the MOCC generalized adjoint function is equivalent to the CP generalized source importance.

From the relationship between $\Gamma^{*g}(\vec{r},\vec{\Omega}_l)$ and $\Gamma^{\dagger g}(\vec{r},\vec{\Omega}_l)$, the integration of (I.44) over angular domain and region j results in the CP multiplications using definitions in (I.18),

$$[\Gamma^*] = [P_{VV}][\Gamma^\dagger] \tag{I.59}$$

where $[\Gamma^\dagger]$ is the vector of the generalized scalar flux importances.

Applying (I.59) to (I.57), the generalized flux importance equation are obtained,

$$[\Gamma^\dagger] = [Q^*_\Gamma] = \left[[\Sigma_s]^T + \lambda\,[[\chi]\cdot[\nu\Sigma_f]]^T\right][P_{VV}][\Gamma^\dagger] + [S^\dagger] \tag{I.60}$$

where $[S^*] = [S^\dagger]$. One may again see that the generalized flux importances are the total generalized adjoint sources of the integro-differential generalized adjoint transport problem.

I.3.3 Evaluation of the Perturbed Transport Operators

Here we present two approximation methods for the perturbed integral transport functional $\left\langle \phi^{\dagger g}, (\Delta\mathcal{L}^g - \lambda\Delta\mathcal{F}^g)\Phi^g \right\rangle$. We first present the approximation of the perturbed integro-differential transport functional $\left\langle \Phi^{*g}, (\Delta A^g - \lambda\Delta B^g)\Phi^g \right\rangle$ where the adjoint angular functions are assumed isotropic (COURAU, 2001). Then we present the isotropic approximation method for the perturbed integral transport functional by assuming that the source terms in the modified transport equations and adjoint functions are isotropic. This functional is found equivalent to the approximated perturbed integro-differential transport functional. Secondly, when the source terms in the modified transport equations are assumed anisotropic, we introduce a method that linearizes the term $([P_{VV}(\Sigma+\Delta\Sigma)]-[P_{VV}(\Sigma)])[Q]$ (which is indirectly associated with these anisotropic sources) with respect to the total cross-sections of each group and mixture.

Let us first evaluate the $\left\langle \Phi^{*g}, (\Delta A^g - \lambda\Delta B^g)\Phi^g \right\rangle$ term. Using,

$$\begin{aligned} \Delta A^g\Phi^g &= \Delta\Sigma^g\Phi^g(\vec{r},\vec{\Omega}_l) - \sum_{g'=1}^{G}\Delta\Sigma_s^{g\leftarrow g'}\phi^{g'}(\vec{r}) \\ \Delta B^g\Phi^g &= \sum_{g'=1}^{G}\chi^g\Delta(\nu\Sigma_f^{g'})\phi^{g'}(\vec{r}) \end{aligned} \tag{I.61}$$

where $\Delta\chi$ is assumed very small and negligible we can write:

$$\begin{aligned} \left\langle \Phi^{*g}, (\Delta A^g - \lambda\Delta B^g)\Phi^g \right\rangle = &\left\langle \Phi^{*g}, \Delta\Sigma^g\Phi^g \right\rangle \\ &- \left\langle \Phi^{*g}, \sum_{g'=1}^{G}(\Delta\Sigma_s^{g\leftarrow g'} + \lambda\chi^g\Delta(\nu\Sigma_f^{g'}))\phi^{g'} \right\rangle \end{aligned} \tag{I.62}$$

Since only Φ^{*g} depends on $\vec{\Omega}_l$ in the last term on the RHS of (I.62), the angular summation associated with the scalar product yields ϕ^{*g} in this case. For the

first term on the RHS of (I.62) the angular summation requires both Φ^{*g} and Φ^{g}. Here we will assume that Φ^{*g} is isotropic ($\Phi^{*g}(\vec{r},\vec{\Omega}_l) \approx \phi^{*g}(\vec{r})$) so that the angular summation over Φ^{g} can also be performed analytically. We then obtain

$$\left\langle \Phi^{*g}, (\Delta A^g - \lambda \Delta B^g)\Phi^g \right\rangle \approx \left\langle \phi^{*g}, \Delta\Sigma^g \phi^g - \sum_{g'=1}^{G} (\Delta\Sigma_s^{g\leftarrow g'} + \lambda \chi^g \Delta(\nu\Sigma_f^{g'}))\phi^{g'} \right\rangle \tag{I.63}$$

If we use the integral transport equation, we need to to evaluate $\left\langle \phi^{\dagger g}, (\Delta\mathcal{L}^g - \lambda\Delta\mathcal{F}^g)\Phi^g \right\rangle$ to first order:

$$\begin{aligned}
\Delta\mathcal{L}^g\Phi^g &\approx -\Delta(\mathcal{T}^{g,-1}) \sum_{g'=1}^{G} \Sigma_s^{g\leftarrow g'} \phi^{g'}(\vec{r}) - \mathcal{T}^{g,-1} \sum_{g'=1}^{G} \Delta\Sigma_s^{g\leftarrow g'} \phi^{g'}(\vec{r}) \\
\Delta\mathcal{F}^g\Phi^g &\approx \Delta(\mathcal{T}^{g,-1}) \sum_{g'=1}^{G} \chi^g \nu\Sigma_f^{g'} \phi^{g'}(\vec{r}) + \mathcal{T}^{g,-1} \sum_{g'=1}^{G} \chi^g \Delta(\nu\Sigma_f^{g'}) \phi^{g'}(\vec{r})
\end{aligned} \tag{I.64}$$

where $\Delta(\mathcal{T}^{g,-1}) = \mathcal{T}_p^{g,-1} - \mathcal{T}^{g,-1}$

Using (I.29), (I.55) and (I.64) in $\left\langle \phi^{\dagger g}, (\Delta\mathcal{L}^g - \lambda\Delta\mathcal{F}^g)\Phi^g \right\rangle$, we can obtain,

$$\begin{aligned}
\left\langle \phi^{\dagger g}, (\Delta\mathcal{L}^g - \lambda\Delta\mathcal{F}^g)\Phi^g \right\rangle &\approx -\left\langle [\phi^\dagger], ([P_{VV}(\Sigma+\Delta\Sigma)] - [P_{VV}(\Sigma)])\,[Q] \right\rangle \\
&\quad -\left\langle [\phi^\dagger], [P_{VV}(\Sigma)]\,([\Delta\Sigma_s][\phi] + \lambda[\chi][\Delta(\nu\Sigma_f)][\phi]) \right\rangle \\
&\approx -\left\langle [\phi^\dagger], [\Delta P_{VV}][Q] \right\rangle \\
&\quad -\left\langle [\phi^*], ([\Delta\Sigma_s][\phi] + \lambda[\chi][\Delta(\nu\Sigma_f)][\phi]) \right\rangle
\end{aligned} \tag{I.65}$$

where,

$$\left\langle [X],[Y] \right\rangle \equiv [X]^T[V][Y]$$

$$[\Delta P_{VV}] = [P_{VV}(\Sigma + \Delta\Sigma)] - [P_{VV}(\Sigma)]$$

$$[Q] = [[\Sigma_s] + \lambda[\chi][\nu\Sigma_f]]\,[\phi]$$

$[V]$ the matrix of the regional volumes, and the flux importance and adjoint functions are assumed constant within each region. The term $[\Delta P_{VV}][Q]$ will be approximated using 2 methods: the isotropic approximation (IA) and linear approximation (LA) methods. For the IA method, we first add the term $\Delta\Sigma^g\Phi^g$ to both sides of the neutron transport equation (I.1),

$$\vec{\Omega}_l \cdot \vec{\nabla}\Phi^g(\vec{r},\vec{\Omega}_l) + \Sigma^g\Phi^g(\vec{r},\vec{\Omega}_l) + \Delta\Sigma^g\Phi^g(\vec{r},\vec{\Omega}_l) = \sum_{g'=1}^{G}[\Sigma_s^{g\leftarrow g'} + \lambda\chi^g\nu\Sigma_f^{g'}]\phi^{g'}(\vec{r}) + \Delta\Sigma^g\Phi^g(\vec{r},\vec{\Omega}_l) \qquad \text{(I.66)}$$

We know that the flux solutions of the transport equation (I.66) are the same as the solutions of the transport equation (I.1). By assuming that $\Delta\Sigma^g\Phi^g$ on RHS of (I.66) is isotropic, we can write the solutions of (I.1) and (I.66) in the CP form (MARLEAU, 2001),

$$\phi_j^g = \sum_{i=1}^{N_J} p_{j\to i}^g q_i^g = \sum_{i=1}^{N_J} \tilde{p}_{j\to i}^g (q_i^g + \Delta\Sigma\phi_i^g) \qquad \text{(I.67)}$$

where $\tilde{p}_{j\to i}^g \equiv p_{j\to i}^g(\Sigma + \Delta\Sigma)$

The equation (I.67) in the matrix form is,

$$[\Delta P_{VV}][Q] = -[P_{VV}(\Sigma + \Delta\Sigma)][\Delta\Sigma][\phi] \approx -[P_{VV}(\Sigma)][\Delta\Sigma][\phi] \qquad \text{(I.68)}$$

Applying (I.68) into (I.65), we find that the approximated perturbed integral transport functional (I.65) using IA method is equivalent to the approximated perturbed integro-differential transport functional $\left\langle \Phi^{*g}, (\Delta A^g - \lambda \Delta B^g)\Phi^g \right\rangle$ in (I.63).

For the LA method, when the term $\Delta\Sigma^g\Phi^g$ on RHS of (I.66) is assumed anisotropic, equation (I.67) becomes,

$$\begin{aligned}
\phi_j^g &= \sum_{i=1}^{N_J} p_{j\to i}^g \cdot q_i^g \\
&= \sum_{i=1}^{N_J} \left[\tilde{p}_{j\to i}^g \cdot q_i^g + \frac{1}{V_j} \int_{V_j} d^3r \int_{V_i} d^3r' \frac{e^{-\tau^g((\Sigma+\Delta\Sigma),\vec{r'},\vec{r})}}{\|\vec{r'} - \vec{r}\|^2} \delta_i(\vec{r'}) \Delta\Sigma^g \Phi^g(\vec{r'}, \vec{\Omega}_l) \right] \\
&= \sum_{i=1}^{N_J} \left[\tilde{p}_{j\to i}^g \cdot q_i^g + \Xi_{j\to i}^g \Delta\Sigma_i^g \right] \qquad \text{(I.69)}
\end{aligned}$$

where,

$$\Xi_{j\to i}^g = \frac{1}{V_j} \int_{V_j} d^3r \int_{V_i} d^3r' \frac{e^{-\tau^g((\Sigma+\Delta\Sigma),\vec{r'},\vec{r})}}{\|\vec{r'} - \vec{r}\|^2} \delta_i(\vec{r'}) \Phi^g(\vec{r'}, \vec{\Omega}_l) \qquad \text{(I.70)}$$

with $\Delta\Sigma^g(\vec{r'}) = \Delta\Sigma_i^g$ for $\vec{r'}$ a point in V_i. We can finally write equation (I.69) in the matrix form,

$$[\Delta P_{VV}][Q] = -[\Xi][\Delta\Sigma] \qquad \text{(I.71)}$$

Because the direct computation for the $\Xi_{j\to i}^g$ factors in (I.69) may be complicated, we can indirectly approximate $[\Xi]$ matrix as follows,

$$[\Xi][\Delta\Sigma] \approx \sum_{m=1}^{N_{MIX}} [\hat{\Xi}_m][\Delta\Sigma_m] \qquad \text{(I.72)}$$

with N_{MIX} is the number of mixtures used in the problem. Here $[\hat{\Xi}_m]$ is a $(N_J \times G)$

by $(N_J \times G)$ diagonal matrix containing the linearization factors $\hat{\Xi}^g_{m,j}$, and $[\Delta\Sigma_m]$ is a vector of dimension $N_J \times G$ containing the total cross-section perturbations of the m-th mixture. The linearization factors of the m-th mixture are pre-evaluated using,

$$\hat{\Xi}^g_{m,j} = -\frac{1}{d\Sigma^g_m}\sum_{i=1}^{N_J}(p^g_{j\to i}(\Sigma^g + d\Sigma^g_m) - p^g_{j\to i}(\Sigma^g))q^g_i \tag{I.73}$$

where we will use $d\Sigma^g_m = 10^{-4}\Sigma^g_m$. To determine these linearization factors, we use the MOCC algorithm to perform $G \times N_{MIX}$ scanning over tracking lines (to evaluate $[P_{VV}(\Sigma + d\Sigma)][Q]$ for each group and mixture). In the GPT based on the CP equations (COURAU and MARLEAU, 2003) there is an equivalent correction scheme based on the evaluation of the correction factors associated with the term

$$([P_{VV}(\Sigma)][Q] - [P_{VV}(\Sigma + d\Sigma)]([\Sigma_s] + \lambda[\chi][\nu\Sigma_f] + [d\Sigma])[\phi])$$

Note that this scheme needs long computing time to evaluate the N_{MIX} CP matrices associated with the total cross-section perturbation $[d\Sigma_m]$ of each group and mixture.

The same procedures are applied to evaluate the perturbed transport functionals

$$\left\langle \Gamma^{*g}, (\Delta A^g - \lambda\Delta B^g)\Phi^g \right\rangle \qquad \text{and} \qquad \left\langle \Gamma^{\dagger g}, (\Delta \mathcal{L}^g - \lambda\Delta \mathcal{F}^g)\Phi^g \right\rangle$$

where the generalized adjoints and flux importances are assumed isotropic and constant within each region.

I.4 Solutions of Generalized Adjoint Transport Equations

The generalized adjoint solution algorithm is implemented in the lattice code DRAGON (MARLEAU, 2001; ASSAWAROONGRUENGCHOT and MARLEAU, 2005) where the generalized adjoint transport calculations proceed as follows. First the geometries of the fuel assemblies are analyzed and tracked. The tracking lines with the cyclic angles are generated over the discretized geometries using an adequate angular quadrature for the polar and azimuthal angles. The macroscopic cross sections are extracted from a microscopic cross section data library or provided as user input data. The external generalized adjoint sources are evaluated using the pre-computed forward fluxes and the cross-sections associated with the GPT functional.

Next the generalized adjoint functions are initialized and the MOCC generalized adjoint solution algorithm is called. This algorithm here is similar to that used for the adjoint MOCC solutions and is generally composed of three levels of iterations: the power iteration over adjoint fission sources and external generalized adjoint sources, the multigroup iteration over the adjoint scattering sources and the spatial iteration over the tracking lines respectively (see figure I.2). The adjoint fission sources are evaluated and added to the external generalized adjoint sources in the power iteration loop. These adjoint sources are then transferred into the multigroup iteration loop where they will be assumed constant. The adjoint scattering sources are then evaluated and added to the total generalized adjoint sources. The group-reduction procedure is implemented to avoid the iterations for the generalized adjoint functions in the converged groups as well as the group-splitting procedure (ASSAWAROONGRUENGCHOT and MARLEAU, 2005; ASSAWAROONGRUENGCHOT and MARLEAU, 2007b) for speeding up the multigroup iterations. The spatial iterations are performed by scanning over the cyclic tracking lines to

determine a closed form using the generalized adjoint characteristics equations (Eq. (I.49)) and the computed total generalized adjoint sources. Here the closed forms (Eq. (I.51)) for generalized adjoint angular functions on each cyclic tracking line are used to evaluate the average generalized adjoint angular functions (Eq. (I.50)) on each segment of cyclic tracking lines. The generalized adjoints in each region are then calculated using the average generalized adjoint scalar equation (Eq. (I.52)).

After each spatial iteration is complete, the multigroup rebalance technique (ASSAWAROONGRUENGCHOT and MARLEAU, 2005) is performed to correct the generalized adjoints using the multigroup adjoint balance equations. The multigroup convergence test routine verifies the convergence of generalized adjoints in each multigroup iteration. After the multigroup convergence is reached, the orthogonal generalized adjoints are extracted from the biased generalized adjoints using decontamination scheme. Various biasing/decontamination schemes are discussed in the next section. The convergence test routine verifies the convergence of the generalized adjoints after each power iteration. At the end of the iteration process, a decontamination is performed and the selected solutions (Γ_β^{*g} and $\Gamma_\beta^{\dagger g}$) are determined according to the methods used in the evaluation of the perturbed transport operators.

I.4.1 Biasing and Decontamination Schemes

Because of the negative external generalized adjoint sources, direct use of these sources in the adjoint solution algorithm shall result in the negative generalized adjoints (unlike the forward fluxes and adjoint functions which are strictly positive). During the multigroup iterations, using such negative values in the adjoint rebalance scheme (ASSAWAROONGRUENGCHOT and MARLEAU, 2007b) can cause errors in the rebalance factors and numerical oscillations in the solutions (e.g.

the negative rebalance factors change the signs of the generalized adjoints which then induce numerical oscillations). The rebalance scheme then becomes less effective to speed up the solutions. This problem arises because, in the adjoint balance equations, adjoint functions and spatial-integrated adjoint balance sources (adjoint fission plus external sources) must be positive, and the cancellations between positive and negatives sources may lead to inadequate rebalance factors. To avoid this problem, the generalized adjoints are made positive using a biasing scheme defined as follows,

$$[\Gamma^*_{\text{bias}}] = [\Gamma^*] + C_{\text{bias}}[\phi^*] \tag{I.74}$$

$$C_{\text{bias}} = \max_{i,g}\left(\frac{f_b q_i^{*g} - S_i^{*g}}{q_i^{*g}}\right) \tag{I.75}$$

$$q_i^{*g} = \sum_{g'=1}^{G}(\Sigma_{s,i}^{g'\leftarrow g} + \frac{1}{k_{eff}}\chi_i^{g'}\nu\Sigma_{f,i}^{g})\phi_i^{*g'} \tag{I.76}$$

where C_{bias} is the biasing factor. f_b is a predetermined positive source biasing factor. Index i indicates the i-th region. q_i^{*g} are the standard adjoint fission plus scattering sources. The adjoint functions are used in the biasing because they are also the homogeneous solutions of the generalized adjoint transport equations and they are strictly positive. The biased generalized adjoints are determined so that they result in positive total generalized adjoint sources. For a specific f_b, the biasing factor may not always result in positive generalized adjoints. The selection of f_b is discussed in the section I.5. After the multigroup iteration is completed, the orthogonal generalized adjoints $\Gamma_\perp^{*g}$ are extracted using a decontamination scheme,

$$[\Gamma^*_\perp] = [\Gamma^*_{\text{bias}}] - C_{\text{decon}}[\phi^*] \tag{I.77}$$

$$C_{\text{decon}} = \frac{[\Gamma^*_{\text{bias}}]^T[\phi^*]}{[\phi^*]^T[\phi^*]} \tag{I.78}$$

in order to satisfy $[\Gamma^*_\perp]^T[\phi^*] = 0$, where C_{decon} is the required decontamination factor. One can find that the decontamination scheme removes the homogeneous solutions from the total inhomogeneous solutions (biased adjoints). Note that this decontamination scheme is performed only in the power loop. When the convergence is reached, we then evaluate the selected solution $[\Gamma^*_\beta]$ using Eq. (I.40). In our study, we examine three types of biasing and decontamination schemes as follows,

- *Scheme 1* consists of a 2 step biasing/decontamination scheme. In the first step the generalized adjoints are biased once in the first power iteration loop using Eq. (I.74). We then use these biased generalized adjoints in the power and multigroup iterations. The rebalance procedure in the multigroup iteration is turned on but the decontamination procedure is turned off in this step. When the biased generalized adjoints converge, the orthogonal generalized adjoints are extracted using Eq. (I.77). The first step is stopped and then the second step power iteration begins. In this second step the generalized adjoints are kept unbiased. The orthogonal generalized adjoints are directly used in the power and multigroup iterations. The rebalance procedure is turned off as well as decontamination in the power iterations. When the second step power iterations converge, the last decontamination is performed to extract the required orthogonal generalized adjoints Γ^{*g}_β.

- *Scheme 2* consists of a single-step biasing/decontamination scheme that is performed in each power iteration loop. The generalized adjoints are biased at the beginning of each power iteration loop and then used in the power and multigroup iterations. When multigroup iterations converge, the orthogonal generalized adjoints are extracted and used in the next power iteration loop. The convergence of multigroup iterations relies on the biased generalized adjoints while convergence of power iterations relies on the orthogonal generalized adjoints.

- *Scheme 3* is a 2 step biasing/decontamination scheme similar to Scheme 1 except that, in the first step, the biasing and decontamination are performed in each power iteration (as described in Scheme 2).

I.5 Numerical Results

I.5.1 17×17 PWR lattice

In the numerical simulation, the two-dimensional 17×17 PWR lattice (MARLEAU et al., 2000) is discretized into 135 regions according to the exact geometries with the use of 1/8 symmetrical property (see Figure I.3). Reflective boundary conditions are used in this problem. The 69 energy group nuclear cross sections are obtained from the WIMS-AECL library (MARLEAU et al., 2000). The resonance self-shielding model (MARLEAU et al., 2000) is applied to correct the cross sections in the resonance energy groups. The azimuthal angular integration is performed using a 19 point Gaussian quadrature (ROY et al., 1991) while the polar integration consists in a 10 point Gauss-Legendre quadrature. The tracking density is 20 lines/cm. The convergence criterion is 1.0×10^{-6} for both power and multigroup iterations. Here, we compare our results with the generalized source importances obtained by the CP method (COURAU, 2001; COURAU and MARLEAU, 2002) where the same cyclic tracking procedure is considered. The testing computer is a PENTIUM 4-3.2GHz CPU with 1 GB RAM on an Intel D865GLC motherboard. The relative error (ϵ_f) between the MOCC generalized adjoints and CP generalized source importances is defined as,

$$\epsilon_f = \frac{\|[\Gamma^*_{MOC}] - [\Gamma^*_{CP}]\|}{\|[\Gamma^*_{CP}]\|} \tag{I.79}$$

where $[\Gamma^*_{MOC}]$ and $[\Gamma^*_{CP}]$ are the MOCC generalized adjoints and CP generalized source importances respectively.

The functionals of reaction rate ratio used in the numerical simulations are the one-group homogenized cross sections defined as,

$$\Sigma_x^H = \frac{\left\langle \Sigma_x^g, \phi^g \right\rangle}{\left\langle \phi^g \right\rangle} \tag{I.80}$$

where Σ_x^H is the homogenized total (Σ^H), transport correction (Σ_{tc}^H), fission neutron production ($\nu\Sigma_f^H$), fission (Σ_f^H), absorption (Σ_a^H) or scattering (Σ_s^H) cross sections.

We first determine the forward fluxes, adjoint functions and k_{eff} using the MOCC (ASSAWAROONGRUENGCHOT and MARLEAU, 2007b) and CP methods for the forward and adjoint problems. The CP forward and adjoint k_{eff} results are 1.2623630 and 1.2623640 respectively, while the MOCC forward and adjoint k_{eff} results are 1.2623630 and 1.2623628. These results all agree to within 9.5×10^{-7} as expected. The maximum relative error ϵ_f between the forward fluxes by MOCC and CP methods is 6.0×10^{-7}, and ϵ_f for the adjoint functions is 3.2×10^{-7}.

I.5.1.1 Biasing Technique and Convergence Analysis

The results we obtained for the 6 types of generalized adjoints associated with homogenized cross sections defined above are shown in Table I.1. As one can see, selecting $f_b = 10^4$ (in Eq. (I.75)) for the biasing/decontamination schemes 1 and 3 gives the lowest number of one-group solutions (TNOS) and a maximum relative error $\epsilon_f = 1.5 \times 10^{-6}$. For the scheme 2, we select $f_b = 500$ which gives the lowest TNOS and the relative error as low as 3.8×10^{-6}.

For the scheme 1 and 3, increasing f_b causes lower TNOS because the orthogo-

nal generalized adjoints have small magnitude and the larger biased generalized adjoints cause a reduction in the convergence error

$$\epsilon_n = \frac{\max_{i,g} |\Gamma_i^{*g,(n)} - \Gamma_i^{*g,(n-1)}|}{\max_{i,g} |\Gamma_i^{*g,(n)}|} \tag{I.81}$$

in the n-th iteration. For the cases using $f_b = 10^5$, the convergence rate diminishes. This is because of the early convergence (in the first step) due to large magnitude of biased generalized adjoints that reduces the convergence error and subsequently results in the longer iterations in the second step (where the rebalance scheme is turned off). In these cases ϵ_f is low because in the second step, the power iterations are performed using the unbiased generalized adjoints.

For scheme 2 with $f_b \leq 100$, we find that some biased generalized adjoints become negative because the decontamination extracts the negative orthogonal component which the pre-evaluated biasing factor can not take into account. These negative generalized adjoints then cause long TNOS in the low f_b cases. When $f_b \geq 10^3$, ϵ_f is increased because of early convergence due to the large biased generalized adjoints. To use scheme 2, we then need to verify the appropriate f_b that ensures the positive biased generalized adjoints and total generalized adjoint sources. Among the schemes proposed, the solution using scheme 2 is the most efficient because the rebalance technique can be used at each power iteration.

The results of computing time using the MOCC and CP methods are shown in Table I.2. The total computing time by the MOCC method is longer than the total time by the CP method. The pre-evaluation of the CP matrices is more efficient than using MOCC method (to perform the spatial and angular integrations over adjoint sources) to compute the 6 types of generalized adjoints in our study. The maximum relative errors of the generalized adjoints using scheme 1 to 3 all agree to within 3.8×10^{-6}.

As can be seen in Table I.3, the TNOS depends on the magnitude of generalized adjoint source $||S^*||$ as well as f_b. The TNOS for Σ^H and Σ_s^H is high due to the high $||S^*||$ as shown in Table I.3 while the TNOS is low for the $\nu\Sigma_f^H$, Σ_f^H and Σ_a^H cases in scheme 2 due to the low $||S^*||$. For scheme 1 and 3 the overbiasing causes high TNOS for Σ_f^H and Σ_a^H cases.

I.5.1.2 GPT Estimates

The GPT estimates of variations in cell averaged cross sections, due to perturbations in the temperature of fuel, clad and coolant by 1, 10, 25 and 50%, are shown in Table I.4 and I.5. As one can see, the absolute relative errors

$$\epsilon_r = \left| \frac{R_p - R_{GPT}}{R_u} \right| \tag{I.82}$$

of our GPT estimates are within 2.3×10^{-4} for perturbation in temperature as large as 10%. The GPT estimates using IA method are comparable to the results using LA method. This is because the angular neutron fluxes are relatively isotropic in the PWR problem due to the fuel rods that are uniformly positioned over the spatial domain. The high-order angular terms in $\Delta\Sigma^g\Phi^g$ then produce low effect in GPT estimates.

The sensitivity coefficients of eigenvalue and homogenized cross-sections to various lattice parameters are shown in Table I.6 to I.9. Plots of sensitivity against energy spectrum are shown in Figure I.4 to I.7. The reference sensitivities for parameter P (here P can represent the eigenvalue or an average cross section) are evaluated using

$$S_{P,ref}^q = \frac{\alpha_q}{\Delta\alpha_q P}(P_+ - P_-) \tag{I.83}$$

where $P_{\pm}$ is computed using a direct calculation with $\pm 0.1\%$ perturbation in boron density ($N_{\mathrm{B_{nat}}}$), coolant density ($N_{\mathrm{H_2O}}$) and fuel temperature (T_f). For U^{235} enrichment, the reference sensitivities are calculated using $\pm 0.01\%$ perturbation in U^{235} enrichment percentage (e.g. $(3.25 \pm 0.01)\%$ enrichment). The sensitivities of homogenized cross section and eigenvalue using GPT method are evaluated (using equations (I.47) and (I.48) respectively) with $+1.0\%$ perturbation in boron density ($N_{\mathrm{B_{nat}}}$), coolant density ($N_{\mathrm{H_2O}}$), fuel temperature (T_f) and $+0.10\%$ perturbation in U^{235} enrichment percentage (e.g. $(3.25+0.1)\%$ enrichment).

The sensitivities evaluated using the LA method result in lower absolute relative error

$$\epsilon_s = \left| \frac{(S_{ref} - S_{GPT})}{S_{ref}} \right| \tag{I.84}$$

than the sensitivities using the IA method. The main exceptions are for the sensitivities $S^{T_f}_{\Sigma^H}$ and $S^{T_f}_{\Sigma^H_s}$ where the LA method will give large error due to the nonlinear effect in Doppler broadening and the reference sensitivities are evaluated at different perturbations. However, if we re-evaluate the $S^{T_f}_{\Sigma^H}$ and $S^{T_f}_{\Sigma^H_s}$ using LA method and $\pm 0.1\%$ perturbation, we obtain $S^{T_f}_{\Sigma^H} = -0.00387687$ and $S^{T_f}_{\Sigma^H_s} = -0.00428919$ which give low ϵ_s of 1.3×10^{-6} and 1.8×10^{-4} respectively. Because the linearization factors for the LA method are pre-evaluated using small perturbations ($d\Sigma^g_m = 10^{-4}\Sigma^g_m$), then the sensitivity results give lower error than when the IA method is selected.

For the sensitivity of eigenvalue to fuel temperature ($S^{T_f}_{\lambda}$) as shown in Figure I.4, the positive sensitivity in range $E = 1.0eV$ to $10keV$ is mostly due to the Doppler broadening that increase the absorption rates in the U^{238} resonance regions (corresponding to the increasing T_f). The negative sensitivity in range $E = 0.1$ to $1.0eV$ is caused by the increasing scattering reaction rate of oxygen atoms in fuel.

The positive sensitivity in range $E = 0.01$ to $0.1eV$ results from the increasing collision rates with respect to the increasing total cross section of oxygen atoms.

For the sensitivity of eigenvalue to boron concentration in coolants ($S_\lambda^{N_{\mathrm{B_{nat}}}}$) in Figure I.5, the positive sensitivity is due to the absorption rate in the range $E = 10^{-5}eV$ to $0.1keV$. In case of the sensitivity of eigenvalue to H_2O density ($S_\lambda^{N_{\mathrm{H_2O}}}$) in Figure I.6, the dominant negative sensitivity in the range $E = 0.01eV$ to $1.0keV$ results from the increasing scattering reaction rate. But the positive effects in the range $E = 10keV$ to $10MeV$ is from the increasing collision rate of hydrogen and oxygen atoms at high energy.

For the sensitivity of eigenvalue to U^{235} enrichment ($S_\lambda^{\mathrm{U^{235}}}$) in Figure I.7, the positive sensitivity in the range $E = 0.01eV$ to $1.0keV$ is from the absorption rates of U^{235} atoms. But the absorption-to-fission reactions contribute mainly to the negative sensitivity via the fission neutron production in the high energy range ($E = 0.1$ to $10MeV$).

I.5.2 37 Pin CANDU Assembly

A 2D 37 pin CANDU assembly (MARLEAU et al., 2000) is discretized into 42 regions according to the exact geometries (see Figure I.8). The 69 energy group nuclear cross sections are obtained from WNEALIB nuclear library. Reflective boundary conditions are also used in this problem. The tracking density, azimuthal and polar quadrature sets are the same as those used for the PWR case.

GPT estimates of variations in cell averaged cross sections, due to perturbations in the temperature of fuel, clad and coolant by -1,-10, -25 and -50% are considered. The estimates are presented in Table I.10 and I.11. Here the LA method provides more accurate estimations than the IA method for the perturbations of 0% to -

10%. This is because the CANDU fuel bundle is located at the center of the lattice leading to the angular neutron fluxes those are somewhat anisotropic. In fact the angular fast fluxes are mainly outward-directed while thermal angular fluxes are directed toward center of the cell. As a result, the high-order terms in $\Delta\Sigma\Phi$ introduce more effective corrections to the GPT estimates.

I.6 Conclusions

Here we have studied the generalized perturbation theory (GPT) for the estimations of eigenvalue and linear reaction rate ratio based on the integral neutron transport equation. The advantage of using the integral transport equation is that the GPT estimates take into account the variations in the cross sections and the neutron transfer characteristics between each region. In addition, for problems with isotropic sources, these estimates depend on the generalized scalar flux importances while GPT estimates based on the integro-differential transport equation still depend on the generalized angular source importance functions.

The relationship between generalized adjoint function and generalized flux importance is defined in order to transform the generalized flux importance integral transport equations into the integro-differential form. The generalized adjoint scalar functions are related to the generalized flux importances by the linear transformation using CP matrix, i.e. $[\Gamma^*] = [P_{VV}][\Gamma^\dagger]$. The resulting adjoint and generalized adjoint transport equations are then solved using the MOCC method.

The numerical results of a 17×17 PWR test case show that the MOCC generalized adjoint functions are similar to the CP generalized source importances. The biasing and decontamination schemes in each power iteration loop (scheme 2) results in the lowest computing time among the 3 schemes proposed. This is because, in

each power iteration, the decontamination scheme extracts the orthogonal generalized adjoints and in the meantime remove the undesired contaminated components which are the linear function of the standard adjoint functions. Therefore the orthogonal generalized adjoint functions converge faster than the generalized adjoint functions, which are iterated with the contaminated components allowed, in scheme 1 and 3.

To evaluate the perturbed integral transport functionals in the GPT estimates, the isotropic approximation (IA) and linear approximation (LA) methods are applied to approximate the term $\Delta(\mathcal{T}_l^{g,-1})$. Using the IA method, the first order GPT estimate based on the integral transport equations is found equivalent to the GPT estimate based on the integro-differential transport equation where the adjoint angular functions are assumed isotropic as reported in the GPT based on the CP equation (COURAU and MARLEAU, 2003). The GPT estimates of the homogenized cross-sections due to the perturbations in the fuel, clad and coolant temperature result in the absolute relative error as low as 2.3×10^{-4} for the perturbations in temperature of 10% or less. The GPT estimate using IA method is comparable to the estimate using the LA method because in the PWR lattice the angular neutron fluxes are relatively isotropic due to the fuel rods are uniformly distributed over the assembly. Therefore the high-order angular terms in $(\Delta\Sigma^g\Phi^g)$ produce low effect in the GPT estimation using the LA method. For the CANDU case, the angular neutron fluxes are generally more anisotropic and the LA method then results in much more accurate GPT estimates for perturbations in temperature from 0 to -10%. For the sensitivity evaluation, the same behaviors are observed, provided that the linearization factors are evaluated using small perturbed cross-sections ($d\Sigma_m^g = 1.0^{-4}\Sigma^g$).

Finally one could extend the integral-transport based GPT to the anisotropic scattering problem by rearranging for the $\vec{\Omega}$-to-$\vec{\Omega}'$ scattering terms in the generalized

flux importance transport equations.

Acknowledgments

This work was supported in part by the Natural Science and Engineering Research Council of Canada.

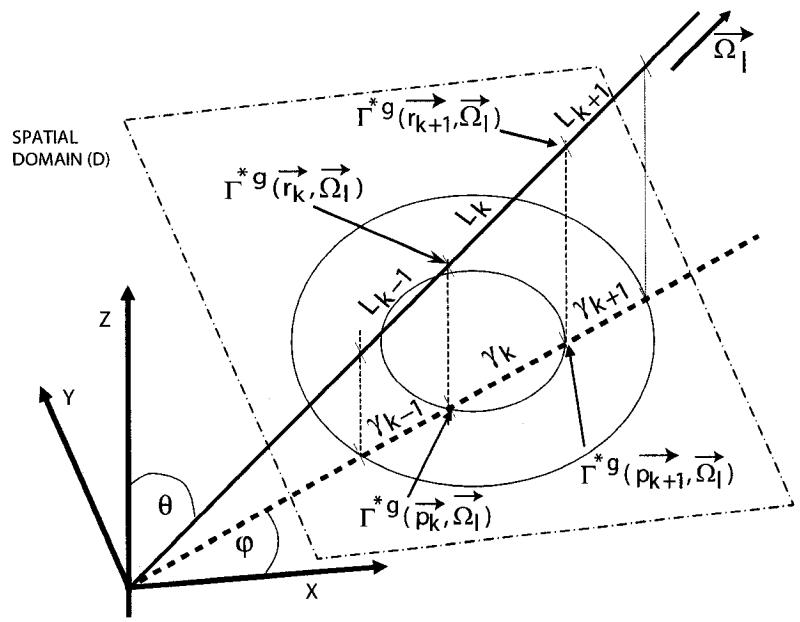

Figure I.1 3D Tracking line in direction $\vec{\Omega}_l$

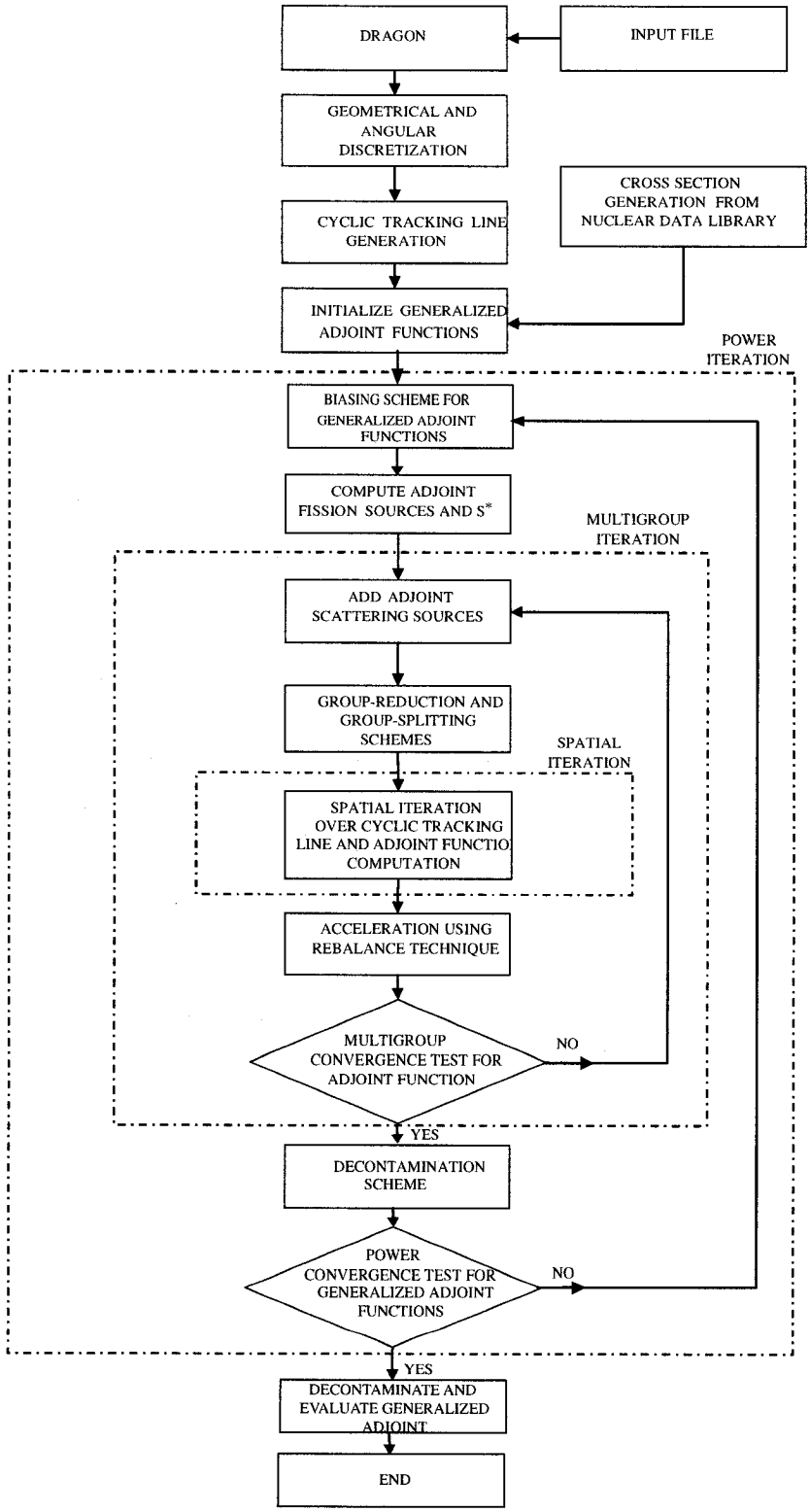

Figure I.2 Generalized adjoint solution flow diagram

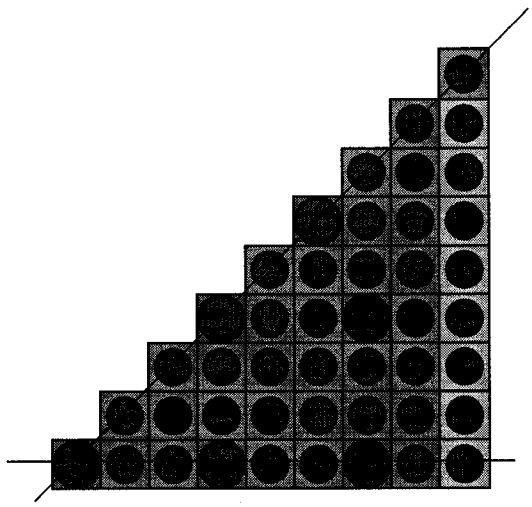

Figure I.3 A 1/8 17 $\times$ 17 PWR lattice

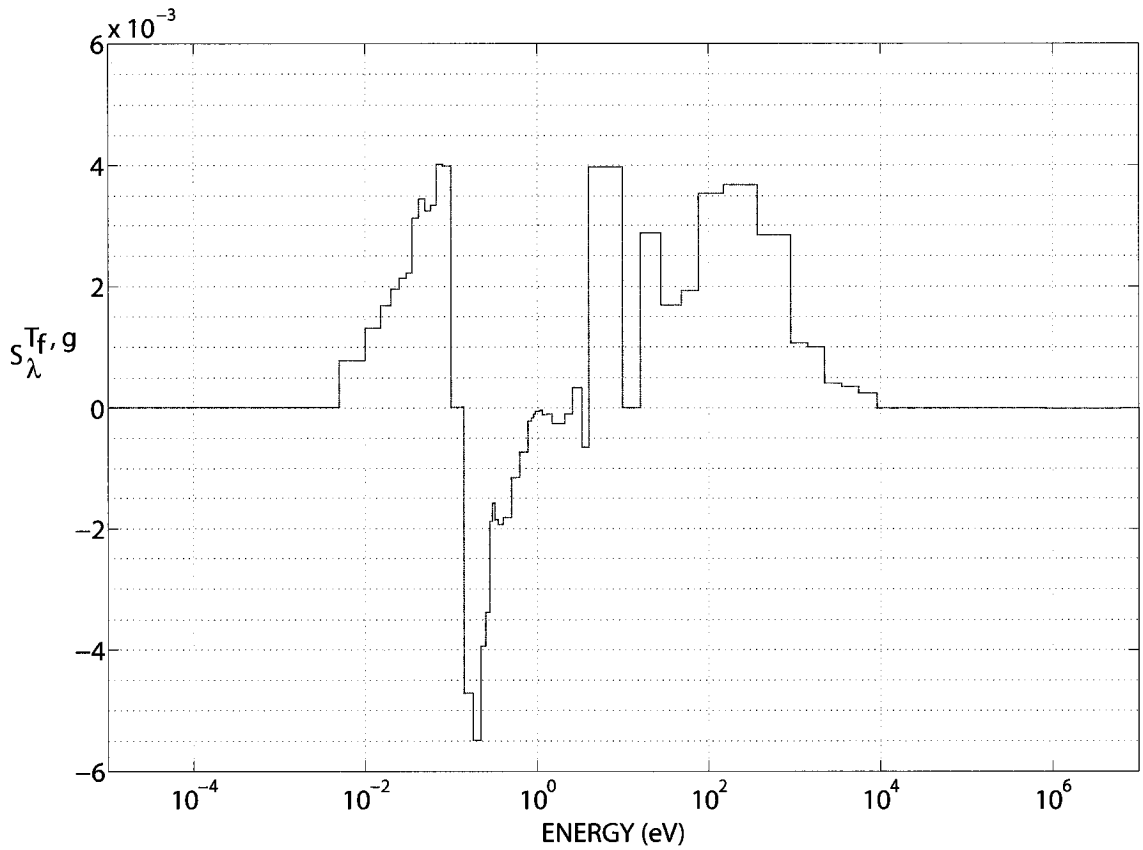

Figure I.4 Sensitivity of eigenvalue to fuel temperature

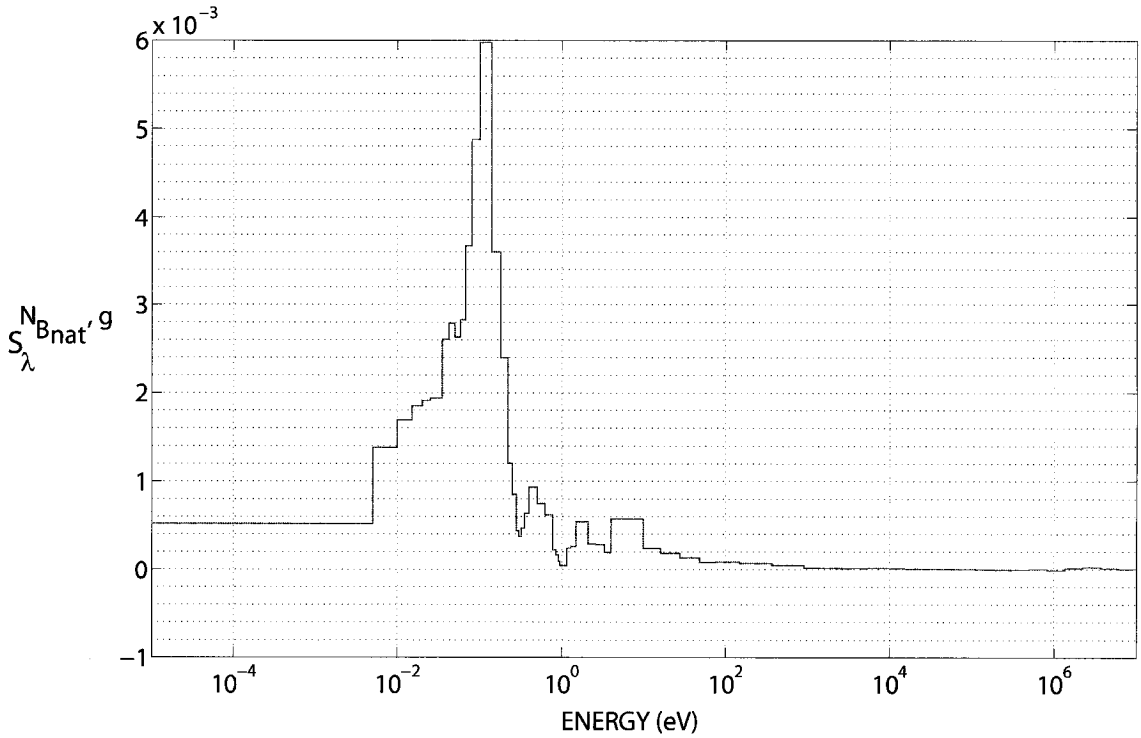

Figure I.5 Sensitivity of eigenvalue to boron concentration in the coolant

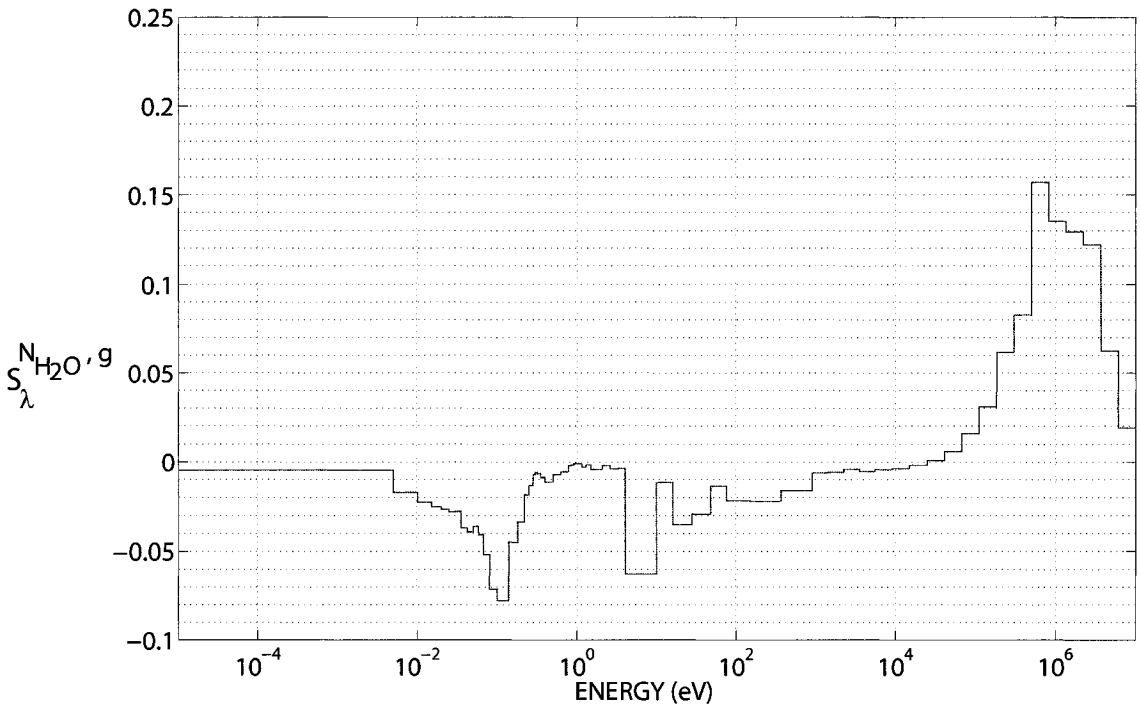

Figure I.6 Sensitivity of eigenvalue to H_2O density in the coolant

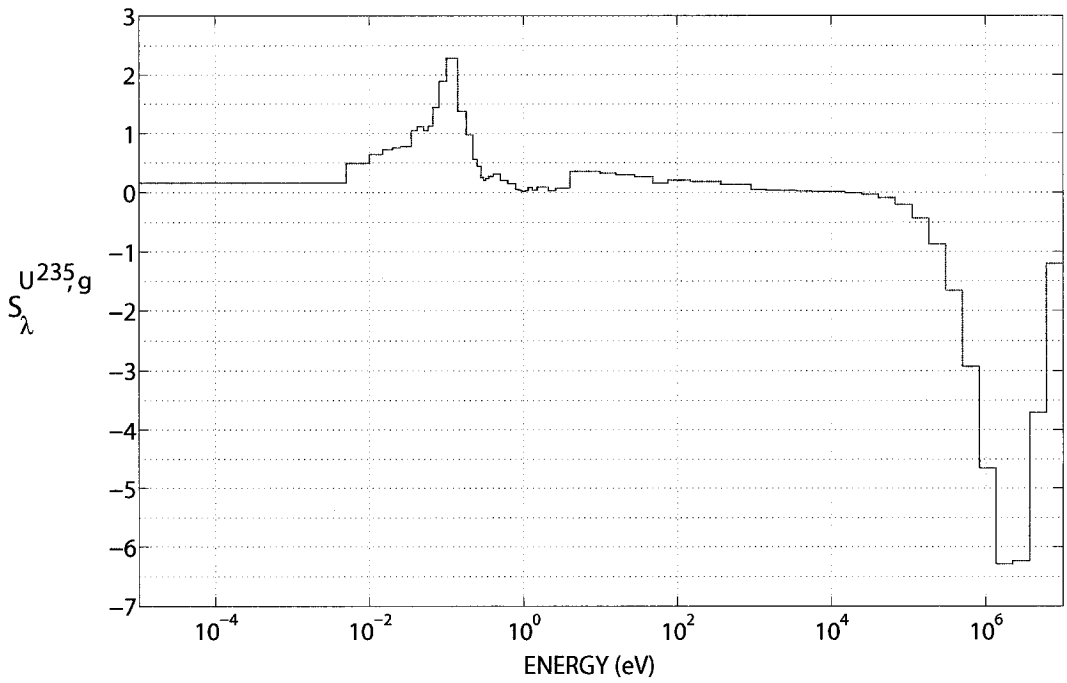

Figure I.7 Sensitivity of eigenvalue to U^{235} enrichment

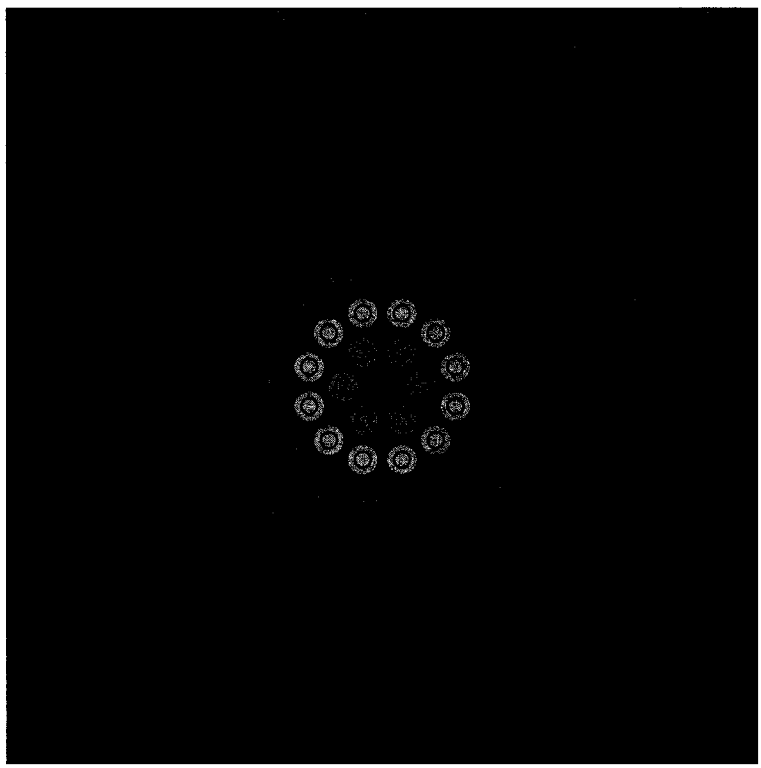

Figure I.8 A 37 pin CANDU assembly

Table I.1 Effect of Source Biasing Factor (f_b) on Total Numbers of One-group Solutions

Source Biasing Factor (f_b)	Scheme 1		Scheme 2		Scheme 3	
	TNOS	ϵ_f	TNOS	ϵ_f	TNOS	ϵ_f
No Biasing/ Rebalance	37787	1.2E-6	34454	1.4E-6	35161	1.4E-6
1.0	25502	1.3E-6	55082[a]	1.5E-3	57494[a]	1.5E-3
10.0	26236	1.2E-6	24193	2.5E-6	27517	1.2E-6
100.0	24652	1.3E-6	20558	3.0E-6	25106	1.2E-6
500.0	22214	1.4E-6	18250	3.8E-6	24960	1.2E-6
1.0E+3	22598	1.3E-6	16621	1.0E-5	21955	1.3E-6
1.0E+4	21951	1.5E-6	11010	2.9E-4	20817	1.4E-6
1.0E+5	22939	1.3E-6	5977	2.2E-3	23590	1.3E-6

[a] : *unconverged in* Σ_a^H *iteration*

Table I.2 CPU Time Used in MOCC and CP Methods with Various Generalized Adjoint Sources

Types of GPT Functional	CP Method Scheme 1 (min)	MOCC Scheme 1 (min)	MOCC Scheme 2 (min)	MOCC Scheme 3 (min)
Σ^H	0.28	336.0	352.5	354.1
Σ^H_{tc}	0.32	282.2	352.7	283.1
$\nu\Sigma^H_f$	0.35	262.6	204.4	262.0
Σ^H_f	0.36	374.6	186.5	298.0
Σ^H_a	0.62	382.5	189.3	336.7
Σ^H_s	0.35	329.9	350.7	332.3
CP Matrix Computing Time	1359.0	—	—	—
Total Computing Time	1361.3	1967.9	1636.1	1866.2

The total computing time for forward fluxes and adjoint functions using CP (excluding CP evaluation) and MOCC methods are 0.37 and 319.5 min. respectively

Table I.3 The Total Numbers of One-group Solutions

Types of GPT Functional	$\|\|S^*\|\|$	S^*_{max}	S^*_{min}	Scheme 1 ($f_b = 10^4$) TNOS	Scheme 2 ($f_b = 500$) TNOS	Scheme 3 ($f_b = 10^4$) TNOS
Σ^H	2.49E+0	2.42E-1	-1.61E-2	3748	3932	3950
Σ^H_{tc}	8.71E-1	1.23E-2	-6.18E-2	3148	3934	3158
$\nu\Sigma^H_f$	8.81E-1	9.35E-2	-7.75E-4	2929	2280	2922
Σ^H_f	3.63E-1	3.85E-2	-3.15E-4	4179	2080	3324
Σ^H_a	4.69E-1	4.92E-2	-6.14E-4	4267	2112	3756
Σ^H_s	2.46E+0	2.40E-1	-1.56E-2	3680	3912	3707
Max ϵ_f	-	-	-	1.5E-6	3.8E-6	1.40E-6

The total number of one-group solutions for the combined forward and adjoint solution (ASSAWAROONGRUENGCHOT and MARLEAU, 2007b) is 5410 iterations.

Table I.4 PWR: GPT Estimates for Perturbations (Δ) in Fuel, Clad and Coolant Temperatures Using Isotropic Approximation (IA) Method

Δ	k_{eff}		Σ^H (cm^{-1})		$\nu\Sigma_f^H$ (cm^{-1})		Σ_s^H (cm^{-1})	
	GPT	ϵ_r	GPT	ϵ_r	GPT	ϵ_r	GPT	ϵ_r
0%	1.262363	-	6.61101E-1	-	2.78388E-2	-	6.39048E-1	-
1%	1.261930	7.5E-7	6.61132E-1	8.1E-7	2.78185E-2	4.7E-7	6.39088E-1	8.4E-7
10%	1.258089	1.9E-5	6.61350E-1	5.4E-5	2.76328E-2	2.1E-4	6.39385E-1	6.2E-5
25%	1.251947	1.6E-4	6.61949E-1	3.6E-4	2.73201E-2	1.3E-3	6.40124E-1	4.1E-4
50%	1.242350	6.7E-4	6.63065E-1	1.3E-3	2.68056E-2	4.9E-3	6.41475E-1	1.5E-3

Table I.5 PWR: GPT Estimates for Perturbations (Δ) in Fuel, Clad and Coolant Temperatures Using Linear Approximation (LA) Method

Δ	k_{eff}		Σ^H (cm^{-1})		$\nu\Sigma_f^H$ (cm^{-1})		Σ_s^H (cm^{-1})	
	GPT	ϵ_r	GPT	ϵ_r	GPT	ϵ_r	GPT	ϵ_r
1%	1.261929	0.0	6.61133E-1	8.1E-7	2.78185E-2	2.2E-6	6.39089E-1	8.4E-7
10%	1.258074	3.1E-5	6.61361E-1	7.0E-5	2.76322E-2	2.3E-4	6.39396E-1	7.8E-5
25%	1.251928	1.8E-4	6.61975E-1	4.0E-4	2.73190E-2	1.4E-3	6.40150E-1	4.5E-4
50%	1.242330	6.8E-4	6.63117E-1	1.4E-3	2.68038E-2	5.0E-3	6.41528E-1	1.5E-3

Table I.6 PWR: Sensitivities of Eigenvalue to Lattice Parameters

Sensitivity	Direct Calculation	IA method		LA method	
		Sensitivity	ϵ_s	Sensitivity	ϵ_s
$S_\lambda^{T_f}$	2.53097E-2	2.52297E-2	3.2E-3	2.52297E-2	3.2E-3
$S_\lambda^{N_{\mathrm{B_{nat}}}}$	5.33563E-2	5.33079E-2	9.1E-4	5.33269E-2	5.5E-4
$S_\lambda^{N_{\mathrm{H_2O}}}$	-1.25740E-1	-1.27087E-1	1.1E-2	-1.25043E-1	5.5E-3
$S_\lambda^{\mathrm{U}^{235}}$	-6.30958	-6.32400	2.3E-3	-6.30786	2.7E-4

Table I.7 PWR: Sensitivities of One-group Homogenized Total Cross Section to Lattice Parameters

Sensitivity	Direct Calculation	IA method		LA method	
		Sensitivity	ϵ_s	Sensitivity	ϵ_s
$S_{\Sigma^H}^{T_f}$	-3.87687E-3	-3.86779E-3	2.3E-3	-3.84071E-3	9.3E-3
$S_{\Sigma^H}^{N_{\mathrm{B_{nat}}}}$	-1.00529E-2	-1.00348E-2	1.8E-3	-1.00348E-2	1.8E-3
$S_{\Sigma^H}^{N_{\mathrm{H_2O}}}$	8.42317E-1	8.40955E-1	1.6E-3	8.42109E-1	2.5E-4
$S_{\Sigma^H}^{\mathrm{U}^{235}}$	-3.55951	-3.578886	5.4E-3	-3.559142	1.0E-4

Table I.8 PWR: Sensitivities of One-group Homogenized $\nu\Sigma_f^H$ Cross Section to Lattice Parameters

Sensitivity	Direct Calculation	IA method		LA method	
		Sensitivity	ϵ_s	Sensitivity	ϵ_s
$S_{\nu\Sigma_f^H}^{T_f}$	-1.77648E-2	-1.76707E-2	5.3E-3	-1.76840E-2	4.5E-3
$S_{\nu\Sigma_f^H}^{N_{\mathrm{B_{nat}}}}$	-4.34573E-2	-4.33902E-2	1.5E-3	-4.34103E-2	1.1E-3
$S_{\nu\Sigma_f^H}^{N_{\mathrm{H_2O}}}$	6.90526E-1	6.92367E-1	2.7E-3	6.89623E-1	1.3E-3
$S_{\nu\Sigma_f^H}^{\mathrm{U}^{235}}$	1.04159E+1	1.04422E+1	2.5E-3	1.04137E+1	2.1E-4

Table I.9 PWR: Sensitivities of One-group Homogenized Σ_s^H Cross Sections to Lattice Parameters

Sensitivity	Direct Calculation	IA method		LA method	
		Sensitivity	ϵ_s	Sensitivity	ϵ_s
$S_{\Sigma_s^H}^{T_f}$	-4.28997E-3	-4.26243E-3	6.4E-3	-4.23442E-3	1.3E-2
$S_{\Sigma_s^H}^{N_{\mathrm{B_{nat}}}}$	-1.07261E-2	-1.07261E-2	0.0	-1.07167E-2	8.8E-4
$S_{\Sigma_s^H}^{N_{\mathrm{H_2O}}}$	8.51890E-1	8.50463E-1	1.7E-3	8.51694E-1	2.3E-4
$S_{\Sigma_s^H}^{\mathrm{U}^{235}}$	-3.82411	-3.84454	5.3E-3	-3.82355	1.5E-4

Table I.10 CANDU: GPT Estimates for Perturbations (Δ) in Fuel, Clad and Coolant Temperatures Using Isotropic Approximation (IA) Method

Δ	k_{eff}		Σ^H (cm^{-1})		$\nu\Sigma_f^H$ (cm^{-1})		Σ_s^H (cm^{-1})	
	GPT	ϵ_r	GPT	ϵ_r	GPT	ϵ_r	GPT	ϵ_r
0%	1.112581	-	3.92741E-1	-	3.38072E-3	-	3.89702E-1	-
-1%	1.112118	1.7E-4	3.88794E-1	1.8E-4	3.35663E-3	1.9E-3	3.85775E-1	2.0E-4
-10%	1.107525	1.1E-3	3.53268E-1	1.5E-3	3.13981E-3	1.5E-2	3.50434E-1	1.6E-3
-25%	1.097669	1.2E-4	2.94060E-1	2.2E-3	2.77848E-3	2.1E-2	2.91532E-1	2.4E-3
-50%	1.069817	1.1E-2	1.95383E-1	1.3E-3	2.17645E-3	2.1E-2	1.93366E-1	1.4E-3

Table I.11 CANDU: GPT Estimates for Perturbations (Δ) in Fuel, Clad and Coolant Temperatures Using Linear Approximation (LA) Method

Δ	k_{eff}		Σ^H (cm^{-1})		$\nu\Sigma_f^H$ (cm^{-1})		Σ_s^H (cm^{-1})	
	GPT	ϵ_r	GPT	ϵ_r	GPT	ϵ_r	GPT	ϵ_r
-1%	1.112231	7.1E-5	3.88719E-1	7.9E-6	3.36323E-3	2.2E-5	3.85695E-1	8.1E-6
-10%	1.108761	2.7E-5	3.52517E-1	4.1E-4	3.20585E-3	4.1E-3	3.49629E-1	4.4E-4
-25%	1.101319	3.4E-3	2.92183E-1	2.6E-3	2.94359E-3	2.7E-2	2.89519E-1	2.8E-3
-50%	1.080279	2.0E-2	1.91629E-1	1.1E-2	2.50666E-3	1.2E-1	1.89342E-1	1.2E-2

APPENDIX II

ARTICLE II: MULTIGROUP ADJOINT TRANSPORT SOLUTION USING THE METHOD OF CYCLIC CHARACTERISTICS

Monchai Assawaroongruengchot and Guy Marleau

Nuclear Science and Engineering,
Volume 155, Number 1, January 2007, Pages 37-52

Abstract

Most perturbation theory calculation methods for neutron transport problems are based on the assumption that the solution to the adjoint transport problem is known. Here we develop an adjoint transport solution based on the method of cyclic characteristics (MOCC) for two dimensional fuel assembly problems with isotropic scattering. The main advantages of the MOCC method are: it requires lower computing time and memory spaces than the collision probability method (CP); it does not require the boundary surface currents as for the method of characteristics (MOC) with the isotropic tracking. In the MOCC method the adjoint characteristics equations associated with a cyclic tracking line are formulated in such a way that a closed form for the adjoint angular function can be obtained. The mathematical relationship between the adjoint function obtained by CP method and the adjoint function by MOCC method is also presented. In order to speed up the MOCC solution algorithm, group-reduction and group-splitting techniques based on the structure of the adjoint scattering matrix are implemented. In addition, a combined forward flux/adjoint function iteration scheme, based on the group-splitting technique and the common use of large numbers of variables storing tracking-line data and exponential values, is proposed to reduce the computing time. To demonstrate the efficiency of these algorithms, calculations are performed on a 17×17 PWR lattice, a 37 pin CANDU cell and the Watanabe-Maynard benchmark. Comparisons of adjoint function and k_{eff} results obtained by the MOCC and CP methods are presented.

II.1 Introduction

In static perturbation theory the adjoint functions are required for various calculations including sensitivity coefficients, uncertainty analysis and estimation of k_{eff} variations due to small changes in reactor core compositions. (RONEN, 1986) Such perturbation theory methods have been mostly applied to problems using the multigroup neutron diffusion equation in general geometries or one-group transport equation in homogeneous geometries. On the other hand, analyses of perturbation problems using multigroup neutron transport and adjoint transport equations in heterogeneous geometries are more limited. In fact the adjoint transport equation has been solved using the S_N discrete ordinate method, (CARLSON and LATHROP, 1968; SJODEN, 2002) the variational nodal method, (LAURIN-KOVITZ and LEWIS, 1996b) the collision probability method (CP) (COURAU, 2001; COURAU and MARLEAU, 2002) and the Monte Carlo method. (HOOGENBOOM, 1981)

Here we propose to develop an adjoint transport solution algorithm based on the MOCC method. This method is similar to the CACTUS (HALSALL, 1980) method and uses the cyclic tracking procedure and MOCC forward flux routines programmed in DRAGON. (ROY et al., 1991; MARLEAU, 2001) The exact geometries can be treated directly in the algorithm. The tracking line with cyclic angles (MARLEAU, 2001) is composed of a finite set of segments periodically translating along the line in the rectangular spatial domain unfolded to infinity using either reflective or periodic boundary conditions. The advantage of the cyclic tracking procedure is that we are able to derive a closed form for the adjoint angular function on an infinite line based on the solution for a finite number of line segments. The MOCC method does not need the boundary surface currents as it is the case when the method of characteristics (MOC) with isotropic tracking procedure is considered. (HONG and CHO, 1998; ZIKA and ADAMS, 2000) The MOCC method

performs only one cycle of scanning over the cyclic tracking lines in each spatial iteration loop. Therefore the spatial iteration time is lower in the MOCC method than in the MOC method when the same tracking lines are used.

In section II.2 we present the formulation of the adjoint characteristics equation including a closed form for adjoint angular function and average adjoint scalar function. Section II.3 presents the mathematical relationship between the adjoint scalar function associated with the MOCC method and the adjoint scalar function obtained using CP method. Section II.4 describes the structure of the solution algorithm including the group-reduction, group-splitting and rebalance techniques. We also discuss the combined flux/adjoint iteration scheme. Section II.5 presents the numerical results for a 17 × 17 PWR lattice, a 37 pin CANDU cell and the Watanabe-Maynard benchmark. Then we conclude in the last section.

II.2 Characteristics Formulation of the Adjoint Transport Problem

Here we derive the adjoint characteristics equation associated with a cyclic line segment using the integro-differential adjoint transport equation. We will start with the multigroup discrete ordinate neutron transport equation in direction $\vec{\Omega}_l$ for a multiplicative k_{eff} problem with isotropic scattering as follows, (LEWIS, 1993)

$$\frac{d\Phi^g(\vec{r}+S\vec{\Omega}_l,\vec{\Omega}_l)}{dS}+\Sigma^g(\vec{r}+S\vec{\Omega}_l)\Phi^g(\vec{r}+S\vec{\Omega}_l,\vec{\Omega}_l)=q^g(\vec{r}+S\vec{\Omega}_l) \qquad \text{(II.1)}$$

where

$$q^g(\vec{r})=\sum_{g'=1}^{G}[\Sigma_s^{g\leftarrow g'}(\vec{r})+\frac{1}{k_{eff}}\chi^g(\vec{r})\nu\Sigma_f^{g'}(\vec{r})]\phi^{g'}(\vec{r}) \qquad \text{(II.2)}$$

with $\vec{\Omega}_l$, the l-th discretized unit angular directional vector. Here $\Phi^g(\vec{r},\vec{\Omega}_l)$ and $\phi^g(\vec{r})$ are the forward angular and scalar fluxes respectively. $\Sigma^g(\vec{r})$ and $\Sigma_s^{g\leftarrow g'}(\vec{r})$

are the transport-corrected total and isotropic scattering cross sections respectively where the transport correction takes partially into account the linearly anisotropic contributions to the scattering cross sections. (MACFARLANE, 1984) Finally, $\Sigma_f^g(\vec{r})$ is the fission cross sections, $\chi^g(\vec{r})$ is the fission production spectrum, and ν is the average number of neutrons generated per fission. Note that the scalar flux is approximated using an angular quadrature technique as follows,

$$\phi^g(\vec{r}) = \sum_{l=1}^{N^\Omega} W_l^\Omega \Phi^g(\vec{r}, \vec{\Omega}_l) \tag{II.3}$$

where W_l^Ω and N^Ω are respectively the weight and order of the angular quadrature defining the cyclic tracking lines.

One can associate with the forward transport equation (Eqs. (II.1) and (II.2)) written in the following compact form:

$$\mathcal{H}[\Phi(\vec{r}, \vec{\Omega}_l)] - \mathcal{S}[\phi(\vec{r})] = \frac{1}{k_{eff}} \mathcal{F}[\phi(\vec{r})]$$

an adjoint equation:

$$\mathcal{H}^*[\Phi^*(\vec{r}, \vec{\Omega}_l)] - \mathcal{S}^*[\phi^*(\vec{r})] = \frac{1}{k_{eff}^*} \mathcal{F}^{*g}[\phi^*(\vec{r})]$$

where the operators $\mathcal{H}^*$, $\mathcal{S}^*$ and $\mathcal{F}^*$ are defined in such a way as to preserve the scalar products: (LEWIS, 1993)

$$\begin{aligned}
\left\langle [\Phi^*(\vec{r}, \vec{\Omega}_l)], \mathcal{H}[\Phi(\vec{r}, \vec{\Omega}_l)] \right\rangle &= \left\langle \mathcal{H}^*[\Phi^*(\vec{r}, \vec{\Omega}_l)], [\Phi(\vec{r}, \vec{\Omega}_l)] \right\rangle \\
\left\langle [\Phi^*(\vec{r}, \vec{\Omega}_l)], \mathcal{S}[\phi(\vec{r})] \right\rangle &= \left\langle \mathcal{S}^*[\phi^*(\vec{r})], [\Phi(\vec{r}, \vec{\Omega}_l)] \right\rangle \\
\left\langle [\Phi^*(\vec{r}, \vec{\Omega}_l)], \mathcal{F}[\phi(\vec{r})] \right\rangle &= \left\langle \mathcal{F}^*[\phi^*(\vec{r})], [\Phi(\vec{r}, \vec{\Omega}_l)] \right\rangle
\end{aligned}$$

with

$$\left\langle [\Phi^*(\vec{r},\vec{\Omega}_l)],[\Phi(\vec{r},\vec{\Omega}_l)] \right\rangle \equiv \sum_{l=1}^{N_\Omega}\sum_{g=1}^{G}\int_D d^3r\Phi^{*g}(\vec{r},\vec{\Omega}_l),\Phi^g(\vec{r},\vec{\Omega}_l)$$

and D is a spatial domain. k^*_{eff}=k_{eff}, namely, the eigenvalues for the forward and adjoint problems are identical. We may also note that for the multigroup transport equation, $\mathcal{S}^* = \mathcal{S}^T$ and $\mathcal{F}^* = \mathcal{F}^T$, where the transposition is with respect to the groups.

One can then associate with the forward transport problem presented in equation (II.1), the following adjoint transport equation: (LEWIS, 1993)

$$\frac{d\Phi^{*g}(\vec{r}-S\vec{\Omega}_l,\vec{\Omega}_l)}{dS}+\Sigma^g(\vec{r}-S\vec{\Omega}_l)\Phi^{*g}(\vec{r}-S\vec{\Omega}_l,\vec{\Omega}_l)=q^{*g}(\vec{r}-S\vec{\Omega}_l) \qquad \text{(II.4)}$$

with

$$q^{*g}(\vec{r})=\sum_{g'=1}^{G}[\Sigma_s^{g'\leftarrow g}(\vec{r})+\frac{1}{k_{eff}}\chi^{g'}(\vec{r})\nu\Sigma_f^g(\vec{r})]\phi^{*g'}(\vec{r}) \qquad \text{(II.5)}$$

Here $\Phi^{*g}(\vec{r},\vec{\Omega}_l)$ and $\phi^{*g}(\vec{r})$ are the adjoint angular and adjoint scalar functions (usually called adjoint angular and adjoint scalar fluxes (HENRY, 1975; LEWIS, 1993; ROZON, 1998)) respectively. The adjoint scalar function is approximated using an angular quadrature technique identical to that considered for the flux (see equation II.3):

$$\phi^{*g}(\vec{r})=\sum_{l=1}^{N^\Omega}W_l^\Omega\Phi^{*g}(\vec{r},\vec{\Omega}_l) \qquad \text{(II.6)}$$

The general boundary conditions used in neutron transport problems are of the form,

$$\Phi^{g,-}(\vec{r_s},\vec{\Omega}'_l)=\alpha\cdot\Phi^{g,+}(\vec{r}_s,\vec{\Omega}_l) \qquad \text{(II.7)}$$

where $(+)$ and $(-)$ indicate the outgoing and incoming directions, α is the albedo

or the transmission coefficient at the domain boundary, and $\vec{r}_s$ and $\vec{r}_s'$ are the points on the boundary.

For reflective boundary conditions, the variables in (II.7) become,

$$\begin{aligned}
&\vec{r}_s' = \vec{r}_s \\
&\vec{\Omega}_l' = \vec{\Omega}_l - 2(\vec{n} \cdot \vec{\Omega}_l)\vec{n} \\
&\vec{\Omega}_l' \cdot \vec{n} < 0 \text{ and } \vec{\Omega}_l \cdot \vec{n} > 0
\end{aligned}$$

where $\vec{\Omega}_l$ and $\vec{\Omega}_l'$ are the unit directional vectors of the angular functions impinging on and reflecting from boundary at point $\vec{r}_s$, and $\vec{n}$ is the unit outward vector normal to boundary surface at $\vec{r}_s$.

When periodic boundary conditions are considered, the variables in (II.7) become,

$$\begin{aligned}
&\vec{r}_s' = \vec{\mathcal{T}}(\vec{r}_s \rightarrow \vec{r}_s', \vec{\Omega}_l) \cdot \vec{r}_s \\
&\vec{\Omega}_l' = \vec{\Omega}_l
\end{aligned}$$

where $\vec{\mathcal{T}}(\vec{r}_s \rightarrow \vec{r}_s', \vec{\Omega}_l)$ is the periodicity or translation operator.

The boundary conditions associated with the adjoint transport problems that arise from the derivation of adjoint transport equations are,

$$\Phi^{*g,+}(\vec{r}_s, \vec{\Omega}_l) = \alpha \cdot \Phi^{*g,-}(\vec{r}_s', \vec{\Omega}_l') \tag{II.8}$$

When void boundaries ($\alpha = 0$) are considered, equation (II.8) give the zero neutron importance of outgoing neutron flux at boundary. (HENRY, 1975) Therefore, contrary to the forward neutron transport problems, we need to solve the adjoint transport equation in the backward direction ($-\vec{\Omega}_l$).

Here, in order to derive the adjoint characteristics equations, we follow a derivation similar to that used when solving the forward neutron transport equation. (ROY, 1998) First, we multiply both sides of (II.4) by,

$$e^{\tau^g(\vec{r}-S\vec{\Omega}_l,\vec{r})} = e^{\int_0^S \Sigma^g(\vec{r}-S'\vec{\Omega}_l)dS'} \tag{II.9}$$

where $\tau^g(\vec{r}-S\vec{\Omega}_l,\vec{r})$ is the optical path between $\vec{r}-S\vec{\Omega}_l$ and $\vec{r}$. We then integrate the resulting equation over dS from $S=0$ to t,

$$\begin{aligned}\Phi^{*g}(\vec{r}-t\vec{\Omega}_l,\vec{\Omega}_l) &= \Phi^{*g}(\vec{r},\vec{\Omega}_l)e^{-\tau^g(\vec{r}-t\vec{\Omega}_l,\vec{r})} \\ &+ e^{-\tau^g(\vec{r}-t\vec{\Omega}_l,\vec{r})}\int_0^t dS q^{*g}(\vec{r}-S\vec{\Omega}_l)e^{\tau^g(\vec{r}-S\vec{\Omega}_l,\vec{r})}\end{aligned} \tag{II.10}$$

Now, let us consider the spatial domain (D) having infinite length along the Z-axis as shown in Figure II.1. A tracking line generated across the spatial domain in direction $\vec{\Omega}_l$ is composed of line segments indexed by L_k, where $k=1$ to K identifies each segment on the tracking line. We will now assume that the outgoing adjoint angular function $\Phi^{*g}(\vec{r}_{k+1},\vec{\Omega}_l)$ of segment L_k is known. Within each region, the adjoint scalar functions are assumed to have uniform distribution. The nuclear cross sections and adjoint sources are also assumed constant in each region. The adjoint sources and total cross sections at point $(\vec{r}_{k+1}-S\vec{\Omega}_l)$ on the segment L_k are defined as,

$$q^{*g}(\vec{r}_{k+1}-S\vec{\Omega}_l) = q_k^{*g} \tag{II.11}$$

$$\Sigma^g(\vec{r}_{k+1}-S\vec{\Omega}_l) = \Sigma_k^g \tag{II.12}$$

for $S \in [0, L_k]$, and q_k^{*g} and Σ_k^g are the adjoint sources and total cross sections associated with segment L_k respectively. The optical path between points $(\vec{r}_{k+1}-$

$S\vec{\Omega}_l)$ and $\vec{r}_{k+1}$ becomes,

$$\tau^g(\vec{r}_{k+1} - S\vec{\Omega}_l, \vec{r}_{k+1}) = \Sigma_k^g S \quad \text{for S} \in [0, L_k] \tag{II.13}$$

Using equations (II.12) and (II.13) in (II.10), we write the adjoint characteristics equation for the segment L_k as follows,

$$\Phi^{*g}(\vec{r_k}, \vec{\Omega}_l) = \Phi^{*g}(\vec{r}_{k+1}, \vec{\Omega}_l)e^{-\Sigma_k^g L_k} + \frac{q_k^{*g}}{\Sigma_k^g}[1 - e^{-\Sigma_k^g L_k}] \tag{II.14}$$

The adjoint characteristics equation (II.14) is in the same form as the characteristics equation for the forward neutron transport problem except that the adjoint characteristics equation is derived in direction $(-\vec{\Omega}_l)$. (ROY, 1998)

For two-dimensional problems, $\Phi^{*g}(\vec{r}, \vec{\Omega}_l)$ is independent of Z. The adjoint characteristics equation (II.14) is rewritten as,

$$\Phi^{*g}(\vec{p}_k, \vec{\Omega}_l) = \Phi^{*g}(\vec{p}_{k+1}, \vec{\Omega}_l)e^{-\frac{\Sigma_k^g \gamma_k}{\sin(\theta)}} + \frac{q_k^{*g}}{\Sigma_k^g}[1 - e^{-\frac{\Sigma_k^g \gamma_k}{\sin(\theta)}}] \tag{II.15}$$

where $L_k = \gamma_k / \sin(\theta)$, and $\vec{p}_k$ and $\vec{p}_{k+1}$ are the projection of $\vec{r_k}$ and $\vec{r}_{k+1}$ on the X-Y plane respectively. The average adjoint angular function on the segment L_k in the direction $\vec{\Omega}_l$ is,

$$L_k \overline{\Phi}_k^{*g}(\vec{\Omega}_l) = \int_0^{L_k} dt \Phi^{*g}(\vec{r}_{k+1} - t\vec{\Omega}_l, \vec{\Omega}_l) \tag{II.16}$$

Using (II.10), (II.12) and (II.13) in (II.16), we obtain,

$$L_k \overline{\Phi}_k^{*g}(\vec{\Omega}_l) = \frac{\Phi^{*g}(\vec{p}_{k+1}, \vec{\Omega}_l)}{\Sigma_k^g}[1 - e^{\frac{-\Sigma_k^g \gamma_k}{\sin(\theta)}}] + \frac{q_k^{*g}}{\Sigma_k^g \Sigma_k^g}\left[\frac{\Sigma_k^g \gamma_k}{\sin\theta} - [1 - e^{\frac{-\Sigma_k^g \gamma_k}{\sin(\theta)}}]\right] \tag{II.17}$$

In the cases where the segment L_k is located in a void region,

$$\Sigma^g(\vec{r}_{k+1} - S\vec{\Omega}_l) = \Sigma_k^g = 0 \tag{II.18}$$

$$\tau^g(\vec{r}_{k+1} - S\vec{\Omega}_l, \vec{r}_{k+1}) = \Sigma_k^g S = 0 \tag{II.19}$$

for $S \in [0, L_k]$. Using (II.19) in (II.15), the adjoint characteristics equation for the segment L_k in the void region becomes,

$$\Phi^{*g}(\vec{p}_k, \vec{\Omega}_l) = \Phi^{*g}(\vec{p}_{k+1}, \vec{\Omega}_l) + \frac{\gamma_k}{\sin\theta} q_k^{*g} \tag{II.20}$$

while the average adjoint angular function equation is given by,

$$L_k \overline{\Phi}_k^{*g}(\vec{\Omega}_l) = \Phi^{*g}(\vec{p}_{k+1}, \vec{\Omega}_l)\frac{\gamma_k}{\sin\theta} + \left[\frac{\gamma_k}{\sin\theta}\right]^2 \frac{q_k^{*g}}{2} \tag{II.21}$$

These average adjoint angular equations are similar to those used for the forward fluxes. (ROY, 1998) The main difference is the fact that the average angular flux $\overline{\Phi}_k^g(\vec{\Omega}_l)$ depends on the incoming angular flux $\Phi^g(\vec{p}_k, \vec{\Omega}_l)$, while the average angular adjoint $\overline{\Phi}_k^{*g}(\vec{\Omega}_l)$ depends on the outgoing angular adjoint $\Phi^{*g}(\vec{p}_{k+1}, \vec{\Omega}_l)$.

II.2.1 Closed Form of Adjoint Angular Function in an Infinite Medium

In a rectangular spatial domain unfolded to infinity using reflective boundary conditions as shown in Figure II.2, a cyclic tracking line is defined in such a way that each line starts and ends at the same point after periodically translating along the infinite tracking lines. (MARLEAU, 2001) These lines can also be obtained by following the neutrons as they travel through a finite spatial domain with the specular boundary conditions. The same set of consecutive segments (e.g. A-B-C-D-A) is then obtained. In addition, the cyclic tracking lines for periodic boundary

conditions are shown in Figure II.3. For a cyclic tracking line having K segments in direction $\vec{\Omega}_l$, we can write the adjoint characteristics equation (derived in direction $(-\vec{\Omega}_l)$) as follows,

$$\Phi^{*g}(\vec{p}_1, \vec{\Omega}_l) = \Phi^{*g}(\vec{p}_{K+1}, \vec{\Omega}_l) \prod_{k'=1}^{K} [H(k')\beta_{alb}(k')] + M(K) \qquad \text{(II.22)}$$

where

$$M(K) = \sum_{k=1}^{K} \left[\left(\prod_{k'=1}^{k-1} [H(k')\beta_{alb}(k')] \right)^{\varrho(k)} \left(\frac{1 - e^{\frac{-\Sigma_k^g \gamma_k}{\sin\theta}}}{\Sigma_k^g} \right)^{\vartheta(k)} \left(\frac{\gamma_k}{\sin\theta} \right)^{(1-\vartheta(k))} \right] q_k^{*g}$$

$$H(k) = e^{\frac{-\Sigma_k^g \gamma_k}{\sin\theta}}$$

$$\varrho(k) = \begin{cases} 1 & \text{when } k > 1 \\ 0 & \text{otherwise} \end{cases}$$

$$\vartheta(k) = \begin{cases} 0 & \text{when segment } L_k \text{ is in void a region} \\ 1 & \text{otherwise} \end{cases}$$

$$\beta_{alb}(k) = \begin{cases} \alpha(k) & \text{when segment } L_k \text{ is in contact with the boundary at } \vec{p}_k \\ 1 & \text{otherwise} \end{cases}$$

$\vec{p}_1$ and $\vec{p}_{K+1}$ are the starting and ending points of cyclic tracking line, $M(K)$ represents the summation of the adjoint sources q_k^{*g}, for $k = 1$ to K, that contributes to adjoint function $\Phi^{*g}(\vec{p}_1, \vec{\Omega}_l)$ via the transmission coefficients defined as follows,

$$\Xi(q_k^{*g} \rightarrow \Phi^{*g}(\vec{p}_1, \vec{\Omega}_l)) = \left[\left(\prod_{k'=1}^{k-1} [H(k')\beta_{alb}(k')] \right)^{\varrho(k)} \left(\frac{1 - e^{\frac{-\Sigma_k^g \gamma_k}{\sin\theta}}}{\Sigma_k^g} \right)^{\vartheta(k)} \left(\frac{\gamma_k}{\sin\theta} \right)^{(1-\vartheta(k))} \right]$$

Since the starting and ending points of a cyclic tracking line are effectively the

same point in the finite domain, we can then write,

$$\Phi^{*g}(\vec{p}_{K+1}, \vec{\Omega}_l) = \Phi^{*g}(\vec{p}_1, \vec{\Omega}_l) \tag{II.23}$$

when $M(K)$ is finite and the following condition is satisfied,

$$[\prod_{k'=1}^{K} H(k')\beta_{alb}(k')] < 1$$

Using (II.23) in (II.22), the closed form for the adjoint angular function $\Phi^{*g}(\vec{p}_1, \vec{\Omega}_l)$ is determined by,

$$\Phi^{*g}(\vec{p}_1, \vec{\Omega}_l) = \frac{M(K)}{[1 - \prod_{k'=1}^{K}[H(k')\beta_{alb}(k')]]} \tag{II.24}$$

The adjoint angular function (II.24) is used in calculations of the incoming and outgoing adjoint angular functions of each segment using the adjoint characteristics equations. Then we use these angular adjoint to evaluate the average angular adjoint on each segment and the scalar adjoint functions in each region as discussed in the next section.

II.2.2 Determination of Average Adjoint Scalar Function

In the characteristics formalism a tracking line $\vec{T}(\vec{P}, \vec{\Omega})$ is defined by its reference starting point $\vec{P}$ and a direction vector $\vec{\Omega}$. (WU and ROY, 2003) Γ is the characteristics domain composed of subdomains $\pi_{\vec{P}}$ and $\pi_{\vec{\Omega}}$, where $\pi_{\vec{P}}$ is the two-dimension spatial subdomain of a plane, containing the point $\vec{P}$ perpendicular to the angular direction $\vec{\Omega}$. $\pi_{\vec{\Omega}}$ is the sub-domain of the unit angular directional vector $\vec{\Omega}$ represented by polar angle θ and azimuthal angle φ where $\theta \in [0, \pi]$ and $\varphi \in [0, 2\pi]$.

The average adjoint scalar function in region j of the spatial domain (D) is,

$$V_j \phi_j^{*g} = \int_{V_j} d^3r \int_{\pi_{\vec{\Omega}}} d^2\Omega \cdot \Phi^{*g}(\vec{r}, \vec{\Omega}) \tag{II.25}$$

where ϕ_j^{*g} is the average adjoint scalar function in group g in region j, where $j = 1$ to N_J, and N_J is the total number of regions in the spatial domain (D). Here V_j is the volume of region j.

Using the characteristics formalism, we can rewrite (II.25) as,

$$V_j \phi_j^{*g} = \int_{\Gamma} d^4T \int_0^{+\infty} dt \cdot F_j(\vec{T}, \vec{P} + t\vec{\Omega}) \cdot \Phi^{*g}(\vec{P} + t\vec{\Omega}, \vec{\Omega}) \tag{II.26}$$

where we have used,

$$\begin{aligned} \int_{V_j} d^3r \int_{\pi_{\vec{\Omega}}} d^2\Omega \cdot f(\vec{r}, \vec{\Omega}) &= \int_{\pi_{\vec{P}}} d^2P \int_{\pi_{\vec{\Omega}}} d^2\Omega \int_0^{+\infty} dt \cdot F_j(\vec{T}, \vec{P} + t\vec{\Omega}) \cdot f(\vec{r}, \vec{\Omega}) \\ &= \int_{\Gamma} d^4T \int_0^{+\infty} dt \cdot F_j(\vec{T}, \vec{P} + t\vec{\Omega}) \cdot f(\vec{r}, \vec{\Omega}) \end{aligned} \tag{II.27}$$

for $f(\vec{r}, \vec{\Omega})$ an arbitrary function. $F_j(\vec{T}, \vec{P}+t\vec{\Omega})$ is equal to 1 when the point $(\vec{P}+t\vec{\Omega})$ on tracking line $\vec{T}(\vec{P}, \vec{\Omega})$ is located in the region j, otherwise it takes a value of 0. The discretized form of average adjoint scalar equation (II.26) with the use of (II.16) is,

$$V_j \phi_j^{*g} = \sum_{l=1}^{N^{\Omega}} \sum_{i=1}^{N^{\perp}(l)} W_i^{\perp} W_l^{\Omega} \sum_{k=1}^{K} [F_j(\vec{T}(\vec{P}_i, \vec{\Omega}_l), \vec{p}_{k+1/2}) L_k \overline{\Phi}_k^{*g}(\vec{\Omega}_l)] \tag{II.28}$$

where

$$\int_{\pi_{\vec{P}}} d^2P \int_{\pi_{\vec{\Omega}}} d^2\Omega \cdot f(\vec{P}, \vec{\Omega}) \approx \sum_{l=1}^{N^{\Omega}} \sum_{i=1}^{N^{\perp}(l)} W_i^{\perp} W_l^{\Omega} \cdot f(\vec{P}_i, \vec{\Omega}_l)$$

$\overline{\Phi}_k^{*g}(\vec{\Omega}_l)$ is the average adjoint angular function for the segment L_k on $\vec{T}(\vec{P}_i, \vec{\Omega}_l)$,

$W_i^{\perp}$ is the quadrature weight for a starting point $\vec{P}_i$ of $\vec{T}(\vec{P}_i, \vec{\Omega}_l)$, $N^{\perp}(l)$ is the total number of tracking lines in direction $\vec{\Omega}_l$, and $\vec{p}_{k+1/2}$ is the center point of segment L_k.

II.3 Mathematical relationship between adjoint functions by MOCC and CP methods

Here we show that performing the adjoint angular function integrations over the tracking lines and characteristics domains using the MOCC procedure is equivalent to integrating the collision probability over the adjoint sources. (COURAU, 2001; COURAU and MARLEAU, 2002) Let us first rewrite the adjoint transport equation (II.4) in the direction $\vec{\Omega}$ as follows,

$$-\frac{d\Phi^{*g}(\vec{r}+S\vec{\Omega},\vec{\Omega})}{dS}+\Sigma^g(\vec{r}+S\vec{\Omega})\Phi^{*g}(\vec{r}+S\vec{\Omega},\vec{\Omega})=q^{*g}(\vec{r}+S\vec{\Omega}) \qquad \text{(II.29)}$$

Multiplying both side of (II.29) by,

$$e^{-\tau^g(\vec{r}+S\vec{\Omega},\vec{r})}=e^{-\int_0^S \Sigma^g(\vec{r}+S'\vec{\Omega})dS'}$$

and integrating over dS from $S=0$ to R, we obtain,

$$\begin{aligned}\Phi^{*g}(\vec{p}+t\vec{\Omega},\vec{\Omega}) &= \Phi^{*g}(\vec{p}+t_K\vec{\Omega},\vec{\Omega})\cdot e^{-\tau^g(\vec{p}+t_K\vec{\Omega},\vec{p}+t\vec{\Omega})} \\ &\quad+\int_0^{t_K-t} dS\cdot q^{*g}(\vec{p}+(t+S)\vec{\Omega})\cdot e^{-\tau^g(\vec{p}+(t+S)\vec{\Omega},\vec{p}+t\vec{\Omega})} \qquad \text{(II.30)}\end{aligned}$$

where we have used $\vec{r}=\vec{p}+t\vec{\Omega}$ and $t_K=R+t$.

In the infinite spatial domain, we find that,

$$e^{-\tau^g(\vec{p}+t_K\vec{\Omega},\vec{p}+t\vec{\Omega})} \rightarrow 0 \quad \text{when} \quad t_K \rightarrow \infty \tag{II.31}$$

Using (II.27), (II.30) and (II.31) in the average adjoint scalar equation (II.26), we obtain,

$$V_j\phi_j^{*g} = \int_{V_j} d^3r \int_{D_\infty} d^3r' \cdot \frac{e^{-\tau^g(\vec{r'},\vec{r})}}{\|\vec{r'}-\vec{r}\|^2} \cdot q^{*g}(\vec{r'}) \tag{II.32}$$

where,

$$\vec{r} = \vec{p} + t\vec{\Omega}$$
$$\vec{r'} = \vec{r} + S\vec{\Omega}$$
$$d^3r' = d^2\Omega \cdot dS \cdot S^2$$
$$S = \|\vec{r'}-\vec{r}\|$$

Here D_∞ is the infinite spatial domain that is composed of the finite spatial domain (D) unfolded to infinity.

We can rewrite (II.32) using the collision probability definition as follows, (COURAU, 2001; COURAU and MARLEAU, 2002)

$$\begin{aligned}\phi_j^{*g} &= \frac{1}{V_j}\sum_{i=1}^{N_J}\left[\int_{V_j} d^3r \int_{V_i} d^3r' \cdot \frac{e^{-\tau^g(\vec{r'},\vec{r})}}{\|\vec{r'}-\vec{r}\|^2} \cdot q^{*g}(\vec{r'})\right] \\ &= \sum_{i=1}^{N_J} p_{j\rightarrow i}^g \cdot q_i^{*g}\end{aligned} \tag{II.33}$$

where we assume that the total adjoint source $(q^{*g}(\vec{r'}) = q_i^{*g})$ is constant over the

region i with,

$$q_i^{*g} = \sum_{g'=1}^{G} [\Sigma_{s,i}^{g' \leftarrow g} + \frac{1}{k_{eff}} \chi_i^{g'} \nu \Sigma_{f,i}^{g}] \phi_i^{*g'} \tag{II.34}$$

$$p_{j \rightarrow i}^{g} = \frac{1}{V_j} \int_{V_j} d^3r \int_{V_i} d^3r' \frac{e^{-\tau^g(\vec{r'},\vec{r})}}{\|\vec{r'} - \vec{r}\|^2} \tag{II.35}$$

We can write the MOCC average adjoint scalar function equation (II.33) in matrix form,

$$[\phi_{MOCC}^*] = [P_{VV}][Q^*] \tag{II.36}$$

where

$$[Q^*] = \left[[\Sigma_s]^T + \frac{1}{k_{eff}} [[\chi] \cdot [\nu \Sigma_f]]^T \right] [\phi_{MOCC}^*] \tag{II.37}$$

$[P_{VV}]$ is the collision probability matrix, $[\Sigma_s]$ and $[\nu \Sigma_f]$ are matrices of scattering and fission cross section respectively, and $[\chi]$ is the matrix of probability of fission neutron production.

The adjoint CP equation or flux importance equation is in the form, (COURAU, 2001; COURAU and MARLEAU, 2002)

$$[\phi_{CP}^*] = \left[[\Sigma_s]^T + \frac{1}{k_{eff}} [[\chi] \cdot [\nu \Sigma_f]]^T \right] [P_{VV}][\phi_{CP}^*] \tag{II.38}$$

where $[\phi_{CP}^*]$ is the adjoint function solutions (flux importance function (RONEN, 1986)) to the adjoint CP equation. The source importance function is related to the flux importance by: (RONEN, 1986; COURAU and MARLEAU, 2002)

$$[\phi_{CP}^+] = [P_{VV}][\phi_{CP}^*] \tag{II.39}$$

Using (II.38) in (II.39), we obtain the source importance CP equation as follows,

$$[\phi_{CP}^{+}] = [P_{VV}] \left[[\Sigma_s]^T + \frac{1}{k_{eff}} [[\chi] \cdot [\nu\Sigma_f]]^T \right] [\phi_{CP}^{+}] \qquad \text{(II.40)}$$

The source importance function is the solution of the integro-differential adjoint neutron transport equation. (RONEN, 1986; COURAU and MARLEAU, 2003) Since the MOCC adjoint function is derived from the integro-differential adjoint transport equation and the MOCC average adjoint equation (II.36) is equivalent to the source importance CP equation (II.40), therefore the MOCC adjoint function is equivalent to the source importance function derived by the CP method:

$$[\phi_{MOCC}^{*}] = [\phi_{CP}^{+}]$$

II.4 MOCC Solution of Adjoint Transport Problems

The lattice code DRAGON (MARLEAU, 2001) contains a collection of models that can simulate the neutron behavior of a unit cell or a fuel assembly in a nuclear reactor. It includes all of the functions that characterize a lattice cell code, including multigroup and multidimensional neutron flux calculations based on CP and MOCC methods. The two-dimensional cyclic tracking procedure (ROY et al., 1991) (EXCELT module) in DRAGON is developed to generate the tracking lines in the rectangular spatial domain with the specular boundary conditions. These cyclic tracking lines are used in the CP evaluation and MOCC forward flux solution.

The MOCC forward flux solution algorithm (ROY, 1998) (MOCC module) was developed for k_{eff} and buckling-mode neutron transport problems in a two-dimensional heterogeneous fuel assembly. The forward transport calculations proceed as follows. First the geometries of the fuel assemblies are analyzed and tracked. The tracking

lines with the cyclic angles are generated over the discretized geometries using an adequate angular quadrature for the polar and azimuthal angles (e.g. Gaussian quadrature formula) (ROY et al., 1991). The macroscopic cross sections required for the transport calculations can be extracted from a microscopic cross section data library or provided as user input data. The MOCC forward flux algorithm is then called. The MOCC algorithm is generally composed of three levels of iterations: the power iteration over fission sources, the multigroup iteration over the scattering sources and the spatial iteration over the tracking lines respectively. The fission sources are first initialized in the power iteration loop and then transferred into the multigroup iteration loop where these fission sources are assumed constant. The scattering sources are then added to the fission sources. The spatial iteration is performed to evaluate the forward scalar fluxes.

In the forward multigroup iterations, the convergence rate depends on the within-group scattering to- and up-scattering to total cross-section ratios of reactor materials. Higher up-scattering cross-sections (from thermal-to-intermediate/intermediate-to-fast groups) result in the higher scattering sources in the intermediate/fast groups which then cause longer multigroup iterations (the convergence of thermal fluxes depend on the convergence of intermediate/fast fluxes). When the within-group scattering to total cross-section ratio approaches to unity, the convergence of multigroup iteration becomes unacceptably slow. To speed up the multigroup iterations, the forward rebalance technique is then called to correct the forward fluxes using the multigroup neutron balance equations. This rebalance technique is limited to reflective or periodic boundary conditions with unit albedos. The multigroup convergence test routine verifies the convergence of the forward fluxes after each multigroup iteration. After the multigroup convergence is reached, the forward k_{eff} is evaluated and the forward fluxes are normalized in such a way that the normalized fluxes result in a unit neutron production rate. The power con-

vergence test routine verifies the convergence of the normalized forward fluxes and k_{eff} in each power iteration.

II.4.1 Implementation of Adjoint MOCC Module

The adjoint MOCC solution algorithm is similar to the MOCC forward solution algorithm (see Figure II.4). The adjoint algorithm is programmed using the double-precision variables for adjoint functions, rebalance factors, tracking-line integrating variables and variables storing exponential values. Only the variables storing nuclear cross-section data are programmed in single-precision. The forward MOCC algorithm was also upgraded using the double-precision arithmetics. We have chosen the double-precision computation because Intel Pentium 4 CPU is optimized for the acceleration of double-precision computation with SSE2 architechture (RICE, 2000; Intel, 2005). For the single-precision computation, the additional operations for single-to-double precision conversion may cause longer computing time. We have tested for the computing time for a forward k_{eff} problem of a 135-regions 69-groups PWR lattice using Pentium 4-3.2GHz CPU computer. It shows that the computing time using single-precision variables (for fluxes and tracking-line integrations) is longer than using double-precision variables by approximately 30% (144 and 86 min. for single and double precision computations respectively).

The adjoint MOCC algorithm is composed of 3 levels of iterations, the same as the MOCC forward solution algorithm. The adjoint function solution performs as follows: in the power iteration loop the adjoint fission sources are initialized and then transferred into the multigroup iteration loop where these adjoint fission sources are assumed constant. The adjoint scattering sources are then added to the adjoint fission sources. The group-reduction procedure is then implemented to avoid the iterations for the adjoint functions in the converged groups as well as

the group-splitting procedure for speeding up the multigroup iterations as we will discuss in II.4.2. Since these procedures can also be used to speed-up the forward algorithm the next logical step is to combine the forward and adjoint schemes as we will discuss in II.4.3.

The spatial iterations are performed by scanning over the cyclic tracking lines to evaluate the terms $[M(K)]$ and $[1 - \prod_{k'=1}^{K}[H(k')\beta_{alb}(k')]]$ using the adjoint characteristics equations and the computed adjoint fission and scattering sources. The closed forms for adjoint angular functions on each cyclic tracking line are used to evaluate the average adjoint angular functions on each segment of cyclic tracking lines. The adjoint scalar functions in each region are then calculated using the average adjoint scalar function equation.

After each spatial iteration is completed, the rebalance technique described in II.4.4 is performed to correct the adjoint scalar functions using the multigroup adjoint balance equations. The non-leakage probability approach (MARLEAU, 2004b) is implemented for both forward and adjoint rebalancing schemes to take in account cell leakage. The multigroup convergence test routine verifies the convergence of the adjoint scalar functions after each multigroup iteration. After the multigroup convergence is reached, k^*_{eff} is evaluated and the adjoint scalar functions are normalized (unit adjoint production rate). The power convergence test routine verifies the convergence of the normalized adjoint scalar functions and k^*_{eff} in each power iteration.

II.4.2 Group-splitting and Group-reduction Techniques

Here we consider the group-splitting technique where the energy groups are divided according to the structure of the adjoint scattering matrix. We may first write the

forward scattering matrix for a mixture that contains up-scattering cross sections at the highest energy group (see Figure II.5). The adjoint scattering matrix is obtained by transposing the forward scattering matrix. From the adjoint scattering matrix, we can divide the energy groups into two sets. The first set contains all the groups without up-scattering (G_1: $g \leq g_u$ groups, where g_u is the lowest group containing no up-scattering). The second set contains the remaining groups (G_2: $g > g_u$ groups) where the adjoint scattering sources depend only on adjoint functions in G_2. We can improve the multigroup iterations by first solving the G_2 adjoint transport equations to obtain the converged adjoint function solutions which are then used to compute the adjoint scattering sources required for solving the G_1 adjoint transport equations. Note that in the non-splitting scheme, these G_1 adjoint scattering sources are computed with the un-converged G_2 solutions. Therefore inefficient computations in G_1 can be avoided in such a group-splitting procedure. In addition, we perform the backward iteration (G_1^-) from g_u to 1 groups because the adjoint scattering matrix is upper triangular in this group set (adjoint scattering sources in higher groups depend on the adjoint functions in lower groups). Here G_x^+ and G_x^- represent the forward and backward group iterations on the group set G_x respectively (e.g. G_1^+ represents the forward group iteration from 1 to g_u groups).

In addition to the group-splitting technique, we also consider the group-reduction technique. During the multigroup iteration, the adjoint functions over energy groups do not converge simultaneously. From the fact that up-scattering cross sections are low from thermal to fast/intermediate groups, the adjoint scattering sources ($q_{sc}^{*g}(\vec{r}) = \sum_{g'=1}^{G} \Sigma_s^{g' \leftarrow g} \phi^{*g'}(\vec{r})$) in thermal groups depend mainly on the thermal adjoint functions (while the considerable down-/up-scattering cross sections contribute to adjoint scattering sources in fast/intermediate groups). Therefore, when the adjoint fission sources are fixed during multigroup iterations, the

adjoint functions in thermal groups will converge before the adjoint functions in the fast/intermediate groups (for forward problems the fast fluxes converge before the thermal fluxes due to the low up-scattering cross sections from thermal/intermediate to fast groups). The group-reduction procedure consists in monitoring the convergence of the adjoint functions in the most thermal groups and activating the multigroup iterations only on the un-converged groups.

II.4.3 The Combined Forward-Adjoint Iteration Scheme

Here we propose to combine the forward and adjoint iteration schemes to reduce the computing time when both forward and adjoint solutions are required. The combined iteration scheme implemented in the multigroup iteration is based on the group-splitting technique and the common use of the large number of routine variables such as those used for storing exponential values and tracking line data. From the forward and adjoint scattering matrices we can divide the energy groups into 2 sets (G_1: $g \leq g_u$ and G_2: $g > g_u$) as discussed previously. As seen from the scattering matrices, the G_1 forward scattering sources ($q_{sc,G1}$) depend only on the fluxes (ϕ_{G1}). Similarly the G_2 adjoint scattering sources ($q^*_{sc,G2}$) depend only on the G_2 adjoint functions (ϕ^*_{G2}). Therefore we may divide the multigroup iteration into 3 steps as follows,

- The first step is the flux iteration for G_1. Because $q_{sc,G1}$ depend only on ϕ_{G1}, we first solve the G_1 forward transport equations to obtain the converged flux ϕ_{G1} which are then used to compute $q_{sc,G2}$ for solving the G_2 function transport equations in next step. The forward group iterations G_1^+ is performed because the forward scattering matrix is lower triangular (forward scattering sources in lower groups depend on forward fluxes in higher groups).

- The second step is the combined forward and adjoint iterations for G_2. The large number of exponential function evaluation and tracking-line variables calculations that are used both by the flux and adjoint function computation algorithms are the key to reduce the computing time. We then solve simultaneously group-by-group the G_2 forward and adjoint transport equations to obtain the converged solutions ϕ_{G2} and ϕ^*_{G2}.

- The third step consists in solving the adjoint functions for G_1 where the adjoint scattering sources $q^*_{sc,G1}$ are computed using the converged adjoint functions ϕ^*_{G2}. The backward group iterations G_1^- is performed because the adjoint scattering matrix is upper triangular in this case.

During the combined forward-adjoint iterations, the flux and adjoint function converge at different rates. We have isolated the convergence checking routines for flux and adjoint function in such a way that they can be turned off independently when either the flux or the adjoint has converged.

II.4.4 Multigroup Rebalance Technique

In the multigroup adjoint iterations, the convergence rate depends on the ratio of the within group and up-scattering cross section to the total cross section. From the fact that the thermal adjoint functions converge before the intermediate and fast adjoint functions (the convergence of intermediate and fast adjoint funtions also depend on the convergence of thermal adjoint funtions). The higher up-scattering cross-sections from the thermal to intermediate groups, result in higher thermal adjoint scattering sources ($q^{*g}_{sc}(\vec{r}) = \sum_{g'=1}^{G} \Sigma_s^{g' \leftarrow g} \phi^{*g'}(\vec{r})$) those cause longer multigroup iterations. When the within-group scattering to total cross-section ratio approaches to unity, the multigroup iteration convergence slowly (similar to the

forward multigroup iterations). In fact the adjoint function must satisfy both adjoint transport and balance equations. By correcting the adjoint scalar functions using the adjoint balance equations after each spatial iteration loop, one can accelerate the calculation process. For the problems with the albedo boundary conditions, the adjoint balance equations are obtained by integrating (II.4) over all angles and domain volume as follows,

$$\Theta^{*g}[\phi^*] = Q^{*g} \tag{II.41}$$

where

$$\Theta^{*g}[\phi^*] = \mathcal{L}^{*g} + \sum_{j=1}^{N_J} \Sigma_j^g \phi_j^{*g} V_j - \sum_{j=1}^{N_J} \sum_{g'=1}^{G} \Sigma_{s,j}^{g' \leftarrow g} \phi_j^{*g'} V_j \tag{II.42}$$

$$Q^{*g} = \frac{1}{k_{eff}} \sum_{j=1}^{N_J} \sum_{g'=1}^{G} \chi_j^{g'} \nu \Sigma_{f,j}^{g} \phi_j^{*g'} V_j \tag{II.43}$$

$\mathcal{L}^{*g}$ is the total adjoint leakage in group g, and the subscript j indicates the variable associated with region j.

The total adjoint leakage $\mathcal{L}^{*g}$ can be determined indirectly by, (MARLEAU, 2004b)

$$\mathcal{L}^{*g} = \sum_{j=1}^{N_J} \left[\left(1 - P_{NL,j}^{g}\right) \sum_{g'=1}^{G} \left(\Sigma_{s,j}^{g' \leftarrow g} + \frac{1}{k_{eff}} \chi_j^{g'} \nu \Sigma_{f,j}^{g} \right) \phi_j^{*g'} V_j \right] \tag{II.44}$$

where

$$P_{NL,j}^{g} = \sum_{i=1}^{N_J} p_{j \to i}^{g} \Sigma_i^g \tag{II.45}$$

$P_{NL,j}^{g}$ is the non-leakage probability of a neutron in region j in energy group g. We can determine $P_{NL,j}^{g}$ using MOCC method by solving the adjoint transport

equations with the imposed adjoint sources defined as follows,

$$q_i^{*g} = \Sigma_i^g \tag{II.46}$$

Using the MOCC adjoint scalar equation (II.33) in CP form, we can find that the adjoint results with adjoint sources (II.46) are equal to the non-leakage probabilities.

We can then rewrite (II.41) using (II.44) and (II.45) as follows,

$$\sum_{j=1}^{N_J} \Sigma_j^g \phi_j^{*g} V_j - \sum_{j=1}^{N_J} P_{NL,j}^g \sum_{g'=1}^{G} \Sigma_{s,j}^{g' \leftarrow g} \phi_j^{*g'} V_j = \frac{1}{k_{eff}} \sum_{j=1}^{N_J} P_{NL,j}^g \sum_{g'=1}^{G} \chi_j^{g'} \nu \Sigma_{f,j}^g \phi_j^{*g'} V_j \tag{II.47}$$

The corrected adjoint scalar function is defined as follows,

$$\widetilde{\phi}_j^{*g} = f_c^g \phi_j^{*g} \tag{II.48}$$

where f_c^g is the correction factor associated with energy group g. Applying (II.48) to the LHS of (II.47), we then solve the G resulting equations to obtain the correction factors f_c^g. All final correction factors shall converge to 1.0 at the end of multigroup iterations. For the problems with no leakage ($\alpha = 1$), $P_{NL,j}^g$ are set to unity.

II.5 Numerical Results

The adjoint solution algorithm is tested for a 17×17 PWR lattice, a 37 pin CANDU cell and the 3×3 Watanabe-Maynard benchmark. We compare the k_{eff} and adjoint function with the k_{eff} and adjoint results obtained using the CP method. (COURAU, 2001; COURAU and MARLEAU, 2002) The azimuthal angular integration is performed using an 11 point Gaussian quadrature while the polar inte-

gration consists in a 6 point Gauss-Legendre quadrature. (ROY et al., 1991) The tracking density is 20 lines/cm. The convergence criterion is 1.0×10^{-6} for both power and multigroup iterations. The cyclic tracking procedure is commonly used for both the collision probability evaluation and MOCC adjoint solutions. The testing computer is Prosys Ultra GLC with Intel D865GLC motherboard, PENTIUM 4-3.2GHz CPU and 1 GB RAM.

II.5.1 A 17 × 17 PWR Lattice

A 2-D 17 × 17 PWR lattice is discretized into 135 regions according to the exact geometries with the use of 1/8 symmetrical property (see Figure II.6). (MARLEAU, 2001) The 69 energy group nuclear cross sections are obtained from the WIMS-AECL library. Reflective boundary conditions are used for this problem.

The k_{eff} results by MOCC and CP methods are shown in Table II.1. All the values for k_{eff} agree to within 2×10^{-7} as expected. The forward k_{eff} result is similar to the adjoint k^*_{eff} result as expected. The comparisons between the source importance functions obtained by CP method and the adjoint functions by MOCC method are performed. The maximum absolute relative error observed in this case for the 135×69 adjoint function values is 2.3×10^{-6}.

The results for computing time using MOCC and CP methods are shown in Table II.2. The adjoint function computing time is lower in MOCC method than CP method (include CP evaluation time) by approximately 71.79%. This is because the numerical integration in collision probability evaluation is time-consuming and a large number of collision probability evaluations is required ($69 \times 135 \times 135$ values), while MOCC method requires only one cycle of scanning over the cyclic tracking lines to evaluate the closed forms and average adjoint scalar functions in

each spatial iteration loop. On the other hand, we may consider that the collision probabilities have already been evaluated and the adjoint function computing time by CP method is then reduced to 1.7 second. Note that the CP evaluation is programmed in double-precision because the tracking line integration is performed on the large number of exponential values and tracking-line data. When the CP evaluation finishes, the CP matrices are stored in single-precision format in order to reduce the permanent memory space (e.g. $\approx$ 20 MB for single-precision CP matrices of PWR). The CP solution is programmed in single-precision but changing the algorithm to double-precision will affect the total computing time by less than 1 second.

For the group-splitting iteration, we have found that group 27 is the highest energy group containing up-scattering cross sections. We then divide the energy groups into two sets: (G_2: 27 to 69) and (G_1: 1 to 26) groups. In the G_1 groups we perform the backward iteration G_1^- because the adjoint scattering sources in higher energy groups depend on the adjoint functions in the lower groups. In the G_2 groups, the forward iteration G_2^+ results in the lowest number of one-group adjoint function solutions as shown Table II.3. As a result of group-splitting, the total number of one-group solutions is decreased by approximately 24.5% compared with the (1 to 69) non-splitting case.

The combined forward-adjoint iterations with the forward iteration G_2^+ in the second step gives the lowest computing time and number of one-group solutions. The total computing time is approximately 19.3% lower than the total computing time for individual forward and adjoint calculations by MOCC method.

II.5.2 A 37 Pin CANDU Cell

A 2-D 37 pin CANDU cell is discretized into 42 regions according to the exact geometries (see Figure II.7). (MARLEAU, 2001) The 69 energy group nuclear cross sections are obtained from WNEALIB nuclear library. Reflective boundary conditions are also used in this problem.

The k_{eff} results by MOCC and CP methods are shown in Table II.4. All the values for k_{eff} agree to within 2×10^{-6}. The maximum absolute relative error of adjoint functions in this case is 4.03×10^{-6}. The adjoint function computing time is again lower in MOCC than CP method (include CP evaluation time) by approximately 61.1% (Table II.5). For the group-splitting iteration, the energy groups are divided into two sets as for the PWR case. In the G_2 groups, the backward iteration G_2^- results in the lowest number of one-group solutions which is approximately 18.2% lower than the (1 to 69) non-splitting case (see Table II.6).

The combined forward-adjoint iterations procedure with the forward iteration G_2^+ in the second step produces the lowest computing time and number of one-group solutions. The computing time for combined iterations is 19.4% lower than the total computing time required for individual forward and adjoint calculations by MOCC method.

II.5.3 The Watanabe-Maynard Benchmark

The 2-D 3×3 Watanabe-Maynard benchmark with fission sources and internal void regions is discretized into 300 regions with the use of 1/2 symmetrical property (see Figure II.8). (MARLEAU, 2001) The 2 energy group nuclear cross sections are shown in Table II.7. Reflective boundary conditions are also used in this problem.

The k_{eff} results by MOCC and CP methods are shown in Table II.8. All the values for k_{eff} agree to within 8×10^{-7}. The maximum absolute relative difference between the source importance functions obtained by CP method and the adjoint functions by MOCC method is 1.08×10^{-4}. The large relative error obtained in this case is because of the high scattering and low absorption cross sections in the mixture 2. This is also because flux solution algorithm based on the CP method is programmed using single precision variables while the MOCC method uses double precision. If we reduce the within-group scattering cross sections in the mixture 2 by 50%, the maximum absolute relative error is decreased to about 1.4×10^{-6} (the CP computing time is only slightly lower because it is dominated by the CP integration time which remains the same, but the MOCC computing time is reduced by a factor of nearly 2).

The results of computing time by MOCC and CP methods are shown in Table II.9. The total forward and adjoint computing time by MOCC method is higher than the total time by CP method. But the combined forward-adjoint scheme gives the lowest computing time among the methods for the total forward and adjoint calculations.

II.6 Conclusions

The MOCC method is a good alternative solution method for the adjoint transport problems in two-dimensional heterogeneous geometries. The adjoint function and k_{eff} results by MOCC method are similar to the source importance function and k_{eff} results by CP method as expected. Since the source importance CP equation can be derived from the MOCC adjoint scalar function equation, the source importance function by CP method can be shown to be equivalent to the adjoint function by MOCC method.

In order to satisfy the boundary conditions in the adjoint transport problems, we need to solve the $\vec{\Omega}$-directed adjoint transport equation along the tracking line in the backward direction $(-\vec{\Omega})$. The adjoint characteristics equation is in the same form as the characteristics equation in neutron transport problem except the adjoint characteristics equation is formulated in the direction $(-\vec{\Omega})$. With the use of closed form, the solution of adjoint angular function associated with the cyclic tracking line is directly determined.

By taking into account the structure of adjoint scattering matrix, the group-oriented and group-splitting iterations result in speed-up of computations. Because the adjoint functions converge faster in the thermal groups than in the fast groups, the group-reduction procedure is implemented by monitoring the convergence in the most thermal groups and activating the multigroup iterations only for the adjoint functions in the un-converged groups.

The combined forward-adjoint iterations scheme based on the group-splitting technique and the common use of the large number of routine variables storing tracking line data and exponential values give lower computing time than the total time required for the individual forward and adjoint calculations. The 3 step scheme (e.g. 1 to 26 (forward), 27 to 69 (forward & adjoint) and 26 to 1 (adjoint)) can be applied for both PWR and CANDU cases. This is because the forward fluxes converge slower than the adjoint functions in these cases. The iterations in the second step rely on the convergence of the flux iterations where the iteration for 27 to 69 groups give lower computing time than the iterations for 69 to 27 groups.

The current implementation of the MOCC method is very efficient and requires a lower computing time than the CP method for a single adjoint function calculation.

Acknowledgments

This work was supported in part by the Natural Science and Engineering Research Council of Canada.

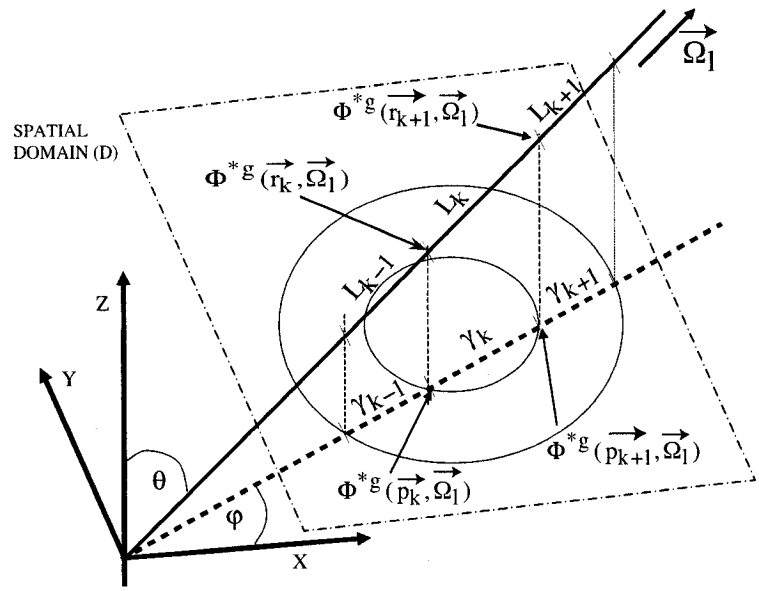

Figure II.1 3-D tracking line in direction $\vec{\Omega}_l$

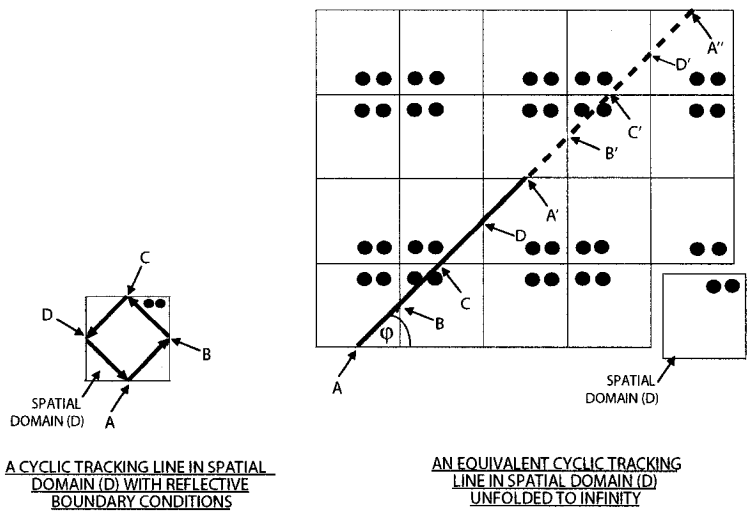

Figure II.2 A cyclic tracking line in rectangular spatial domain unfolded to infinity using reflective boundary conditions

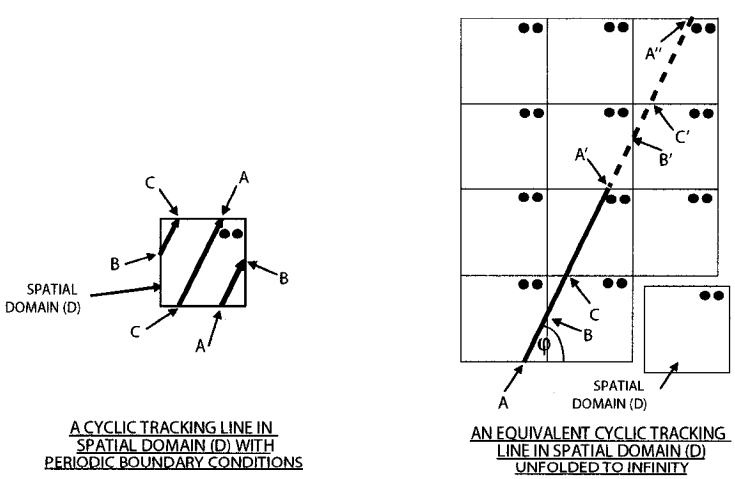

Figure II.3 A cyclic tracking line in rectangular spatial domain unfolded to infinity using periodic boundary conditions

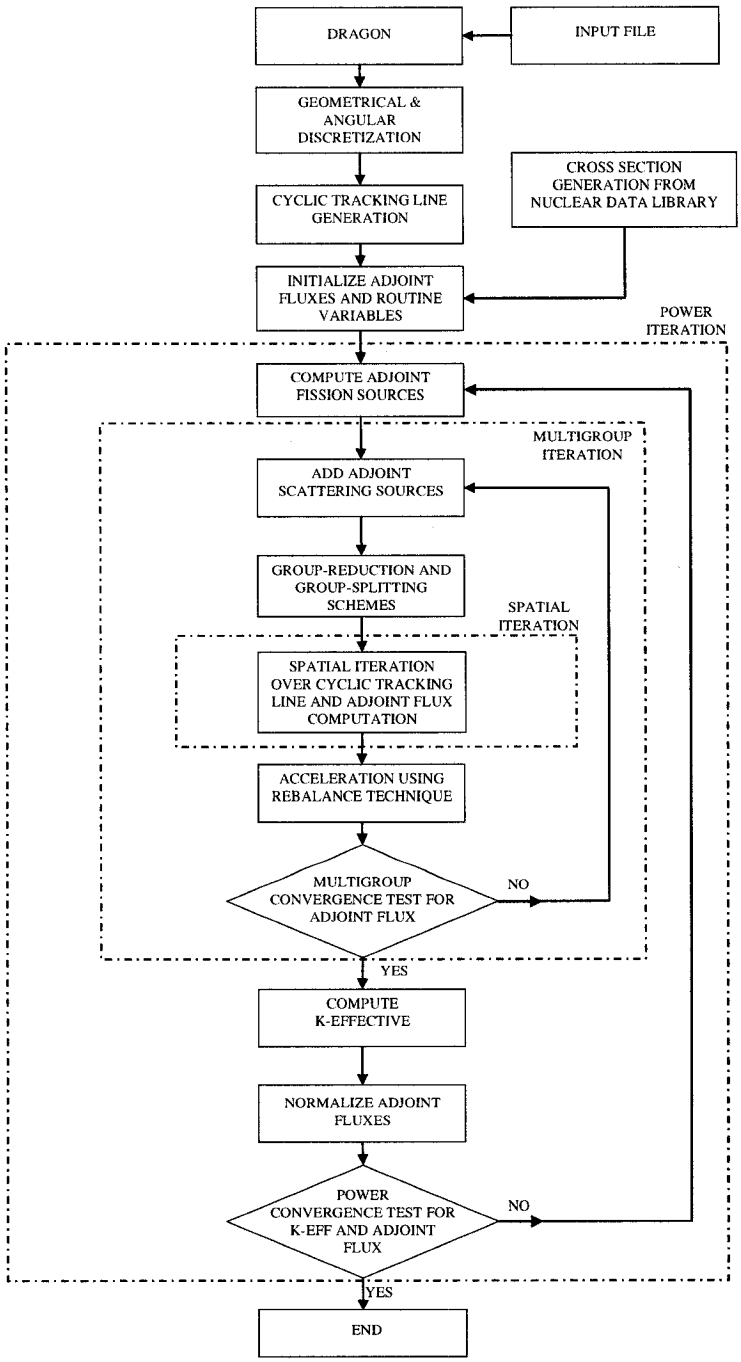

Figure II.4 MOCC flow diagram for adjoint transport problem

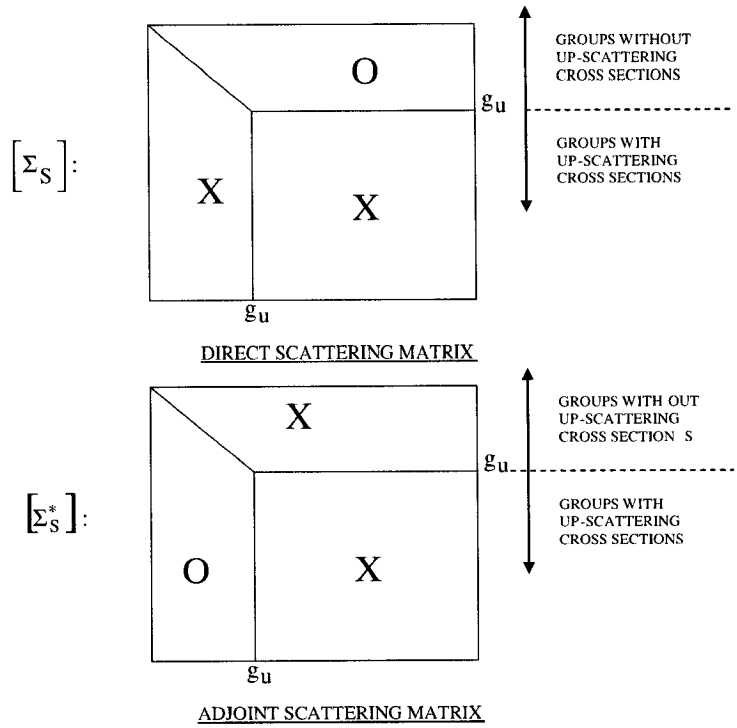

Figure II.5 Direct and adjoint scattering matrices containing up-scattering cross sections at highest energy group

Table II.1 k_{eff} for MOCC and CP solutions of the PWR Test Case

Solution method	k_{eff}
Forward CP	0.7062190
Adjoint CP	0.7062192
Forward MOCC	0.7062191
Adjoint MOCC	0.7062191

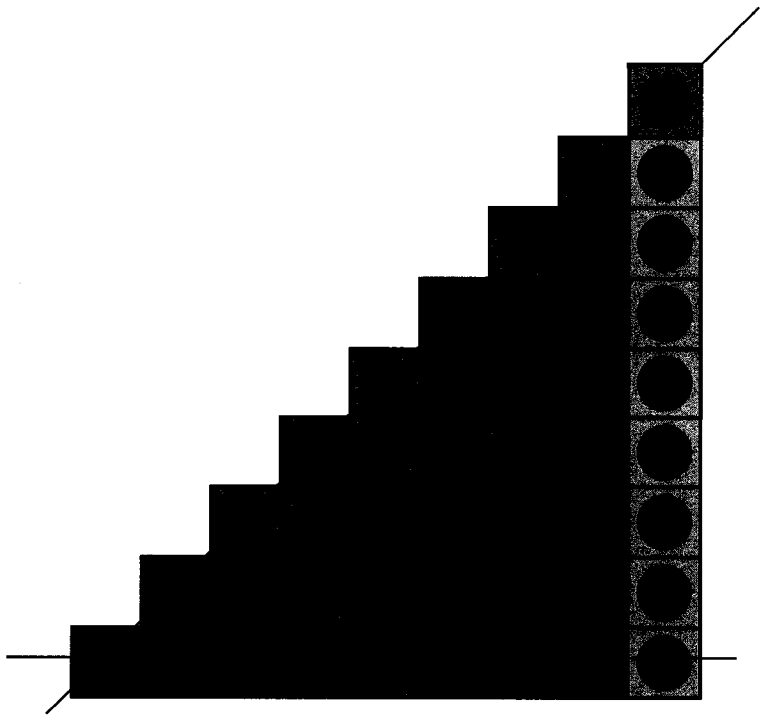

Figure II.6 A 2-D 17 × 17 PWR lattice

Table II.2 Computing Time for MOCC and CP Solution of PWR Test Case

Solution method	Computation time		
	CP evaluation	Flux solution	Total
Forward CP	226 min 48 sec	1.5 sec	226 min 51.2 sec
Adjoint CP	—	1.7 sec	
Forward MOCC $(G_1^+ + G_2^+)$	—	86 min	150 min
Adjoint MOCC $(G_2^+ + G_1^-)$	—	64 min	
3 steps combined MOCC Iteration: $(G_1^+ + G_2^+ + G_1^-)^a$	—	121 min	121 min
3 steps combined MOCC Iteration: $(G_1^+ + G_2^- + G_1^-)^a$	—	132 min	132 min

[a] : *The first set of groups is for the fast flux only, the second set is for the thermal flux and adjoint function, and the last set is for fast adjoint function only.*

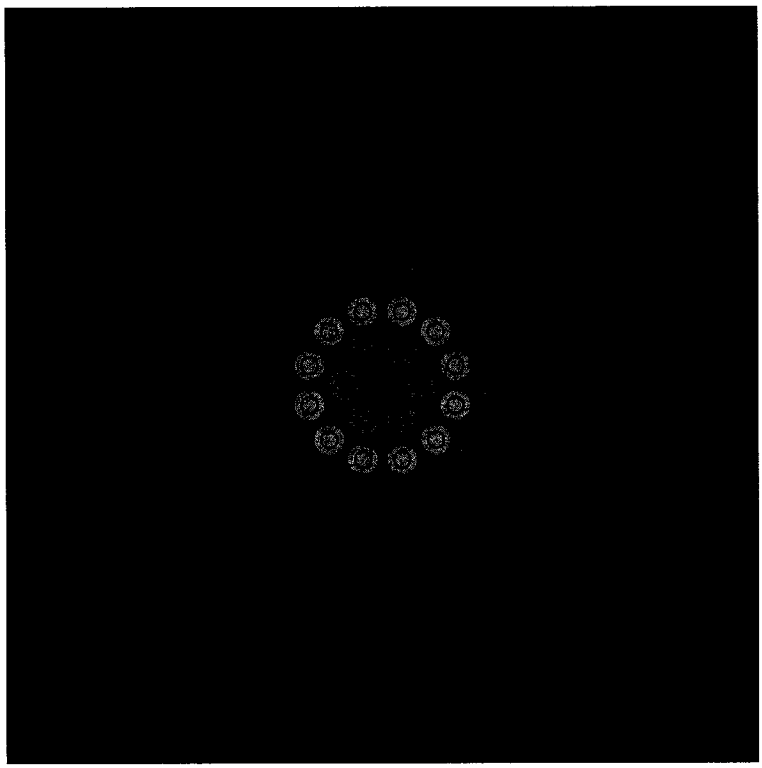

Figure II.7 A 2-D 37 pin CANDU cell

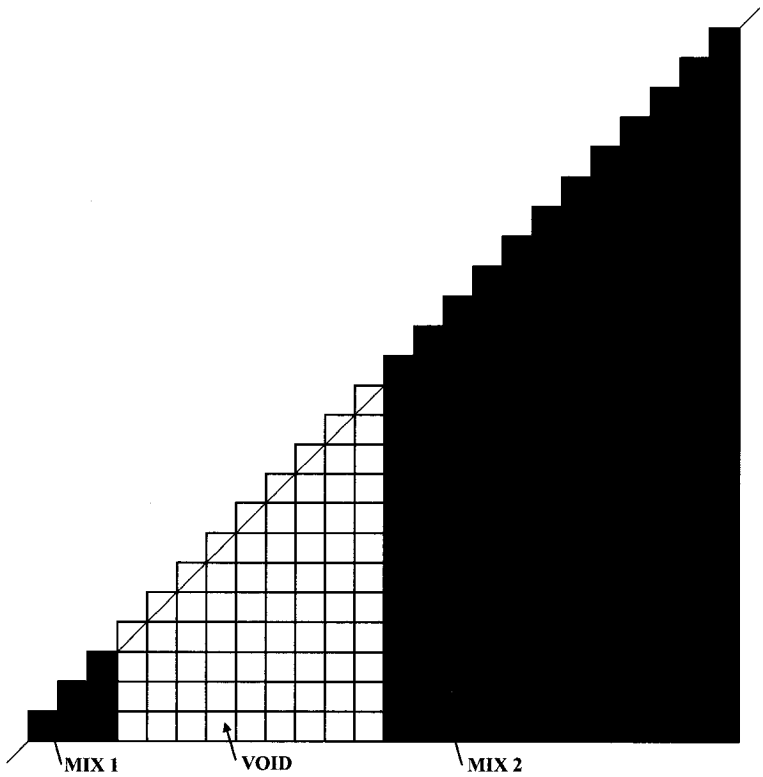

Figure II.8 The 2-D 3×3 Watanabe-Maynard benchmark

Table II.3 Total Number of Iterations Using a Group-splitting Technique for the PWR Test Case

Group-splitting option	Number of power iterations	Number of multigroup iterations	Number of one-group flux solution
Non-splitting iteration: (1 to 69)	6	70	4111
Non-splitting iteration: (69 to 1)	5	83	5392
Group-splitting iteration: $(G_2^+ + G_1^+)$	6	(53 + 55)	3389
Group-splitting iteration: $(G_2^- + G_1^-)$	5	(70 + 48)	4017
Group-splitting iteration: $(G_2^+ + G_1^-)$	5	(52 + 45)	3104
3 steps combined algorithm iteration: $(G_1^+ + G_2^+ + G_1^-)^a$	8	(64+85+60)^a	5549
3 steps combined algorithm iteration: $(G_1^+ + G_2^- + G_1^-)^a$	5	(57+103+45)^a	6056

Notes: 4180 one-group flux solutions for forward problem.
^{a} *: The first set of groups is for the fast flux only, the second set is for the thermal flux and adjoint function, and the last set is for fast adjoint function only.*

Table II.4 k_{eff} for MOCC and CP solutions of the CANDU Test Case

Solution method	k_{eff}
Forward CP	1.1126080
Adjoint CP	1.1126095
Forward MOCC	1.1126075
Adjoint MOCC	1.1126080

Table II.5 Computing Time for MOCC and CP Solution of CANDU Test Case

Solution method	Computation time		
	CP evaluation	Flux solution	Total
Forward CP	84 min 50 sec	0.30 sec	84 min 50.42 sec
Adjoint CP	—	0.12 sec	
Forward MOCC $(G_1^+ + G_2^+)$	—	39 min	72 min
Adjoint MOCC $(G_2^- + G_1^-)$	—	33 min	
3 steps combined MOCC iteration: $(G_1^+ + G_2^+ + G_1^-)^a$	—	58 min	58 min
3 steps combined MOCC iteration: $(G_1^+ + G_2^- + G_1^-)^a$	—	59 min	59 min

[a] : *The first set of groups is for the fast flux only, the second set is for the thermal flux and adjoint function, and the last set is for fast adjoint function only.*

Table II.6 Total Number of Iterations Using a Group-splitting Technique for the CANDU Test Case

Group-splitting option	Number of power iterations	Number of multigroup iterations	Number of one-group flux solution
Non-splitting iteration: (1 to 69)	4	42	2628
Non-splitting iteration: (69 to 1)	4	37	2418
Group-splitting iteration: $(G_2^+ + G_1^+)$	4	(33 + 41)	2416
Group-splitting iteration: $(G_2^- + G_1^-)$	4	(31 + 32)	2151
Group-splitting iteration: $(G_2^+ + G_1^-)$	4	(33 + 32)	2199
3 steps combined algorithm Iteration: $(G_1^+ + G_2^+ + G_1^-)^a$	6	$(57 + 37 + 33)^a$	3391
3 steps combined algorithm Iteration: $(G_1^+ + G_2^- + G_1^-)^a$	6	$(57 + 42 + 33)^a$	3501

Notes: 2408 one-group flux solutions for forward problem.
[a] : The first set of groups is for the fast flux only, the second set is for the thermal flux and adjoint function, and the last set is for fast adjoint function only.

Table II.7 Two Group Cross Sections for the Watanabe-Maynard Benchmark

Cross Sections	Mix 1	Mix 2
Σ^1	0.392175	0.449812
Σ^2	0.622581	1.355650
$\nu\Sigma_f^1$	0.022141	0.0
$\nu\Sigma_f^2$	0.496970	0.0
χ^1	1.0	1.0
χ^2	0.0	0.0
$\Sigma_s^{1\to1}$	0.361893	0.411998
$\Sigma_s^{1\to2}$	0.000715	0.021280
$\Sigma_s^{2\to1}$	0.001451	0.002672
$\Sigma_s^{2\to2}$	0.358282	1.335170

Table II.8 k_{eff} for MOCC and CP solutions of the Watanabe-Maynard Test Case

Solution method	k_{eff}
Forward CP	0.2096349
Adjoint CP	0.2096349
Forward MOCC	0.2096354
Adjoint MOCC	0.2096346

Table II.9 Computing Time for MOCC and CP Solution of Watanabe-Maynard Test Case

	Computation time		
Solution method	CP evaluation	Flux solution	Total
Forward CP	35.9 sec	0.3 sec	36.5 sec
Adjoint CP	—	0.3 sec	
Forward MOCC	—	18.9 sec	42.5 sec
Adjoint MOCC	—	23.6 sec	
Combined MOCC	—	27.8 sec	27.8 sec

APPENDIX III

ARTICLE III: COOLANT VOID REACTIVITY ADJUSTMENTS IN ADVANCED CANDU LATTICES USING ADJOINT SENSITIVITY TECHNIQUE

Monchai Assawaroongruengchot and Guy Marleau

Accepted for Publication (July 2007) in Annals of Nuclear Energy

Abstract

Coolant void reactivity (CVR) is an important factor in reactor accident analysis. Here we study the adjustments of CVR at beginning of burnup cycle (BOC) and k_{eff} at end of burnup cycle (EOC) for a 2-D Advanced CANDU Reactor (ACR) lattice using the optimization and adjoint sensitivity techniques. The sensitivity coefficients are evaluated using the perturbation theory based on the integral neutron transport equations. The neutron and flux importance transport solutions are obtained by the method of cyclic characteristics (MOCC). Three sets of parameters for CVR-BOC and k_{eff}-EOC adjustments are studied: 1) Dysprosium density in the central pin with Uranium enrichment in the outer fuel rings, 2) Dysprosium density and Uranium enrichment both in the central pin, and 3) the same parameters as in the first case but the objective is to obtain a negative checkerboard CVR-BOC (CBCVR-BOC). To approximate the EOC sensitivity coefficient, we perform constant-power burnup/depletion calculations using a slightly perturbed nuclear library and the unperturbed neutron fluxes to estimate the variation of nuclide densities at EOC. Our aim is to achieve a desired negative CVR-BOC of -2 mk and k_{eff}-EOC of 0.900 for the first two cases, and a CBCVR-BOC of -2 mk and k_{eff}-EOC of 0.900 for the last case. Sensitivity analyses of CVR and eigenvalue are also included in our study.

Keyword: Coolant-void reactivity (CVR); CANDU reactor; Advanced CANDU Reactor (ACR); Sensitivity Coefficient; Sensitivity Analysis

III.1 Introduction

Advanced CANDU Reactor (ACR) is the next generation CANDU reactor developed by AECL (OVANES et al., 2002). The main characteristics of the ACR

are: undermoderated tight lattice, heavy water moderator, light water coolant and CANFLEX fuel bundles. A typical ACR lattice geometry is shown in Figure III.1. The CANFLEX fuel bundle contains 43 pin fuel rods: the central pin is composed of Dysprosium-poisoned natural Uranium-oxide, and the remaining fuel pins are composed of slightly enriched Uranium-oxide. The moderator is separated from the coolant channels by means of the pressure and calendria tubes with a CO_2 gap. In ACR lattices, where the moderator is isolated from the coolant, loss-of-coolant accidents reduce the absorption and moderation in the coolant, and in the mean time increase the fast fission in fuel rods. This generally leads to positive reactivity change upon the coolant voiding. To mitigate this effect, Dysprosium oxide is introduced in the central pin of each fuel bundle. Because of its large resonance absorption, the fast fission effects are then partly overridden. For the nominal (cooled) conditions, the fission neutron productions by natural Uranium in the central pin compensate the thermal absorptions in Dysprosium. A similar technique could also be used for the CANDU-6 lattices by introducing a mixture of Gadolinium and slightly enriched Uranium in the central pin of the fuel bundle (AECL R&D Advisory Panel, 1992). CVR studies were previously performed for the fresh-fuel CANDU and ACR lattices. The positive CVRs were observed for both cases (CONSTANTIN and BEALACEANU, 2002; CONSTANTIN et al., 2003; COTTON et al., 2004; COTTON et al., 2005). Remarkably CVR studies of ACR checkerboard-voided patterns as presented in Figure III.2 reveal a higher positive CVR (CBCVR) than that of the 100% coolant-voided case (e.q. CBCVR $\simeq$ +7.8 mk ; CVR $\simeq$ +3.5 mk) (COTTON et al., 2005; TALEBI et al., 2006).

For a reference compositions of the ACR fuel, CVR is found to be as high as +3.99 mk at beginning of burnup cycle, then attain a maximum value (+5.15 mk) at about 5 FPD, and gradually decreases to approximately -4.28 mk at the end of the burnup cycle. In fact, the CVR remains positive for the first 120 days and become

negative afterward. Here we propose to use the optimization and adjoint sensitivity techniques to adjust Dysprosium density and Uranium enrichment percentage and obtain the desired CVR-BOC, and k_{eff}-EOC (to meet the exit-burnup requirement) for an ACR lattice. A perturbation theory method based on the integral transport equations with isotropic scattering is used to determine the sensitivity coefficients (ASSAWAROONGRUENGCHOT and MARLEAU, 2006; ASSAWAROONGRUENGCHOT and MARLEAU, 2007c). This method is chosen because it provides more accurate sensitivity coefficients than the method with the integrodifferential transport equations for the lattice problems with the anisotropic neutron fluxes (COURAU and MARLEAU, 2002; ASSAWAROONGRUENGCHOT and MARLEAU, 2006; ASSAWAROONGRUENGCHOT and MARLEAU, 2007c) (such as ACR or CANDU-6). In addition the angular flux importance functions are definitely isotropic in the isotropic scattering problems. The neutron and flux importance transport solutions are obtained by the method of cyclic characteristics in DRAGON (ASSAWAROONGRUENGCHOT and MARLEAU, 2006; ASSAWAROONGRUENGCHOT and MARLEAU, 2007b; ASSAWAROONGRUENGCHOT and MARLEAU, 2007c). To approximate the EOC sensitivity coefficient, we estimate the variations in nuclide densities at EOC by introducing a very small perturbation in the lattice parameters at BOC and perform constant-power burnup/depletion calculations for 600 full power days (FPD) using the unperturbed neutron fluxes.

In the next section we present the optimization method, adjoint sensitivity calculation technique and the approximation of sensitivity coefficients at BOC and EOC as well as the positive CBCVR effect in 2×2 ACR lattices. In section III.3 we present sensitivity analyses of CVRs and eigenvalues to Dysprosium density and Uranium enrichment. Section III.4 presents the effects of U235 enrichment and Dysprosium to CVR-BOC and CBCVR-BOC. The optimization results of CVR-

BOC, CBCVR-BOC and k_{eff}-EOC for the ACR lattice are presented in Section III.5. Finally the conclusions are presented in the last section.

III.2 The Optimization and Adjoint Sensitivity Techniques

Our objective is to obtain the desired CVR-BOC (or CBCVR-BOC) and k_{eff}-EOC by adjusting %wt Dysprosium (Dy) density and Uranium (U235) enrichment percentage. Here we study 3 situations: 1) the simultaneous adjustment of Dy density in the central pin and U235 enrichment in the outer fuel rings, 2) the adjustment of Dy density and U235 enrichment both in the central pin, and 3) the adjustment of Dy and U235 enrichment similar to the first case but to obtain the negative CBCVR-BOC.

Dy is selected for the adjustment because it has wide and large resonance capture cross sections. Increasing Dy density shall result in higher absorption rate partly caused by the hardened neutron spectrum and subsequently lower the CVR. Because the increasing Dy density also lowers the k_{eff} of the cooled lattice, one needs to increase fission rates by adjusting U235 to compensate the higher Dy absorption rate. In our study the target CVR-BOC is set to -2 mk so that the maximum CVR ($\sim$1.2 mk higher than CVR-BOC) is offset to -0.8 mk. The target k_{eff}-EOC is set to 0.900 to meet the burnup requirement of the discharged fuel bundles.

III.2.1 The Optimization Problem

In order to obtain the desired CVR-BOC and k_{eff}-EOC, we define an optimization problem to search for the Dy density and U235 enrichment that minimizes a cost

functional J,

$$\begin{aligned} J &= W_c(CVR_{tar,BOC} - CVR_{BOC})^2 + W_\lambda(\lambda_{tar,EOC} - \lambda_{EOC})^2 \\ &\quad + W_F F_{50mk}^2(\lambda_{o,BOC} - \lambda_{BOC}) \end{aligned} \tag{III.1}$$

where $CVR = (\lambda - \lambda_{void})$ and $\lambda = 1/k_{eff}$. W_c, W_λ and W_F are the weights of CVR_{BOC}, λ_{EOC} and function $F_{50mk}(\lambda_{BOC} - \lambda_{o,BOC})$ respectively. The function F_{50mk} serves as a penalty function for λ_{BOC} where $F_B(x) = x$ when $|x| > B$, otherwise 0. By defining the penalty function for λ_{BOC}, the optimal solution shall not result in the λ_{BOC} change larger than 50 mk. In fact, our optimal Dy and U235 result in lower k_{eff} (min. ~-9.06 mk change) at BOC for 3 cases as shown in Section III.5. $CVR_{tar,BOC}$ and $\lambda_{tar,EOC}$ are the target CVR_{BOC} and λ_{EOC} respectively. $\lambda_{o,BOC}$ is the nominal eigenvalue of the lattices at BOC. For the CBCVR adjustment in the third case, CVR is replaced by CBCVR in Equation (III.1).

III.2.2 Sensitivity Calculation using Perturbation Theory

We first define the integral neutron transport equation in direction $\vec{\Omega}_l$ for a multiplicative k_{eff} problem with isotropic scattering as follows,

$$(\mathcal{L}^g - \lambda\mathcal{F}^g)\Phi^g(\vec{r}, \vec{\Omega}_l) = 0 \tag{III.2}$$

where

$$\begin{aligned}
\mathcal{L}^g\Phi^g(\vec{r},\vec{\Omega}_l) &= \Phi^g(\vec{r},\vec{\Omega}_l) - \mathcal{T}_l^{g,-1}\sum_{g'=1}^{G}\Sigma_s^{g\leftarrow g'}(\vec{r})\phi^{g'}(\vec{r}) \\
\mathcal{F}^g\Phi^g(\vec{r},\vec{\Omega}_l) &= \mathcal{T}_l^{g,-1}\sum_{g'=1}^{G}\chi^g(\vec{r})\nu\Sigma_f^{g'}(\vec{r})\phi^{g'}(\vec{r}) \\
\mathcal{T}_l^{g,-1}(\vec{r}) &= \mathcal{T}^{g,-1}(\vec{r},\vec{\Omega}_l) = (\vec{\Omega}_l\cdot\vec{\nabla}+\Sigma^g(\vec{r}))^{-1}
\end{aligned} \tag{III.3}$$

and $\mathcal{T}_l^{g,-1}$ is the inverse transport operator. We apply the perturbation theory method based on the integral neutron transport equations in Eq. (III.2) to determine the eigenvalue sensitivity coefficient to parameter P_i defined as follows (ASSAWAROONGRUENGCHOT and MARLEAU, 2007c),

$$\begin{aligned}
\frac{\partial\lambda_{V,X}}{\partial P_i} &= \frac{1}{\Delta P_i}\frac{\langle\Phi^{\dagger g},(\Delta\mathcal{L}^g-\lambda\Delta\mathcal{F}^g)\Phi^g\rangle_{V,X}}{\langle\Phi^{\dagger g},\mathcal{F}^g\Phi^g\rangle_{V,X}} \\
&\approx -\frac{1}{\Delta P_i}\left[\frac{\left\langle[\phi^\dagger],[\Delta P_{VV}][Q]\right\rangle+\left\langle[P_{VV}][\phi^\dagger],([\Delta\Sigma_s][\phi]+\lambda[\chi][\Delta(\nu\Sigma_f)][\phi])\right\rangle}{\langle\Phi^{\dagger g},\mathcal{F}^g\Phi^g\rangle}\right]_{V,X} \\
&\equiv S_{\lambda_{V,X}}^{P_i}=\sum_{g=1}^{G}S_{\lambda_{V,X}}^{g,P_i}
\end{aligned} \tag{III.4}$$

where the inner product is defined,

$$\langle\Phi^{\dagger g}(\vec{r},\vec{\Omega}_l),\mathcal{F}^g(\vec{r},\vec{\Omega}_l)\Phi^g(\vec{r},\vec{\Omega}_l)\rangle = \sum_{g=1}^{G}\sum_{l=1}^{N^\Omega}W_l^\Omega\int_D d^3r\Phi^{\dagger g}(\vec{r},\vec{\Omega}_l)\mathcal{F}^g(\vec{r},\vec{\Omega}_l)\Phi^g(\vec{r},\vec{\Omega}_l) \tag{III.5}$$

and D is the spatial domain for the problem. Φ^g and ϕ^g are respectively the angular and scalar neutron fluxes, while $\Phi^{\dagger g}$ and $\phi^{\dagger g}$ are the angular and scalar flux importance functions, $S_{\lambda_{V,X}}^{g,P_i}$ is a group-based eigenvalue sensitivity coefficient to P_i, $[P_{VV}]$ is the MOCC response matrix, and $[Q]$ is the total scattering and fission sources. P_i is either %wt Dy-BOC density or U235-BOC enrichment percentage,

X is either BOC or EOC, and V is either void or cooled conditions. The spatial vector $\vec{r}$ and directional vector $\vec{\Omega}$ are omitted here for simplicity.

In addition we define the CVR sensitivity coefficient using Eq. (III.4) as,

$$\begin{aligned} \frac{\partial CVR_X}{\partial P_i} &= S^{P_i}_{CVR_X} = \sum_{g=1}^{G} S^{g,P_i}_{CVR_X} \\ &= \frac{\partial(\lambda - \lambda_{void})_X}{\partial P_i} \end{aligned} \tag{III.6}$$

where $S^{g,P_i}_{CVR_X}$ is a group-based CVR sensitivity coefficient to P_i.

III.2.3 The Approximation of Sensitivity Coefficients at BOC and EOC

The burnup sensitivity method was used to compute the eigenvalue sensitivity at EOC for a few group problem (YANG and DOWNAR, 1988; GANDINI, 2001). The method requires to solve the coupled time-dependent adjoint nuclide burnup equations and generalized adjoint transport equations backward in time (when the void coefficients at EOC are required, one also needs to solve another coupled problem associated with the coolant-voided conditions.). One can expect that the solution of these coupled problems would be time-consuming. The method is then useful when various types of sensitivity coefficients are required to evaluate. In our problem we require to compute two types of eigenvalue coefficients $S^{Dy_{BOC}}_{\lambda_{EOC}}$ and $S^{U235_{BOC}}_{\lambda_{EOC}}$ at EOC. We propose to use a simple method to approximate the EOC perturbed nuclide densities with the use of perturbation theory described in the previous section, that requires only the flux importance functions at BOC and EOC.

First we compute the sensitivity coefficients at BOC. One needs to determine the BOC perturbed transport operators ($\Delta\mathcal{L}_{BOC}$ and $\Delta\mathcal{F}_{BOC}$) associated with

the parameter perturbation ΔP_i. We introduce a very small perturbation ΔP_i (e.g. 0.0001% U235-BOC and 0.01%wt Dy-BOC that results in approximately $\Delta\lambda \approx 5 \times 10^{-5}$) in the lattice parameters and construct the BOC perturbed macroscopic cross-section library. Next we perform resonance self-shielding correction to the macroscopic cross sections in this perturbed library and construct the BOC perturbed transport operators for the sensitivity calculations using Eq.(III.4). For the void sensitivity coefficients at BOC, we impose the vacuum condition to the coolant mixtures in the BOC perturbed library, then perform self-shielding correction and evaluate the coolant-voided BOC perturbed transport operators.

To evaluate the sensitivity coefficients at EOC, we need to approximate the EOC perturbed nuclide densities $\tilde{N}_{EOC}$ associated with the perturbed parameter $\tilde{P}_i$ by solving the burnup/depletion equations,

$$\left[\frac{d\tilde{N}_\kappa}{dt}\right] = C([\tilde{N}_\kappa], [\phi_\kappa], \tilde{P}_i) \tag{III.7}$$

with the use of DRAGON-EVO module (MARLEAU et al., 2006), where C is the nuclide burnup and decay functions, $\tilde{P}_i = P_i + \Delta P_i$, and κ is the burnup step. We perform the constant-power burnup/depletion calculation on the BOC perturbed library from 0 to 600 FPDs using the unperturbed fluxes (which have been calculated using the unperturbed library at each burnup periods). The differences between the perturbed and unperturbed fluxes due to this very small perturbation are assumed small. Once the EOC nuclide densities have been obtained, we perform self-shielding correction on the resulting EOC perturbed library, then approximate the perturbed transport operators $\Delta\mathcal{L}_{EOC}([\tilde{N}_{EOC}], [\phi_{EOC}], \tilde{P}_i)$ and $\Delta\mathcal{F}_{EOC}([\tilde{N}_{EOC}], [\phi_{EOC}], \tilde{P}_i)$, and evaluate the EOC sensitivity coefficients using Eq. (III.4). For the evaluation of EOC void sensitivity coefficients, similar procedures are performed as for the BOC void coefficient.

A more accurate procedure consists in performing burnup/depletion calculations using the perturbed fluxes associated with their perturbed library. However this method is time-consuming due to the evaluation of perturbed fluxes required at each burnup steps. Here this method will only be used to evaluate the reference group-based coefficients for sensitivity analyses.

III.2.4 The Optimization Procedure

In order to compute the neutron and adjoint transport solutions for sensitivity approximations, we first discretize a 2-D 43 pin ACR lattice into 66 regions according to the exact geometries (see Figure III.1). The 69 energy group nuclear cross sections are obtained from the WIMS-AECL library with 63 burnup/depleted nuclides. The azimuthal angular integration for the MOCC method is performed using a 19 point Gaussian quadrature (ROY et al., 1991) while the polar integration consists in a 10 point Gauss-Legendre quadrature. The tracking density is 21 lines/cm. Periodic boundary conditions are used for this problem. For the lattice burnup/depletion calculations, we perform the calculation for 600 FPDs using the constant 35kW/kgU burnup power to evaluate the neutron fluxes, CVR, cooled and void k_{eff} at each burnup step. The flux importance functions of the cooled and void lattices are computed at BOC and EOC. The 22 burnup steps are at 0, 1, 5, 10, 20, 30, .., 50, 70, 90, ..,150, 200, 250, ..., 600 FPDs. The cooled and voided macroscopic cross sections in the library are corrected separately to take into account the self-shielding effects due to heavy nuclides at each burnup step.

One can see that the optimization problem defined in (III.1) is a two variable problem. We can easily find the optimal Dy density and U235 enrichment percentage by scanning through the ranges of Dy density and U235 enrichment with the step change (e.g. 0.001). The cooled and void eigenvalues associated with the new

parameters are approximated and applied in the cost functional for the optimal search,

$$\lambda_{V,X,new} = \lambda_{o,V,X} + \sum_{i}^{N_p} \frac{\partial \lambda_{V,X}}{\partial P_i}(\tilde{P}_i - P_{i,o}) \tag{III.8}$$

where $\tilde{P}_i$ is either the step-searching Dy or U235, $P_{i,o}$ is the nominal values of Dy-BOC or U235-BOC of the lattices for which the coefficients are evaluated, and λ_o is the eigenvalue of the lattices associated with the parameters $P_{i,o}$.

In the first step of the optimizing process, we compute the fluxes, flux importance functions and sensitivity coefficients of the lattices with the nominal Dy and U235. Then we use these coefficients to search the optimal Dy and U235 that minimizes the cost functional. Next we apply the computed optimal Dy and U235 to the lattices, build the new lattice library, and compute the new CVR-BOC and k_{eff}-EOC. If these new CVR-BOC and k_{eff}-EOC do not meet their target values, we begin the second step and reevaluate the fluxes, flux importance functions and sensitivity coefficients of the new lattices with the optimal Dy and U235 obtained from the previous step. The same procedures are repeated until the CVR-BOC and k_{eff}-EOC meet their target values. The stopping criteria are to obtain the absolute relative errors (%) of the CVR-BOC and k_{eff}-EOC less than ϵ and 0.1ϵ respectively, where ϵ is a small real value.

III.2.5 Positive CBCVR Effect in the 2 × 2 ACR Lattice

Similar to the positive CVR effect in the ACR lattices, the positive CBCVR mainly results from the decreasing coolant-absorption and -moderation that causes hardened flux spectrum and the increasing fast fission. The main difference is that the checkerboard void (CBVOID) flux spectrum is less hardened than the fully void

spectrum. This is because the ACR lattice is undermoderated causing the strong spatial coupling among the adjacent lattices. During the checkerboard voiding the adjacent cooled lattices contribute to the thermalization of neutrons born in the void lattices (as well as that for the neutrons born in the cooled and slowed down inside the void cells). This results in the less hardened CBVOID spectrum and the lower resonance absorptions. One can compute the 2 group spatial-integrated absorption, scattering and neutron production rates for the cooled, CBVOID and fully void lattices as presented in Table III.1. The reaction rates are normalized with respect to the unit total neutron production rate. The result shows that the CBVOID lattices have the lowest absorption rates among all cases. One can see that the decreased fast capture reaction in CBVOID lattices (compared with fully void cells) results from the increasing down-scattering reaction. The neutron saving from resonance capture, and the absence of coolant absorption results in more thermal fissions and the higher k_{eff} and CBCVR than that in the fully void lattices.

This is unlike the CANDU-6 reactor where the lattices are overmoderated and neutrons are well thermalized in moderator yielding the weak spatial couplings among the lattices. The CANDU coolant-voided spectrum is comparatively less hardened than the ACR lattices and localized in each void lattice (TALEBI et al., 2006). In the CBVOID CANDU lattice, the CBVOID flux spectrum is relatively localized and less hardened than the fully void spectrum. The fast fission due to the hardened spectrum is increased in the void lattices but this effect is less important in the adjacent cooled lattices. Due to loss of coolant-moderation (e.g. slowing-down of fast neutrons and up-scattering of thermal neutrons by hot coolant into resonance region), the resonance absorption is lower in the void than the adjacent cooled lattices. The overall effect is that the CBVOID lattices have lower fast fission and higher resonance absorption than the 2×2 fully void lattices. The resulting CBCVR is then lower than the CVR in the CANDU lattices.

III.3 Sensitivity Analysis of CVR and Eigenvalues

The sensitivity analysis is regarded as a analytical tool for nuclear reactor analysis (LEWINS and BECKER, 1982). It can be applied to study the effects of a parameter on the energywise reactor characteristics. In this section we consider the sensitivity coefficients of CVR, CBCVR and eigenvalues (at BOC and EOC) to Dysprosium density in the central pin, and U235 enrichment in the central pin and the outer rings. Note that the group-based sensitivity coefficients are evaluated for the initial-designed ACR lattice with 4.6% Dy and 0.7114% U235 enrichment in the central pin, and 2% U235 enrichment in the outer rings. To compute the EOC perturbed nuclear library (where U235 and Dy are perturbed by 0.01 and 0.046% respectively), their burnup/depletion equations are solved using the perturbed fluxes associated with the perturbed nuclear library at each step.

III.3.1 Sensitivity Coefficients of CVRs and Eigenvalues with respect to Dysprosium

We first consider the sensitivity coefficients of CVR and eigenvalues to Dysprosium density. The group sensitivity of cooled and void eigenvalues (at BOC) to Dysprosium density (%wt) presented in Figure III.3 are positive due to the increasing absorption rate corresponding to the increasing Dysprosium. The sensitivity of void eigenvalue is higher than that of the cooled because, during coolant voiding, the neutrons are less thermalized and the neutron spectrum becomes hardened. Since the Dysprosium has large resonance absorption cross sections, the hardened fluxes then result in higher absorption rates. One can see that these increasing absorptions in Dy shall compensate the decreasing coolant absorptions and mitigate the positive CVR effect during coolant voiding.

The group sensitivity of cooled and void eigenvalues at EOC to Dysprosium density are presented in Figure III.4. The group coefficients are positive between 10^{-5} to 10^{3} eV due to the fact that some Dysprosium still remain in the pin and because there are higher U235 and converted Pu239 contents at EOC (when Dy-BOC is increased by 0.46%, U235-EOC and Pu239-EOC are increased approximately by 2.3E-2 and 2.1E-2 %). The hardened spectrum due to loss of coolant also results in more positive sensitivity of void eigenvalue at low energy. The negative sensitivity at high energy is due to increasing fission neutron productions. This is because the burnable poisons including Dy are mainly consumed and the presence of higher remaining U235 and Pu239 with their fast fissions becomes the dominant effect. More negative sensitivity of void eigenvalue at high energy is due to higher fast fissions produced by the hardened fluxes.

The group sensitivity coefficients of CVR at BOC and EOC to Dysprosium density in Figure III.5 are mainly negative as a result of the increasing absorptions by the hardened neutron spectrum as mentioned above. The positive sensitivity between 10^{-1} to 10 eV is due to the decreasing coolant absorptions. CVR-EOC sensitivity at low energy becomes more negative than that at BOC because the higher absorptions are caused by the remaining U235 and Pu239 contents, and the fact that the fluxes at EOC are more hardened than at BOC. More positive CVR-EOC sensitivity at high energy is due to the increasing fast fissions by U235 and Pu239.

The group sensitivities of checkerboard void (CBVOID) eigenvalue (at BOC and EOC) to Dy density are similar to the group sensitivities of fully void eigenvalue at BOC and EOC except that their magnitudes are smaller. This is because CBVOID flux spectrum is softer than the fully void spectrum. Similarly the CBCVR sensitivity has the same structure as the CVR sensitivity except for their smaller magnitudes.

III.3.2 Sensitivity Coefficients of CVRs and Eigenvalues to U235 Enrichment Percentage in the Outer Rings

The group sensitivity of cooled and void eigenvalues (at BOC) to Uranium enrichment in the outer rings are presented in Figure III.6. The sensitivity coefficients are positive in the range 10^{-5} to 10^{3} eV due to the increasing absorption rate corresponding to the increasing U235. But an increase in absorption-to-fission reaction rate also results in negative sensitivities at high energy. The sensitivity of void eigenvalue at low energy is higher than sensitivity of cooled eigenvalue because the hardened flux spectrum during coolant voiding causes higher absorptions in the increasing U235.

The sensitivity of void eigenvalue at high energy is slightly more positive than the cooled sensitivity. This results from an increase in the fast fission contribution (due to lower coolant-moderation and the undermoderated lattices). On the other hand the hardened flux spectrum upon coolant voiding causes higher resonance capture in the increasing U235. The thermal fission is also lower due to the hardened spectrum. In addition the increasing fast fission are partially suppressed by the absorption by Dy that has the large resonance cross section between 100 eV to 10 keV (when the coolant is voided and spectrum are hardened, Dy can be seen as the inserted absorber at the central pin.). These effects of Dy absorption also appears in the flux importance weighting. At high energy we find that the void flux importances in the most outer ring are lower than the cooled, while the increasing fast fissions due to the hardened spectrum are mostly from this ring.

The group sensitivity of cooled and void eigenvalues (at EOC) to Uranium enrichment in the outer rings in Figure III.7 are similar to those at BOC except the magnitude is smaller because U235 are mainly consumed at EOC. The main difference is that the void sensitivity at high energy is more negative than the cooled

sensitivity. This is because the poisons are mostly depleted and we also find that Pu239 at EOC increases with the U235 (e.g. Pu239-EOC reaches the maximum value at 5.0% U235). Fission from Pu239 then starts to dominate at EOC and contributes to the negative sensitivity coefficients at high energy. As one can see in Figure III.8, CVR-EOC sensitivity is more negative than CVR-BOC sensitivity at low energy. This is a result of the flux spectrum at EOC that is more hardened than the spectrum at BOC. The CVR-BOC sensitivity is negative at high energy because the fast fission is lowered by the increasing U235 resonance capture and partially eliminated by the Dy absorptions; on the other hand, the CVR-EOC sensitivity becomes positive due to the dominating fission from Pu239 at EOC. The positive CVR sensitivity between 10^{-1} to 1 eV is because of the decreasing absorption rate by loss of coolant.

For the group sensitivity of CBVOID eigenvalues and CBCVR (at BOC and EOC) to Uranium enrichment in the outer rings are similar to those of fully void lattices except that the magnitude is smaller. As mentioned earlier, this is because CBVOID flux spectrum is softer than the fully void spectrum.

III.3.3 Sensitivity Coefficients of CVRs and Eigenvalues to U235 Enrichment in Central Pin

The group sensitivity of cooled and void eigenvalues (at BOC) to U235 enrichment in the central pin in Figure III.9 are similar to the case for U235 enrichment in the outer rings except the magnitude is much smaller (due to the sensitivity coefficients to U235 in a single pin). The void sensitivity becomes more negative than the cooled at high energy because the increased U235 directly reduces the Dy and U238 absorption probabilities in the same pin. The fast fission effect in the central pin is then higher upon coolant voiding. At high energy we find that the void flux

importance in the central pin is higher than the cooled flux importance that causes more negative void sensitivity. This may suggest that, during coolant voiding, the neutron flux importance in the central pin is more important for the voided than the cooled case because the neutrons have more chances to undergo fission.

The group sensitivity of cooled and void eigenvalues (at EOC) to Uranium enrichment in the central pin are similar to those group sensitivity at BOC except the magnitude is much larger. This is because the poisons are mainly depleted at EOC, the EOC fluxes are more hardened than the BOC fluxes, and U235 in the central pin also burns slower than U235 in the outer rings.

III.3.4 The Exact Sensitivity Coefficients

The exact CVR and eigenvalue sensitivity coefficients to Dy and U235 at BOC and EOC presented in Table III.2 and III.3 are approximated using,

$$\left(\frac{\partial \lambda_{V,X}}{\partial P_i}\right)_{ex} = S^{P_i}_{\lambda_{V,X},ex} \approx \frac{(\lambda_{P_i^+} - \lambda_{P_i^-})_{V,X}}{(P_i^+ - P_i^-)} \tag{III.9}$$

where $P_i^{\pm} = P_{i,o} \pm \Delta P_{ex,i}$, and $\Delta P_{ex,i}$ is either 0.01% for Dy-BOC or 0.0001% U235-BOC. $\lambda_{P_i^{\pm}}$ is the eigenvalue computed using the nuclear library with $P_i^{\pm}$.

For the coefficients computed by the perturbation theory method, the maximum absolute relative error is approximately 4.0 and 27.25% for BOC and EOC coefficients. Large error is found in the EOC sensitivity to U235. This is because of the nonlinearity of the problem where the increasing U235 will affect the amount of the fission products, Pu densities and the flux spectrums along the burnup period, and the fact that it is a rather large perturbation of U235 in 42 out of the 43 fuel

pins. An improvement to reduce the error in these coefficients is by approximating the perturbed EOC nuclide densities using their perturbed fluxes from 300 to 600 FPDs. The maximum error at EOC is then decreased to about 10.0%.

III.4 Effects of U235 Enrichment and Dysprosium Density on CVR and CBCVR

Next we study the effects of U235 enrichment in the central pin to CVR-BOC and CBCVR-BOC in Figure III.10. As one can see, both CVRs increase linearly with the U235 enrichment because the increasing U235 having large fission cross-sections reduce the Dy and U238 absorption probabilities in the same pin. U235, U238 and Dy also see the same hardened fluxes. Upon voiding the increase in U235 directly results in an increase in fast fissions. As mentioned earlier, CBCVR is larger than CVR because the CBVOID lattices have lower resonance capture and higher thermalized neutrons due to the spatial-coupled coolant-moderation of the neutrons between the void and cooled lattices. Subsequently there are higher thermal fissions in the CBVOID lattices than in the fully void lattices.

The effects of U235 enrichment in the outer rings on CVR-BOC and CBCVR-BOC is illustrated in Figure III.11. Both CVRs decrease with the increasing U235 enrichment between 0 to 5% because the increasing U235 directly results in the higher resonance capture that lowers the voiding fast fission. For U235 enrichment higher than 5%, the fast fissions become important (the system tends to behave like a fast reactor) and dominate over the Dy and U238 resonance absorptions. Both CVRs are then increased with these fast fissions. At U235 $< 1\%$ the lattices tend to have a higher moderation ratio (higher $(D^2 + H^1)$/U235 atomic ratio) and weaker spatial-coupling that is analogous to the CANDU lattice mentioned previously. The CBVOID flux spectrum is relatively localized and less hardened than the fully void spectrum. The CBVOID resonance absorption is then higher

(weaker coupling) but the CBVOID fissions and CBCVR are lower than those of fully void lattices.

The effects of Dy density in the central pin on CVR-BOC and CBCVR-BOC is presented in Figure III.12. The increasing Dysprosium density directly decreases CVRs because its large resonance absorption partially eliminates the fast fission effect in the fuel pins. When the Dysprosium density is greater than 40%, the CVRs decrease more slowly because of spatial self-shielding of the Dy mixture that already suppresses thermal and resonance neutron fluxes in the central pin and surrounding regions. When Dy is decreased, both CVR and CBCVR become higher and closer because lower Dy causes lower resonance absorption and more hardened flux spectrum giving the higher void and CBVOID k_{eff}. Because of the lower resonance absorption in Dy (that makes CVR lower than CBCVR), the CVR then rises toward the CBCVR.

On the plot of CVR of the initial lattices against burnup period in Figure III.13, one first observes an increase before attaining a maximum at 5th FPD. This is because the Xe (and marginally Sm) density rise quickly to its saturation at 5th FPD. The higher Xe also lower the cooled k_{eff}. When coolant is voided, the resonance absorptions in Xe are also lower due to loss of coolant-moderation. The cooled and void k_{eff} become far apart and result in higher CVR than CVR-BOC. One can test this case by setting the zero Xe density and find that the CVR peak is directly decreased. Because of the accumulation of other fission products, CVR is then decreased gradually after 5th FPD.

The plot of CBCVR versus the burnup period is presented in Figure III.17. CBCVR first increases, attains the maximum at 5th FPD and then continues decreasing afterward. This peaking effect is due to the Xe buildup similar to the CVR peaking. After 150th FPD the CBCVR starts increasing again and reach the second peak

at 500th FPD. This is a result of the Dy depletion that causes the rising CBCVR. During the CBVOID the decreasing of Dy lowers thermal and resonance absorption and increases fast fission. With the coupled coolant-moderation, the CBCVR-EOC becomes positive. For the fully void lattice, there are many resonance isotopes produced at EOC such as Pu240, U236, U238 etc. that compensates the decreasing resonance absorption in Dy, and the fact that the fully void flux spectrum is more hardened than the CBVOID spectrum. The CVR-EOC then becomes negative. We also test this problem by setting the zero Dy density at EOC. We find that the CBCVR-EOC is increased from 9.89 mk to 13.94 mk, and the CVR-EOC is also increased from -4.23 mk to 3.77 mk. The second CBCVR peak is also lower when one inserts higher Dy at BOC. In addition, we empty the U235 at the 4th ring, and Pu239 densities, then we obtain the CBCVR-EOC of 10.16 and 10.00 mk (CVR-EOC is -4.08 and -4.24 mk) respectively. The 2nd CBCVR peaking may collectively result from the decreasing of U235 and Dy, and the increasing of Pu239 production and fission-product poisonings.

III.5 Optimization Results

In the optimization process, we first calculate the sensitivity coefficients as presented in Section III.2.2 and III.2.3, and proceed the optimization procedure as presented in Section III.2.4. The weights W_c, W_λ and W_F are set equal to unity so that the CVR-BOC, k_{eff}-BOC and k_{eff}-EOC are optimized with the equal importance. For the convergence criteria, we choose $\epsilon = 1$. The optimization process is then stopped when the absolute relative errors of the CVR-BOC and k_{eff}-EOC are less than 1.0% and 0.1% respectively.

The first case is the simultaneous adjustment of Dy density (%wt) in the central pin and U235 enrichment in outer fuel rings. The adjustment results in each step

are presented in Table III.4. From this table, the CVR-BOC sensitivity of Dy and U235 are both negative but the EOC eigenvalue sensitivity coefficients are of opposite sign. For this case the optimal Dy density and U235 enrichment are close to their original values. It then requires 2 adjustment steps to attain the optimal Dy and U235. The final Dy density and U235 enrichment are 8.26% and 2.107% which are within the practicable limits. As a result of the final adjustment, CVR remains negative over the full burnup period as shown in Figure III.13. The k_{eff} plot versus burnup period is shown in Figure III.14.

For the second case the adjustment results of Dy and U235 both in the central pin are presented in Table III.5. The CVR and eigenvalue sensitivity coefficients of Dy and U235 are of opposite signs. Because of these opposite signs, the effect of U235 increment directly opposes to the effect of Dy increment. Subsequently many steps are required to attain the target CVR-BOC and k_{eff}-EOC. The final adjusted Dy density is 19.614% wt but the final U235 enrichment is as high as 20.995% that may cause expensive fuel cost and not be available in the fuel market (enrichment is of ~3.5% for PWR fuel). From the final adjustment result, CVRs are negative over burnup period as shown in Figure III.15 and the k_{eff} plot versus burnup period are also shown in Figure III.16.

For the third case the adjustment results of Dysprosium in the central pin and U235 enrichment in the outer fuel rings are presented in Table III.6. The CBCVR sensitivity of Dy and U235 are both negative but the eigenvalue sensitivity are of the opposite sign. In the nominal lattice, the CBCVR sensitivity coefficients of Dy and U235 are lower than CVR coefficients by approximately 30 to 50 %. One may foresee that many adjustment steps are required to lower the initial CBCVR of +9.51 mk down to its target value of -2.0 mk using such CBCVR coefficients. The magnitudes of the CBCVR and eigenvalue sensitivity coefficients to Dy become smaller when Dy density is higher. As mentioned previously, this is in accordance

with the Dy effect on CBCVR where the self-shielding effects in the central pin become important at high Dy density. For very high Dy density $\geq 90\%$, the central pin is discretized into finer regions (from 3 to 10 regions) to take in account the higher self-shielding effects and optical thickness, and obtain a finer adjustment. More discretized regions shall result in slower Dy consumption (competing with U235 absorption) and subsequently higher U235 left at EOC. The CBCVR-BOC and maximum CBCVR at the final step are -1.18 and -0.54 mk respectively. In this case the CBCVR-BOC can not meet the target value of -2 mk because the final Dy density is 99.838% wt that approaches to its maximum limit in the central pin. In fact, the CBCVR-BOC can be decreased further by increasing the U235 enrichment but it shall result in higher k_{eff}-EOC. In this case one would seek new extended burnup period for which the optimal Dy and U235 exist within the limits. In addition the CVR-BOC and maximum CVR-BOC at the final step are -20.45 and -19.49 mk respectively. As a result of the final adjustment, the CVR and CBCVR are entirely negative over our burnup period as shown in Figure III.17 and III.18. The k_{eff} plot is also presented in Figure III.19.

III.6 Conclusions

The simple optimization and adjoint sensitivity techniques are applied to adjust the CVR-BOC, CBCVR-BOC and k_{eff}-EOC of the ACR lattices. In the first adjustment case, the optimal Dy density in the central pin and U235 enrichment in the outer rings are of 8.26 %wt and 2.107% that gives approximately the CVR-BOC and k_{eff}-EOC of -2.0 mk and 0.900. By slightly altering Dy and U235 to their optimal values, one can adjust the positive CVRs (for the first 120 FPDs) to be negative over the burnup period. In the second case, we obtain the optimal Dy and U235 of 19.614%wt and 20.995% both in the central pin. The resulting CVRs are

all negative as expected. In the last case, the optimal CBCVR-BOC is of -1.18 mk while its target is -2.0 mk. This is because the Dy approaches its maximum limit in the central pin. By increasing the burnup period in this case, one could determine the new Dy and U235 that would result in the desired target CBCVR-BOC and k_{eff}-EOC. According to the optimal Dy and U235 of 99.838%wt and 2.406% the resulting CBCVRs are entirely negative, while the initial CBCVRs are all positive.

In addition the sensitivity analysis method is used in analyzing the groupwise characteristics of eigenvalues, CVR and CBCVR (at BOC and EOC) with respect to the Dy and U235. Besides the Dy adjustment in the central pin, one may consider to replace Dy with Gadolinium (Gd). The advantage of Gd is its fast-burnt poison that reduces the BOC excess reactivity. The lattice then remains with the higher k_{eff}-EOC for which one may consider to lower the U235 enrichment. By using these simple techniques, one can design lattices that meet both safety and burnup performance requirements.

Acknowledgments

This work was supported in part by the Natural Science and Engineering Research Council of Canada.

Table III.1 Reaction Rates in Cooled, Checkerboard Voided and Fully Voided ACR Lattices

Spatial Integrated Reaction Rates	Group 1			Group 2		
	Cooled	CBVOID	VOID	Cooled	CBVOID	VOID
Integrated Flux	6.1658E+1	7.3882E+1	9.1552E+1	6.9898E+1	6.4448E+1	6.2952E+1
Total Collision	1.9506E+1	2.0880E+1	2.3185E+1	3.0901E+1	2.5528E+1	2.1550E+1
${}^{1}_{0}n$ Production ($< \nu\Sigma_f\phi >$)	9.8295E-2	1.0940E-1	1.2758E-1	9.0171E-1	8.9060E-1	8.7242E-1
Absorption	1.8990E-1	2.0387E-1	2.3492E-1	6.2028E-1	5.9680E-1	5.7127E-1
Scattering from Group 1	1.8695E+1	2.0078E+1	2.2378E+1	6.2061E-1	5.9719E-1	5.7174E-1
Scattering from Group 2	3.3811E-4	3.8699E-4	4.6836E-4	3.0280E+1	2.4931E+1	2.0978E+1

Cutoff energy for 2 group condensation is 4.0 eV.

Table III.2 Exact Cooled Eigenvalue Sensitivity Coefficients at BOC and EOC

Exact Sensitivity Coefficients	AT BOC [mk/%]	AT EOC [mk/%]
$S^{Dy_{BOC}}_{\lambda,ex}$	3.99488E+0 (0.21%)[a]	4.28095E+0 (1.99%)
$S^{U^{235}{}_{BOC}}_{\lambda,ex}$	-1.01743E+2 (0.03%)	-1.52207E+2 (27.25%)
$S^{U^{235}{}_{BOC,cp}}_{\lambda,ex}$	-2.68003E+0 (0.00%)	-3.96617E+0 (2.33%)

cp: Central Pin

$(.)^a$: absolute relative error between exact and adjoint sensitivity coefficients

Table III.3 Exact Void-, CBVOID-Eigenvalue, CVR and CBCVR Sensitivity Coefficients at BOC

Exact Sensitivity Coefficients	AT BOC [mk/%]
$S^{Dy_{BOC}}_{\lambda_{void},ex}$	5.72582E+0 (0.00%)[a]
$S^{U235_{BOC}}_{\lambda_{void},ex}$	-9.14494E+1 (0.04%)
$S^{U235_{BOC,cp}}_{\lambda_{void},ex}$	-3.07592E+0 (0.00%)
$S^{Dy_{BOC}}_{\lambda_{\mathrm{CBVOID}},ex}$	4.82887E+0 (0.03%)
$S^{U235_{BOC}}_{\lambda_{\mathrm{CBVOID}},ex}$	-9.53909E+1 (0.13%)
$S^{Dy_{BOC}}_{\mathrm{CVR,ex}}$	-1.73094E+0 (0.48%)
$S^{U235_{BOC}}_{\mathrm{CVR,ex}}$	-1.02933E+1 (0.02%)
$S^{U235_{BOC,cp}}_{\mathrm{CVR,ex}}$	3.95889E-1 (0.00%)
$S^{Dy_{BOC}}_{\mathrm{CBCVR,ex}}$	-8.34549E-1 (0.55%)
$S^{U235_{BOC}}_{\mathrm{CBCVR,ex}}$	-6.67630E+0 (3.98%)

cp: Central Pin
$(.)^a$: absolute relative error between exact and adjoint sensitivity coefficients

Table III.4 Adjustment Results for Case 1

Step	Dy	U235 in Outer Rings	$S^{Dy_{BOC}}_{\mathrm{CVR_{BOC}}}$ $S^{Dy_{BOC}}_{\lambda_{EOC}}$ [mk/%]	$S^{U235_{BOC}}_{\mathrm{CVR_{BOC}}}$ $S^{U235_{BOC}}_{\lambda_{EOC}}$ [mk/%]	CVR_{BOC} CVR_{MAX} [mk]	$k_{eff,BOC}$ $k_{eff,EOC}$
1	4.600%	2.000%	-1.73922E+0 4.19581E+0	-1.02908E+1 -1.10729E+2	3.99 5.15	1.234298 0.897071
2	7.905%	2.135%	-1.92856E+0 5.14526E+0	-7.01726E+0 -1.11994E+2	-1.79 -0.57	1.239252 0.903398
3	8.260%	2.107%	-	-	-1.99 -0.77	1.233968 0.899057

Table III.5 Adjustment Results for Case 2

Step	Dy	U235 in Central Pin	$S^{Dy_{BOC}}_{\mathrm{CVR_{BOC}}}$ $S^{Dy_{BOC}}_{\lambda_{EOC}}$ [mk/%]	$S^{U235_{BOC,cp}}_{\mathrm{CVR_{BOC}}}$ $S^{U235_{BOC,cp}}_{\lambda_{EOC}}$ [mk/%]	CVR_{BOC} CVR_{MAX} [mk]	$k_{eff,BOC}$ $k_{eff,EOC}$
1	4.600%	0.711 %	-1.73922E+0 4.19581E+0	3.90224E-1 -3.87950E+0	3.99 5.15	1.234298 0.897071
2	9.444 %	6.891 %	-1.98489E+0 6.28405E+0	4.20737E-1 -2.82673E+0	0.54 1.82	1.230367 0.898547
3	14.950%	13.490%	-2.22372E+0 7.56566E+0	3.41115E-1 -2.076259E+0	-1.37 -0.03	1.226168 0.897758
4	19.614%	20.995%	-	-	-1.97 -0.58	1.225400 0.899265

Table III.6 Adjustment Results for Case 3

Step	Dy	U235 in Outer Rings	$S^{Dy_{BOC}}_{\mathrm{CBCVR_{BOC}}}$ $S^{Dy_{BOC}}_{\lambda_{EOC}}$ [mk/%]	$S^{U235_{BOC}}_{\mathrm{CBCVR_{BOC}}}$ $S^{U235_{BOC}}_{\lambda_{EOC}}$ [mk/%]	CBCVR_{BOC} CBCVR_{MAX} [mk]	$k_{eff,BOC}$ $k_{eff,EOC}$
1	4.600%	2.000%	-8.39113E-1 4.21443E+0	-6.94191E+0 -1.03694E+2	9.51 10.16	1.234298 0.897071
2	14.822%	2.420 %	-2.15826E-1 1.51408E+0	-3.58174E+0 -1.11639E+2	3.03 3.74	1.260364 0.924263
3	37.376%	2.465 %	-5.32440E-2 3.92651E-1	-1.59958E+0 -1.12799E+2	0.28 0.97	1.245293 0.913696
4	80.138%	2.466 %	-1.61898E-2 2.02822E-1	-2.14471E+0 -1.18058E+2	-0.88 -0.20	1.230621 0.907132
5	99.838%	2.426 %	-9.87304E-3 7.25470E-2	-1.88599E+0 -1.17012E+2	-0.97 -0.74	1.223195 0.901892
6	99.838%	2.406 %	-	-	-1.18 -0.54	1.220766 0.899420

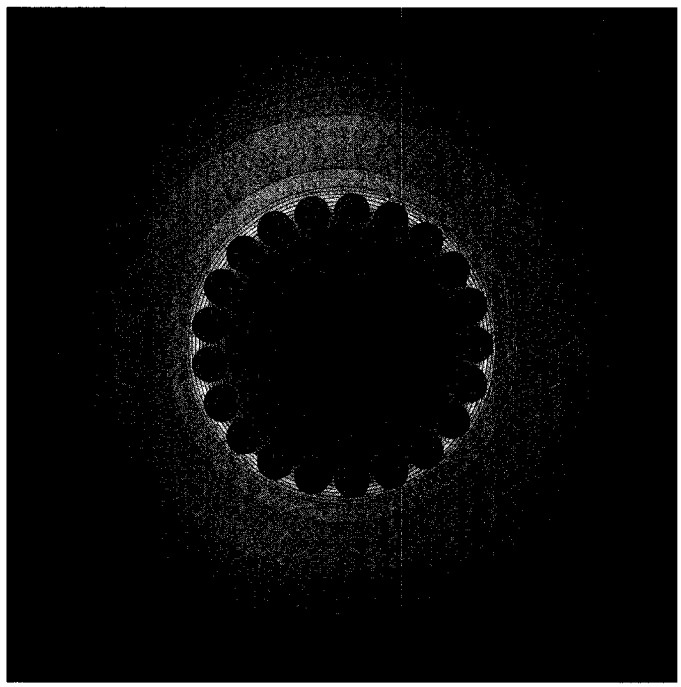

Figure III.1 CANFLEX fuel geometry for ACR type reactor

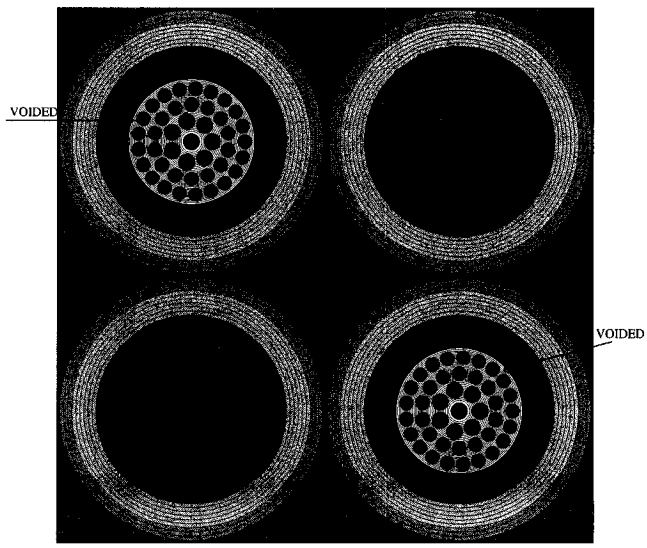

Figure III.2 2 × 2 ACR assembly for checkerboard voiding study

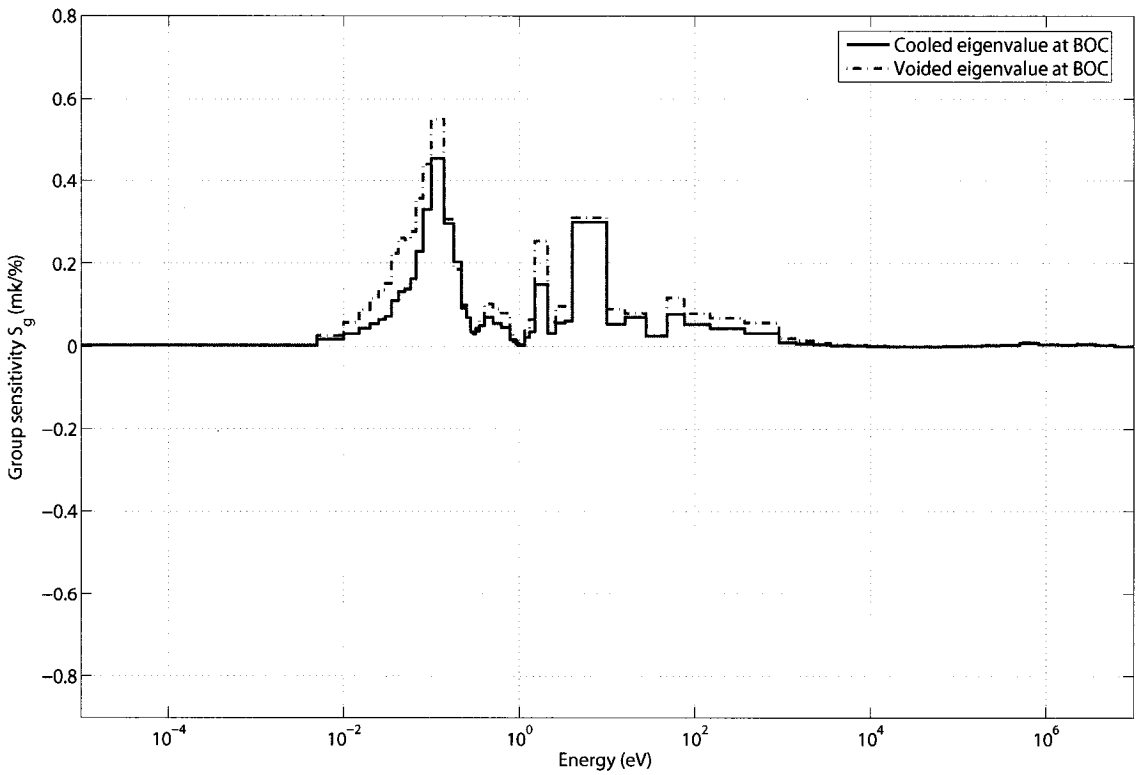

Figure III.3 Group sensitivity of cooled and void eigenvalues (at BOC) to Dysprosium density

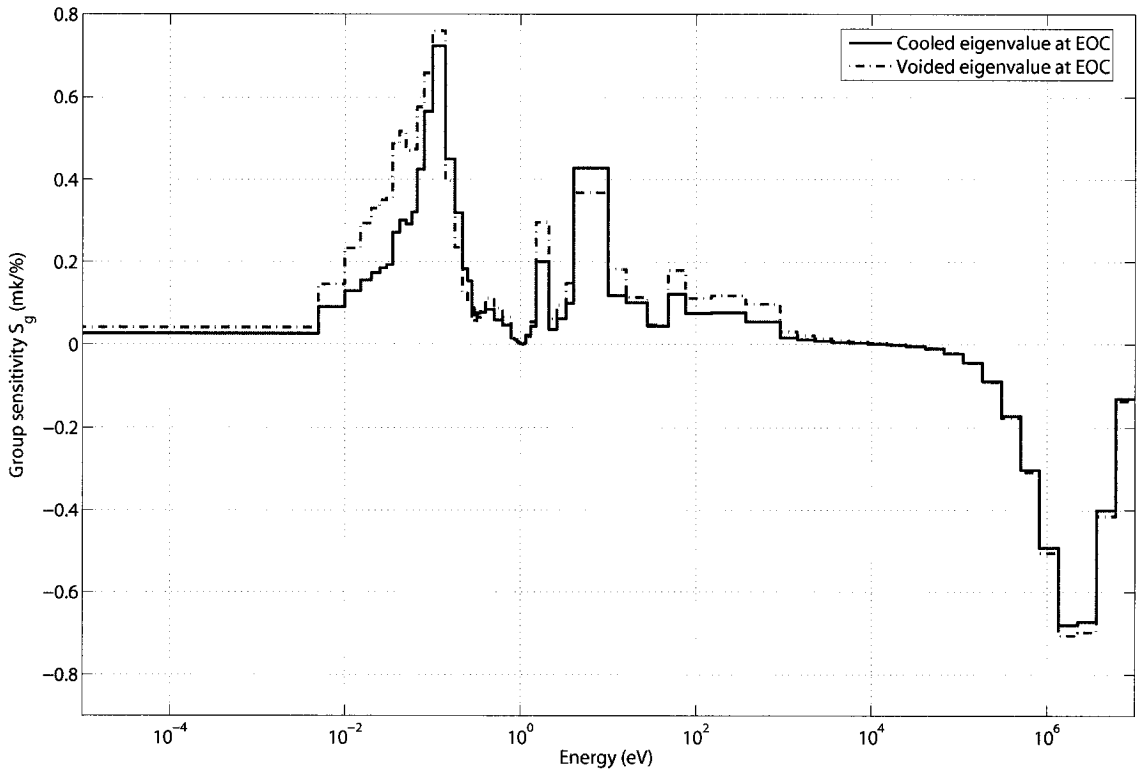

Figure III.4 Group sensitivity of cooled and void eigenvalues (at EOC) to Dysprosium density

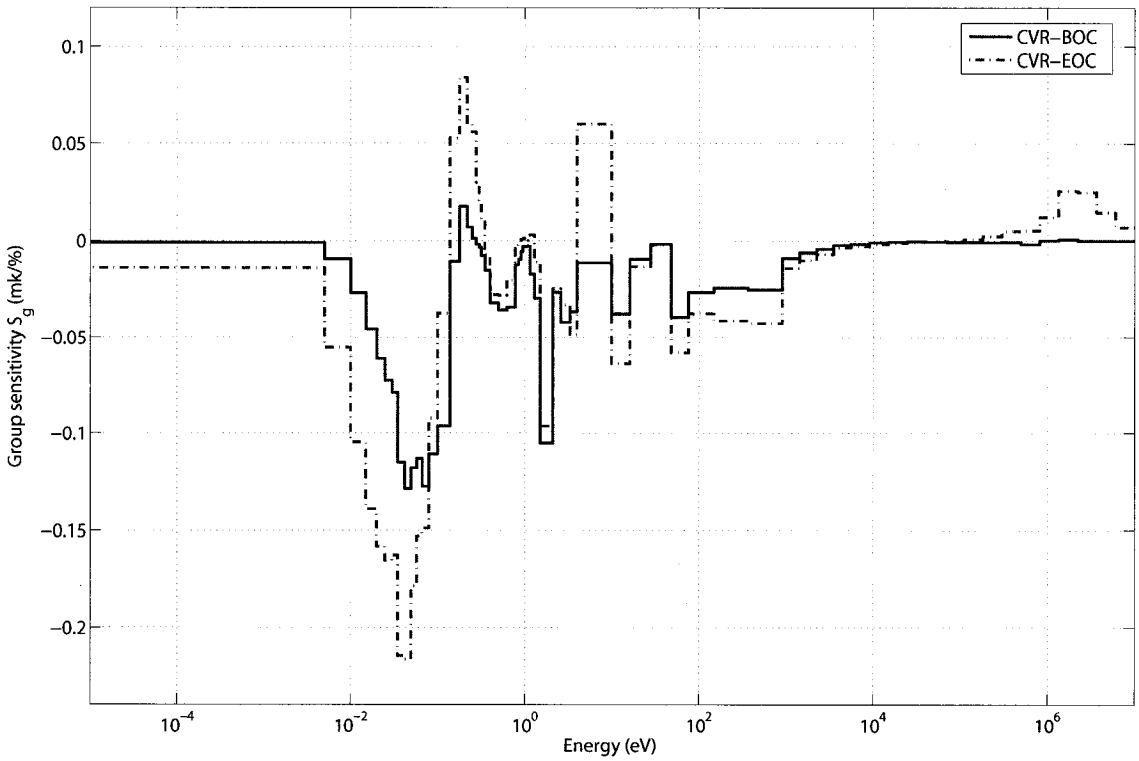

Figure III.5 Group sensitivity of CVR-BOC and CVR-EOC to Dysprosium density

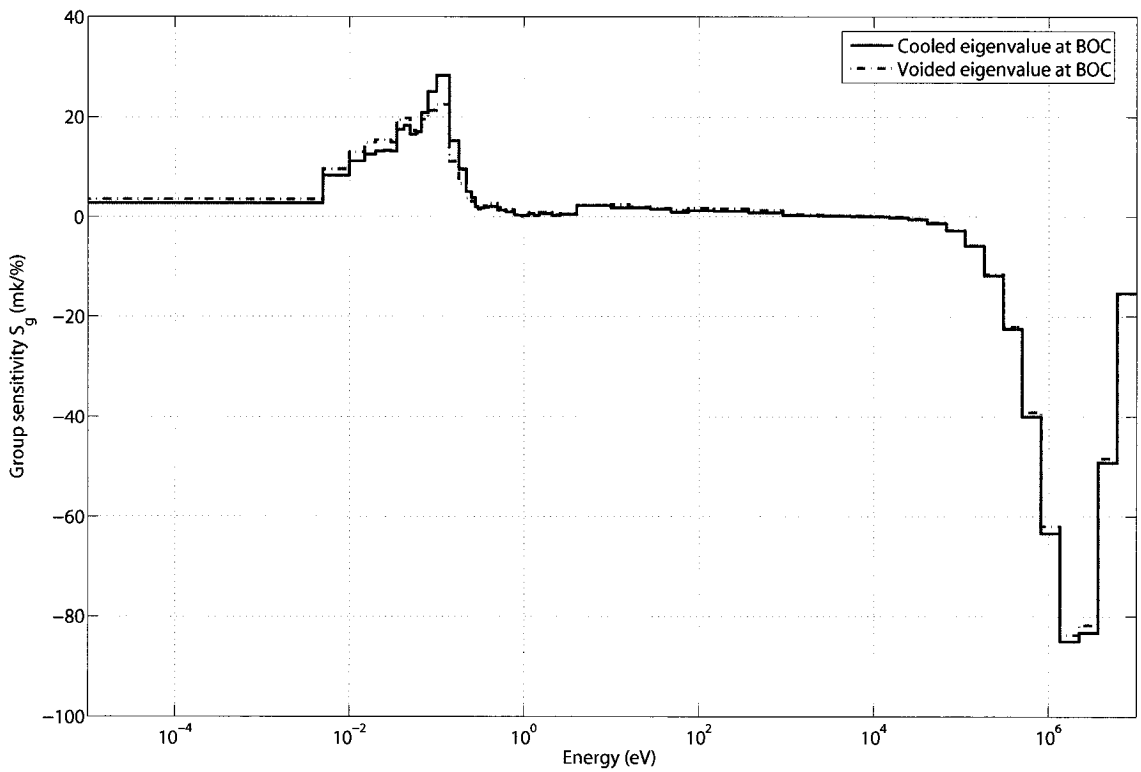

Figure III.6 Group sensitivity of cooled and void eigenvalues (at BOC) to U235 enrichment

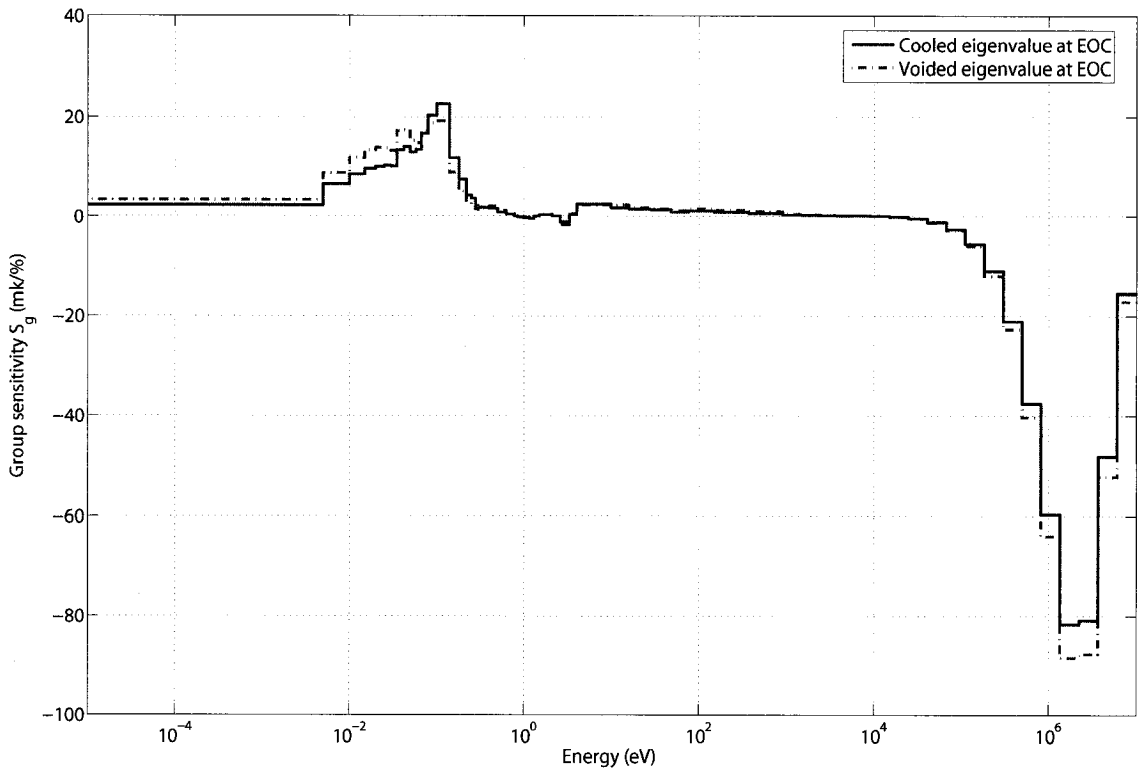

Figure III.7 Group sensitivity of cooled and void eigenvalues (at EOC) to U235 enrichment

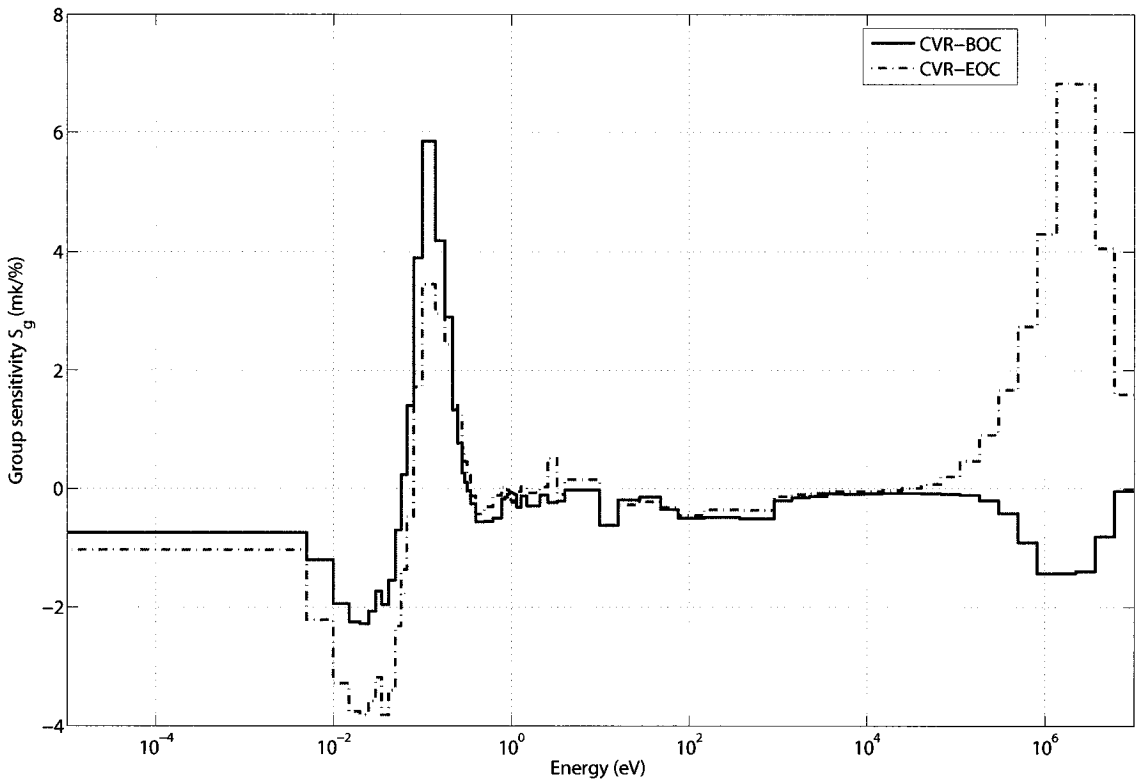

Figure III.8 Group sensitivity of CVR-BOC and CVR-EOC to U235 enrichment

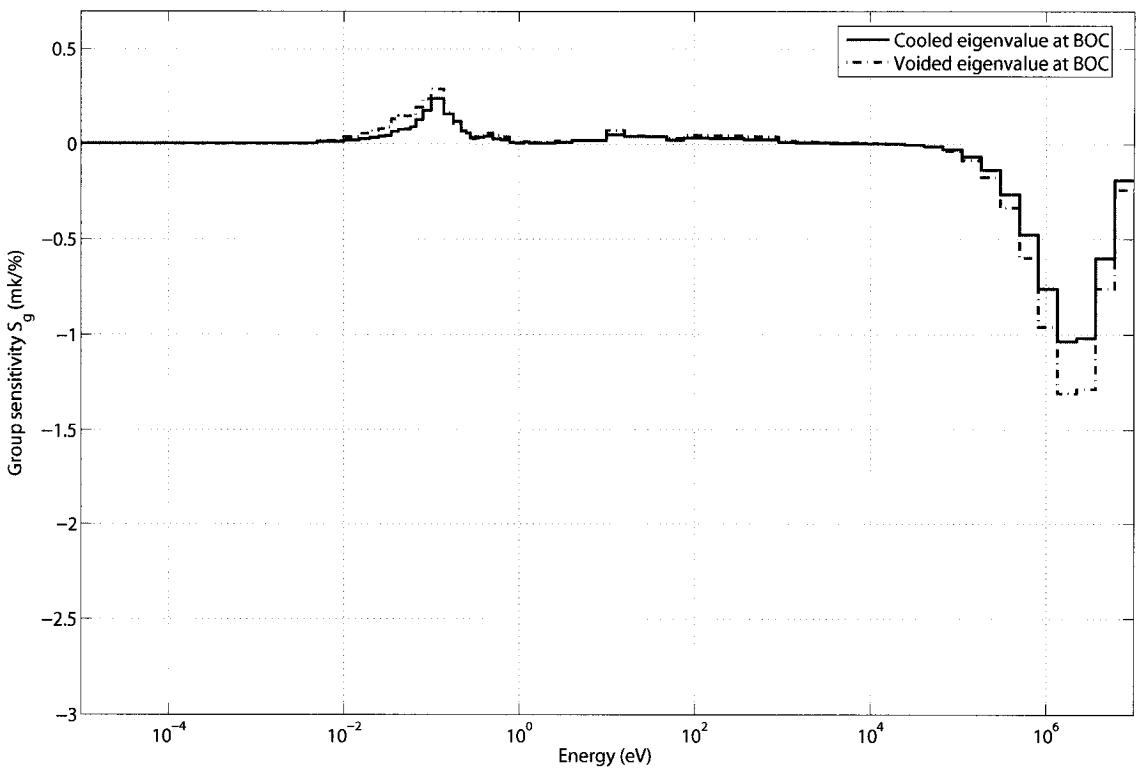

Figure III.9 Group sensitivity of cooled and void eigenvalues (at BOC) to U235 enrichment in central pin

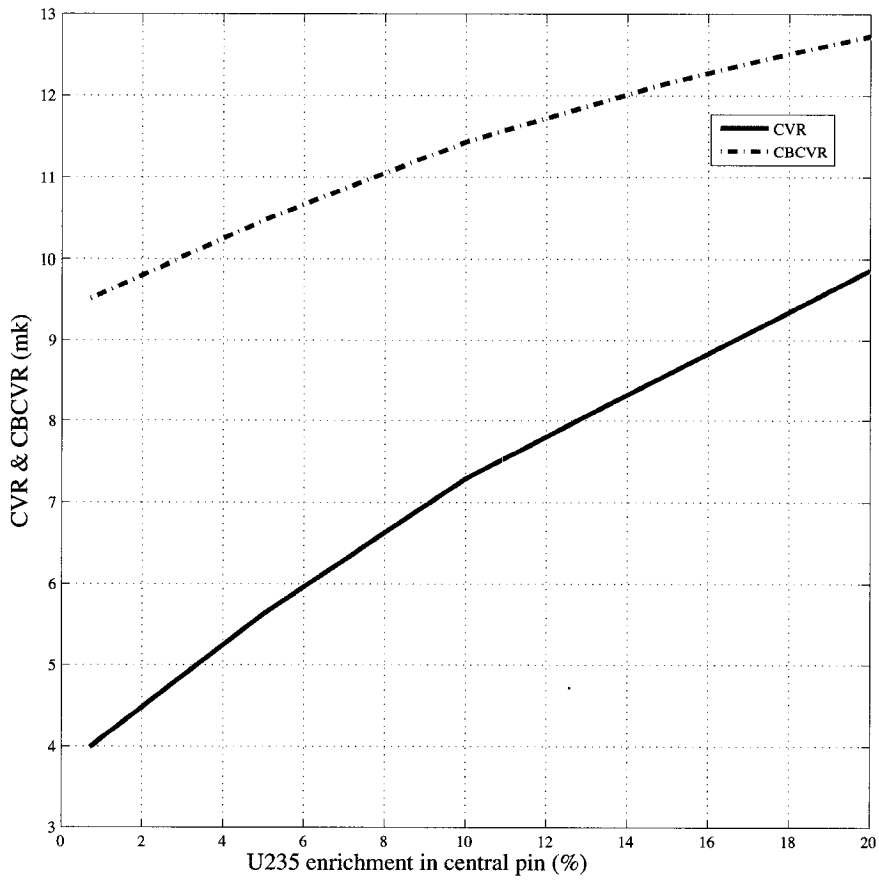

Figure III.10 CVR-BOC and CBCVR-BOC versus U235 enrichment(%) in central pin

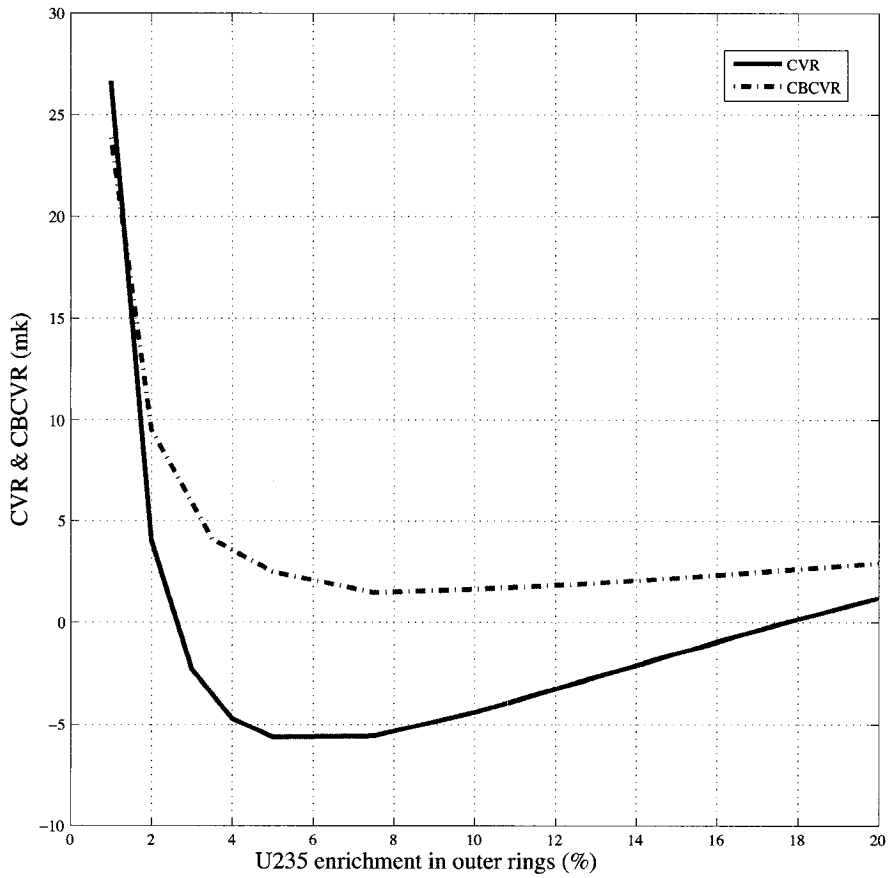

Figure III.11 CVR-BOC and CBCVR-BOC versus U235 enrichment(%) in outer rings

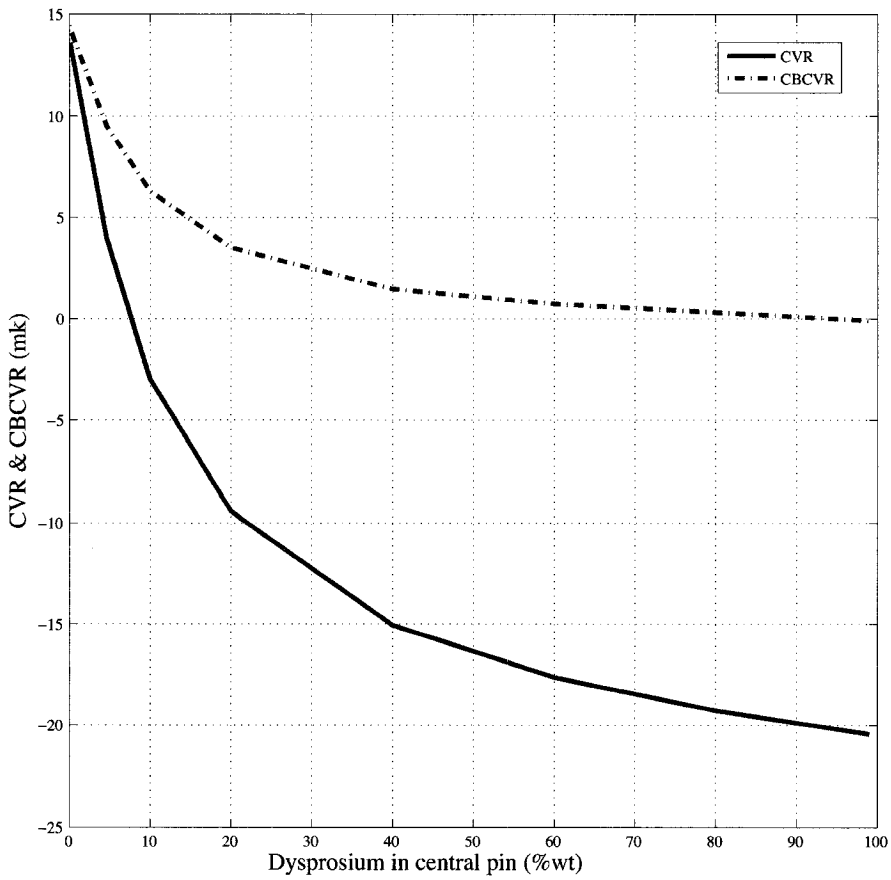

Figure III.12 CVR-BOC and CBCVR-BOC versus Dysprosium (%w) in central pin

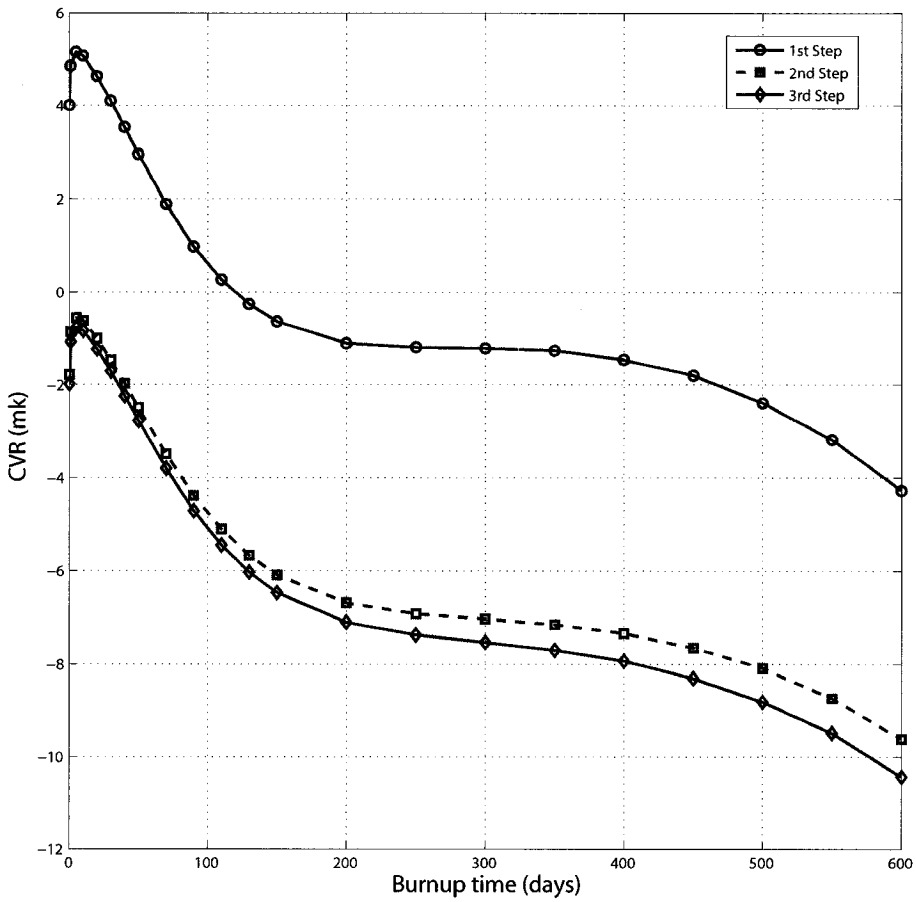

Figure III.13 CVR versus burnup time for Case 1

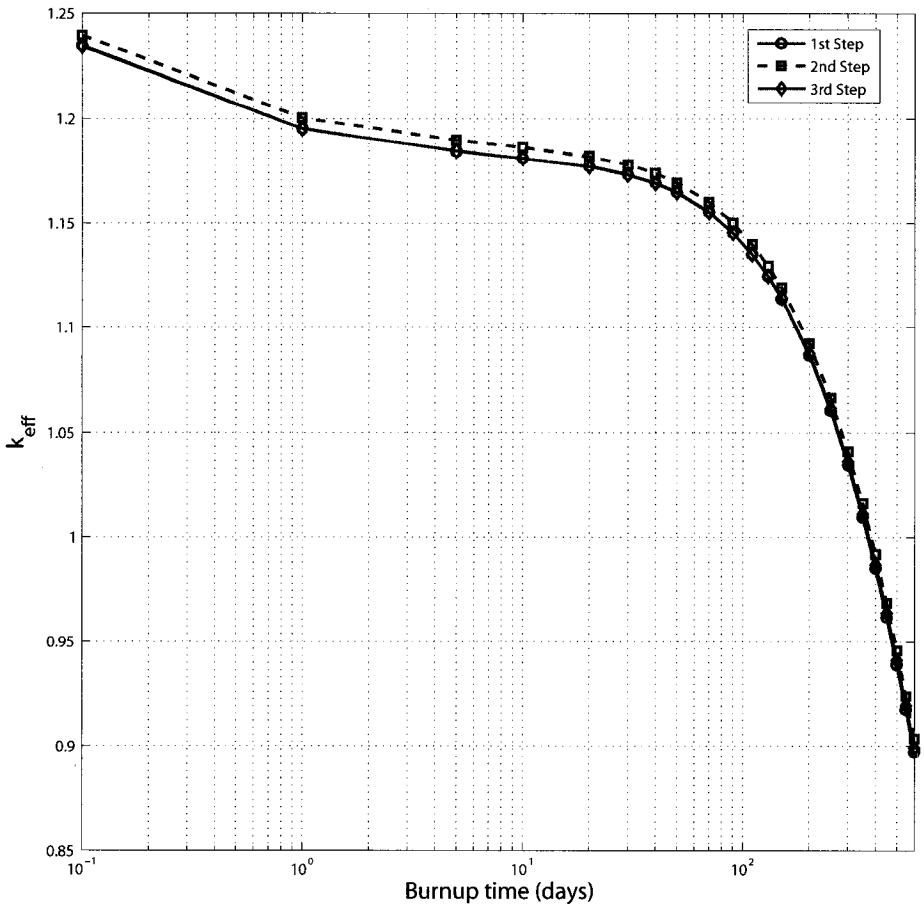

Figure III.14 k_{eff} versus burnup time for Case 1

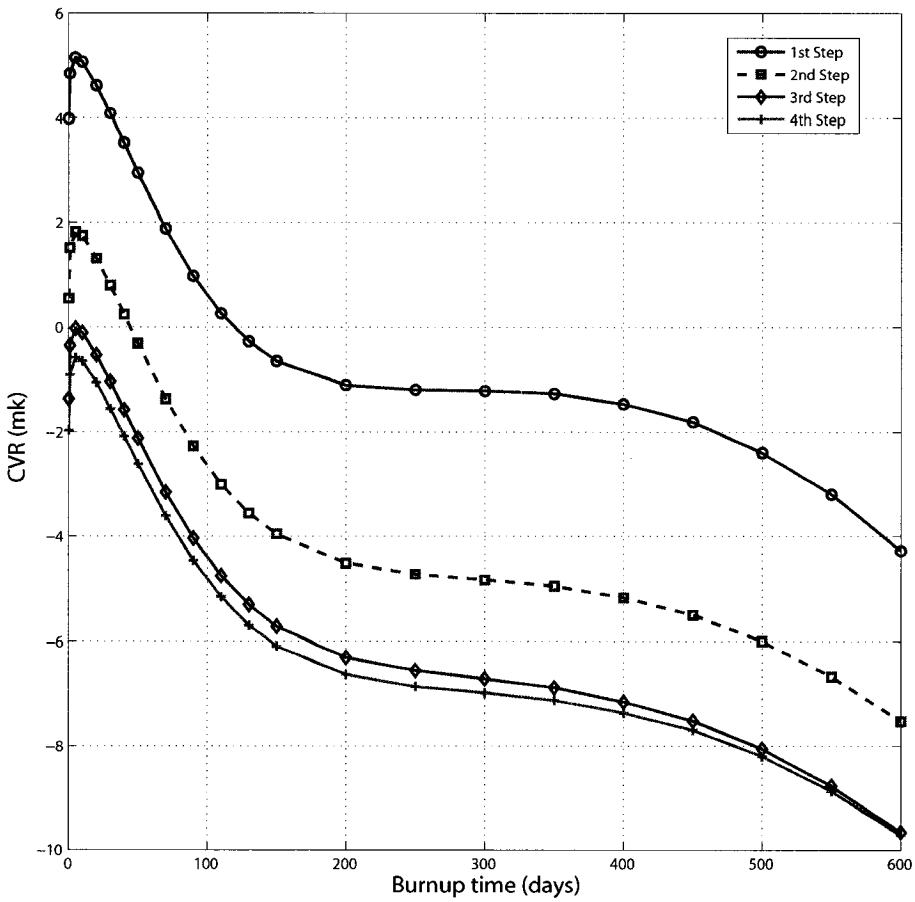

Figure III.15 CVR versus burnup time for Case 2

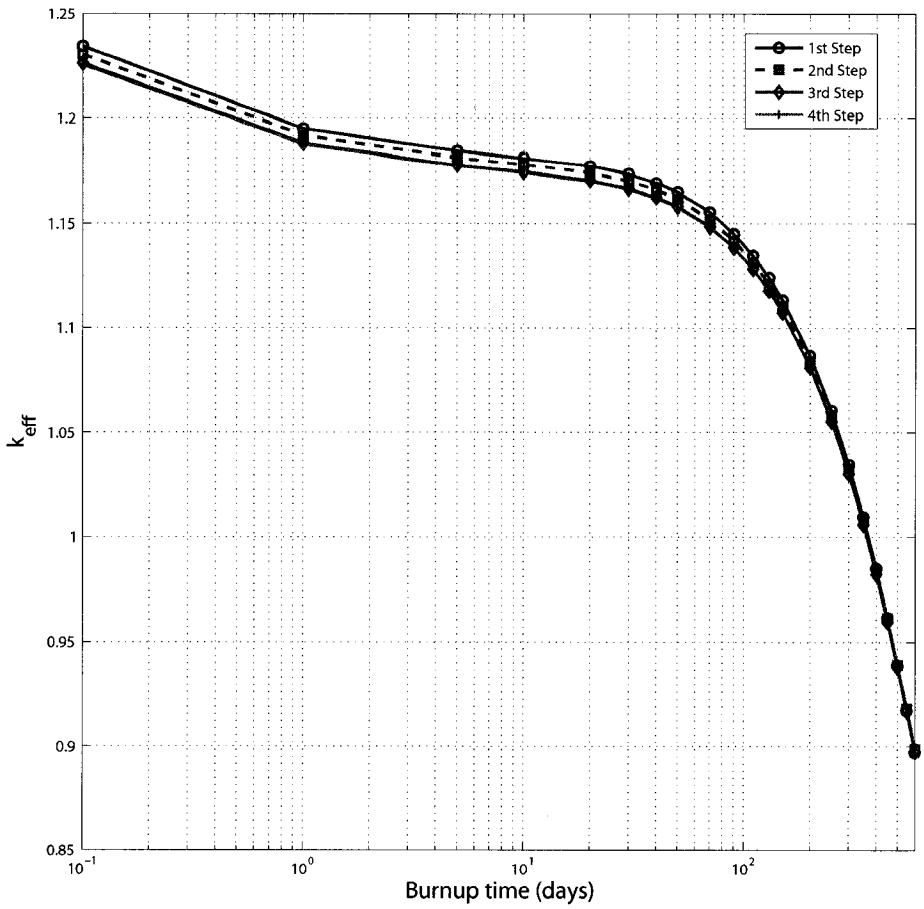

Figure III.16 k_{eff} versus burnup time for Case 2

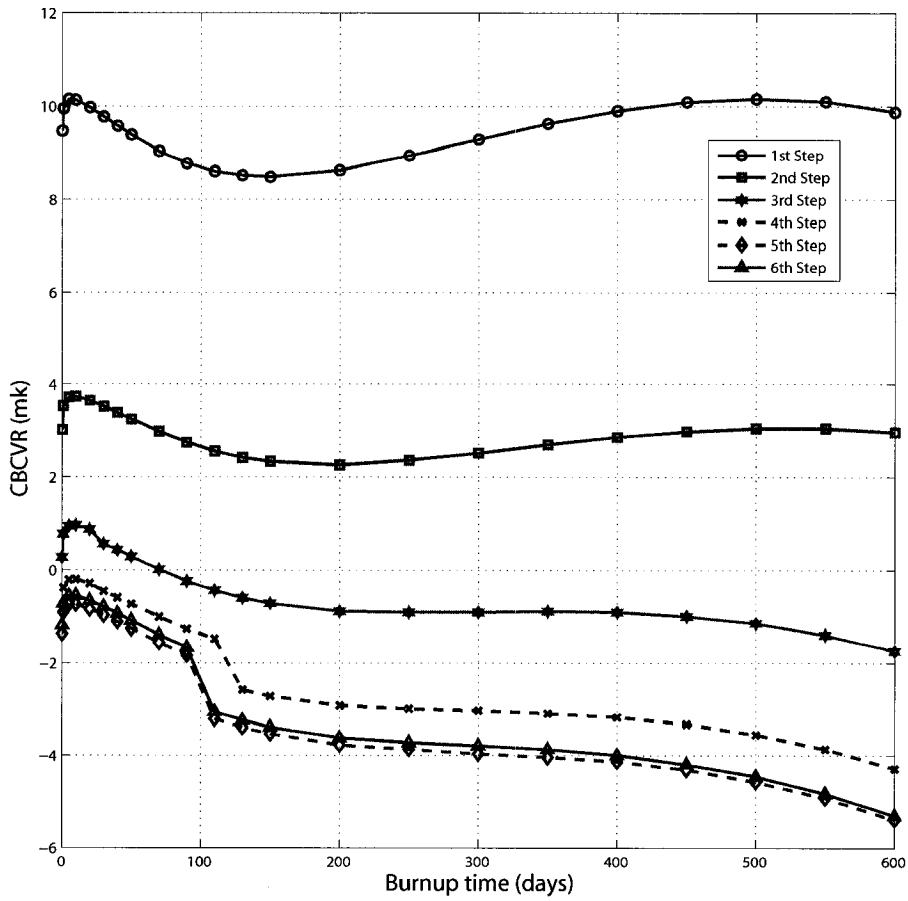

Figure III.17 CBCVR versus burnup time for Case 3

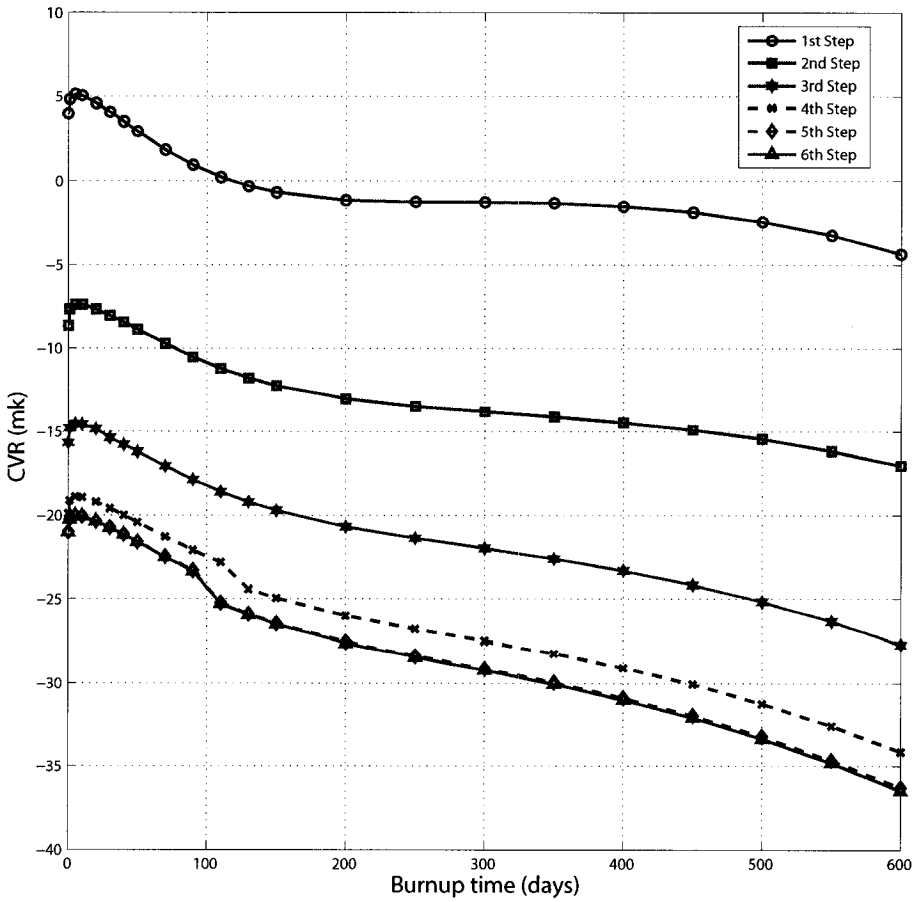

Figure III.18 CVR versus burnup time for Case 3

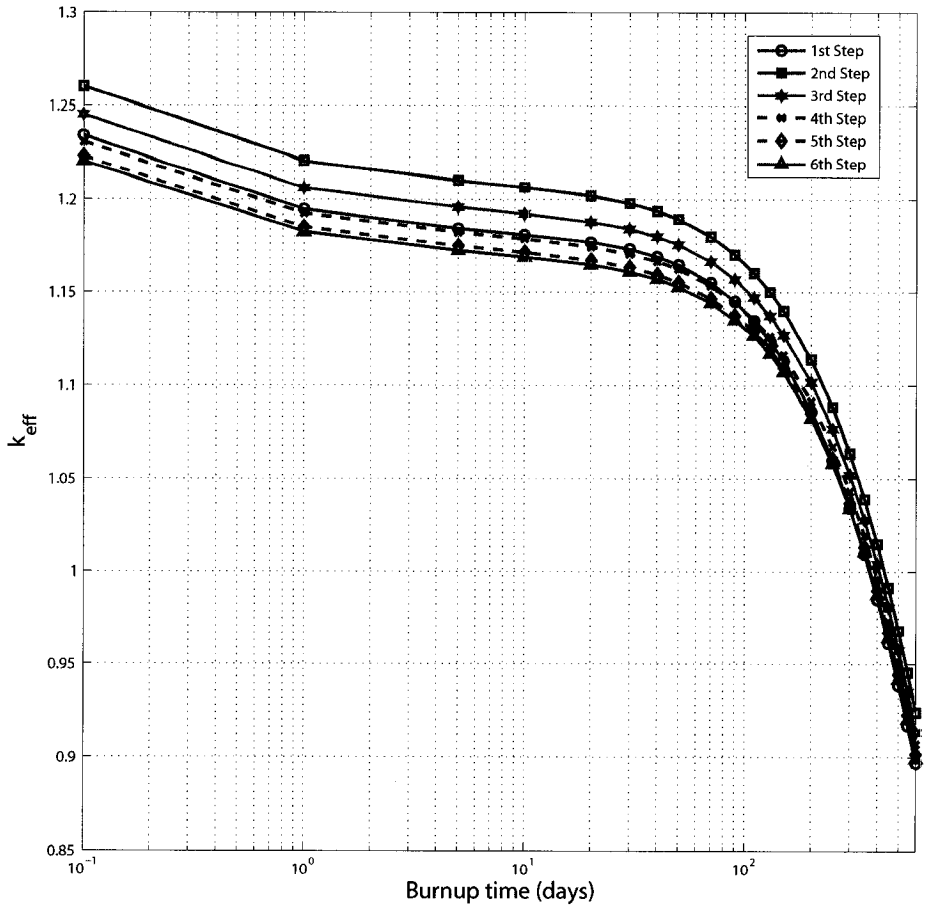

Figure III.19 k_{eff} plot versus burnup time for Case 3